On the Formation of the Particle Surface Composition during Spray Drying of Milk Powder

Martin Foerster

Dipl.-Ing.

A thesis submitted for the degree of Doctor of Philosophy at Monash University in 2017

Department of Chemical Engineering

Copyright Notice

Table of Contents

Abstract

Milk is often spray-dried to powder for improved preservation, easier handling and economy of transportation through lower bulk volume. The particle surface composition that is formed during the spray drying process strongly affects the functional powder properties. Typically, an unwanted overrepresentation of fat occurs on the particle surfaces during spray drying and leads to detrimental effects on the powder properties, including impaired reconstitution behavior, lower oxidative stability and greater stickiness. This necessitates additional post-processing steps, such as lecithination. With the governing driving forces of this component segregation being still under debate, in most reports the discussion has been restricted to the drying stage and the components' differences in diffusivity, solubility and interaction with the air/water interface have been perceived as the potential mechanisms. Yet, a few studies have recently indicated that the atomization stage might have a decisive impact on the final particle surface composition. In the present work, two convective drying methods, spray and single droplet drying, were employed to obtain a better insight about the component segregation in drying milk droplets.

In a comparison between the surface composition of spray-dried model milk particles and their corresponding atomized droplets, the atomization stage was found to exert the decisive influence on the final particle surface composition. In a second step, the emulsions were modified prior to spray drying by the addition of λ-carrageenan, a natural and food-safe polysaccharide. Emulsion stabilization was achieved at certain carrageenan concentrations, translating into improved fat encapsulation upon spray drying. Rheological investigation showed that the presence of a dispersed fat phase significantly reduced the extensional viscosity, which was raised again by stabilization with λ-carrageenan. It was concluded that under extensional stress during atomization the milk model emulsions were least stable against disintegration along the oil/water interfaces of the fat globules and hence preferably broke up along these, leading to the observed fat coverage as soon as individual droplets had been formed.

A modified single droplet drying technique allowed tracking the surface composition of model milk droplets after discrete drying times, in addition to the changes in temperature, diameter and mass with proceeding drying. Also here, the fat accumulated at the surface during droplet generation. The hydrophobic fat shell resulted in less droplet shrinkage and greater resistance to evaporation in comparison to a protein-rich shell. The experimentally determined drying and shrinkage kinetics were implemented into a numerical model to simulate the distribution of lactose, protein and fat during drying. The calculated concentration profiles highlighted the value of the new single droplet drying method to find accurate initial surface compositions as initial condition for such a model and to validate the results. The simulation work confirmed that the initial surface composition upon droplet generation was not caused by diffusive component segregation, but by the droplet generation mechanism itself.

Publications during Enrolment

The following peer reviewed articles were published (or accepted) in course of this research work (listed in order of their appearance in this thesis):

Invited Review Articles

Foerster, M., Woo, M.W., Selomulya, C., Component segregation during spray drying of milk powder, Elsevier Reference Module of Food Science, 2017, 1-11, DOI: dx.doi.org/10.1016/B978-0-08-100596-5.21155-4

Foerster, M., Woo, M.W., Selomulya, C., Single droplet drying, Elsevier Reference Module of Food Science, 2017, 1-9, DOI: dx.doi.org/10.1016/B978-0-08-100596-5.21154-2

Original Research Articles

Foerster, M., Gengenbach, T., Woo, M.W., Selomulya, C., The impact of atomization on the surface composition of spray-dried milk droplets, Colloids and Surfaces B: Biointerfaces (5-year impact factor 2015: 4.269), 2016, Vol. 140, p. 460-471, DOI: dx.doi.org/10.1016/j.colsurfb.2016.01.012

Foerster, M., Liu, C., Gengenbach, T., Woo, M.W., Selomulya, C., Reduction of surface fat formation on spray-dried milk powders through emulsion stabilization with λ-carrageenan, Food Hydrocolloids (5-year impact factor 2015: 4.703), 2017, Vol. 70, p. 163-180, DOI: dx.doi.org/10.1016/j.foodhyd.2017.04.005

Foerster, M., Gengenbach, T., Woo, M. W., Selomulya, C., The influence of the chemical surface composition on the drying process of milk droplets, Advanced Powder Technology (5-year impact factor 2015: 2.414), 2016, Vol. 27, p. 2324–2334, DOI: dx.doi.org/10.1016/j.apt.2016.07.004

Putranto, A., Foerster, M., Woo, M.W., Chen, X.D., Selomulya, C., A continuum-approach modelling of surface composition and ternary component distribution inside low fat milk emulsions during single droplet drying, AIChE Journal (5-year impact factor 2015: 2.317), 2017, Vol. 63, p. 2535–2545, DOI: dx.doi.org/10.1002/aic.15657

‘Thesis Including Published Works’ Declaration

I hereby declare that this thesis contains no material which has been accepted for the award of any other degree or diploma at any university or equivalent institution and that, to the best of my knowledge and belief, this thesis contains no material previously published or written by another person, except where due reference is made in the text of the thesis.

This thesis includes two review articles (Chapter 1) and three original research articles (Chapter 4, Chapter 5 and first part of Chapter 6) that have been published after peer-review with me as the first author (see publications listed on page II and table below). The core theme of the thesis is the formation of the particle surface composition during spray drying of milk powder. The ideas, development and writing up of all these papers in the thesis were the principal responsibility of myself, the student, working within the Department of Chemical Engineering under the supervision of Professor Cordelia Selomulya and Dr Meng Wai Woo.

The inclusion of co-authors reflects the fact that the work came from active collaboration between researchers and acknowledges input into team-based research. Chapter 2 recites the review articles in their original wording. Chapter 3, 4 and 5 each recite one of the research articles of which I am first author in their original wording. These chapters are introduced by an additional, prefacing paragraph to embed the individual studies into the wider context of this thesis.

In case of Chapter 6, the publication of which I am first author is amended by a subchapter based on a peer-reviewed publication of which I am a co-author. The corresponding graphs and writing are presented in revised form. My contribution to this publication involved: provision of the experimental data, development of the original concept of the mathematical model, discussion of the code and the simulation results (excluding coding and solving the equations), and assistance in writing the manuscript.

I have renumbered the chapters, tables and figures of the published articles and harmonized the nomenclature in order to generate a consistent presentation within the thesis. For all publications, one consolidated bibliography and one consolidated list of acknowledgements are presented in this thesis.

Student signature: [redacted] Date: 23 March 2017

The undersigned hereby certify that the above declaration correctly reflects the nature and extent of the student’s and co-authors’ contributions to this work. In instances where I am not the responsible author I have consulted with the responsible author to agree on the respective contributions of the authors.

Main supervisor signature: [redacted] Date: 23 March 2017

Thesis chapter	Publication title	Status	Nature and % of contribution	Co-author names, nature and % of co-author's contribution	Co-author Monash student?
2	Single droplet drying	Published	90% (concept, manuscript preparation)	1) Woo: 5% (discussion of manuscript) 2) Selomulya: 5% (discussion of manuscript)	No No
2	Component segregation in spray-dried milk powder	Accepted	90% (concept, manuscript preparation)	1) Woo: 5% (discussion of manuscript) 2) Selomulya: 5% (discussion of manuscript)	No No
4	The impact of atomization on the surface composition of spray-dried milk droplets	Published	80% (concept, experiments, manuscript preparation)	1) Gengenbach: 5% (XPS analysis) 2) Woo: 7.5% (discussion of experiments and manuscript) 3) Selomulya: 7.5% (discussion of experiments and manuscript)	No No No
5	Reduction of surface fat formation on spray-dried milk powders through emulsion stabilization with λ-carrageenan	Accepted	70% (concept, experiments, manuscript preparation)	1) Liu: 10% (assistance in experiments) 2) Gengenbach: 5% (XPS analysis) 3) Woo: 7.5% (discussion of experiments and manuscript) 4) Selomulya: 7.5% (discussion of experiments and manuscript)	Yes No No No
6	The influence of the chemical surface composition on the drying process of milk droplets	Published	80% (concept, experiments, manuscript preparation)	1) Gengenbach: 5% (XPS analysis) 2) Woo: 7.5% (discussion of experiments and manuscript) 3) Selomulya: 7.5% (discussion of experiments and manuscript)	No No No
6	A continuum-approach modelling of surface composition and ternary component distribution inside low fat milk emulsions during single droplet drying	Published as co-author	30% (provision of experimental data, concept of model, discussion of model, assistance in preparing manuscript)	1) Putranto: 50% (first author) 2) Woo: 7.5% (discussion of model and manuscript) 3) Chen: 5% (discussion of model) 4) Selomulya: 7.5% (discussion of model and manuscript)	No No No No

Acknowledgements

The academic support that I received during my studies, particularly from my supervisors, Cordelia Selomulya and Meng Wai Woo, is very much appreciated.

Cordelia was impressively quick with replying to emails and proof-reading, which was critical for the fast progress of my work in the last three years. My supervisors always had an open door for discussions and advice. They never revealed any eccentricities, were always fair and gave me all the freedom that I could have wished for. For that reason: thank you for making my PhD life a pleasant one, Cordelia and Wai! In the years to come I will look back proudly about having been part of this great research group.

Many thanks also go to all the postgraduate students in our group who created a positive and supportive atmosphere and particularly to Ruohui Lin for the comprehensive training on single droplet drying.

I am sincerely grateful for the time invested by and the input received from the examiners of my PhD milestones, the editors and reviewers of my publications, and the examiners of this thesis.

Monash University is acknowledged for the provision of my scholarships and the Australian Research Council is acknowledged for the research funding through the Linkage program (LP140100922).

The XPS measurements conducted at CSIRO were crucial for my project. Thomas Gengenbach, thank you for your valuable time and expertise!

Chang Liu, I'm certain you're having a very successful career ahead of you. Thanks for your commitment as well as the brilliant team work, and best of luck for your own PhD studies!

The confocal laser scanning microscopy work was performed at the Melbourne Centre for Nanofabrication (MCN) in the Victorian Node of the Australian National Fabrication Facility (ANFF). I also wish to acknowledge use of facilities within the Monash Centre for Electron Microscopy. The extensional viscosity measurements were conducted by Amarin McDonnell and Leslie Yeo at RMIT University, School of Engineering. CSIRO Agriculture & Food, Werribee, is gratefully acknowledged for provision of spray-dried skim milk powder samples. The support by Zhenkai Liao in installation of the microfluidic multi-jet spray dryer is highly appreciated, as well as the valuable discussions with Svenja M. Beck.

On a less formal note, a big shout out to all the great people I have met on this journey, too many to list them all.

It was a pleasure to be a part of an amazing community at our department, which would have not been the same without these lovely people: Kim Phu, Scot Sharman, Lilyanne Price, Harry Bouwmeester,

Joanne Tanner, Kahlil Desai, Tristan Lambert, Ross Ellingham, Jill Crisfield and everyone volunteering for CEPA. Keep it up, folks!

In research it can, at times, be hard to perceive a noticeable progress. It was also for this reason that it felt so good to advance every week, km by km, with RunMonash. Trevor Vincent, and the whole gang, you're such an inspiration!

Cheers, everyone. I'm out of here. But hey, let's stay in touch.

I say it as it is: it is such a good feeling to write these final words of my thesis. Nonetheless, with my graduation I am leaving behind countless friends and places close to my heart. What makes this process easier is to think of the brilliant people on the other side of the globe that I have been seeing too rarely for the last three years.

First and foremost, I owe this achievement to my fantastic parents, their continuous support and the independence as well as confidence they have given me to go my own way. Mom and dad, I'm grateful for everything you've done, everything to come, and all the love you are giving, which means so much to me and has made me the man that I am today.

Credit also goes to my grandma, who certainly helped finishing the PhD in time by keeping a wary eye on me coming back sooner rather than later.

Svenja Beck, this thesis would not have been possible without the strength, understanding and joy you are giving me. The best part of any working day, no matter how good or bad, has been coming home to you. Together, nothing can stop us.

Nomenclature

Abbreviations

CFD	Computational fluid dynamics
CLSM	Confocal laser scanning microscopy
d.m.	Dry matter
EDX	Energy dispersive X-ray analysis
ESCA	Electron spectroscopy for chemical analysis
FBRM	Focused beam reflectance measurement
LFMM	Low-fat model milk
LN_2	Liquid nitrogen
MFMJSD	Microfluidic multi-jet spray dryer
REA	Reaction engineering approach
RFMM	Regular-fat model milk
SAW	Surface acoustic wave
SD	Spray drying
SDD	Single droplet drying
SEM	Scanning electron microscopy
TEM	Transmission electron microscopy
XPS	X-ray photoelectron spectroscopy

Formula Symbols

Latin Symbols

a	[-]	Fitting parameter (normalized activation energy)
A	[m^2]	Surface area
b	[-]	Fitting parameter (normalized activation energy)
B	[-]	Fitting parameter (normalized radius)
c	[-]	Fitting parameter (normalized activation energy)
c_p	[$J \cdot K^{-1}$]	Heat capacity
C	[$kg \cdot m^{-3}$]	Concentration
d	[m]	Diameter
D	[$m^2 \cdot s^{-1}$]	Diffusion coefficient
$D(4,3)$	[m]	Volume weighted mean diameter
f	[-]	Diffusivity correction factor
h_h	[$W \cdot m^{-2} \cdot K^{-1}$]	Convective heat transfer coefficient

h_m	[m·s^{-1}]	Convective mass transfer coefficient
k	[W·m^{-1}·K^{-1}]	Thermal conductivity
k_a	[m·s^{-1}]	Kinetic adsorption parameter
k_d	[s^{-1}]	Kinetic desorption parameter
K_B	[J·K^{-1}]	Boltzmann's constant
m	[kg]	Mass
n	[-]	Number
N	[mol/l]	Normality
Oh	[-]	Ohnesorge number
PV	[milliequiv. peroxide/kg fat]	Peroxide value
Q	[kg·m^{-2}]	Surface concentration
r	[m]	Radial coordinate
r^2	[-]	Coefficient of determination
R	[m]	Radius
$\mathcal{R}$	[J·mol^{-1}·K^{-1}]	Universal gas constant
S	[ml]	Titration volume
t	[s]	Time
T	[K]	Temperature
v_r	[m·s^{-1}]	Shrinkage velocity
V	[m^3]	Volume
x	[m]	Diffusion length
X	[kg·kg^{-1}]	(Local) moisture content
$\overline{X}$	[kg·kg^{-1}]	Global moisture content

Greek Symbols

γ	[N·m^{-1}]	Surface tension
τ	[s]	Diffusion time
ΔE_{vap}	[J·mol^{-1}]	Apparent activation energy of evaporation
ΔH_{vap}	[J·kg $^{-1}$]	Enthalpy of water evaporation
μ	[Pa·s]	Dynamic viscosity
ρ	[kg·m^{-3}]	Density
Φ	[-]	Packing volume fraction
ψ	[-]	Fractionality coefficient

Subscripts

0	Initial condition
b	Bulk

d	Droplet
e	Equilibrium
ext	Extensional
fat	Fat
i	Component index
j	Size class
lac	Lactose
max	Maximum
prot	Protein
s	Surface
sat	Saturation
v	Vapor
vap	Evaporation
w	Water

1 Introduction

Spray drying of milk emulsions to powder form entails the benefits of better preservation, easier handling as well as further processing, and a reduced bulk volume for economy of transportation. In Australia, for instance, 35 % of the produced milk is currently spray-dried into whole milk, skim milk or infant formula powders (dairyaustralia.com.au, 2015/16). An efficient production process of milk powder with desirable functional properties, which are strongly influenced by the chemical particle surface composition, is therefore of particular importance for the dairy industry. Yet, the manufacture of milk powder at both industrial and laboratory scale is characteristically afflicted by a fat coverage on the particle surface that is formed in the course of the spray drying process. The surface fat impacts the product shelf life detrimentally due to increased susceptibility to fat oxidation. It also impedes further processing because of an impaired reconstitution behavior and deteriorated flow properties. This can result in the consumer experiencing a compromised product quality and in reduced production efficiency, as considerable product losses or the necessity of additional processing steps, such as coating with lecithin, can emerge. In light of this, it is of great scientific as well as industrial interest to identify the mechanism(s) that are responsible for the formation of surface fat during the convective drying of milk droplets. For this purpose, the following three research gaps are to be addressed:

Firstly, the governing driving forces for the observed component segregation between lactose, protein and fat in a drying milk droplet are still under debate. The discussion has been mostly restricted to the drying stage of the spray drying process, with the component's differences in diffusivity, surface activity and solubility being typically perceived as potential reasons. Only a few studies have discussed the possibility that an atomization induced mechanism might already impact the component distribution ahead of the actual drying process. These studies have usually been limited to an analysis of the surface composition of the dried particles, while the atomization process and the thereby generated droplets were not investigated. This proved to be insufficient for drawing a reliable conclusion about whether the atomization stage or the subsequent drying stage exerts the dominant influence on the chemical surface composition of the product powder.

Secondly, as the mechanism that primarily governs the component segregation has not been identified yet, no targeted attempts to inhibit the surface fat formation in spray-dried milk powder have been published so far, either.

Thirdly, whilst the detrimental influence of surface fat on the final particle characteristics has already been studied extensively, it has not been investigated yet how the fat surface alters the droplet's drying and shrinkage kinetics. Single droplet drying experiments allow to obtain such information from measuring the changes in droplet temperature, mass and size during convective drying. A detailed knowledge

of the kinetics will be helpful in spray drying applications for optimization of process design and product characteristics. In addition, hitherto single droplet drying has not been utilized to track the changes in surface composition over drying time, though this promises to give new insights into the component segregation that occurs between generation of the droplets and completion of the drying. Availability of such data would also support the development of a reliable numerical model for computation of the component distribution inside a convectively drying milk droplet. Simulation of the spatiotemporal concentration profiles of lactose, protein and fat can further help understanding the component segregation mechanism. It can also be applied in industrial computational fluid dynamics (CFD) simulation for spray-dryer design and prediction of product properties. No such model has been published yet, although a few numerical approaches have been reported in literature that allow calculation of the concentration profile of one or two solutes in a drying droplet (e.g. an aqueous lactose/protein solution). These models, however, entailed weaknesses in describing the evaporation rate and diffusion of moisture through the solidifying crust as well as in defining the droplet shrinkage rate. Moreover, the predicted changes in surface composition over time were not validated experimentally.

In the following literature review chapter, the research gaps will be described in more detail and possible investigation techniques to address them will be discussed.

2 Literature Review

2.1 Preface

The component segregation and surface fat formation during spray drying of milk droplets has briefly been described in the introduction of this thesis and will be elaborated in more detailed in the following literature review. It was endeavored to establish a profound understanding of the potential segregation mechanisms that are discussed in literature to be aware of which concepts need to be taken into consideration for this study.

Further, the literature has been reviewed in respect to analysis techniques that are available for investigation of the component segregation in convectively drying droplets. In the following summary, an overview about different single droplet drying approaches will be given with a focus on the advantages and limitations of free falling single droplet drying and suspended single droplet drying. A combination of these two methods was utilized in this work by employing microfluidic jet spray drying as a form of falling single droplet drying (Chapter 3-5) together with suspended single droplet drying (Chapter 6).

The following work has been published by Elsevier B.V.:

Foerster, M., Woo, M.W., Selomulya, C., Component segregation during spray drying of milk powder, Elsevier Reference Module of Food Science, 2017, 1-11, DOI: dx.doi.org/10.1016/B978-0-08-100596-5.21155-4

Foerster, M., Woo, M.W., Selomulya, C., Single droplet drying, Elsevier Reference Module of Food Science, accepted, 2017, 1-9, DOI: dx.doi.org/10.1016/B978-0-08-100596-5.21154-2

2.2 Component Segregation during Spray Drying of Milk Powder

2.2.1 Synopsis

The formation of the chemical surface composition in convectively dried milk droplets has been investigated in a range of experimental and numerical studies. The process is complex and of particular importance for the functional properties of spray-dried milk powder, as its surface composition has been found to differ considerably from its bulk composition. The surface of milk powder is usually characterized by a distinct accumulation of fat and, in case of milk emulsions with low fat content, a less pronounced overrepresentation of protein in comparison to the bulk composition. Based on experimental

studies on the drying process of milk powder using various analysis techniques of its surface composition, a number of different concepts have been proposed in literature to explain this segregation mechanism. Furthermore, numerical models of increasing complexity have been developed over the years to contribute towards a better understanding of the segregation process and to predict the powder properties as a function of drying and feed conditions applied.

2.2.2 Introduction

2.2.2.1 Bulk Composition of Whole Milk

Whole milk, skim milk and infant formula emulsions are regularly spray-dried to powder form at large industrial scale for preservation with increased stability against oxidative rancidity, reduced bulk volume for economy of transportation, and easier processing as ingredient in food products (Schuck, 2002, Vega and Roos, 2006). While the exact composition of bovine whole milk can vary considerably, on average it has a solid content of 12-13 % w/w and, as presented in Table 2.1, the major components are lactose with an approximate content of 41 % w/w in dry matter (d.m.), fat with 31 % w/w and protein with 27 % w/w.

Table 2.1: Typical composition of bovine whole milk (Bylund, 2003).

Species	Concentration [% w/w]
Water	87.5
Lactose	4.8
Fat	3.9
Protein, total	3.4
Casein	2.71
α_{s1}-casein	1.04
α_{s2}-casein	0.27
β-casein	1.05
κ-casein	0.34
Whey protein	0.65
α-lactalbumin	0.13
β-lactoglobulin	0.33
Miscellaneous	0.19
Fat globule membrane proteins	0.04
Minerals, vitamins	0.8

The milk fat is dispersed inside the aqueous continuous phase in form of spherical fat globules of 0.1-10 µm in diameter (Michalski et al., 2002). The globules are stabilized by a surrounding layer of fat globule membranes, which are composed of a complex combination of phospholipids, lipoproteins, other proteins, organic acids, bound water, traces of metals and enzymes (Singh and Gallier, 2016). About 80 % of the total protein content in bovine milk is made of caseins. These phosphoproteins are

held together in form of submicron-sized micelles by hydrophobic interaction and calcium ions (Müller-Buschbaum et al., 2007). In studies that investigate milk model emulsions, native casein is often replaced by sodium caseinate as emulsifier. It is produced from precipitated casein by the addition of sodium hydroxide and is soluble in water without developing a micelle structure (Jost, 2002). The remaining protein fraction in milk consists of whey proteins, which are primarily comprised of α-lactalbumin and β-lactoglobulin. Whey protein is also known as milk serum protein due to its greater water solubility than that of casein.

2.2.2.2 Powder Surface Composition after Spray Drying

The main components at the surface of spray-dried milk powder usually differ substantially in proportion from the bulk composition of the original milk emulsion because of an overrepresentation of fat at the surface. The surface layer of fat is unwanted, as the chemical surface composition strongly influences the functional powder properties, with surface fat leading to several detrimental effects on the product characteristics (Vignolles et al., 2007). This includes enhanced lipid oxidation during storage and thus faster expiration (Granelli et al., 1996, Hardas et al., 2000, Keogh et al., 2001a), reduced reconstitution behavior (Fäldt and Bergenståhl, 1996b, Millqvist-Fureby et al., 2001) and greater stickiness (Kim et al., 2005a, Nijdam and Langrish, 2006). This can cause a deteriorated product quality for the end user, as well as lower production efficiencies due to significant product losses and the requirement of additional processing steps, such as coating with lecithin. Furthermore, an enrichment of protein at the surface of particles from low-fat milk emulsions is sometimes observed. Although being less of a concern for skim and whole milk, in powders that contain particularly high proportions of native casein the rehydration behavior can also be detrimentally affected by too much surface protein as a result of a network formation between the casein micelles (Havea, 2006, Mimouni et al., 2010, Schuck et al., 2007). It is therefore of great interest to identify the segregation mechanism that induces the surface fat formation or other component segregation processes during spray drying of milk powders. A better understanding will help to find technical solutions to establish more desirable surface compositions. Moreover, knowledge about the chemical surface formation in drying milk droplets is relevant for modeling purposes of industrial applications to predict the functional product properties and to optimize spray dryer designs.

An analysis of the whole manufacturing process of milk powder has indicated that spray drying is the determining step, whereas the following fluidized bed and handling stages have a negligible influence on the surface composition (Kim et al., 2009b). As such, the studies on the surface formation of milk particles reported in literature have mostly focused on the drying process itself. It has been attempted to explain the component segregation by mechanisms occurring during the drying stage between droplet generation and completion of the spray drying process (segregation induced by diffusivity, surface activity and crust formation), or prior to this during disintegration of the feed emulsion into individual droplets (segregation induced by atomization). It is still under debate which of those potential mecha-

nisms is in fact the predominating driving force, with the respective studies providing either one specific segregation concept as explanation (Table 2.2) or a combination of two or more (Table 2.3).

2.2.3 Chemical Surface Composition of Milk Particles

2.2.3.1 Presence of Surface Fat and Effect of Spray Drying Conditions

In general, Table 2.2 and Table 2.3 show that there is a wide agreement in the observation of a dominant presence of surface fat on convectively dried milk powder, which could not be prevented by variation of the drying parameters or spray dryer type. For milk (model) emulsions with fat contents similar to whole milk, the particles were found to be covered by an almost consistent fat layer that occupied more than 85 % of the outmost surface area (Chew et al., 2015, Kim et al., 2003, Murrieta-Pazos et al., 2012, Shamaei et al., 2016). This corresponds to a fat surface overrepresentation of approximately three times in relation to the feed bulk composition. Skim milk (model) emulsions and milk protein concentrates were observed to also translate into a fat accumulation on the powder surface with 3.5-45.9 % surface fat for fat contents of 0.6-1.5 % in the bulk (Fyfe et al., 2011, Kelly et al., 2015, Kim et al., 2009a, Murrieta-Pazos et al., 2012, Nikolova et al., 2014). This corresponds to a surface overrepresentation of 6-30 times in comparison to the bulk composition. Nevertheless, in contrast to whole milk particles, it has been shown that the surface of skim milk and milk protein concentrate powders is not dominated by fat because of the low overall fat proportion. The remaining surface area of low-fat milk powders was found to primarily consist of protein (42.0-62.7 % in the first few nanometers of the surface area for 35.0-38.5 % in the bulk), indicating a slight surface enrichment in protein during drying. Independent from the overall fat content, a distinct lack in lactose has been consistently reported for all milk powders that were subject of the studies listed in Table 2.2 and Table 2.3, with lactose being sometimes almost completely absent from the outmost surface region (Gaiani et al., 2006, Nijdam and Langrish, 2006).

To some degree, within the above described range of surface compositions, the exact amount of fat and protein at the particle surface has been reported to be influenced by the drying conditions. Fyfe et al. (2011) studied commercial skim and whole milk powders as wells as powders obtained from laboratory and pilot scale spray drying. Comparison of the powders showed that there was a difference in surface composition depending on the spray dryer type, albeit always featuring a distinct fat overrepresentation and, for skim milk powders, additionally a moderate protein overrepresentation. Commercial milk powders consisted of more fat and less protein at the surface than the powders produced with laboratory and pilot spray dryers. It remained unclear if this can be ascribed to a larger particle size and higher feed solid content of the industrial drying processes or to the differences in atomization techniques applied. Some studies have indicated that the final particle surface composition will conform more with the bulk composition if the drying rate is increased, for instance by means of a higher drying temperature or a smaller droplet size as influenced by the atomization pressure (Gaiani et al., 2010, Kelly et al., 2002, Nikolova et al., 2015a).

Table 2.2: Summary of studies on component segregation in droplets consisting of milk protein and fat: organized by concepts provided as explanation – part 1: only one concept per study.

Concept	System	Surface composition (XPS)	Analysis	Author
Diffusivity	Aqueous solution of sucrose/ caseinate in agar gel matrix	20% protein overrepresentation	XPS	(Meerdink and van't Riet, 1995)
Diffusivity	Industrial spray dried skim and whole milk	Overrepresentation of fat (whole milk: 98% on surface / 29% total, skim milk: 18% on surface / 1% total), also enrichment of protein near the surface	XPS, free fat extraction	(Kim et al., 2003)
Diffusivity	Single droplet drying of whole and skim milk	Hydrophobic surface due to surface fat	Dissolution behavior	(Fu et al., 2011a)
Diffusivity	Spray drying of skim milk in pilot scale	Overrepresentation of fat (5.8-7.4 % on surface / 0.9 % total) and protein (43.0–49.8 % on surface / 36.9% total), slight increase in segregation with longer drying	XPS	(Nikolova et al., 2014, Nikolova et al., 2015a)
Surface activity	Spray drying of lactose/ soybean oil/ whey protein or sodium caseinate	Overrepresentation of fat for whey protein, better fat encapsulation with sodium caseinate (whey protein: 45 % on surface, caseinate: 3% on surface / 30% total)	XPS	(Fäldt and Bergenståhl, 1995, Fäldt and Bergenståhl, 1996a)
Surface activity	Spray drying of sucrose/ whey protein or sodium caseinate	Overrepresentation of protein (up to 50-58% / 0.5-1 % total)	XPS	(Adhikari et al., 2009)
Surface activity	Spray drying of phosphor-caseinate/ lactose/ milk fat	Overrepresentation of fat (14.5-18.7 % on surface / 0.4 % total)	XPS	(Gaiani et al., 2006)
Surface activity/ hydrophobicity	Spray drying of milk protein concentrate with various protein contents	Overrepresentation of fat (3.5-10.2 % on surface / 0.6-1.4 % total) and protein (62.7-97.2 % on surface / 35.4-85.8 % total)	XPS	(Kelly et al., 2015)
Crust formation	Industrial spray dried skim and whole milk	Overrepresentation of fat (whole milk: 93.3 % first 5 nm, 58.6 % first µm / 28.4 % total, skim milk: 45.9 % first 5 nm, 22.8 % first µm / 1.5 % total) and slight overrepresentation in protein for skim milk (45.1% first 5 nm, 34.4 % first µm / 38.5 % total)	XPS, EDX, free fat extraction	(Murrieta-Pazos et al., 2012)

Table 2.3: Summary of studies on component segregation in droplets consisting of milk protein and fat: organized by concepts provided as explanation – part 2: combinations of concepts.

Concept	System	Surface composition (XPS)	Analysis	Author
Diffusivity, surface activity	Spray drying of lactose and fat with casein or whey protein	Overrepresentation of fat for all powders and of protein for many powders, less fat enrichment for casein instead of whey protein and for higher temperatures	XPS	(Gaiani et al., 2010)
Diffusivity, surface activity	Spray drying of lactose/ rapeseed oil/ whey protein	Overrepresentation of fat (55-65 % on surface / 30 % total)	XPS, free fat extraction	(Millqvist-Fureby et al., 2001)
Surface activity, crust formation	Spray drying of whole and skim milk	Overrepresentation of fat (significant) and protein (less distinct)	XPS	(Nijdam and Langrish, 2005, Nijdam and Langrish, 2006)
Surface activity, crust formation	Spray drying of walnut oil and skim milk (with Tween 80 or maltodextrin)	Overrepresentation of fat (85.6-92.5 % on surface / 50 % total)	XPS, free fat extraction	(Shamaei et al., 2016)
Diffusivity, surface activity, crust formation	Single droplet and spray drying of milk model emulsions at various fat contents and of milk protein concentrate	Overrepresentation of fat (milk emulsion with 76-87 % fat on surface / 29-42 % total, milk protein concentrate: 17-27 % on surface / 1.5 % total)	XPS	(Chew et al., 2014, Chew et al., 2015)
Surface activity, crust formation, atomization	Spray drying of whole and skim milk (lab and pilot scale), compared with commercial powders	Overrepresentation of fat in form of thin patches on all powders (e.g. commercially dried skim milk: on surface 16.5 % / 0.7 % total, pilot scale: about 14 % and laboratory scale: about 7 % on surface)	XPS, CLSM	(Fyfe et al., 2011)
Diffusivity, surface activity, crust formation, atomization	Spray drying of whey protein/ sunflower oil/ maltodextrin	Overrepresentation of fat (17.7-34.1 % on surface / 10 % total) and protein (19.8-42.7 % on surface / 10 % total)	XPS	(Xu et al., 2013)
Diffusivity, surface activity, crust formation, atomization	Industrially spray-dried powders of skim and whole milk	Overrepresentation of fat (whole milk: >90 % on surface / 26 % total, skim milk >18 %on surface / 1 % total), slight protein overrepresentation for skim milk (42 % on surface / 35 % total)	XPS	(Kim et al., 2009a, Kim et al., 2009b)

Diffusivity, surface activity, atomization	Spray drying of skim milk	High fat overrepresentation and lower protein overrepresentation, surface fat content already high directly after atomization	XPS, flash freezing of atomized droplets	(Wu et al., 2014)

Furthermore, the properties of the feed emulsion can affect the particle surface composition. A higher droplet viscosity and earlier crust formation due to an increased feed solid content have been reported to reduce the extent of component segregation during drying of skim milk (Kim et al., 2009b, Wu et al., 2014). The fat encapsulation efficiency was improved by a stronger reduction in fat globule size during homogenization in studies conducted by Kim et al. (2009b) and Millqvist-Fureby (2003), whereas the surface composition data sets provided by Xu et al. (2013) and Keogh and O'Kennedy (1999) did not demonstrate such a statistically significant relationship for the range of droplet sizes investigated. Gaiani et al. (2010) and Fäldt and Bergenståhl (1996a) observed an influence of the kind of milk protein employed as emulsifier. The use of casein, particularly in the presence of lactose, resulted in less surface fat than the use of whey protein, presumably due to casein's greater surface activity and resistance to denaturation under heat (Vega and Roos, 2006).

2.2.3.2 Analysis Techniques of Component Distribution

X-ray photoelectron spectroscopic analysis (XPS), also referred to as electron spectroscopy for chemical analysis (ESCA) in this context, is the prevailing method to quantify the chemical surface composition of milk particles. In this sensitive surface analysis technique, the powder samples are irradiated with an X-ray beam of a well-defined energy level under high vacuum, and electrons are emitted if their binding energy is surpassed by the photon energy. Detection of the number of emitted electrons and their respective kinetic energy, which is characteristic for each chemical element, yields the sample composition and the chemical state of the elements. Fäldt et al. (1993) suggested a transformation of the obtained elemental particle surface concentrations, i.e. the relative amounts in carbon, nitrogen and oxygen, into the surface percentages that are covered by lactose, protein and fat by means of a matrix linearization based on each component's representative structural formula. This approach has been widely adopted in literature, and the surface compositions presented in Table 2.2 and Table 2.3 were determined in this manner. Nikolova et al. (2015b) discussed the possibility of a distortion of the XPS analysis towards higher carbon contents as a result of organic pollution inside the vacuum chamber and therefore proposed a modified approach where the linearization matrix is derived from experimental measurements of XPS spectra for lactose, protein and lipid standard samples. Either way, it is generally accepted that component compositions derived from XPS atomic spectra should be considered as semi-quantitative estimations only. In addition, it needs to be noted that XPS analysis accounts only for the first few nanometers of the sample surface (about 0-10 nm), with the exact sampling depth being difficult to quantify because of the surface curvature of the milk particles. As such, it only describes the outmost surface

layer of the analyzed powders, which does not allow a conclusion about the overall amount of free surface fat, especially for high-fat milk powders.

The total amount of free surface fat, often expressed by the encapsulation efficiency of a powder sample, is frequently quantified by surface fat extraction. In this method, the mass of extracted fat is determined by measuring the sample weight before and after extraction with a nonpolar, organic solvent, such as hexane or petroleum ether. In terms of powder concentration, duration of the extraction process and intensity of the contact between powder and solvent during mixing, no standard procedure has been established yet and the techniques reported in literature vary considerably amongst each other, as summarized by Vega and Roos (2006). The amount of extracted fat further depends on the particle size and porosity (Twomey et al., 2000, Vignolles et al., 2007). A significant amount of extractable fat is believed to not originate from the particle surfaces, but from inner free fat that is extracted from the inside of the particles through pores and cracks, in particular at relatively intense mixing and long exposure times to the solvent (Buchheim, 1982, Buma, 1971). For this reason, the results from fat extraction of milk powder samples might most often represent the amount of free fat instead of the amount of free surface fat (Kim et al., 2005b). As a consequence, free (surface) fat extraction might provide a more suitable technique than XPS in order to quantify the total amount of surface fat, but is typically limited to a qualitative comparison amongst samples analyzed with the same extraction technique, rather than giving robust absolute values.

Other, less frequently employed analysis methods include confocal laser scanning microscopy (CLSM) for the protein and fat distribution throughout the whole particle volume (Taneja et al., 2013), transmission electron microscopy (TEM) for protein-lipid or protein-protein interactions (McKenna et al., 1999), and Energy Dispersive X-ray (EDX) analysis of the atomic surface composition at a sampling depth of about 1 µm (Murrieta-Pazos et al., 2012). As these techniques describe the particle composition at different distances from the extreme surface, often various combinations are employed to obtain a comprehensive insight into the component distribution, such as XPS measurements together with free fat extraction and CLSM investigation (Vignolles et al., 2009a) or XPS together with EDX analysis (Murrieta-Pazos et al., 2012).

2.2.4 Potential Segregation Mechanisms

2.2.4.1 Diffusivity

As illustrated in Figure 2.1b, Meerdink and van’t Riet suggested that the component segregation could occur due to differences in the components’ diffusivities (Meerdink, 1994, Meerdink and van't Riet, 1995), a concept that has been adopted in a series of subsequent studies (Chew et al., 2014, Fu et al., 2011a, Kim et al., 2003, Nikolova et al., 2015a). As water evaporates from the droplet surface, radial gradients in the component concentrations are formed and cause the components to diffuse towards the

inside of the droplet. Because the diffusivity of a species increases with decreasing hydrodynamic radius, the outer droplet region might become depleted in the smaller, faster diffusing components, such as lactose. As a first approximation of the binary diffusion coefficient of a species in liquid medium, there is an inverse proportionality between the hydrodynamic radius of the species and its diffusivity according to the Stokes-Einstein equation (Cussler, 2009). In homogenized, bovine whole milk, the radius is in the range of 100-10,000 nm for lipid globules (Leman et al., 1989, Michalski et al., 2002), 50-300 nm for casein micelles (Dewan et al., 1974, Müller-Buschbaum et al., 2007) and 0.1-1 nm for lactose (Bylund, 2003). Thus, the diffusivity of lactose is 2-5 orders of magnitude greater than the diffusivity of the fat globules. The longer the drying process takes (for instance the lower the drying temperature or the higher the initial water content), the stronger might the diffusivity effect influence the component segregation (Kentish et al., 2005, Nikolova et al., 2015a, Vehring et al., 2007).

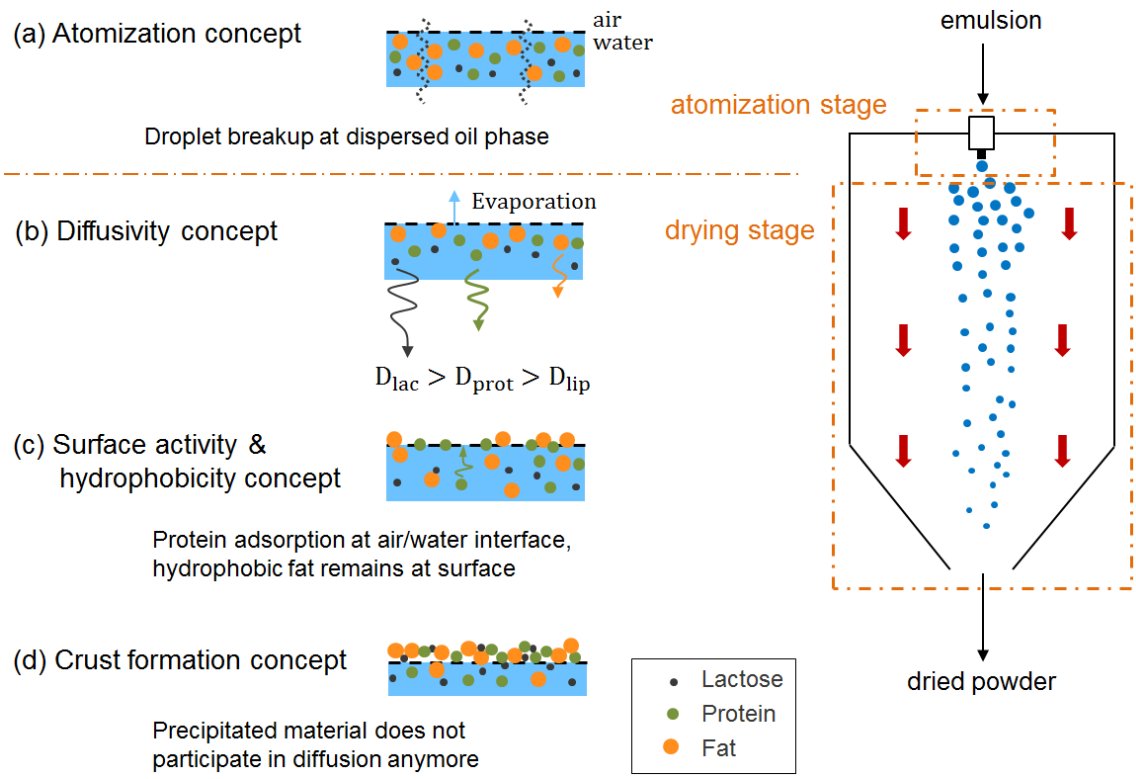

Figure 2.1: Explanations proposed in literature for the component segregation in drying milk droplets: Schematics of (a) atomization concept, (b) diffusivity concept, (c) protein surface activity and fat hydrophobicity concept, (d) crust formation concept.

2.2.4.2 Protein Surface Activity and Fat Hydrophobicity

Furthermore, the surface composition of milk powder might be influenced by the components' interaction with the air/water interface (Figure 2.1c). Milk protein's surface activity, i.e. its tendency to adsorb at an interface between air and water in an orientated configuration under a reduction of the surface tension of the liquid phase and a reduction of the entropy of the system, has mostly been used as explanation of the protein surface overrepresentation observed in several studies. Milk proteins and particu-

larly casein, due to its relatively flexible molecule structure, feature a high degree of surface activity as a result of their amphiphilic nature (Leman et al., 1989). Thus, their adsorption at the air/water interface has been widely reported, with the movement to the interface being primarily controlled by diffusion, although other factors such as convection as a result of temperature and pressure gradients can also have an influence (Graham and Phillips, 1979, Landström et al., 1999). Fäldt and Bergenståhl observed a migration of milk protein to the surface of drying emulsion droplets consisting of soybean oil, lactose and either whey protein or sodium caseinate and explained this by the protein's surface activity (Fäldt and Bergenståhl, 1995, Fäldt and Bergenståhl, 1996a). This concept has been adopted in other studies (Adhikari et al., 2009, Gaiani et al., 2006). Additionally, as the adsorbed protein is bound to the air/water interface, this impacts the gradient in protein concentration inside the droplet and counteracts any concentration driven diffusion processes away from the surface (compare to Section 2.2.4.1). Similarly, the hydrophobic nature of milk fat might attenuate diffusion away from the droplet surface towards the inside of the droplet for fat globules that have already accumulated at the air/water interface (Fu et al., 2011a). Further, it has even been suggested that the hydrophobicity causes fat globules to migrate from the droplet center towards the surface (Kelly et al., 2015).

2.2.4.3 Crust Formation Concept

It has additionally been proposed that the final particle surface composition might be subject to the crust formation and the solubility of the dissolved protein and lactose solutes (Figure 2.1d), as first discussed by Charlesworth and Marshall (1960) and later adopted by others on dairy droplets (Kim et al., 2009b, Wang and Langrish, 2009). These reports argued that the precipitated solutes, once part of the solidified crust, do not participate in the diffusion process anymore. Assuming a decreasing water concentration from the droplet center to the surface due to evaporation, saturation concentrations and consequent precipitation are first reached near the droplet surface. A lower solubility of one component could thus lead to enrichment near the surface in comparison to the other components.

Further, it has been suggested that upon advanced solidification of the dying droplet the fat phase might move through the crust's network of cracks and pores as driven by overpressure imposed by internal vacuoles and capillary forces (Nijdam and Langrish, 2005). As a result of mechanical stress during drying or atomization, the fat globule membranes might become ruptured to some extent and the lipid phase could hence spread freely inside the drying particle and on its surface at the elevated temperatures of the spray drying process, thus forming a consistent fat surface film (Xu et al., 2013).

2.2.4.4 Atomization Concept

As Table 2.2 and Table 2.3 illustrate, the component segregation in drying milk droplets has primarily been presumed to take place during the drying stage of the spray drying process, with different combinations of the three concepts described above being most often presented as potential driving forces. However, a smaller number of reports have considered the possibility that an atomization induced seg-

regation mechanism might take place prior to the drying stage (Figure 2.1a). In a study by Fyfe et al. (2011), a pilot-scale spray dryer resulted in a considerably greater fat overrepresentation on skim milk particles' surfaces in comparison to the same powders produced with a laboratory-scale spray dryer, despite both instruments employing the same atomizer type and drying air temperature profile. It was speculated whether this observation can be ascribed to an influence of the different pressure and shear levels during atomization on the disintegration process of the feed emulsion film. Xu et al. (2013) investigated powders that were produced with a bench-top spray dryer from emulsions consisting of sunflower oil, maltodextrin and whey protein. An increasing fat content on the particle surface with larger fat globule size of the emulsions after homogenization was found. This was explained by liquid fat leakage and consequent spreading of a thin fat film at the particle surface caused by rupture of the fat globule membranes, which become less stable with larger globule sizes. The rupture was supposed to take place either during atomization as a result of shearing or during the drying stage as a result of differential stress on the membranes as they shrink at constant fat globule volume.

Kim et al. (2009b) reported respective surface fat contents of more than 90 % and 18 % on whole milk and skim milk particles that had been dried at a drying air inlet temperature of 205 °C. Because of the intense heat exposure and the consequent fast solidification and immobilization of the components during the drying stage, it was concluded that the surface fat must have already been formed, at least in part, during the preceding atomization stage. Kim et al. (2009b) proposed that the atomization induced fat accumulation on freshly generated milk droplets might originate from the impact of the dispersed fat phase on the disintegration behavior of the emulsion feed. A perforation mechanism was provided as explanation where the milk emulsions preferably disintegrate along the fat globules, causing the fat globules to cover the surface as soon as individual droplets have been formed. This hypothesis was based on earlier photographic investigations of the break-up behavior of emulsions as a function of oil content (Dombrowski and Fraser, 1954, Zakarlan and King, 1982).

As it is difficult to draw reliable conclusions about the impact of the atomization step from the powder characteristics after completed spray drying, Wu et al. (2014) compared the surface composition of atomized skim milk droplets immediately after atomization, as obtained by cryogenic flash freezing, with the one of the corresponding spray-dried particles. Surface fat was observed on the particles and their work showed that this was caused by the atomization stage. After atomization the milk droplets featured surface fat contents of 28.6-34.0 % fat for feed emulsions of 0.7 % fat (dry matter basis), and the surface fat remained or even slightly increased throughout the following drying stage (37.7-38.8 % after completed spray drying).

2.2.5 Relevant Mathematical Modeling Approaches

Mathematical simulation of the component distribution in drying milk droplets promises further insight into the segregation mechanism and a useful tool for the theoretical prediction of powder properties at

certain drying conditions. A number of modeling approaches on the convective drying of droplets are available in literature, such as models that incorporate the concept of the characteristic drying curve (Harvie et al., 2002, Keey, 1991, Langrish and Kockel, 2001, Tran et al., 2016) or the lumped reaction engineering approach (REA) (Chen and Putranto, 2013, Lin and Chen, 2005). The former approach divides the drying process into a perfect shrinkage stage (shrinkage proportional to volume reduction as governed by a constant evaporation rate) and a second stage defined by a falling evaporation rate, whereas the latter approach utilizes empirical correlations between the overall droplet moisture content and the water vapor pressure at the surface as well as the droplet diameter. Although in their simplest form these approaches only incorporate a global mass balance without computation of concentration gradients, some basic models allowing spatiotemporal resolution of one or more species concentrations emerged from these in the 1970s and 1980s and were further refined in recent times. The majority of models discussed in the following chapters was developed for description of food material droplets during spray drying and was validated against the drying kinetics obtained from single droplet drying experiments. Their accuracy is usually limited by the difficulty of finding reliable formulations for the influence of the forming crust on the droplet shrinkage rate, on the effective diffusivities of water and the components due to a rising viscosity and mass transport resistance of the solidified material, and on the partial vapor pressure at the surface and thus on the evaporation rate (Kentish et al., 2005).

2.2.5.1 Approaches with a Spatiotemporal Water Mass Balance

The earliest spatiotemporal approaches modeled water concentration profiles in drying skim milk droplets (Cheong et al., 1986, Ferrari et al., 1989, Sano and Keey, 1982, Wijlhuizen et al., 1979). An evaporation term was set as outer boundary condition and Fick’s second law of diffusion was incorporated along the droplet radius for the water mass balance. The challenge to describe the effective diffusivity and evaporation rate more accurately was addressed in ensuing models. A work by Seydel et al. (2004) described the formation of hollow salt particles by simulating the radius-dependent change in particle density. The model was unique in its attempt to account for component precipitation by means of a population balance that was solved independently from the mass and energy balances. Handscomb et al. (2009) formulated a model that aimed to predict shrinkage and shell thickening rates by balancing capillary contraction forces with the structural strength. The complexity of the crust properties and their effect on evaporation and shrinkage was further highlighted in a study by Vehring et al. (2007) on the drying of a protein-in-water droplet. Using the Peclet number, the model predicted the drying time until commencement of precipitation to stop the simulation at that point, because from then on a sufficient accuracy in simulating the declining evaporation rate was considered to be not feasible. Particularly, the effective diffusion coefficient of moisture through a solidified porous crust medium is difficult to predict with reasonable precision from theoretical equations (Perré, 2015).

2.2.5.2 Approaches with Spatiotemporal Binary Mass Balances

Adhikari and co-workers have been pioneering the simulation of binary component migration in drying droplets to work towards the prediction of the surface composition (compare to Table 2.4), presenting a model on fruit juice samples (Adhikari et al., 2003, Adhikari et al., 2004, Adhikari et al., 2007). Lumping together the juice components into one averaged component, a pseudo-binary system was formulated. The model was based on a discretization of the spatial coordinate, which was divided into equally long increments. Each of the increments represented a spherical disk with homogeneous composition under radial symmetry assumption. Diffusive fluxes were calculated from the differences in concentration and length between the centers of adjacent disks according Fick's first law of diffusion. The increasing evaporation resistance was incorporated *via* estimation of the moisture-dependent water activity in the surface disk and perfect shrinkage was assumed. The differential equations were solved with the method of lines (Iserles, 2009). After the simulated drying kinetics had been compared with suspended single droplet drying experiments for validation, the model was applied on spray drying conditions to predict the particle stickiness from the glass transition temperature.

Table 2.4: Modelling approaches that can be applied for prediction of the surface composition of binary or multicomponent droplets during drying: overview of included segregation mechanisms, consideration of the influence of solidification and experimental validation.

Components	Incorporated segregation concepts					Influence of crust formation on			Validation	Author
	Diffusivity	Surface activity	Hydrophobicity	Precipitation	Atomization	Diffusivity	Evaporation	Shrinkage		
Lumped fruit juice solids	n/a	n/a	n/a	no	no	no	yes	no	Drying rate and temperature during SDD	(Adhikari et al., 2007)
Mannitol	n/a	n/a	n/a	yes*	no	yes*	yes*	yes*	Drying rate and temperature of pure water during SDD	(Gopireddy and Gutheil, 2013)
Lactose, caseinate	yes	yes	n/a	yes	no	no	yes	no	Surface composition after SD and drying rate during SDD	(Wang et al., 2013)
Sucrose, caseinate	yes	yes	n/a	yes	no	yes	yes	no	Experiments used to fit simulation parameters	(Meerdink and van't Riet, 1995)
Sucrose, whey protein	yes	yes	n/a	no	no	no	no	no	-	(Porowska et al., 2015)
Lactose, milk protein, fat	yes	no	no	no	no	yes	no	no	Surface composition after SD	(Chen et al., 2011)
Lactose, milk protein, fat	yes	yes	no	no	yes	yes	yes	yes	Surface composition during SDD	Chapter 6.6

* only early drying stages, SDD = single droplet drying, SD = spray drying

Gopireddy and Gutheil (2013) utilized a description of the diffusion resistance imposed by the solid surface layer and water activity correlations to account for the retardation caused by solidification. Solving a set of differential diffusion and energy equations with a finite difference approach, in this way the concentration profiles of mannitol or polymer solutions during the early stages of single droplet drying were simulated.

2.2.5.3 Approaches with Spatiotemporal Multicomponent Mass Balances

To date, only a few models can be found in literature that allow theoretical prediction of the concentration profiles of more than one component (see Table 2.4). A computation of the component distribution requires a spatiotemporal resolution of the mass balances, either as a set of simple ordinary differential equations by spatial discretization or as a set of partial differential equations. A global energy balance is typically sufficient under the assumption of a uniform temperature profile. This has been validated by dimensionless analysis (Biot numbers well below unity) for spray drying applications and even for significantly larger droplets in single droplet drying configurations (Chen and Peng, 2005, Patel et al., 2005). Further, radial symmetry is generally assumed.

A spatiotemporal multicomponent model by Wang and co-workers was applied to resemble the spray drying process of an aqueous lactose/caseinate solution by variation of the Reynolds number and drying air temperature over time (Wang and Langrish, 2009, Wang et al., 2013). Spatial discretization of the droplet radius comparable to the above described work by Adhikari and co-workers, under the assumption of perfect shrinkage, allowed a simple incorporation of precipitation by comparison between the saturation concentration of each component and the calculated concentration in each disk at each time step. Also the protein surface activity was incorporated into the mass balance of the surface disk. Therefore, the model stands out in respect to its applicability on the component segregation during convective drying of milk droplets. The component diffusivities were expressed as temperature dependent functions, but lacked an influence of the water concentration. The water evaporation rate was governed by an additional term in the water mass balance of the surface disk as a function of local water activity, which was estimated from the components' individual moisture-dependent water activity correlations. As available isotherms describing how the presence of solids affect the water activity have been either generated from liquid phase or fully formed solids, however, using either one to describe the entire drying process may not provide a precise description of the evaporation rate. The model was validated *via* comparison of the simulated surface composition with particles obtained from spray drying experiments. A surface overrepresentation of protein, which was decreasing with higher drying temperature, was predicted. From a sensitivity study it was concluded that the difference in component diffusivities and the protein surface activity were the major driving forces for component segregation, while the components' solubility imposed a subordinate influence.

Three other models were less comprehensive, but nevertheless interesting in their unique approach. Meerdink and van't Riet (1995) described the component segregation during drying of small sucrose/sodium caseinate solution slabs. The model contained Maxwell-Stefan partial differential equations with concentration dependent diffusion coefficients. Since measuring and approximation tools for Maxwell-Stefan multicomponent diffusion coefficients in concentrated aqueous solutions are lacking, the parameters of the diffusivity equations had to be fitted so that the simulated concentration profiles agreed with the experimental results. In the modeling work by Porowska et al. (2015) on drying whey protein/sucrose droplets, the phenomena taking place during crust formation were largely disregarded. The focus was laid on the surface activity of the whey protein and it was supposed that the adsorption process would halt upon commencing shell formation. The protein surface activity was described with the aid of experimental determination of the dynamic surface tension as a function of protein bulk content and time. Also noteworthy, despite not being a spatially resolved model, Chen and co-workers presented an analytical continuum approach to simulate the solid formation in the outermost layer of a drying water droplet with dissolved lactose, fat and milk protein (Chen et al., 2011, Chen et al., 2013, Xiao and Chen, 2014). Under the assumption that the concentration only changes in a thin surface region, an explicit equation for the surface composition was obtained. Protein surface activity was not covered by this model. The Stokes-Einstein equation was introduced in an extended form to account for the concentration dependency of the effective component diffusivities.

In Chapter 6.6 of the present work, the same modified Stokes-Einstein equation will be utilized for a new modeling approach on a drying low-fat milk droplet. For comparison with the previously discussed models, this approach is also included in Table 2.4 and will be described briefly at this point. The model accounted for the protein’s surface activity as a boundary condition. Spatiotemporal balances for energy, momentum and mass of water, lactose, protein and fat formed a set of partial differential equations that was solved with the method of lines. A realistic description of the influence of solidification on the water diffusivity, evaporation rate and particle shrinkage was aspired by incorporation of semi-empirical drying and shrinkage kinetics, which were obtained from suspended single droplet drying experiments and expressed *via* the reaction engineering approach. As such, the model required some experimental work to obviate the need for a perfect shrinkage assumption and for approximations of the effective water diffusivity. A new single droplet drying technique was employed for result validation, which allowed tracking of the changes in chemical surface composition over time (compare to Chapter 6). Solute precipitation and the influence of the fat’s hydrophobic nature on the component distribution were not implemented.

2.2.6 Concluding Remarks

The surface composition of milk powder imposes a critical influence on its functional properties. It is widely accepted that a strong overrepresentation of fat, in comparison to the bulk composition, emerges

on the surface during spray drying at both industrial and laboratory scale with detrimental impact on the powder quality. However, the surface formation process is far from being thoroughly understood. Four different processes might potentially affect the component segregation in drying milk droplets; the components' diffusivities, the components' interaction with the air/water interface (protein's surface activity and the lipid phase's hydrophobicity), the crust formation/precipitation process, and the atomization process. As the degree of influence of each of these mechanisms is still under debate, further experimental work is required to test and validate the different concepts. While the subordinate enrichment of protein is most often perceived to take place during drying due to its lower diffusivity than lactose and primarily due to its surface activity, the atomization stage seems to have a critical impact on the formation of surface fat. Some promising modeling approaches have been published in recent times that are, in principle, capable of simulating the component distribution of drying milk droplets. These should be further developed to account for all of the four potential segregation mechanisms for a better understanding of the surface formation and a more accurate prediction of the powder properties.

2.3 Single Droplet Drying and Microfluidic Jet Spray Drying of Food Materials

2.3.1 Synopsis

Single droplet drying can be a valuable tool to understand the drying characteristics of food droplets with respect to optimization of industrial spray drying processes, because it facilitates the *in situ* monitoring of various droplet properties. For this purpose, the specific single droplet drying technique needs to be evaluated in terms of its comparability with the drying air environment and the droplet features that are expected to exist during spray drying. Single droplet drying can be categorized into four different approaches, each with characteristic advantages and disadvantages in this regard: sessile, suspended, acoustic levitation and free falling single droplet drying.

2.3.2 Introduction

The capability to optimize the design and operation of spray dryers in terms of cost efficiency and product functionality has become more important for many applications in the food industry due to increasing economic pressure and demanding customer requirements. The fine-tuning of the drying conditions in existing spray dryers and the specific design of new processes by numerical simulation require a detailed understanding of the drying behavior of the respective solution, suspension or emulsion to be spray-dried. The effective water and solute diffusion rates, and as such the evaporation rate and droplet temperature, are strongly affected by the complex kinetics of the drying droplet's crust or shell formation as well as by the physical and chemical structure thereof, which are hardly predictable without

empirical data. The lack of sampling points and the size as well as complexity of spray drying instruments does usually not allow tracking the drying characteristics of a material *in situ* at industrial scale. Characteristically, samples can only be taken after spray drying and hence the actual drying process cannot be monitored. In addition, upon atomization the droplets feature a relatively wide distribution in sizes and trajectories. As a result, the drying history and consequent functional characteristics differ to a significant extent amongst the particles (Masters, 1991). Neglecting particle-particle and particle-wall interactions that often occur in spray dryers, the drying process of a material can be observed reproducibly in a simplified environment during convective drying of an individual droplet. In single droplet drying, an isolated droplet is generated and positioned into a conditioned stream of drying air that mimics the environment of the corresponding spray drying process as closely as possible in terms of temperature exposure, drying air flow and humidity. In the course of drying, the changes in parameters, such as droplet temperature, size or mass, are measured over time. There are five general requirements for a single droplet drying system to be suitable for finding a material's drying characteristics for application in spray drying modeling:

1) reproducible generation of droplets with a certain size,
2) fast, stable and low-intrusive positioning of the droplet inside the drying chamber,
3) drying air flow that passes through the drying chamber at a well-defined temperature, moisture content and velocity,
4) measurement techniques of high accuracy and minimal disturbance imposed on the drying droplet,
5) drying conditions with sufficient comparability to spray drying environments.

Single droplet drying was pioneered by Van Krevelen and Hoftijzer (1949) to monitor the mass profiles of drying granulates and by Ranz and Marshall (1952a), who investigated the changes in temperature and size of drying solution droplets. These approaches have been further advanced over the years, and today it can be distinguished between four different single droplet drying techniques by categorizing them according to how the droplets are maintained inside the drying air. Sessile, suspended, levitated and free falling single droplet drying entail different benefits and shortcomings in respect to the five criteria listed above.

2.3.3 Sessile Single Droplet Drying

2.3.3.1 Evaporation of a Sessile Droplet

In sessile single droplet drying, droplets of 0.5-2.5 mm in diameter are usually deposited with a microfluidic syringe on a solid substrate. To restrict the contact area between droplet and substrate and to establish a droplet shape that is as spherical as possible, wetting of the substrate by the typically aqueous droplets is limited by a strong water repellent nature of the substrate's surface. The hydrophobicity is

achieved by coatings consisting of silane (Hampton et al., 2012), modified silica (Manukyan et al., 2013), siloxane (Yu et al., 2012) and polytetrafluoroethylene (Eslamian and Ashgriz, 2007), amongst others (Figure 2.2a). In addition, the repulsion is often further enhanced by certain topographies attained by lithographic patterning of micro-pillars into the hydrophobic substrate (Choi and Kim, 2009, McHale et al., 2005, Sadek et al., 2013, Xu and Choi, 2012) (Figure 2.2b). Though low wettability had been reached in these studies, the droplets still differed substantially from perfect sphericity (initial contact angles of 100-160 °).

Except of the work described in Section 2.3.3.2, sessile single droplet drying has so far mostly been limited to drying at room temperature with drying times of 10-30 min. The evolution of the droplet geometry and dimensions was analyzed by cameras and from that data the evaporation rates were derived. While this did not allow for the drying kinetics to be recorded as accurately as it is possible *via* levitation or suspended single droplet drying, the strength of sessile singe droplet drying lies in its capability to be coupled with various complex and sensitive *in situ* analysis techniques. This includes the visualization of internal flows with spectral radar optical coherence tomography and confocal microscopy (Manukyan et al., 2013), monitoring of the structural evolution with X-ray scattering measurement (Chen et al., 2012), tracking the solute precipitation behavior with a digital high-speed camera (Eslamian and Ashgriz, 2007) and observation of the internal solidification with confocal microscopy (Sadek et al., 2013, Sadek et al., 2016).

In the latter studies, Sadek and co-workers also demonstrated an analysis of the drying rate with improved accuracy by connecting the substrate with a micro-balance the investigation of casein and whey protein solution droplets. Furthermore, in these studies a pendant droplet configuration, resembling suspended single droplet drying, was adopted to avoid a collapse of the shell and to maintain a relatively spherical droplet shape (Figure 2.2c), because shell collapse under pressure and gravity during water evaporation is a common problem in sessile single droplet drying (Chen et al., 2012). Applying such a pendant configuration, Sadek et al. (2014a) observed a good agreement in the obtained morphologies of whey protein / micellar casein particles compared to particles produced at much shorter drying times during free falling single droplet drying. While all of the hitherto summarized studies featured controlled ambient air conditions, they did not include a conditioned flow of drying air, as they were directed towards application in microfluidic devices, coating processes and nanotechnology.

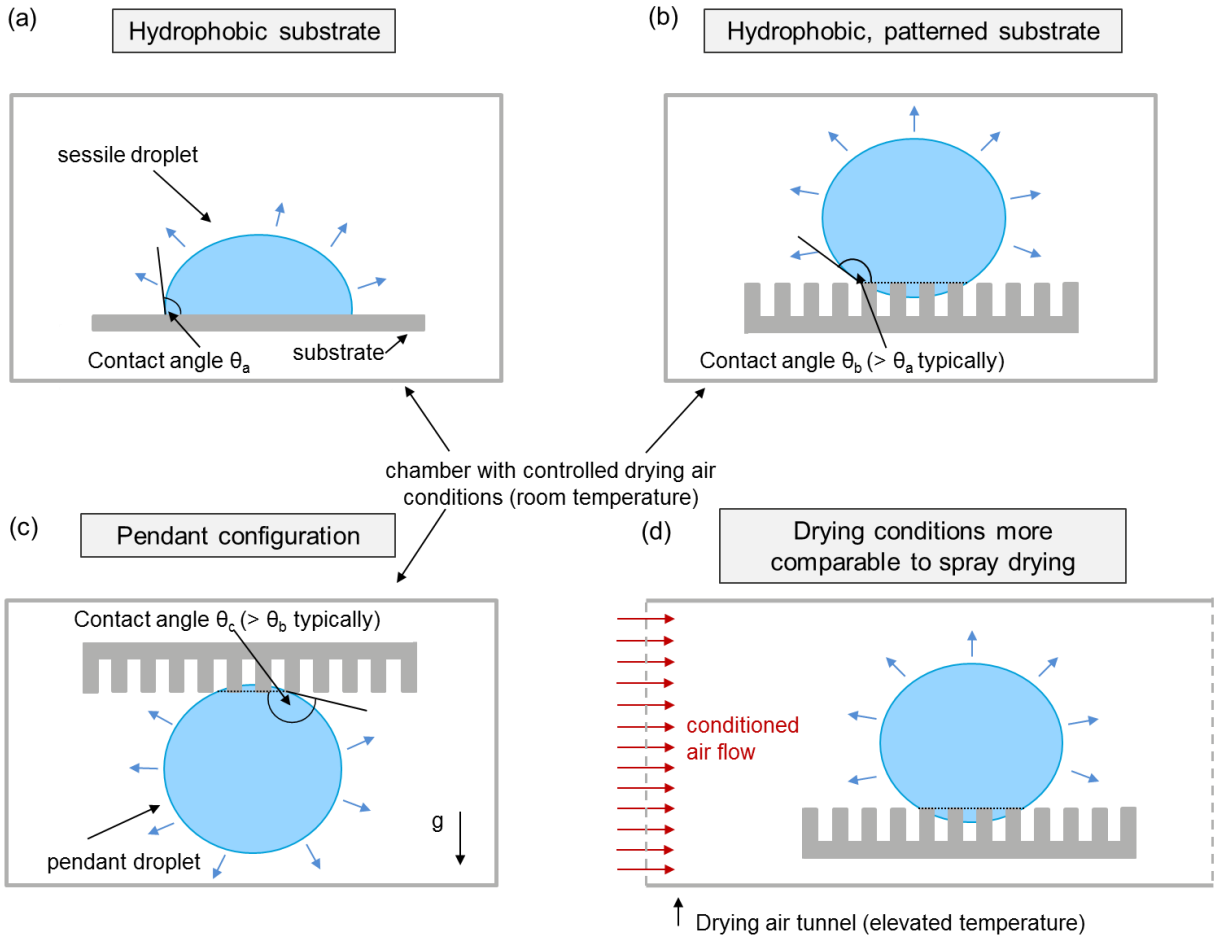

Figure 2.2: Schematic of sessile single droplet drying: (a) sessile droplet on a hydrophobic substrate, (b) sessile droplet on a superhydrophobic substrate, (c) droplet on a superhydrophobic substrate in pendant configuration, and (d) experimental design according to Perdana et al. (2011).

2.3.3.2 Applicability for Spray Drying Studies

Perdana and co-workers demonstrated that sessile single droplet drying can also be conducted at elevated temperatures to establish drying environments that are more related to the conditions in a spray dryer (Perdana et al., 2011, Perdana et al., 2013). The experimental design included a drying air flow through a tunnel with a temperature of 80-100 °C and a velocity of 0.2 m/s (Figure 2.2d). A thin substrate (polypropylene membrane of 0.15 mm thickness on a 1 mm steel plate) was utilized to limit the disturbance of the air flow. Relatively small droplets of 0.5-1.4 mm in diameter were generated and deposited with a pneumatic micro-dispenser. The inactivation of β-galactosidase during drying in a maltodextrin matrix was studied and this information was used for prediction of the residual enzyme activity after laboratory-scale spray drying, which was achieved with reasonable precision. It was highlighted that droplet drying in the sessile configuration could have an advantage over other techniques when conducting high-throughput experimentation where multiple droplets are dried simultaneously.

The utilization of sessile single droplet drying as a model system for spray drying processes is, however, compromised by the presence of the substrate and its contact to the droplet. The droplet shape differs more or less strongly from sphericity with contact angles well below 180 °. Also, the substrate reduces the evaporation rate, impacts the heat and mass transfer and disturbs the flow pattern of the drying air around the droplet (Erbil, 2012, Picknett and Bexon, 1977). All this complicates mathematical modeling of the drying process and makes this approach less suitable for quantitative evaluation of the drying kinetics (Xu and Choi, 2012). This is a particular challenge because the contact angle is decreasing more and more with proceeding drying, and droplets might even collapse into the micro-structure of the patterned support material. Further, it needs to be considered that the contact angle can influence the resulting particle morphology (Sadek et al., 2013). While the above described approaches to couple sessile single droplet drying with various *in situ* imaging techniques are highly interesting for application in spray drying studies, the complex influence of the substrate on the drying process still needs to be better understood.

2.3.4 Suspended Single Droplet Drying

2.3.4.1 Basic Experimental Design and Morphology Studies

In suspended singe droplet drying, also known as filament single droplet drying, it is endeavored to mimic a free droplet more closely than realized by deposition on a substrate. A smaller contact area than in sessile droplet drying is reached by droplet suspension at the tip of a vertical, thin filament. The filament is typically made of glass, its tip is 50-300 µm in diameter and the contact area to the droplet is ideally reduced to a minimum, while still sustaining a static positioning of the droplet inside the drying air stream. The tip of the filament is usually coated with a special layer that repels the solvent of the suspended droplet to prevent it from wetting or climbing up the tip. The flow of the conditioned drying air is guided by a surrounding drying chamber, through which the drying air passes from below with a flat velocity profile across the opening and exits at the top. Ranz and Marshall pioneered the suspended single droplet drying technique and analyzed the droplet temperature and diameter change of various liquids, pure and with suspended or dissolved particles (Ranz and Marshall, 1952a, Ranz and Marshall, 1952b). As characteristic for suspended single droplet drying, the investigated flow regimes and drying air condition were representative for spray drying with Reynold numbers of 0-200 and air temperatures of 85-220 °C, whereas at initial droplet diameters in the range of 0.6 to 1.1 mm the droplets were approximately one order of magnitude larger than what is typically encountered in spray dryers. This relatively simple setup has been employed in a number of studies to understand how the drying air properties, such as velocity and temperature, and the initial solid content affect the physical structure of the particle morphology in order to apply this information on the fine-tuning of spray drying processes. The investigated materials included skim milk, yoghurt, coffee extract, carbohydrate and salt solutions, and the initial droplet sizes ranged between 0.5 to 3 mm in diameter (Charlesworth and Marshall, 1960,

El-Sayed et al., 1990, Fu et al., 2012a, Lin and Gentry, 2003, Sunkel and King, 1993). In such studies, at least one of the drying chamber walls is usually transparent to allow a camera to record the visual changes that are being undergone by the droplet in the course of drying. If required, analyses such as scanning electron microscopy (SEM), X-ray diffraction and solubility measurements are conducted subsequent to drying. Comparison with spray-dried food powders demonstrated a strong similarity between the morphology of industrially produced particles and the single droplet dried particles (Walton, 2000). Beyond phenomenological observation of the particle morphology formation, the design of suspended single droplet drying rigs has been elaborated over time for either continuous online tracking of the drying kinetics or for surface analysis after discrete drying times.

2.3.4.2 Study of Drying Kinetics

For observation of the drying kinetics, the changes in droplet mass with proceeding drying are recorded in order to obtain accurate information about the evaporation rate. For this purpose, the supporting filament is either connected to a micro-balance, as first introduced by Van Krevelen and Hoftijzer (1949), or it is substituted by the arm of a cantilever beam balance (Fu et al., 2011b, Sano and Keey, 1982). In either case the lifting force of the drying air flow must be factored in (Cheong et al., 1986, Lin and Chen, 2002). Also the droplet temperature profiles are typically required, which are monitored by additionally immersing a thermocouple junction into the droplet center or by using a thermocouple as suspension filament. In combination with the shrinkage rate obtained from camera recording, the mass and temperature profiles provide the fundamental kinetics data required for describing the droplet drying process of a given material (Figure 2.3a). Therefore, this approach has been employed in many drying kinetics studies, including food materials, such as solutions of simple sugars and high molecular weight carbohydrates, citric acid solution, slurries, skim and whole milk (Adhikari et al., 2003, Cheong et al., 1986, Fu et al., 2012b, Furuta et al., 1983, Nešić and Vodnik, 1991, Sano and Keey, 1982). The empirical data can be processed by means of shrinkage and evaporation resistance correlations as a function of droplet moisture content, for instance using the Reaction Engineering Approach, to describe the impact of the forming crust on the drying kinetics of food materials and apply these correlations in dryer wide continuous fluid dynamics modeling (Jin and Chen, 2009, Woo, 2016) and numerical droplet simulation models (Mezhericher et al., 2007, Wang et al., 2013).

2.3.4.3 Study of Surface Formation

Furthermore, suspended single droplet drying experiments are sometimes discontinued to monitor the formation of the functional surface properties and of the chemical surface composition with proceeding drying (Figure 2.3b). The drying process is halted by preventing the drying air from entering the chamber before the semi-dried droplets can be studied. After stopping the drying process at discrete drying times in separate drying runs, quantitative analysis has been realized by means of dissolution studies, where the wetting and dissolution behavior was recorded with a camera after attaching a solvent droplet

(Chew et al., 2015, Fu et al., 2011a). Qualitatively, the surface composition of drying milk droplets can be analyzed by flash freezing *via* immersion of the droplets in liquid nitrogen (LN_2). The particles are freeze-dried and undergo spectroscopic investigation of their chemical surface composition.[1]

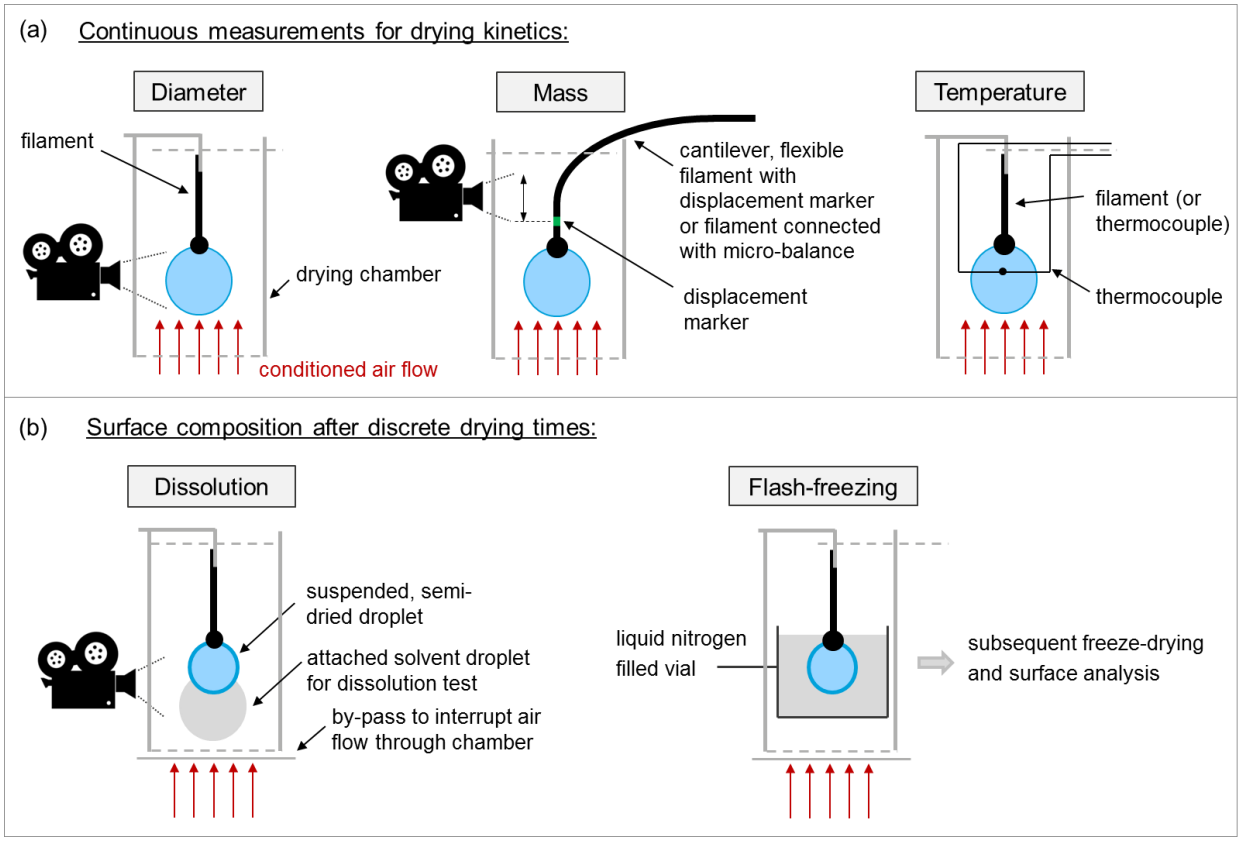

Figure 2.3: Schematic of suspended single droplet drying: (a) continuous droplet diameter, mass and temperature analysis for determination of drying and shrinkage kinetics, and (b) interruption of drying process for qualitative and quantitative investigation of surface composition at certain drying times.

2.3.4.4 Limitations in Comparability with Spray Drying Conditions

Suspended single droplet drying is of intrusive nature due to the contact between the droplet and the filament. However, for a droplet of 1.6 mm in diameter, it has been calculated that the penetration of the supportive filament only contributed to 0.2% of the total droplet volume and the heat transfer through the glass filament accounted for less than 1% of the overall heat input (Charlesworth and Marshall, 1960, Lin and Chen, 2002). Other disadvantages are that the suspension prevents the droplets from rotating freely as they would during spray drying and the contact with the filament tip in combination with the relatively large droplet sizes can lead to the development of an oval instead of a spherical particle shape (Walton, 2004).

Commonly, droplet diameters that are approximately an order of magnitude larger than in spray drying are employed. Diameters below 0.5 mm are not feasible, because the heat conduction along the supporting filament can become significant and the changes in mass or diameter become difficult to measure

[1] This method has been developed as part of the present thesis, see Chapter 6.

with sufficient accuracy. Also, a reproducible droplet generation and the subsequent transfer to the filament without appreciable evaporation prior to drying are limited to larger droplet sizes. Yet, the larger droplet sizes lead to substantially greater drying time scales than observed in spray drying (minutes instead of seconds or milliseconds), which can limit the applicability of the single droplet drying data on spray drying models. At least for sugar solutions and milk emulsions it has been found that in the investigated droplet size range (initial volumes of 1-3 µl) the droplets featured similar shrinkage and drying correlations independent of the droplet size when described by the normalized diameter and the normalized activation energy of evaporation curves of the Reaction Engineering Approach as a function of moisture content (Fu et al., 2011b, Lin and Chen, 2004).

2.3.5 Acoustic Levitation Single Droplet Drying

2.3.5.1 Experimental Design and Observation of Droplet Shrinkage, Temperature and Morphology

In contrast to the previous two techniques, the third single droplet drying method relies on levitation of an individual droplet without solid contact. Tsapis et al. (2005) and Sugiyama et al. (2006) have achieved the levitation by means of a concave hot plate, utilizing the Leidenfrost phenomenon. This approach, however, does not facilitate a drying air environment in the vicinity of the droplet that would feature a flow field and a temperature distribution comparable to spray drying conditions. Another levitation technique is hence more commonly applied, in which an acoustic field supports the droplet (Figure 2.4a). The acoustic, also known as ultrasonic, levitation single droplet drying method employs a piezoelectric transducer and a reflector in vertical arrangement to position a droplet in one of the pressure nodes of the generated standing ultrasound wave (Brenn et al., 1997). The droplets are injected by means of a micro-volumetric syringe into the levitator housing tube, which is ventilated by a conditioned drying air flow. Yarin and co-workers developed the fundamental understanding required for interpreting the drying process of acoustically levitated droplets and validated it experimentally (Yarin et al., 1998, Yarin et al., 1999). Theory was provided about the acoustic boundary layer and acoustic streaming in vicinity of the droplet, which allows derivation of the average Sherwood and Nusselt numbers over the droplet surface. Also the droplet deformation by the acoustic radiation pressure needs to be accounted for, which can be calculated by the boundary element method. It was further shown that Reynold numbers comparable to spray drying conditions can be realized (Schiffter and Lee, 2007a, Yarin et al., 1997).

The vertical position and cross-sectional area of the drying droplet are usually monitored with a camera, and the droplet temperature can be determined *via* infrared thermography. Wulsten and Lee (2008) reported that the droplet temperature is influenced by the acoustic field and cannot be predicted well by acoustic levitation theory. Due to the temperature sensitivity of the transducer, the drying air temperature is somewhat limited, though temperatures of up to 150 °C have been reached through special design

considerations (Mondragon et al., 2011). Levitation single droplet drying has not been as extensively utilized as suspended single droplet drying, particularly in respect to food materials, being primarily limited to pure liquids or relatively simple suspensions of glass beads or silica, for instance. At least, Schiffter and Lee (2007b) found good agreement between the final morphology of mannitol particles after single droplet drying and spray drying. Also, a mathematical model was compared with experimentally obtained shrinkage data of levitating maltodextrin and trehalose droplets by Sloth et al. (2006).

2.3.5.2 Estimation of Evaporation Rates

Accurate determination of the evaporation rate poses a challenge to kinetics studies by acoustic levitation single droplet drying. This technique does not allow for a direct measurement of the changes in droplet mass. Instead, the evaporation rate as a function of moisture content is estimated from droplet size and position data. Kastner et al. (2001) divided the drying process into two stages. The first drying stage was characterized by the occurrence of a significant change in droplet volume and the evaporation rates were estimated using the decreasing droplet diameter. The evaporation rates during the second drying stage, where the volume reduction became minimal, were estimated from the upward motion of the droplet in the acoustic field. This approach was adapted by others, such as Schiffter and Lee (2007b) and Mondragón et al. (2013), with the latter study processing the kinetics data *via* the Reaction Engineering Approach. Groenewold et al. (2002) introduced a hygrometric measurement of the increase in moisture content between the inlet and outlet air to realize a more reliable and universal observation technique of the changes in droplet water content.

2.3.5.3 Comparison with Suspended Single Droplet Drying

An advantage of the acoustic levitation technique over suspended single droplet drying is that it allows for investigation of slightly smaller droplet volumes, because there is no mechanical contact that might disturb the heat and mass transfer. Although most studies were conducted at a range of 1-2 mm in initial droplet diameter, which is also typical for suspended single droplet drying, sizes of 0.5-1 mm have frequently been reported, too (Schiffter and Lee, 2007a, Sloth et al., 2006, Mondragon et al., 2011, Yarin et al., 1999). Yet, interaction between the relatively strong acoustic fields and the levitated droplet occurs at any droplet size, and primary and secondary acoustic streaming alters the heat and mass transfer in comparison to the drying kinetics of an unaffected boundary layer between drying air and droplet (Groenewold et al., 2002, Yarin et al., 1999). Further, the estimation of the drying rate entails a number of uncertainties, such as the requirement of very accurate hygroscopic measurements or a theoretical division of the drying process into two stages with the assumption of perfect shrinkage during the first stage and the assumption of a change in vertical position that only depends on mass loss owing to evaporation during the second stage. As such, for the prediction of drying kinetics under spray drying conditions of more complex systems, such as food solutions and emulsions, suspended single droplet drying might promise more reliable drying data and less complex post-processing.

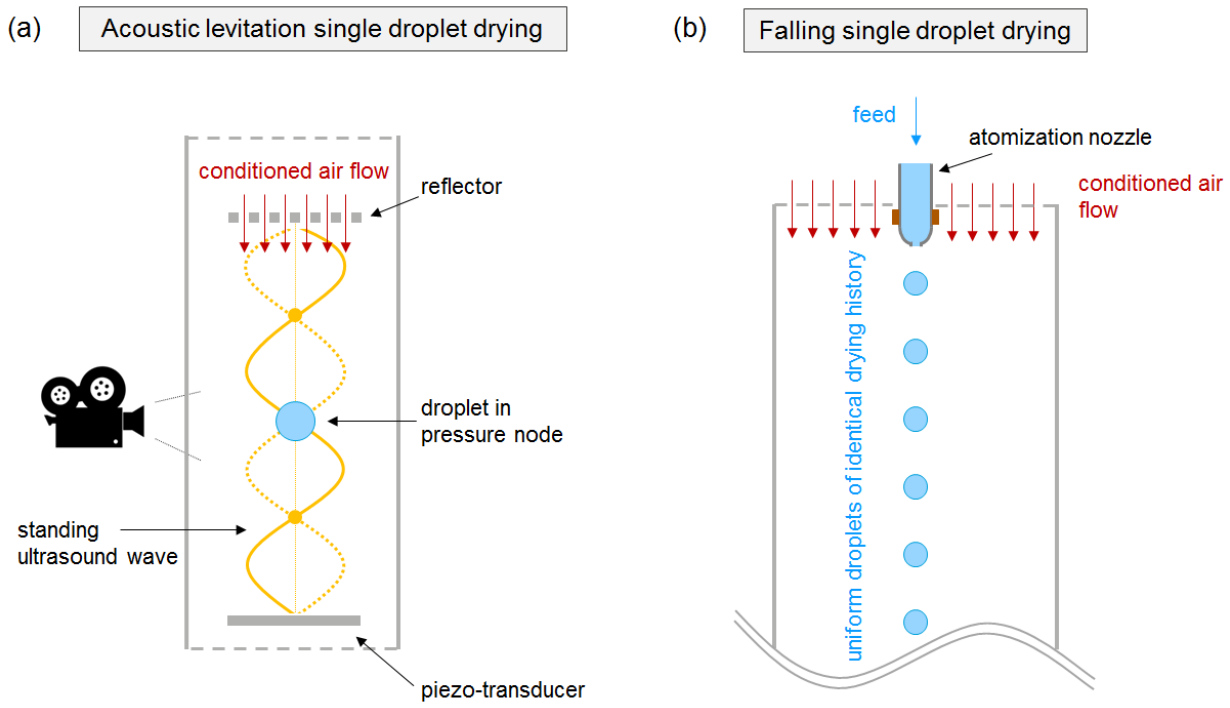

Figure 2.4: Schematic of (a) acoustic levitation single droplet drying, and (b) free falling single droplet drying.

2.3.6 Free Falling Single Droplet Drying

2.3.6.1 Experimental Design

In contrast to the other single droplet drying approaches, free falling single droplet drying is an entirely non-invasive method of exposing the droplet to the drying air, as the droplet is not supported by any means and can interact freely with the drying air without disturbance caused by the positioning technique (Figure 2.4b). At the top of a vertical drying tunnel either an individual droplet is generated with a micro-volumetric syringe or a series of separated droplets with uniform size is generated by means of a microfluidic atomizer (with the latter case being at the interface between single droplet drying and spray drying due to possible droplet-droplet interaction, see Section 2.3.6.3). The micro-sized droplets dry along a well-defined trajectory in the course of their fall through a concurrent drying air stream inside the tunnel. In contrast to conventional spray drying, the droplets are of uniform size and experience identical drying histories, allowing a reliable correlation between the drying or feed conditions and the resulting particle characteristics. The advantage of free falling single droplet drying over other single droplet drying techniques is that the drying conditions of industrial spray dryers are replicated more realistically (Sadek et al., 2014b). The attainable range of droplet sizes and Reynold numbers as well as the drying air temperature profiles are comparable to industrial spray drying environments. This was first demonstrated by Kinzer and Gunn (1951) for pure water droplets of 10-1000 µm in diameter that fell from a pipette down through a hot air tunnel. The evaporation rate was derived mathematically from

measurements of the decrease in velocity as a function of falling time. The droplet velocity at different tunnel heights was determined by flash photography and electrical induction.

2.3.6.2 Limitations in *In Situ* Observation

While for pure liquid droplets the mass and diameter profiles as well as the wet bulb temperature could be calculated from the rate of fall over tunnel height, a meaningful analysis of the drying behavior of free falling droplets becomes more complex for food systems containing colloidal or dissolved solid matter. Due to the droplet movement relative to the drying chamber, a continuous online observation of the droplet characteristics is not feasible. For example, a study by Alexander and Judson King (1985) on free falling food droplets (skim milk, coffee extract, lactose and maltodextrin solutions) was limited to analysis of the morphology and size of the particles at the end of completed drying after a fall distance of 2.71 m. In another study, more information was attained by the addition of eight sampling ports along the dryer column that facilitated a determination of the droplet moisture content after various falling times by droplet collection in dimethyl sulfoxide solvent and subsequent analysis with a combination of titration and high performance liquid chromatography or gravimetric measurement (El-Sayed et al., 1990). Wu et al. (2014) managed to conduct a comparison of the surface composition between mono-dispersed droplets immediately after atomization and the respective particles after completed drying by flash freezing of the atomized droplets in liquid nitrogen and subsequent freeze drying, as first done by Rogers et al. (2008). Vehring (2008) measured the droplet size at discrete locations along the drying tunnel by elastic laser light scattering. However, a continuous observation of the evaporation rate and a tracking of the changes in droplet temperature and diameter have not been achieved in free falling single droplet drying.

2.3.6.3 Droplet Generation and Microfluidic Jet Spray Drying

A matter of particular importance in free falling single droplet drying is the employment of a suitable atomization method for generation of monodisperse droplets that leave the atomizer on a well-defined trajectory and in sufficient distance from each other to ensure identical drying histories and to avoid droplet-droplet interaction. When a series of droplets is to be studied, microfluidic nozzles that are based on jet disturbance at high frequency have emerged as the prevailing method of choice. The functional principle has been adapted from inkjet printer technology and is based either on cone formation under the stress of an external electrical field, on periodic liquid vaporization due to heat pulses, or on pulsed mechanical energy (Le, 1998, Liu et al., 2015). For studies on spray drying of food solutions and emulsions, the latter approach has been most widely applied, for instance on milk protein concentrate and skim milk (Rogers et al., 2012), vitamin B12 and lactose (Wu et al., 2011) and epigallocatechin gallate (Fu et al., 2011c). In these investigations, a laminar feed jet was disintegrated into a series of separate droplets of uniform size by means of a microfluidic atomization nozzle. The nozzle consisted of a glass tube with an orifice of typically 50-150 µm in diameter, which imposed a Rayleigh instability

(Rayleigh, 1879) on the jet by periodic contraction due to the pulse of a piezoelectric ceramic jacket at the tip of the glass tube. A comparable pulsed-orifice droplet generator had previously been reported by Alexander and Judson King (1985), where a single stream of uniform droplets was obtained by means of a liquid jet being subject to an axial vibration that was induced by excitation of a stack of mechanically coupled piezoceramic disks. In these microfluidic jet spray drying techniques, the differentiation between single droplet drying and spray drying is vague. Droplet-droplet interaction can occur when the droplets are generated *via* pulsed mechanical disturbance based on Rayleigh instability, as the distance between the droplet sequence is relatively small (Vehring et al., 2007). An increase in water vapor pressure around a droplet due to evaporation of the adjacent droplets or even droplet collision can occur, because the distance between individual droplets is usually in the order of only a few droplet diameters or less. This has been attempted to be prevented by dispersion of the droplets after atomization, though it must be ensured that the residence time of the droplets remains equal and the drying tunnel is wide enough to sustain a uniform temperature profile experienced by the droplets independent from their radial location (Wu, 2010). Alternatively, commercially available 'droplet-on-demand' type generators allow a droplet production at very low frequencies and thus wide spacing between the droplets, down to single droplets (Vehring et al., 2007).

2.3.7 Concluding Remarks

This summary shows that single droplet drying in its four variations has been studied for a large number of (food) materials, and it has been proven to be a valuable and flexible approach for a better understanding and optimization of spray drying processes. It can be significantly more economical and allow for a more detailed collection of drying data than spray drying trials at pilot or industrial scale. The prediction of particle morphologies and drying kinetics with satisfactory accuracy has been reported throughout all four single droplet drying techniques. Nonetheless, one needs to be aware of the restrictions of each approach in respect to accuracy due to their intrusive nature (sessile, levitated and suspended droplets), limitations in what kind of analyses they can facilitate (especially limited in free falling single droplet drying) and how closely they mimic spray drying conditions (a particular challenge in the sessile droplet configuration, and to lesser extent in acoustic levitation). As such, combinations of two or more single droplet drying techniques, for instance suspended single droplet drying together with free falling single droplet drying, are advisable in order to complement the measurement techniques facilitated by each approach and to validate the results against each other.

3 Research Objectives

In view of the literature review (Chapter 2) and the research gaps summarized in the introduction, the primary objective of the present research was to obtain a better apprehension of the chemical surface formation in the course of spray drying of milk emulsions by means of spray drying and single droplet drying experiments as well as numerical simulation. While spray drying experiments should be used for analysis of the characteristics of the atomized droplets and the corresponding spray-dried particles, single droplet drying allowed investigation of the drying process between droplet generation and completed drying. Furthermore, the gained insights should be tested and applied by working towards an improvement of the fat encapsulation efficiency. This was expected to benefit a more economic and sustainable industrial milk powder production, improved spray drying design and superior milk powder quality for the consumer.

The specific aims were:

Aim 1: It should be found out which of the in literature discussed potential driving forces are in fact responsible for the component segregation in drying milk droplets. For this purpose, it was first of all to be identified during which stage of the spray drying process the surface fat formation primarily takes place by evaluating the impact of the atomization stage in comparison to the subsequent drying stage.

Aim 1 is addressed in Chapter 4.

Aim 2: Once the mechanism responsible for the surface fat formation has been identified, it can be worked towards an inhibition of this mechanism to reduce the amount of surface fat on spray-dried milk powder. Therefore, the understanding gained from aim 1 should be taken as a basis to explore a viable possibility to improve the encapsulation of fat in milk particles.

Aim 2 is addressed in Chapter 5.

Aim 3: How the drying and shrinkage kinetics of convectively dried milk droplets change with a high amount of surface fat should be investigated. For this, conventional single droplet drying was to be conducted and a new technique should be developed to study the change in surface composition over drying time. The observations were to be compared with a suitable numerical model to assist in a reliable interpretation of the results.

Aim 3 is addressed in Chapter 6.

4 The Impact of Atomization on the Surface Composition of Spray-Dried Milk Droplets

4.1 Preface

The aim of the following study was to identify the governing mechanism for the component segregation in drying milk droplets that is responsible for the formation of surface fat. The potential driving forces have been described in Section 2.2 and the characteristics of the various available investigation techniques have been summarized in Section 2.3. It was decided to conduct suspended single droplet drying experiments (Chapter 6) and free falling single droplet drying experiments in form of microfluidic jet spray drying (Chapter 4 and Chapter 5).

It was first of all crucial to determine whether the surface fat formation occurs during the atomization or the drying stage. Therefore, it was aspired to distinguish between the influences of the two stages by analyzing not only the component distribution of the dried particles, but also the one of the corresponding droplets immediately after atomization. A regular-fat milk model emulsion that was similar to bovine whole milk in its dry matter composition and a low-fat milk model emulsion that contained hardly any fat were studied. The main part of this investigation was conducted with a microfluidic multi-jet spray dryer. This instrument allows the production of monodisperse particles with uniform drying history, enabling a reliable correlation between the surface composition, the initial droplet size and the droplet's overall fat content.

The following work has been published by Elsevier B.V.:

Foerster, M., Gengenbach, T., Woo, M.W., Selomulya, C., The impact of atomization on the surface composition of spray-dried milk droplets, Colloids and Surfaces B: Biointerfaces, 2016, Vol. 140, p. 460-471, DOI: dx.doi.org/10.1016/j.colsurfb.2016.01.012

4.2 Abstract

The dominant presence of fat at the surface of spray-dried milk powders has been widely reported in the literature and described as resulting in unfavorable powder properties. The mechanism(s) causing this phenomenon are yet to be clearly identified. A systematic investigation of the component distribution in

atomized droplets and spray-dried particles consisting of model milk systems with different fat contents demonstrated that atomization strongly influences the final surface composition. Cryogenic flash freezing of uniform droplets from a microfluidic jet nozzle directly after atomization helped to distinguish the influence of the atomization stage from the drying stage. It was confirmed that the overrepresentation of fat on the surface is independent of the atomization technique, including a pressure-swirl single-fluid spray nozzle and a pilot-scale rotary disk spray dryer commonly used in industry. It is proposed that during the atomization stage a disintegration mechanism along the oil-water interface of the fat globules causes the surface predominance of fat. X-ray photoelectron spectroscopic measurements detected the outermost fat layer and some adjacent protein present on both atomized droplets and spray-dried particles. Confocal laser scanning microscopy gave a qualitative insight into the protein and fat distribution throughout the cross-sections, and confirmed the presence of a fat film along the particle surface. The film remained on the surface in the subsequent drying stage, while protein accumulated underneath, driven by diffusion. The results demonstrated that atomization induces component segregation and fat-rich surfaces in spray-dried milk powders, and thus these cannot be prevented by adjusting the spray drying conditions.

4.3 Introduction

Many studies on the spray drying of milk or similar emulsions have reported an unwanted fat coverage on the powder surface, concomitant with detrimental effects on the product characteristics, such as deteriorated storage stability (Granelli et al., 1996, Hardas et al., 2000, Keogh et al., 2001b), reduced solubility (Fäldt and Bergenståhl, 1996b, Millqvist-Fureby et al., 2001) and reduced flowability (Kim et al., 2005a, Nijdam and Langrish, 2006). To explain the segregation process of lipid, protein and lactose in the course of spray drying of milk droplets, various concepts have been proposed on the basis of different physical properties of these main components. The component segregation process is often perceived to take place simultaneously to the drying process after atomization. Fäldt and Bergenståhl (1996a) suggested a movement of milk protein to the air/water interface as a consequence of surface activity, an explanation that has been adopted in other studies (Adhikari et al., 2009, Gaiani et al., 2006). Meerdink and van’t Riet proposed that material segregation takes place in a drying milk droplet due to differences in the component diffusivities (Meerdink, 1994, Meerdink and van't Riet, 1995), which has been mentioned in subsequent studies (Chew et al., 2014, Fu et al., 2011a, Kim et al., 2003, Nikolova et al., 2015a). In addition, the crust composition of a drying droplet might be influenced by the solubility of the dissolved solutes (Charlesworth and Marshall, 1960), the concept of which was later applied on dairy systems (Kim et al., 2009b, Wang and Langrish, 2009). It was argued that, once part of the solidified crust, the precipitated material does not undergo diffusion anymore and thus a lower solubility could lead to a higher concentration near the surface. When the fat is in molten state during the drying

process because of the exposure to high temperatures, a convection to the surface through a network of pores and cracks, driven by capillary forces or overpressure of internal vacuoles, is also a potential reason (Nijdam and Langrish, 2005). Different combinations of these hypotheses are often presented as an explanation for fat surface accumulation in spray-dried milk powders, and accordingly the discussion has been restricted to the drying stage in most reports.

However, a small number of studies have discussed the possibility that an atomization induced mechanism might already impact the component distribution ahead of the actual drying process, although the conclusions were based on the final product surface while the atomization process itself was not investigated. Fyfe et al. (2011) compared the surface composition of commercial milk particles (skim milk, whole milk, milk protein concentrate) with the products of a pilot-scale and a laboratory-scale spray dryer. The pilot-scale spray dryer produced skim milk powder with a greater fat overrepresentation at the surface compared to the laboratory-scale spray dryer, despite both instruments utilizing the same drying air temperature profile and nozzle type. It was speculated whether this result could be explained by an impact of the difference in pressure and shear level during atomization on the disintegration process of the feed emulsion. Xu et al. (2013) found that the surface fat content decreased with smaller emulsion droplet sizes in powders comprising different protein isolates, maltodextrin and sunflower oil from a bench-top spray dryer. This was explained by a mechanism of liquid fat leakage and consequent spreading of a thin fat film at the particle surface caused by rupture of the fat globule membranes, which become less stable with larger sizes (Vignolles et al., 2009b). Since Xu et al. (2013) only analyzed the powder properties, their study could not determine whether the supposed rupture occurs due to differential stress on the membranes as they shrink at constant fat globule volume during drying or due to high shear rates imposed on the globules during atomization. Kim et al. (2009b) reported a fat coverage of more than 90 % and 18 %, respectively, on the surface of commercial whole milk and skim milk powders. Significant fat surface overrepresentation was also observed for particles that were dried at very high temperatures and consequently under rapid solidification and material immobilization. Thus, it was concluded that the fat coverage must have occurred, at least in part, during atomization. A film disintegration mechanism during droplet formation along the oil-water interface of lipid globules was proposed as a possible mechanism. In addition, it was hypothesized that the surface becomes further enriched in fat during the subsequent drying process because of the relatively low diffusivity of fat globules. It is difficult to draw a reliable conclusion about the impact of atomization from the final product powder characteristics only. For this reason, Wu et al. (2014) attempted to analyze droplet surface compositions directly after atomization with a microfluidic jet nozzle by flash freezing the droplets in LN_2. Comparison with corresponding spray-dried powders indicated that the atomization step predominantly determines the final surface composition. The study, however, was limited to skim milk and to only one atomization technique that is not used in commercial milk powder manufacturing.

The aim of the present study was to extend the approach by Wu et al. (2014) to conduct a systematic investigation of the impact of atomization on the surface composition of spray-dried milk powders. A microfluidic multi-jet spray dryer was used for the production of monodisperse particles to understand the influences of initial droplet size and emulsion fat content. The results were compared with those from different atomization techniques more common in an industrial setting. Spray-dried particles and flash-frozen droplets were analyzed in terms of surface composition by X-ray photoelectron spectroscopy, internal component distribution by confocal laser scanning microscopy, and size and morphology by light microscopy and scanning electron microscopy, respectively.

4.4 Material and Methods

4.4.1 Feed Preparation

Two model milk emulsions with different fat contents were used. The first was a mixture of dissolved lactose, calcium caseinate and whey protein with a very low fat content of 0.3 % w/w in dry matter to form a low-fat model milk (LFMM) emulsion. The other one was a regular-fat model milk (RFMM) emulsion that featured a composition typical for both bovine whole milk and commercially sold fat-filled milk powder. The solid content of the RFMM emulsion amounted to 20 % w/w, and it contained 40.8 % w/w lactose, 31.1 % w/w fat and 27.0 % w/w protein in d.m. The LFMM emulsion resembled the composition of the RFMM excluding the fat, and thus had a solid concentration of 14 % w/w. For preparation of the RFMM emulsion, commercial skim milk powder (Coles Supermarkets Australia Pty Ltd, Australia) was reconstituted together with sustainably sourced refined *Elaeis guineensis* palm oil fat (Auroma, Australia). For the LFMM emulsion, a mixture of α-lactose monohydrate (Sigma-Aldrich Co., USA), calcium caseinate isolate (Nutrients Direct Pty Ltd, Australia) and whey protein isolate (Nexius Pty Ltd, Australia) with a caseinate/whey ratio of 4:1 was used instead of commercial skim milk powder in order to reduce the fat content as far as possible. Both model systems were prepared with deionized water at 45 °C for 1 h, and then were prehomogenized in a high-speed colloid mill (WiseMix Homogenizer HG-15D, Daihan Scientific, South Korea) at 1000 rpm, followed by homogenization in a high pressure homogenizer (EmulsiFlex-C5, Avestin, Canada) with three passes at 1,000 bar and two subsequent passes at 500 bar. After homogenization the droplet size distribution was analyzed by dynamic light scattering (Zetasizer Nano ZS, Malvern Instruments Ltd, UK) to consistently ensure lipid droplet diameters below 1 µm. Dynamic viscosities were measured at 25 °C with a cone and plate rheometer (Haake Mars, Thermo Fisher Scientific, USA).

Fresh commercial whole milk, which contained 31.1 % w/w fat in d.m. and a solid concentration of 12.5 % w/w, was purchased locally (Pauls Full Cream Milk, Parmalat Australia Pty Ltd, Australia) for comparison with the RFMM emulsion. To investigate the surface composition of skim milk powder

spray-dried under conditions comparable with industrial milk powder production, samples were also taken from a pilot milk processing site (CSIRO Food and Nutrition, Werribee, Australia). Prior to spray drying, raw milk (Tatura Milk Industries Ltd, Australia) was high temperature, short time pasteurized and skimmed in a rotary cream separator to obtain 0.86 % w/w fat in d.m. and a solid content of 9.2 % w/w.

4.4.2 Atomization and Spray Drying with a Microfluidic Multi-Jet Spray Dryer

A microfluidic multi-jet spray dryer (MFMJSD), fabricated by Nantong Dong-Concept New Material Technology Co Ltd, P.R. China, was used to facilitate monodisperse droplet generation with uniform drying history. Depending on the amount of powder required, one to three microfluidic jet nozzles could be operated simultaneously. The design was similar to the nozzle used in the work of Wu et al. (2014), which has been described in detail elsewhere (Wu et al., 2011). In brief, each nozzle consisted of a glass tube with an orifice of 50, 100 or 150 µm in diameter. A piezoelectric ceramic jacket surrounded the nozzle tip, as illustrated in Figure 4.1a, and was electrically connected to a wave generator (DG1000, Rigol Technologies Inc., United States). It imposed a sinusoidal pulse of adjustable frequency on the feed emulsion stream passing through the glass tube and broke it up into individual droplets. The optimum pulse frequency setting was 10 kHz for all feed emulsions, which was found by photographing the jet disintegration with a D7000 digital LSR camera, equipped with an AF Micro-Nikkor 60mm f/2.8D micro-lens and a SB-300 high speed flash light (Nikon Corp., Japan). A typical image of the droplet generation is given in Figure 4.1b. With increasing orifice diameter the feed pressure had to be reduced from 110 to 33 and 17 kPa, respectively, to allow for uniform droplet generation. The nozzles could either be operated detached from the MFMJSD instrument for cryogenic flash freezing of the generated droplets, or positioned onto the drying tower for spray drying. Experiments were conducted with fresh whole milk, RFMM and LFMM emulsions.

A schematic diagram of the MFMJSD is presented in Figure 4.1c. Three individual tubes transferred the feed from 1.5 l steel reservoirs to each nozzle by pneumatic pressure. The nozzles were placed in water-cooled holders, and air streams coming from holes in the nozzle holders dispersed the droplet jets. The droplets then passed through a double-walled stainless steel drying chamber with embedded ceramic fiber insulation of 3.2 m in height and 0.6 m in diameter. The concurrent drying air flow was generated by a ring blower (W2PB-410-H06, XDS, P.R. China) and heated with a 3300 W electrical element, before being evenly dispensed into the tower through two perforated metal sheets. The temperature of the entering air was controlled with a thermocouple, and four thermocouples were inserted into the drying chamber to monitor the temperature gradient along the tower. The data was read out *via* a Picolog USB TC-08 data logger (Pico Technology, United Kingdom) and recorded with a desktop computer. Spray drying was performed at drying air temperatures of 190 °C at the tower top (‘T1’ in Figure 4.1c), 87 °C at the tower bottom (‘T4’), and 132 °C and 102 °C in between (‘T2’ and ‘T3’, respectively).

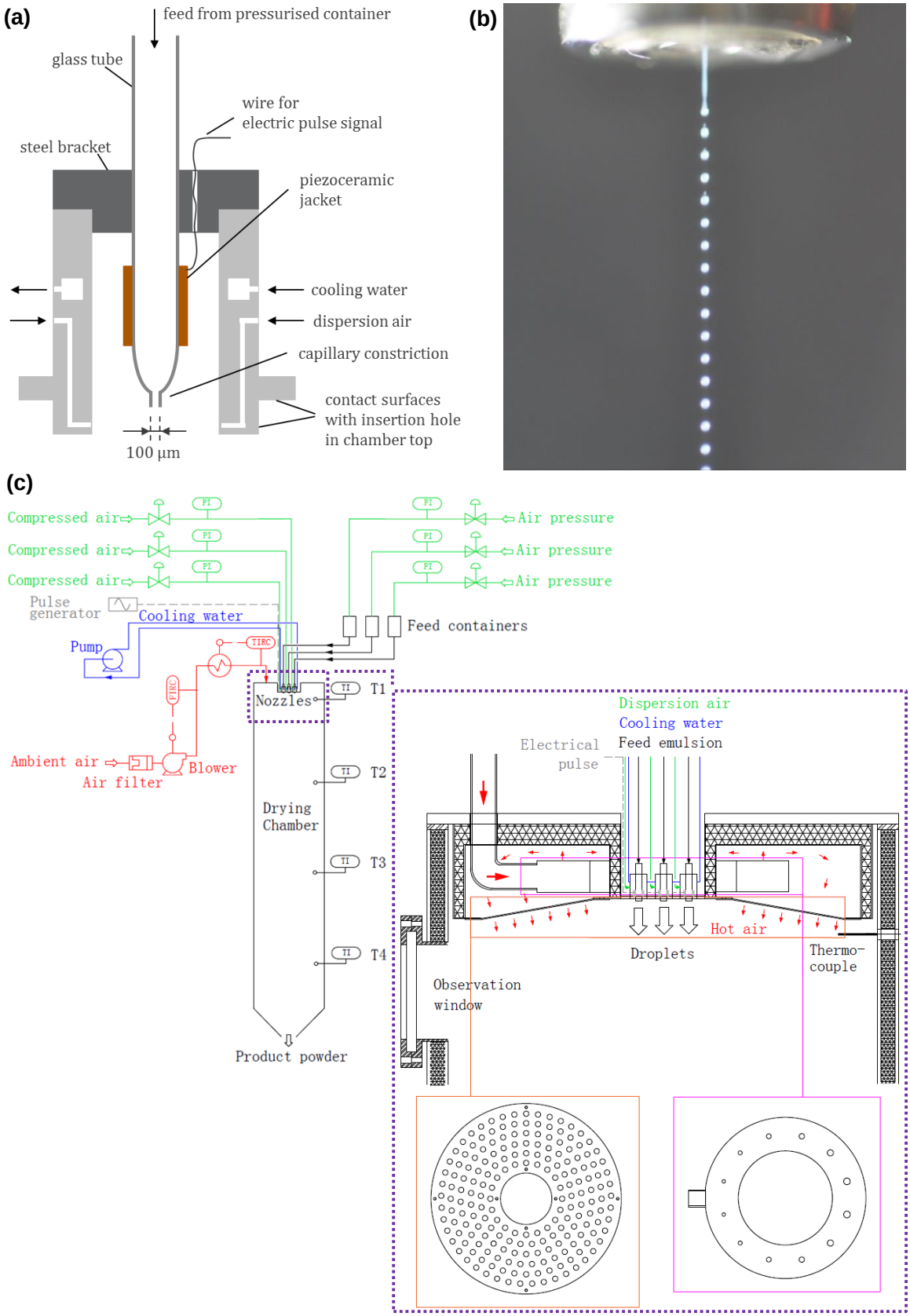

Figure 4.1: The microfluidic multi-jet spray dryer: (a) Schematic of a microfluidic jet nozzle; (b) typical photograph of monodisperse RFMM droplets (20 % w/w solids) generated with a microfluidic jet nozzle; and (c) schematic of the MFMJSD instrument.

4.4.3 Spray Drying with Rotary Pilot-Scale Spray Dryer and Atomization with Pressure-Swirl Nozzle

The freshly prepared skim milk was spray-dried at CSIRO with a pilot-scale spray dryer (Niro, GEA Group AG, Germany), which was equipped with a rotary disc atomizer and had a water evaporation capacity of 15-18 l/h. The feed was preheated to 75 °C, the inlet air temperature was 185 °C and the outlet air temperature was 80 °C. The instrument did not contain an integrated bed, and samples were collected for 1 min at 30 °C.

Furthermore, RFMM and LFMM droplets were flash-frozen subsequent to atomization in pressure-swirl single-fluid spray nozzles (MT Brass Series, AmFog Nozzle Technologies Inc, USA). Two nozzles with different orifices of 0.2 or 0.3 mm in diameter were tested at feed pressures of 450 and 600 kPa.

4.4.4 Cryogenic Flash Freezing and Subsequent Freeze Drying

To investigate the droplets directly after atomization, a modified methodology from Rogers et al. (2008) was applied. Droplets were collected in liquid nitrogen at a distance of 10 cm (if not stated otherwise) from the nozzle, which was operated outside of the spray dryer. The droplet jet required 0.03 ± 0.01 s to travel this distance, as calculated based on the mass flow rate measured by jet collection on a balance and on the approximate jet diameter read out from scaled camera images. The flash-frozen droplets were subsequently kept frozen by storage in dry ice and freeze-dried in a FreeZone 2.5 l benchtop freeze dry system (Labconco Corp., USA) at -80 °C and 0.1 mbar for 48 h.

4.4.5 Confocal Laser Scanning Microscopy

Selected RFMM samples were prepared for CLSM investigation by dual labelling with fluorescent dyes prior to mixing and further processing based on a procedure reported by Taneja et al. (2013). The aqueous solution of already dissolved protein and the molten fat were stained with 0.01 % w/w hydrophilic Fast Green FCF and 0.02 % w/w hydrophobic Nile Red (Sigma Aldrich Co., USA), respectively. After mixing and processing to powder as described above, the labelled powder samples were prepared on a microscope slide with DPX mounting medium (Sigma Aldrich Co., USA) and investigated by CLSM with a Nikon A1+ confocal microscope system (Nikon Corp., Japan). The Fast Green FCF and the Nile Red stains were sequentially excited with a 487 nm argon laser light and a 637 nm helium-neon laser light, respectively. Images were taken with a 60x/1.4 oil immersion objective at a resolution of 512×512 pixels.

4.4.6 Spectroscopic Surface Composition Analysis

Powder surface compositions were determined by XPS using an AXIS Ultra DLD spectrometer (Kratos Analytical Inc., UK) with a monochromated Al K_α source, a hemispherical analyzer operating in the fixed analyzer transmission mode and the standard aperture (analysis area: 0.3 mm × 0.7 mm). The total pressure in the main vacuum chamber during analysis was typically 10-8 mbar. Samples were filled into shallow wells of custom-built sample holders. One lot of each sample was prepared and two different locations were analyzed on each sample at a nominal photoelectron emission angle of 0º with respect to the surface normal. Since the actual emission angle is ill-defined in the case of particles (ranging from 0º to 90º), the sampling depth may have ranged from 0 nm to approximately 10 nm. All elements present were identified from survey spectra. The relative atomic concentrations of the detected elements were calculated using integral peak intensities and the sensitivity factors supplied by the manufacturer. The concentrations in lactose, protein and fat can be assumed to be linear combinations of the atomic surface composition (Fäldt et al., 1993). The surface concentration in each component, expressed in percentage by volume, was hence estimated by linearization based on representative structural formulas for milk protein, lactose and fat as described elsewhere (Chew et al., 2014).

4.4.7 Particle Morphology and Size Distribution Measurement

A field-emission scanning electron microscope (FEI Nova NanoSEM 450 FE-SEM, FEI Corp., USA), operated with a 5 kV electron beam, was employed to study the morphology of spray and freeze-dried powder. Additionally, to study the inner particle structure based on a modified procedure of Rosenberg et al. (1985), powders were suspended in a resin and then cut with a Reichert Ultracut S ultramicrotome (Leica Microsystems, Austria) equipped with a Cryotrim 45 knife (DiATOME, USA). A cold-setting resin (Epofix, Electron Microscopy Sciences, USA), which was cured at room temperature overnight, was used to avoid heat damage to the particles. Both the microtomed and the free powder samples were coated with a 4 nm thick Iridium layer to prevent electrical charging.

Information about particle size distributions was acquired by images taken of the powder samples with a light microscope (B1-211A, Motic, P.R. China) through a 4x objective. By means of ImageJ 1.48 (National Institutes of Health, USA) the projected surface areas were measured of 50 particles for each sample obtained with the microfluidic nozzles and of more than 100 particles for all other samples. The equivalent diameters were calculated from the projected surface areas.

4.5 Results and Discussion

4.5.1 Morphology and Size of Particles Atomized and Spray-Dried in the Microfluidic Multi-Jet Spray Dryer

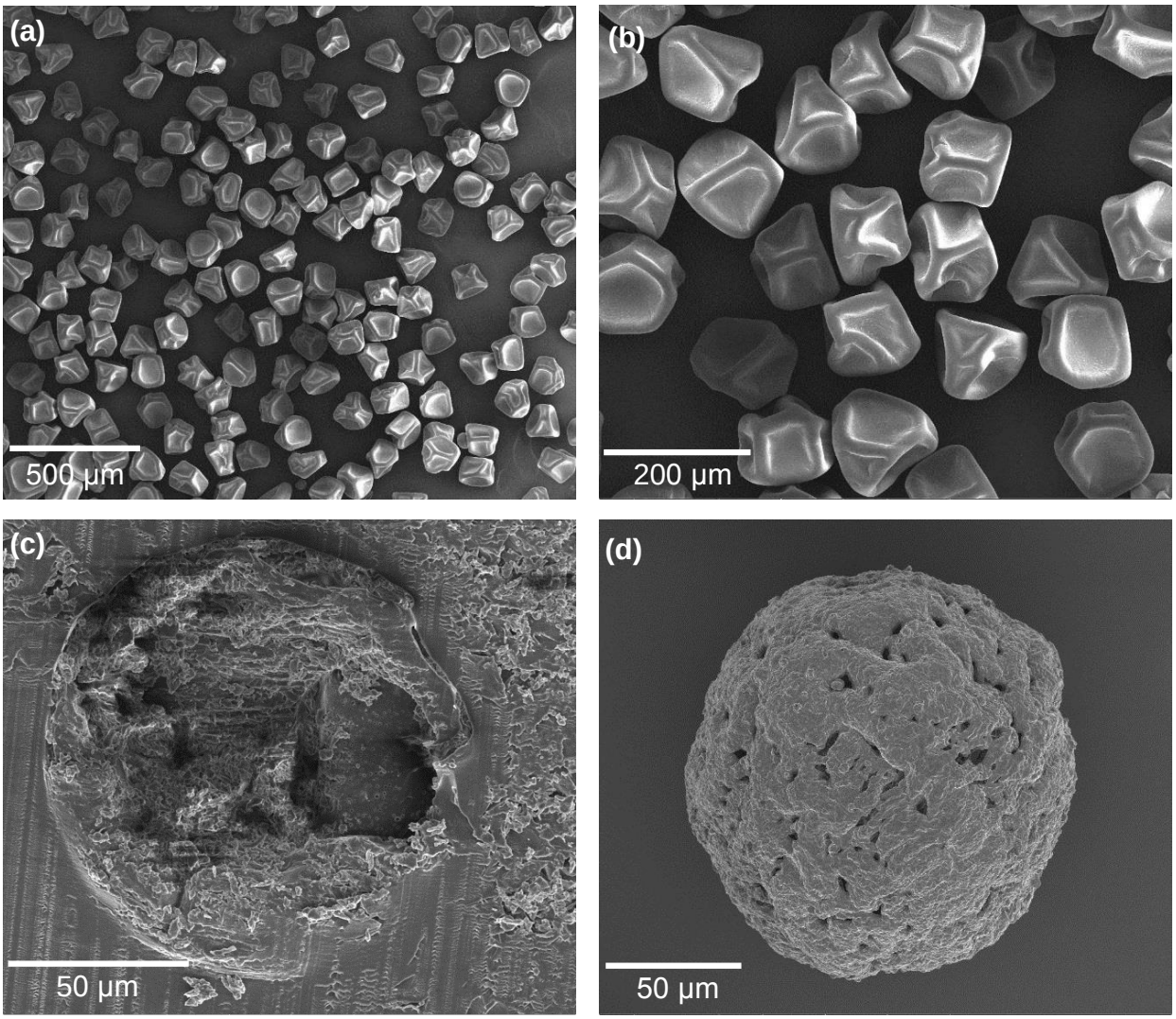

Figure 4.2: SEM images of RFMM particles obtained from three MFMJSD nozzles (100 µm): (a), (b) spray-dried particles; (c) cross-section of such a particle after embedding in resin and microtomic slicing through its middle; and (d) particle that had been flash-frozen after atomization and then freeze-dried.

To better understand the surface formation mechanism during spray drying, the MFMJSD instrument was used to produce monodisperse particles of identical drying histories (Fu et al., 2011c, Rogers et al., 2012). Each spray-dried and freeze-dried powder produced with the microfluidic jet nozzles featured a very narrow size distribution with small standard deviations (refer to Figure 4.8 in Appendix 3.A). Exemplary SEM images are shown in Figure 4.2. The uniformity allowed direct correlations of the impact of different emulsion compositions and orifice sizes on the particle surface composition, which are dif-

ficult to derive from powders produced by conventional spray drying techniques with their wider size and morphology distributions (Masters, 1991). Furthermore, since the atomized droplets were ultra-rapidly flash-frozen at -196 °C and the succeeding freeze drying occurred at a very low drying rate, migration of the solid components and structural changes subsequent to the collection in liquid nitrogen were prevented (Ishwarya et al., 2014). The spray-dried particles had a non-porous crust and were inwardly buckled in shape. This can be explained by an initial inflation due to air expansion in particles of nearly dry condition which is then followed by deflation and shriveling in colder dryer regions (Kim et al., 2009b) or by compressive stress on the particle crust attributable to capillary forces and rapid moisture removal (Rogers et al., 2012, Tsapis et al., 2005). Figure 4.2c displays a typical cross-sectional image of a spray-dried particle that had been embedded and microtomed, containing some hollow areas and internal porosities. The freeze-dried particles were spherical, since they were flash-frozen as freshly generated droplets, and were traversed by porous structures as a result of water sublimation during freeze drying (Figure 4.2d).

As can be seen in Appendix 3.A (Figure 4.8), for the microfluidic jet nozzles of 50, 100 and 150 µm in orifice diameter, there was an almost linear relationship between size of the orifice and the resulting LFMM droplets; a three times bigger orifice diameter lead to a 2.8-fold increase in droplet size. For the same microfluidic jet nozzle size of 100 µm, the LFMM droplets were appreciably larger than the RFMM droplets (diameter of 135.8 and 115.6 µm, respectively). The feed pressure and piezoelectric pulse frequency were identical, and thus the size difference most likely originated from a change in disintegration behavior of the emulsions as a result of their different viscosities or fat contents. Due to its additional fat content, the viscosity of the RFMM emulsion (2.9 mPa·s at a shear rate of 200 s^{-1}) was greater than the one of the LFMM emulsion (2.4 mPa·s). Typically, a higher viscosity results in a delayed disintegration of the jet during atomization, as the Reynolds number is reduced and the jet stability is increased. Thus, an increased viscosity is to be expected to favor the formation of larger droplets (Lefebvre, 1989). Here, however, a converse trend was observed. It was consequently concluded that the presence of more fat reduced the intrinsic stability of the RFMM emulsion jet upon atomization.

The emulsion might have been less stable against disintegration along the oil-water interfaces formed by the lipid globules. With a higher number of fat globules, the emulsions became virtually ‘perforated’ by these areas of lower cohesion, where the emulsion could disintegrate into droplets more easily. Such a perforation mechanism was also discussed in a study by Dombrowski and Fraser (1954), in which fan-shaped flat sheets consisting of either pure water or a soluble oil-water emulsion were generated with a single-hole fan-spray nozzle and the film disintegration was observed by a rapid light flash photographic technique. In the presence of oil the films broke significantly closer to the nozzle. Zakarlan and King (1982) investigated similarly shaped flat sheets of an aqueous sucrose solution with a dispersed phase of peanut oil, and found that the point of disintegration was particularly sensitive to the fat content in a range of 0 to 0.1 % w/w fat. Though the atomization technique and emulsion types were different to the

present study, it seems likely that a comparable perforation mechanism was induced in the RFMM emulsion (lipid level of 6.2 % w/w), and also, at a less pronounced extent, in the LFMM emulsion (lipid level of 0.04 % w/w).

4.5.2 Impact of Microfluidic Jet Atomization on Particle Surface Composition and Influence of Feed Composition

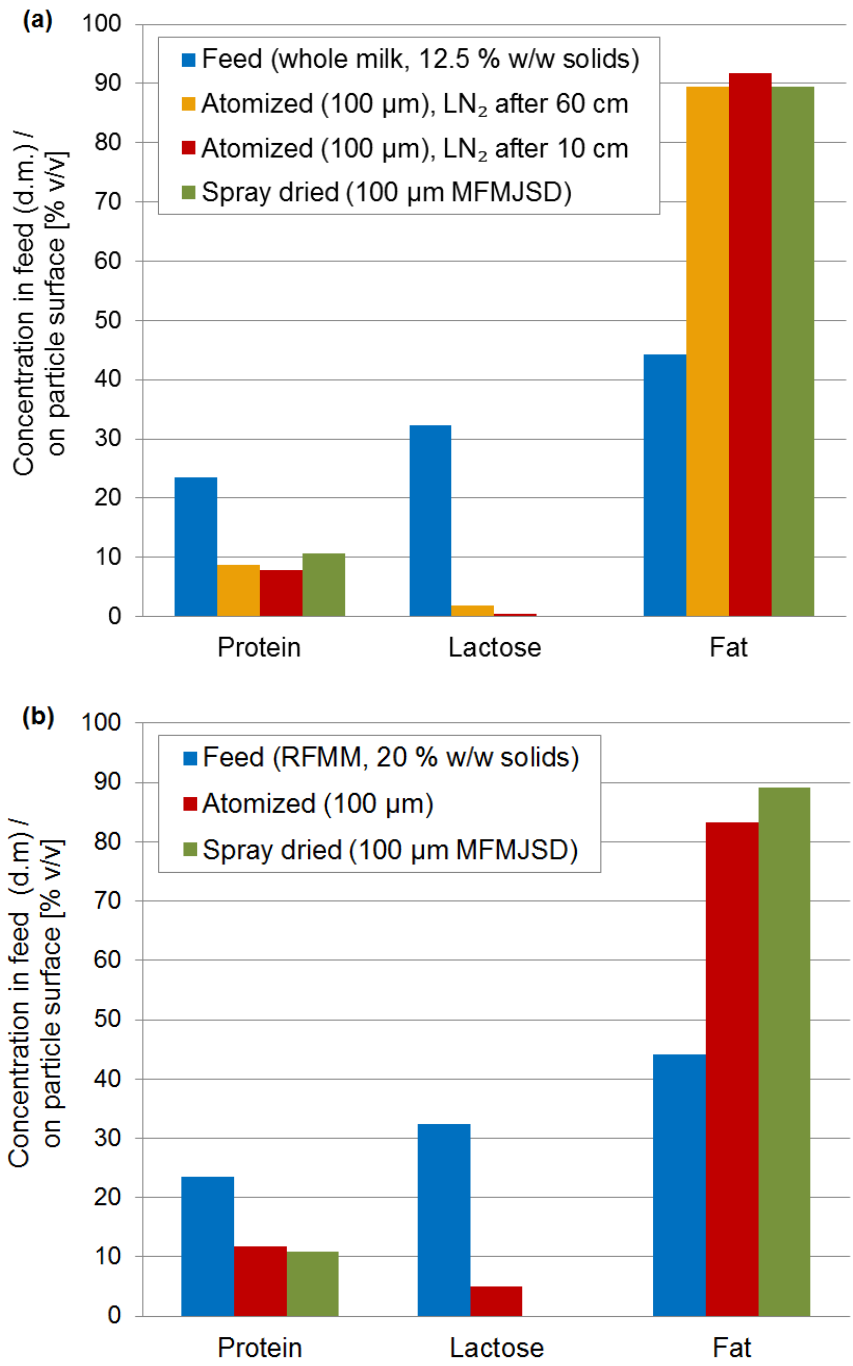

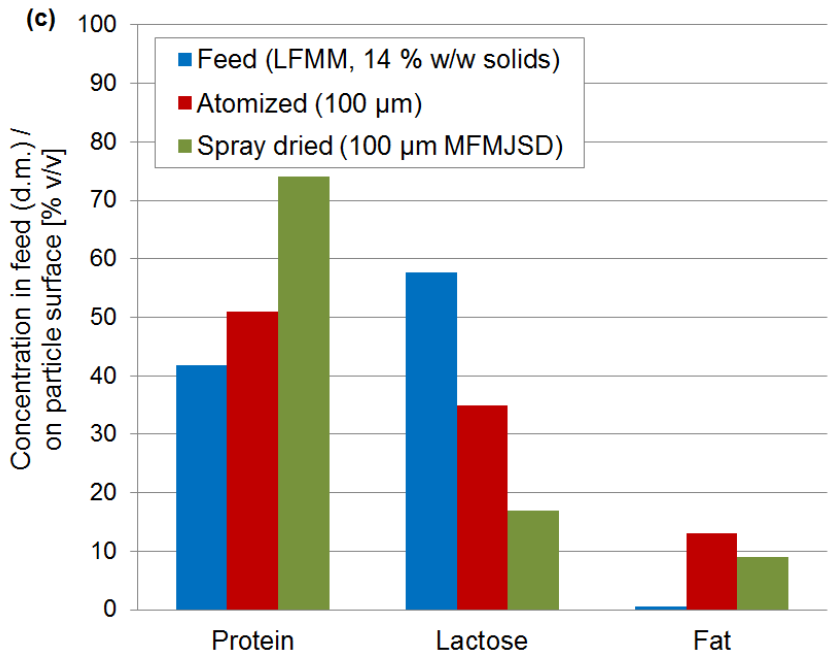

Figure 4.3: Estimated XPS particle surface composition for a MFMJSD with a 100 µm orifice nozzle under variation of the feed emulsions: (a) fresh whole milk, (b) RFMM, and (c) LFMM: Surface composition of particles that were spray-dried and of droplets that were flash-frozen directly after atomization and subsequently freeze-dried, in comparison to the dry matter feed compositions.

Standard deviations of the relative atomic concentrations directly obtained from XPS hardly varied with an average deviation of 1.8 % in the main elements (nitrogen, oxygen, carbon). From this, the component concentrations were estimated from a linearization approach as described in Section 4.4.6 and these values should hence be treated as semi-quantitative only. The RFMM emulsion proved to be a suitable model system for fresh whole milk in terms of surface formation behavior during spray drying, as shown in Figure 4.3a,b for the MFMJSD instrument equipped with a 100 µm nozzle. According to their similar dry matter feed compositions, the droplet and particle surface compositions of the RFMM and fresh whole milk were in good agreement as analyzed by XPS. Most notably it was found that the atomized droplets' surfaces were already covered almost completely by fat. The surface fat contents of the atomized droplets was approximately double that of the dry matter feed fat content, occupying between approximately 83 % and 92 % of the surface. Protein was underrepresented on the droplet surface with occupying only half as much volume as may be expected based on the feed compositions. The results agree with the decline in droplet size with increasing fat content, and further support the hypothesis that the presence of fat globules caused a perforation of the emulsion that resulted in easier jet disintegration along the oil-water interfaces during atomization. As the jet preferably broke up along the fat globules, the fat globules were immediately at the surface as soon as individual droplets had been formed.

The component segregation observed in the flash-frozen particles was a direct result from the atomization step, and was not formed in the time after leaving the nozzle and before entering the liquid nitrogen.

No substantial difference in surface composition was observed for a considerably longer travelling time when the distance between nozzle and liquid nitrogen was increased to 60 cm (Figure 4.3a). Moreover, water evaporation from the droplets, which could have induced a component segregation caused by different diffusivities, was negligible as the temperature between the nozzle and the collection tank was 15 °C. In addition, the droplet residence time of less than 0.05 s between nozzle and liquid nitrogen prevented any appreciable component diffusion to or from the surface driven by, for instance, surface activity or concentration gradients formed during atomization. The diffusion time scales over a diffusion length of 10 µm were estimated to be of 18 and 71 seconds, respectively, for fat globules and protein at 15 °C (refer to Table 4.1 in Appendix 3.B).

Whereas the atomization stage considerably influenced the particle surface composition, no significant impact of the subsequent drying process on the chemical surface composition was observed for regular fat contents (changes smaller than 6 % v/v for every component as shown in Figure 4.3a,b). There was only a minor increase in fat on the RFMM particles. Lactose comprised very small proportions on the surfaces of both the atomized droplets and the spray-dried powders. This demonstrated that the atomization step primarily determined the final surface composition of whole milk powder obtained with a MFMJSD, being responsible for a high fat overrepresentation, and thus strongly influenced the functional product properties. The observation of a pronounced fat accumulation on the droplet surface during atomization in microfluidic jet nozzles was consistent with the study on the atomization of skim milk conducted by Wu et al. (2014), where a feed of 33 % w/w solid content containing 35 % protein and 0.7 % fat in d.m. resulted in 40 % protein and 29 % fat on the surface of the atomized droplets. However, Wu et al. (2014) observed a significant change in surface composition during the following drying step with an increase in protein to 52 % and in fat to 38 %. This was in contrast to the here investigated whole milk and RFMM. In the drying whole milk and RFMM droplets, the dense surface fat layer presumably concealed any underlying component segregation. This was confirmed by spectroscopic analysis of the surface of atomized and spray-dried particles from the LFMM feed (Figure 4.3c). Again, an overrepresentation of surface fat in relation to the dry matter feed concentration was formed during atomization. Yet, due to the low feed fat content, this time the fat did not dominate the surface region analyzed by XPS with a surface proportion of approximately 13 %. This allowed the observation of a small overrepresentation of protein that already emerged during atomization. In course of the following drying stage, a pronounced rise in protein surface coverage from approximately 51 % to 74 % was found.

4.5.3 Development of Component Distribution and Impact of Orifice Size in Microfluidic Multi-Jet Spray Drying

To understand the mechanism that governed the protein migration to the surface during the drying stage of the microfluidic spray drying process, the influence of the droplet drying time was studied by using

nozzles with a smaller and a larger orifice size (Figure 4.4). The protein surface content rose only slightly from 57 % after atomization to 65 % after spray drying for a 50 µm orifice. For a 150 µm orifice, the increase in protein was about double as high from 57 to 77 %. The initial droplet diameters generated with the 50 µm and 150 µm nozzles were 81.5 and 199.5 µm, respectively. The larger the droplets, the longer was the drying time as the drying air temperature profile was kept constant. The drying time

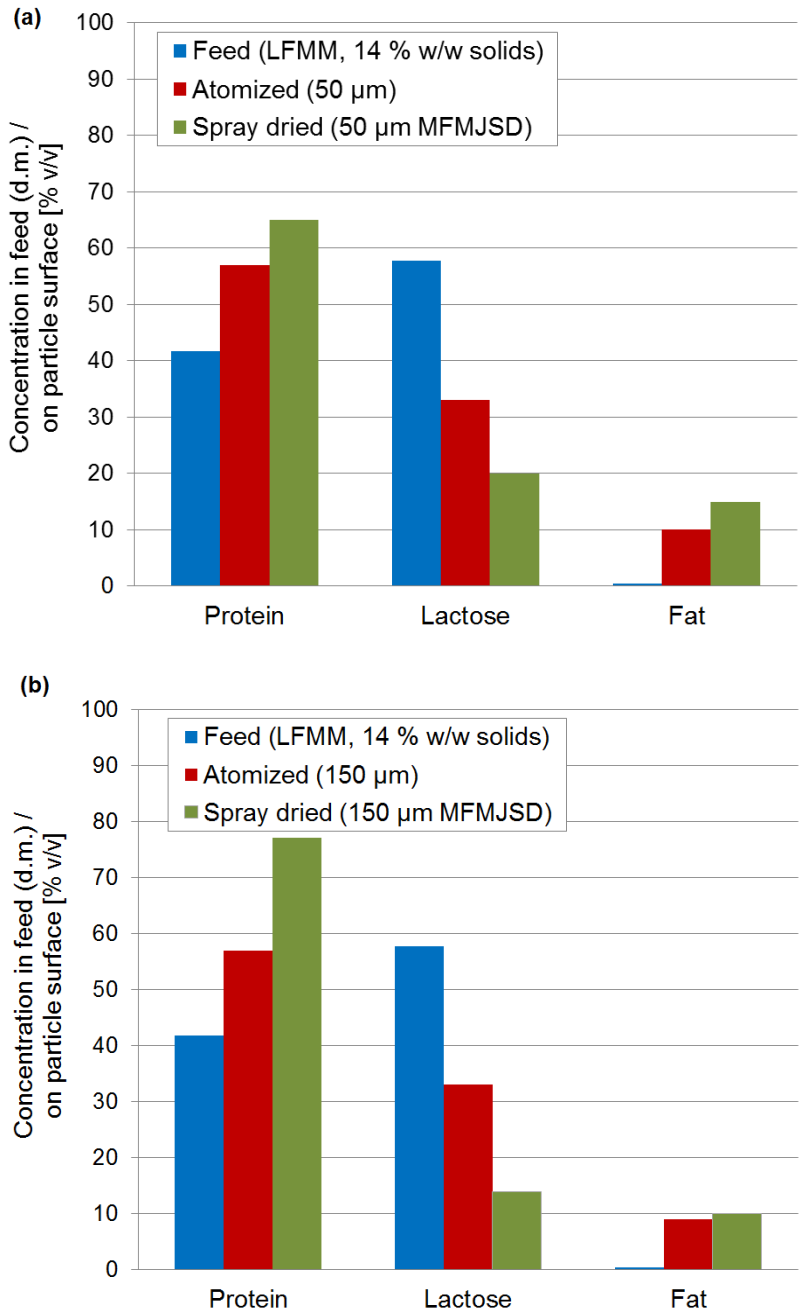

Figure 4.4: Estimated XPS surface composition of LFMM under variation of the MFMJSD nozzle orifice diameter, (a) 50 µm and (b) 150 µm: Surface composition of particles that were spray-dried and of droplets that were flash-frozen directly after atomization and subsequently freeze-dried, in comparison to the dry matter feed composition.

dependency of the extent of protein enrichment near the surface suggested that diffusion controlled the protein migration to the surface. At elevated droplet temperature, 100 °C for instance, such a segregation mechanism seems to be possible, given that the diffusion time scales of the fat globules, casein micelles, calcium caseinate molecules and lactose lied within the droplets' residence time inside the spray dryer (refer to Table 4.1 in Appendix 3.B). Firstly, the protein diffusion to the surface is believed to be mainly driven by the surface activity of milk protein. At a diffusion-controlled rate the proteins travelled to the droplet surface, where they were adsorbed at the air/water interface (Graham and Phillips, 1979). Secondly, the surface accumulation of protein might have been enhanced by a slower diffusivity than the one of lactose. As water evaporates from the surface, the radial water gradient from the particle center to the surface was accompanied by component concentration gradients in opposite direction, causing the components to diffuse towards the center. There was a distinct difference in diffusivities (Table 4.1 in Appendix 3.B), and hence the surface might have become enriched in the larger, slower diffusing species. As the diffusivity of lactose is one to two magnitudes greater than the one of protein, at the surface the protein concentration would increase with a simultaneous reduction of lactose. The fat globule diffusivity is approximately three orders of magnitude lower than the one of lactose, but there was no significant increase in fat surface content from atomized droplet to spray-dried product. A simple mass balance showed that this was because the surface region with 10-15 % v/v fat and a depth of 10 nm (i.e. the penetration depth of the XPS measurements) already comprised approximately the entire fat contained in a LFMM droplet.

The XPS results were compared with the confocal laser scanning microscopy results, which allowed a qualitative insight into the internal component distribution. RFMM particles with labelled protein and lipid were investigated after atomization and after completed spray drying, and typical result images are presented in Figure 4.5. Illustrating the CLSM response intensities of labelled protein and fat in form of individual graphs as obtained from sequential excitation at 487 and 637 nm enabled a discussion of the individual protein and fat distributions. The pixel brightness represented a qualitative measure of the local concentration in each component. In the atomized droplets, a thin layer of fat was formed all around the surface and also underneath this layer the fat content was higher than in the droplet center, whereas the protein was homogeneously distributed throughout the whole droplets (Figure 4.5a,c). This agrees with the XPS observation of an atomization induced fat coverage on the droplet surfaces. The surface fat layer comprised small amounts of protein, which might have been entrapped inside the fat as it had been part of the membranes that surround the fat globules in the homogenized feed emulsions. Thus, the XPS analysis detected less than 100 % surface fat. During the spray drying stage, the fat gradient was further increased with almost all the fat being eventually accumulated near the surface area (Figure 4.5d), which can be ascribed to the hydrophobicity and low diffusivity of the fat globules. The CLSM images indicated that the initial fat layer thickness already exceeded the penetration depth of the XPS analysis. Therefore, the surface fat content as measured by XPS did not increase appreciably from

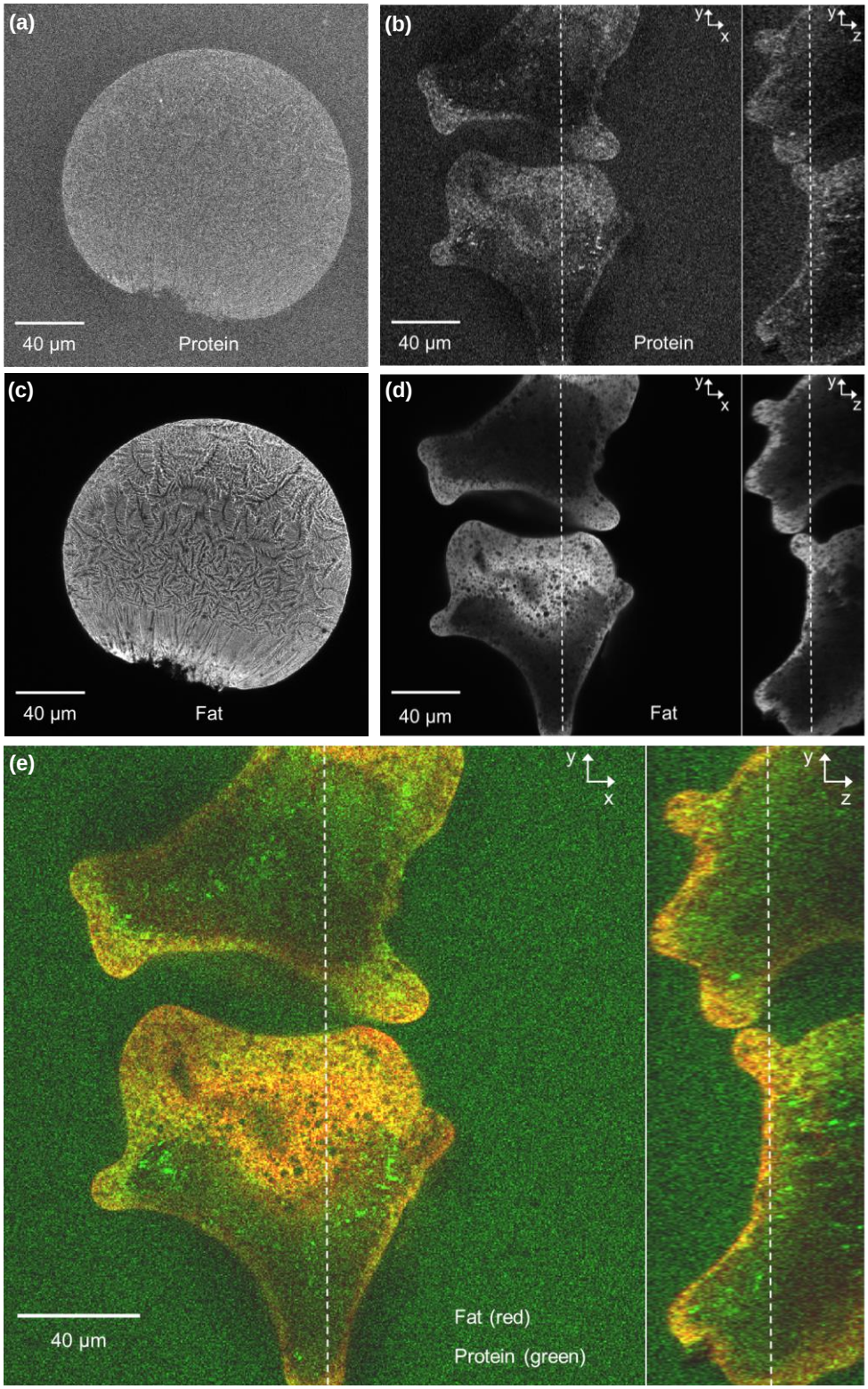

Figure 4.5: CLSM images of protein and fat distribution in RFMM particles: Particles were (a,c) flash-frozen directly after atomization and subsequently freeze-dried (cross-section through middle of particles); and (b,d,e) spray-dried (two cross-sections through three-dimensional image stacks as indicated by the dotted lines). (a)-(d) Split channels: the greater the pixel brightness, the higher the local concentration in Nile Red (fat dye) and Fast Green FCF (protein dye), respectively. (e) Merged channels: Nile Red (fat dye) depicted in red and Fast Green FCF (protein dye) in green.

atomized droplets to spray-dried particles. Also a clear gradient in protein from high concentration close to the surface to very low levels in the particle center was developed during the drying stage (Figure 4.5b), concordant with the XPS measurements. Due to its high diffusivity, lactose dominated in regions far away from the surface inside the spray-dried particles (dark areas). The strong underrepresentation of lactose in surface-near regions, as observed by XPS and CLSM for both model emulsions, presumably had a detrimental impact on the powder's rehydration behavior, since lactose promotes the solubility in high-protein powders (Anema et al., 2006, Baldwin and Truong, 2007). In contrast, the surface fat film reduces the solubility rate of the particles as the wettability is lowered. Recent studies have shown that also a dominant amount of native casein, as present in milk protein concentrate and phosphocaseinate powders, negatively affects the rehydration behavior of aggregated powders in aqueous medium (Gaiani et al., 2007, Mimouni et al., 2010). These powders have been described to feature decelerated water penetration (Schuck et al., 2007) and poor dispersibility (Crowley et al., 2016, Havea, 2006) due to a network of interconnected casein micelles.

While the development of radial concentration gradients in both fat and protein can be seen in the split channel images, these images did not reveal which component is in fact dominating at the surface. For this purpose, the response channels of spray-dried RFMM particles were merged together with protein and fat being depicted in green and red, respectively (Figure 4.5e). Additionally, Video 1[2] provides an animation of the cross-section stack in 1 µm depth steps from the top to about the middle of the particles. It can be seen that fat dominated at the outermost particle surface, as a thin film of fat had been formed around the particles. This corresponds well with the XPS analysis. The existence of a fat film rather than individual lipid islands on the atomized droplets indicated that the fat globules were ruptured during the atomization process, which caused a homogeneous spreading of fat over the particles. Maximal protein concentrations did not typically occur within the first few nanometers of the surface, but immediately underneath that fat film. For the RFMM and fresh whole milk emulsions, the XPS measurements only captured the fat surface layer and thus no increase in protein throughout the drying stage was detected. Because there was only a very thin fat layer (smaller than the XPS penetration depth of 10 nm) in case of the LFMM feed, the adjacent increase in protein was captured by the XPS measurements.

4.5.4 Impact of Conventional Atomization Techniques on Surface Composition

The microfluidic jet nozzles did not represent a droplet generation technique that is typical for commercial milk powder manufacturing. The jet was disintegrated by normal stress imposed *via* sinusoidal pulsation in the microfluidic jet nozzle type, as opposed to industrial-scale spray drying where shear stress significantly contributes to the dispersion of the emulsion films. Employing a spray dryer with a rotary disk atomizer, it was confirmed that a very high surface overrepresentation of fat is also formed under spray drying conditions comparable to industrial milk powder production (Figure 4.6). As the spray

[2] Video 1: CLSM stack animation of protein and fat distribution from the top to about the middle of RFMM particles in 1 µm steps. Available online as supplementary data: dx.doi.org.ezproxy.lib.monash.edu.au/10.1016/j.colsurfb.2016.01.012

dryer did not include any integrated fluidized beds or other powder post-processing steps, the particle surface formation can be attributed to the actual spray drying process, and thus most likely occurred during the atomization stage.

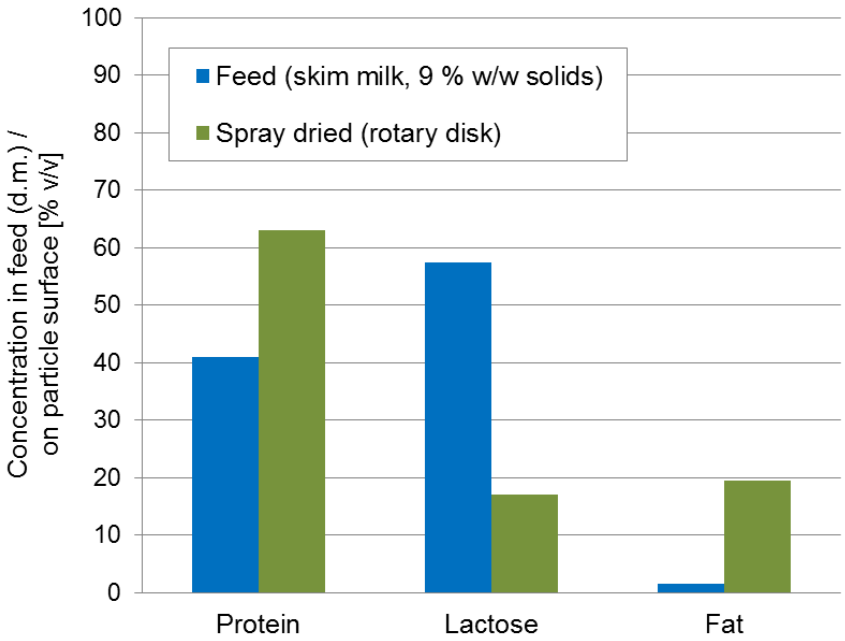

Figure 4.6: Estimated XPS particle surface composition of skim milk powder from a pilot-scale single-stage spray dryer with rotary disk atomizer, in comparison to the dry matter feed composition.

To study a third atomization technique, RFMM and LFMM droplets were generated with a pressure-swirl single-fluid spray nozzle and afterwards were flash-frozen and freeze-dried for XPS analysis (Figure 4.7). The particle surface compositions were similar to the ones obtained from microfluidic jet atomization. The RFMM particle surface consisted of approximately 9 % v/v protein and 92 % v/v fat, and the LFMM particle surface was composed of approximately 63 % v/v protein and 5 % v/v fat. It can thus be concluded that atomization induced component segregation and fat surface coverage take place over a range of different atomization techniques.

In contrast to the droplets and particles obtained from microfluidic jet atomization, the skim milk powder produced with the pilot-scale rotary spray dryer had a wide size distribution of 26.3 ± 13.5 µm in diameter, and the RFMM and LFMM droplets that were atomized with the pressure-swirl nozzle also had a wide size distribution of 24.3 ± 12.2 µm in diameter (results not shown here). The investigated emulsion fat contents and orifice sizes did not have an impact on the mean droplet size generated with the pressure-swirl nozzle. Accordingly, the mean droplet drying time was similar and the droplet surface composition was independent from these two parameters, as depicted by the standard deviations in Figure 4.7. This agrees with the results of Fyfe et al. (2011), where the difference in surface composition between milk powders spray-dried in pilot and lab scale was found to be less than approximately 7 % and 2 % in any of the three main components for skim milk powder and whole milk powder, respective-

ly, despite some differences in nozzle configuration and atomization pressure. Their observation of a discrepancy in comparison with commercial milk powder might be due to the post-processing steps following spray drying in industrial settings, such as fluidized beds, or the application of additives.

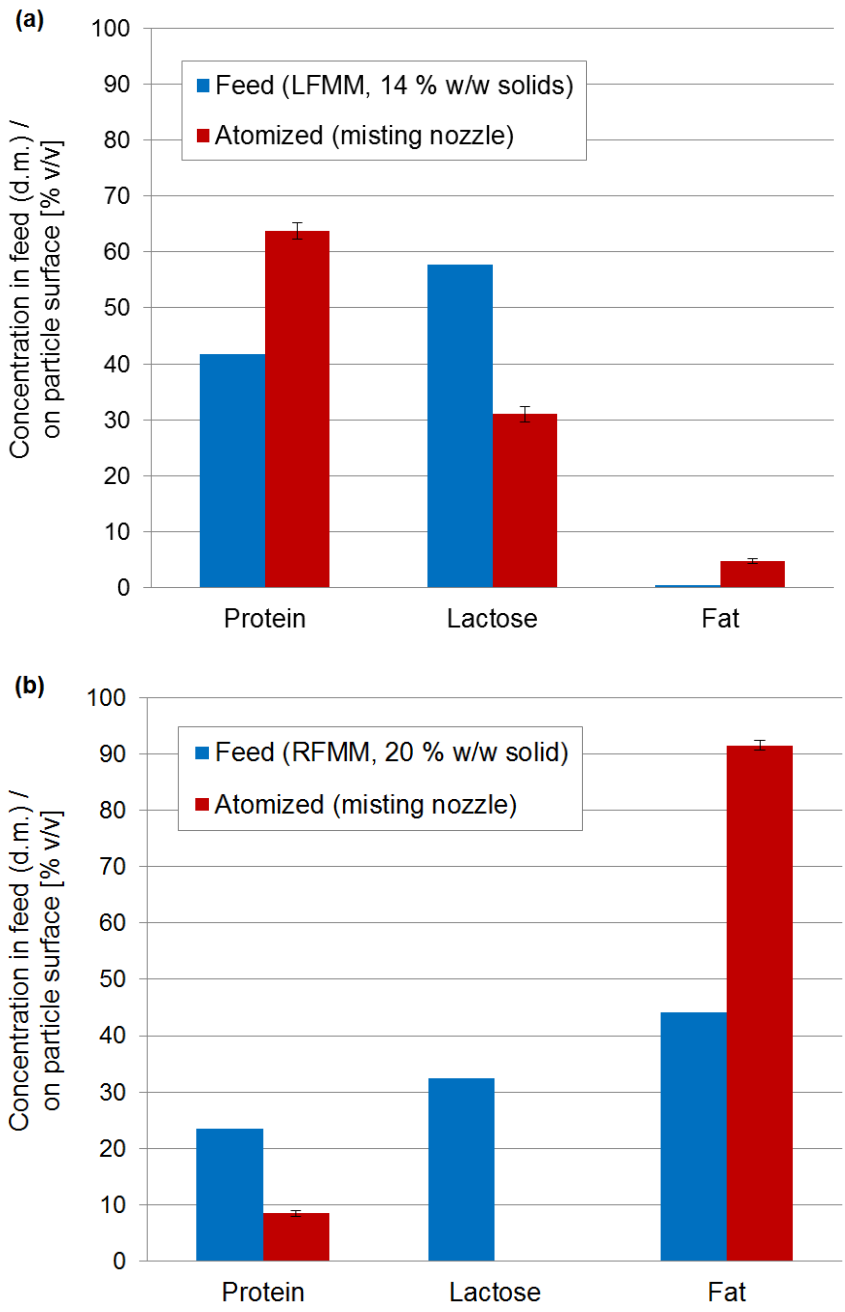

Figure 4.7: Estimated XPS surface composition of droplets atomized with a pressure-swirl single-fluid spray nozzle in comparison with the dry matter feed compositions: (a) LFMM emulsion; and (b) RFMM emulsion. The standard deviations for different spray drying conditions with a feed pressure of 450 or 600 kPa and a nozzle orifice diameter of 0.2 or 0.3 mm are shown. The droplets were flash-frozen directly after atomization and subsequently freeze-dried prior to analysis.

For the range of atomization techniques investigated, atomization induced fat accumulation on spray-dried model milk powders with different fat contents occurred whatever atomization technique was used. Though protein enriched towards the surface region during the drying stage, a fat film always remained at the outmost surface. Therefore, an efficient lipid encapsulation in a shell consisting of protein by adjusting the spray drying conditions seems not to be achievable. Future work is hence needed to investigate whether the perforation mechanism during atomization can be prevented by a specific feed pre-treatment. Furthermore, a numerical multi-component simulation of drying milk droplets can help predicting the final chemical powder surface composition. In such models, the considerable influence of atomization on the material distribution prior to the actual drying step must be taken into account in the form of initial concentration conditions.

4.6 Conclusions

In the present study, a systematic investigation of the impact of atomization on the surface composition of spray-dried model milk powder was conducted on monodisperse particles using a microfluidic multi-jet spray dryer. It was additionally demonstrated that the observed processes also occur in atomization techniques typically used on industrial scale. Cryogenic flash freezing of the droplets allowed the impact of the atomization stage to be distinguished from the drying stage. For the range of emulsions and spray drying techniques investigated, the findings indicate that the component segregation and surface predominance of fat in spray-dried milk powder should not be attributed to the drying stage, but were already formed during atomization. For emulsion fat contents of 0.5 and 44.2 % v/v in d.m., surface fat coverages of 9-13 and 83-92 % v/v, respectively, were detected on the atomized droplets. Because the droplet surfaces were immediately covered by fat after atomization and the droplet size became smaller with higher fat content, it was concluded that a perforation along the oil-water interfaces formed by the fat globules made the emulsions less stable against disintegration with increasing lipid content. However, further studies on the complex relation between the fat content in the presence of milk protein, the emulsion viscosity and the jet stability against disintegration upon atomization need to be conducted. In the following drying stage, the fat film remained on the surface and additional fat enriched near the surface due to its hydrophobicity and low diffusivity. Also protein migrated from the droplet center towards the surface, but accumulated underneath the fat layer and did not penetrate it. Because the protein migration was more distinct for larger droplet sizes and at accordingly longer drying times, it was presumably driven by the protein's surface activity and differences in the component's diffusivities. Beyond milk systems, the presented approach could be applied on other emulsions to investigate whether atomization also induces wanted or unwanted component segregation in other food or pharmaceutical spray drying applications.

4.7 Appendix

4.7.1 Appendix 3.A: Droplet Diameters and Shrinkage in the MFMJSD

In Figure 4.8, the mean particle diameters of powders produced in the MFMJSD with microfluidic jet nozzles of different orifice size and for high and low-fat content are presented together with the corresponding initial droplet diameters immediately after atomization.

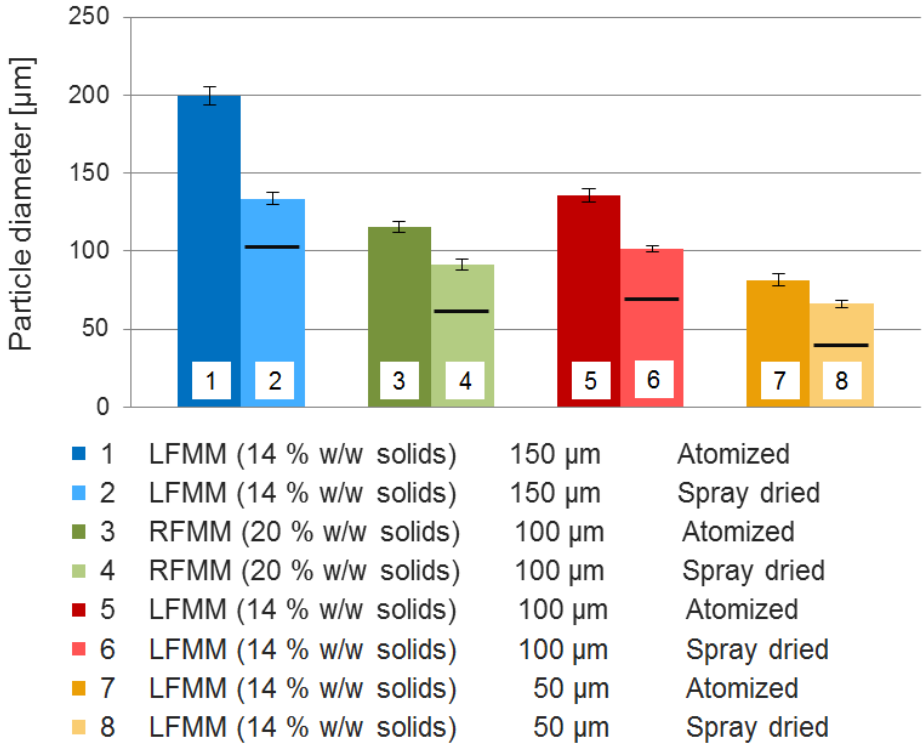

Figure 4.8: Mean diameter and standard deviation of atomized droplets and the corresponding spray-dried particles from the MFMJSD: The microfluidic jet nozzles had orifice diameters of 50, 100 and 150 µm. The atomized droplets were flash-frozen directly after atomization and then freeze-dried. For comparison, the theoretical diameters of dried particles under the assumption of perfect shrinkage are given for each atomized droplet diameter (bold lines).

Both the spray-dried particles and the initial droplets had each small standard deviation in size. For the freeze-dried particles, the equivalent diameter calculated from the projection surface areas in the light microscope images reflected their actual volume due to their spherical shape. Because of the buckled shape of the spray-dried particles, however, their calculated equivalent diameter overestimated the actual particle volume to some degree. A relative comparison between the sizes and shrinkage ratios of the different powders was still possible, nevertheless. The size and shape of the atomized particles could be assumed to be unaffected by the freeze drying step, which gives an accurate knowledge of the initial droplet size. This was useful for discussing the shrinkage behavior and the influence of drying time and

rate on the resulting particle surface composition (Kim et al., 2009b, Pısecký, 1997). In previous studies, the initial droplet size could only be roughly deduced from the final particle size under assumption of a certain shrinkage model (Van Mil et al., 1987). For comparison, the hypothetical product diameters for perfect shrinkage behavior are included in Figure 4.8, which shows that shrinkage was less pronounced for smaller droplets. The measured equivalent diameters of the spray-dried low-fat particles were 28, 48 and 56 % bigger than the corresponding values in case of perfect shrinkage for a 150, 100 and 50 µm orifice, respectively, and 48 % bigger for RFMM and a 100 µm orifice. Because the temperature profile of the drying air was kept identical for all spray drying runs, the smaller droplets reached a dried condition earlier and thus the air enclosed in the particles presumably experienced higher temperatures for the remaining time that the particles spent in the dryer, leading to greater inflation of the internal structures.

4.7.2 Appendix 3.B: Diffusivities of Fat Globules, Protein and Lactose

The diffusion time scales over a diffusion length x of 10 µm were estimated by means of binary diffusion coefficients obtained from Stokes-Einstein's equation (Einstein, 1905):

$$D_i = \frac{k_B T}{6\,\pi\,\mu\,R_i} \tag{4.1}$$

$$\tau_i = \frac{x^2}{D_i} \tag{4.2}$$

where D_i was the binary diffusion coefficient [m^2/s] of component i, K_B the Boltzmann's constant [1.381·10^{-23} J/K], R_i the component radius [m], T the temperature [K], μ the dynamic viscosity of water [Pa·s], and τ_i the diffusion time [s].

The resulting approximation of the components' diffusivities and diffusion time scales are presented in Table 4.1. The values were calculated for 15 °C (temperature in the space between nozzle and liquid nitrogen in the atomization studies) and for 100 °C (estimate for mean particle temperature in spray dryer). The values only give a qualitative impression of the difference in diffusion speed between the three main milk components. The absolute values should be treated with caution considering the limitations of Stoke-Einstein's equation, such as an assumption of infinite dilution.

Table 4.1: Estimation of binary diffusion coefficients and diffusion time scales for 10 µm diffusion length in water at infinite dilution: Values are based on the approximate radius of casein micelles, calcium caseinate and fat globules as measured by dynamic light scattering and the mean radius of lactose in milk according to (Bylund, 2003).

	Mean radius [nm]	Diffusivity [m^2/s]		Diffusion time scale [s]	
		at 15 °C	at 100 °C	at 15 °C	at 100 °C
Fat globules	300	$7.0 \cdot 10^{-13}$	$4.6 \cdot 10^{-12}$	71	11
Protein micelle/caseinate	75	$2.1 \cdot 10^{-12}$	$2.7 \cdot 10^{-11}$	18	3
Lactose	0.5	$4.2 \cdot 10^{-10}$	$2.7 \cdot 10^{-9}$	0.1	0.02

5 Reduction of Surface Fat Formation on Spray-Dried Milk Powders through Emulsion Stabilization

5.1 Preface

In Chapter 4, and also in Chapter 6 for single droplet drying, it was learnt that the fat surface formation in drying milk particles should be ascribed to the atomization step for the range of atomization techniques and model emulsions investigated. It was hence concluded that the surface fat layer on spray-dried milk powder cannot be significantly reduced by adjusting the spray drying conditions or changing the atomization technique. In industry, the unfavorable powder properties that go along with surface fat are typically reduced be an additional coating step subsequent to spray drying. In the following study, it was explored if this processing step can be made obsolete by strengthening the network of RFMM emulsions prior to spray drying in order to reduce the fat globule size and the occurrence of the proposed perforation mechanism for a reduction of the surface fat. The outcomes of the previous chapter indicated that fat was present at the droplet surface immediately after atomization because the emulsions preferably disintegrated along the oil/water-interface of the fat globules. Therefore, this hypothesis was to be tested and a rheological analysis was conducted in the following study to obtain a better understanding of the milk model emulsions' disintegration behavior and how it was influenced by the presence of a dispersed fat phase.

The following work will be published by Elsevier B.V.:

Foerster, M., Liu, C., Gengenbach, T., Woo, M.W., Selomulya, C., Reduction of surface fat formation on spray-dried milk powders through emulsion stabilization with λ-carrageenan, Food Hydrocolloids, accepted for publication on 4 April 2017

5.2 Abstract

The appearance of surface fat during the atomization process in spray drying of milk particles often impairs the functional powder properties. To investigate a possible approach that could minimize the surface fat formation, the interaction between a whole milk model emulsion and λ-carrageenan at various concentrations was studied, as well as how it influences the atomization behavior and the resulting particle characteristics. Carrageenan can stabilize emulsions in the presence of milk protein by adsorp-

tion on the milk fat globule membranes. If too little or too much of the polysaccharide was added, bridging flocculation or depletion flocculation, respectively, occurred inside the emulsions. The best stability and minimal fat globule size were obtained for a carrageenan content of 0.3 % w/w. Rheological investigation indicated that the extensional viscosity can be an important factor influencing the emulsion disintegration behavior during atomization. The λ-carrageenan stabilized emulsions featured a significantly increased extensional viscosity and a better fat encapsulation in the corresponding spray-dried particles, promoting solubility and oxidative stability. Surface fat extraction showed that the most stable emulsion lead to particles with the least amount of surface fat. Though the surface of these particles was still covered by fat according to spectroscopic analysis, this surface fat layer was very thin in comparison to carrageenan-free powder as observed by confocal microscopy. Yet, the addition of carrageenan was also found to have one adverse effect on the intended powder properties, as the strengthened emulsion network translated into denser particles and thus into a deterioration of the powder's reconstitution behavior.

5.3 Introduction

Whole milk, skim milk and infant formula emulsions are spray-dried to powder form at large industrial scale in order to accomplish better preservation, reduced bulk volume for economy of transportation and easier processing as food ingredients. However, during spray drying usually an unwanted layer of fat occurs on the particles' surface and this leads to detrimental effects on the powder properties, including reduced solubility in water (Fäldt and Bergenståhl, 1996b, Millqvist-Fureby et al., 2001), faster expiration due to lipid oxidation (Granelli et al., 1996, Hardas et al., 2000, Keogh et al., 2001a) and greater stickiness (Kim et al., 2005a, Nijdam and Langrish, 2006). This can mean a deteriorated product quality for the end user and a reduction in efficiency during manufacturing due to significant product loss and the necessity of additional processing steps, such as lecithination. For this reason, it is important to identify the driving forces that cause the formation of surface fat during spray drying of milk powder. A few studies previously speculated that the actual drying stage of the spray drying process might not be primarily responsible, but rather an atomization induced mechanism would already determine the eventual chemical surface composition (Fyfe et al., 2011, Kim et al., 2009b, Xu et al., 2013). The hypothesis was supported by recent studies differentiating the impact of the atomization stage from the drying stage (compare to Chapter 4 and Wu et al. (2014)). By comparing the surface composition of the spray-dried particles with the atomized droplets, which were cryogenically flash-frozen immediately after leaving the nozzle, it was learnt that the freshly generated droplets were already covered by a fat film and that this surface fat coverage remained relatively unchanged throughout the following drying process. It was concluded that the surface fat content is hence not significantly reducible by modifying the spray drying conditions. Also, for the range of atomization nozzles investigated, the atomization triggered fat accu-

mulation on the droplet surfaces was independent of the atomization technique. Instead, a promising way to reduce the amount of surface fat seems to modify the emulsion prior to spray drying in order to moderate the segregation between the lipid and the aqueous phase during atomization. Further, it is crucial to understand the actual mechanism that causes the emulsions to disintegrate in a way that results in the fat being present at the surface as soon as individual droplets are formed.

Therefore, the objectives of the present study were, firstly, to contribute towards a better insight into this mechanism and, secondly, to investigate a potential method to improve the properties of milk powder by modifying the emulsion to be spray-dried. Towards the first aim, milk model emulsions of different compositions were investigated in terms of their break-up behavior under shear and extensional stress. There are various possible approaches to address the second aim. As studies have shown, adding a surfactant, such as polysorbate 80 or lecithin, to milk emulsions or oil/milk protein emulsions and subsequent co-spray drying enhanced the product powders' wettability (Fonseca et al., 2011, Lallbeeharry et al., 2014, Millqvist-Fureby and Smith, 2007). Yet, it was also argued that successive spray drying and lecithin coating, as typically done on industrial scale, still remains more efficient (Tian et al., 2014).

Instead, milk emulsion could be modified in a way that strengthens their stability in order to bring about a greater fat encapsulation upon spray drying, thus making subsequent coating redundant. Firstly, by emulsion stability analyses of milk protein containing oil/water emulsions, heat treatment at temperatures above 60 °C (Millqvist-Fureby et al., 2001), a pH value reduction (Dalgleish, 1997) and addition of calcium ions (Agboola and Dalgleish, 1996a, Agboola and Dalgleish, 1996b) were all shown to be not successful in this regard. However, through thermal pre-treatment at 80 °C Wang et al. (2016) attained a cross-linked emulsion of whey protein isolate and fish oil, whose corresponding spray-dried powders featured improved inhibition of lipid oxidation. Secondly, the fat globule size inside oil/water emulsions, as for instance reduced by mechanical treatment during homogenization *via* microfluidization or ultrasonication, also influences the emulsion stability and thus the amount of surface fat. Yet, the ideal size depends on the type of oil, homogenization technique and spray-dried particle diameter (Jafari et al., 2008, Munoz-Ibanez et al., 2016, Soottitantawat et al., 2003). Thirdly, it has been demonstrated that the adsorption of certain polysaccharides on the membranes around the fat globules of various emulsions can enhance the stability against environmental influences, such as thermal and mechanical stress (Drusch et al., 2007, Gharsallaoui et al., 2010, Guzey et al., 2004). A prominent example is pectin, which was for instance found to improve the storage stability of sunflower oil emulsion with whey protein isolate and sodium caseinate as emulsifiers (Einhorn-Stoll et al., 2005). Serfert et al. (2013) obtained enhanced fish oil encapsulation and oxidative stability of powders from an emulsion that comprised of glucose syrup, whey protein and pectin at pH 4. However, while this polysaccharide with its negatively charged carboxylate groups can adsorb at casein below the latter's isoelectric point (pH of approximately 4.6) and is thus used in stabilization of acid dairy drinks, it is not effective at the pH of milk itself (6.4-6.7) (Kravtchenko et al., 1995, Surh et al., 2006). In contrast, carrageenan, a linear sul-

phated polysaccharide, also undergoes attractive electrostatic interaction with κ-casein at neutral milieu (Dalgleish and Morris, 1988, Dickinson, 1998) and therefore is used as stabilizer in pH neutral dairy beverages that are commercially available (Bixler et al., 2001, FAO, 1987, Yanes et al., 2002). The European Food Safety Authority and the US Food & Drug Association, for instance, have concluded that carrageenan as a food additive is considered as safe (FDA, 2016, SCF, 2003).

Carrageenan is a natural hydrocolloid extracted from red algae and is widely used in food applications to form gels and stabilize beverages. It features one, two or three sulphate groups per disaccharide in its kappa (κ), iota (ι) and lambda (λ) form, respectively. Singh et al. (2003) observed an improvement in creaming stability of a soya oil emulsion that contained 3 % w/w sodium caseinate with increasing κ-carrageenan content from 0 to 0.4 % w/w. For a caseinate content of 0.5 % w/w, however, addition of κ-carrageenan impaired the stability due to flocculation. An emulsion containing flaxseed oil and whey protein reached substantially better stability when mixed with any of the three main carrageenan types, with the best result for λ-carrageenan (Stone and Nickerson, 2012). In skim milk emulsions, ι- and κ-carrageenan were found to induce depletion flocculation at temperatures above their coil-helix transition temperature (which is below 60 °C), because only the charge density of their helix structure was great enough to allow adsorption at the casein membranes (Langendorff et al., 2000). Yet, λ-carrageenan remains an active stabilizer at elevated temperature, which might be particularly beneficial for spray drying applications. Furthermore, the higher density of anionic sulphate groups in the λ-form brings along the advantage of gel inhibition and good water solubility even at lower temperature (room temperature).

A few reports have been published about the stabilization of oil/water emulsions in the presence of carrageenan and one type of milk protein. However, there is a lack of investigation hitherto on the impact of carrageenan for a more complete model system that is representative of whole milk, comprising of all its main components (lactose, whey protein, casein and fat). In addition, carrageenan's subsequent effect on the atomization behavior during spray drying and thus the powder properties, particularly in respect to surface fat formation, is still to be studied. In the first part of the present study, a milk model emulsion was investigated to find the optimum λ-carrageenan content in terms of fat globule size and emulsion stability. In the second part, it was studied whether the stabilization with λ-carrageenan translated into optimized powder properties after spray drying. For this purpose, the powders (and selected atomized emulsion droplets) were analyzed in respect to their component distribution *via* X-ray photoelectron spectroscopy, confocal laser scanning microscopy and surface fat extraction. Powder properties including morphology, solubility, wettability and oxidative stability were compared for different carrageenan concentrations. An important connecting link between modified emulsions and spray-dried particle properties was the emulsions' behavior during atomization. Shear and extensional viscosity analyses gave new insights into the disintegration process and how it is influenced by fat and hydrocolloid content.

5.4 Material and Methods

5.4.1 Emulsion Preparation

Stabilization of a milk model emulsion, which resembled the composition of bovine whole milk, was attempted with λ-carrageenan at various concentrations. The emulsion contained 40.8 % w/w lactose, 31.1 % w/w fat and 27.0 % w/w protein in dry matter and featured a solid content of 20 % w/w. It was prepared by dissolving lecithin free, commercial skim milk powder (home brand from Coles Supermarkets Australia Pty Ltd, Australia) in Milli-Q purified water (Merck KGaA, Germany) with stirring at 47 °C for 1 h. Subsequently, sustainably sourced refined *Elaeis guineensis* palm fruit oil (Auroma Pty Ltd, Australia), with a slip melting point of 37-39 °C and a free fatty acid content (as palmitic) of less than 0.09 %, was added. Following prehomogenization in a high-speed colloid mill (WiseMix Homogenizer HG-15D, Daihan Scientific, South Korea) at 1000 rpm for 1 min, different amounts of λ-carrageenan (Melbourne Food Depot Pty Ltd, Australia) were added to form carrageenan contents of 0, 0.1, 0.2, 0.3, 0.4 and 0.5 % w/w in respect to the total emulsion mass. The emulsions were stirred for further 30 min at 47 °C and then were homogenized in a high pressure homogenizer (EmulsiFlex-C5, Avestin, Canada) with three passes at 1,350 bar and two subsequent passes at 650 bar. The homogenization temperature was not directly controlled, but the sample temperature was measured to be between 45 °C at the beginning of the homogenization process and 35 °C at the end. The emulsions were stored at room temperature and were spray-dried and analyzed by the following procedures within 3 h after preparation if not stated otherwise.

5.4.2 Emulsion Analysis

5.4.2.1 Turbiscan Emulsion Stability, Emulsion Microstructure and pH Value

24 h instability tests of each emulsion were conducted with a Turbiscan Classic MA2000 multiple light scattering instrument (Formulaction SA, France) with a pulsed near-infrared light source (wavelength of 850 nm). The backscattering fraction as a function of the emulsion height inside a cylindrical glass measurement cell was determined every 30 min. These results were compared with the microstructure of original emulsion samples that were stored at 6 °C for up to ten days. Images were taken at various locations inside emulsion drops that were contained between a glass microscope slide and a cover slip under 10× magnifications with a conventional optical microscope (B1-211A, Motic, P.R. China). The pH value was measured with a pH meter (H4212, Hanna Instruments, USA) after homogenization.

5.4.2.2 Fat Globule Size Distribution inside Original Emulsions and after Atomization Process

The emulsion droplet size, henceforth described as fat globule size in order to distinguish from the droplet size of the sprays after atomization in the spray dryer nozzle, was analyzed by laser light scattering using a Mastersizer 2000 apparatus (Malvern Instruments, UK) equipped with a Hydro 2000G wet cell.

Approximately 250 ml of the pre-diluted emulsions (oil content of 0.01 % w/w) were added to the wet cell, which was filled with about 1 l of Milli-Q purified water, to establish a laser obscuration level of 5.2-5.5 % to avoid multiple scattering effects. The instrument operated at laser wavelengths of 633 and 466 nm. The pump and stirrer speeds were set to 1000 rpm and 500 rpm, respectively. The physical properties of the fat globules were described with a refractive index of 1.462 and an absorbance index of 0.1. Four samples were taken from each emulsion to conduct individual measurements of 20 s duration, the standard deviation was determined from this and the average was reported as the mean diameter over volume D(4,3) [m]:

$$D(4,3) = \Sigma(n_j d_j^4)/\Sigma(n_j d_j^3) \tag{5.1}$$

where the particle diameter and number of particles in each size class are expressed by d_j [m] and n_j [-], respectively. The size distribution and the corresponding volumetric mean diameters were determined for the original emulsions after homogenization. In addition, they were also measured for the same emulsions after they had been passed through a spray drying atomization nozzle. The nozzle was operated outside of the spray dryer and the atomized emulsions were collected immediately after leaving the nozzle, and thus no contact with drying air occurred. Two different atomization techniques were investigated: a pressure-swirl single-fluid spray nozzle (MT Brass Series, AmFog Nozzle Technologies Inc, USA) with an orifice of 0.2 mm in diameter at a feed pressure of 500 kPa, and a microfluidic jet nozzle that is described in Section 5.4.3.1.

5.4.2.3 Shear Viscosity and Extensional Viscosity of the Emulsions

Dynamic shear viscosities were measured at 25 °C with a cone and plate rheometer (Haake Mars, Thermo Fisher Scientific, USA), which was equipped with a MP60 measuring plate and a C60/1 cone rotor. Each sample's viscosities were investigated at six different shear rates in the range of 50-500 1/s, and the average of three samples taken from the same emulsion was determined together with the respective standard deviation. Also the dynamic shear viscosities of a pure carrageenan solution with a carrageenan/water ratio similar to the emulsion with 0.5 % w/w carrageenan were measured.

The extensional viscosity was of special interest for interpretation of the jet disintegration mechanism of the microfluidic jet nozzle described in Section 5.4.3.1. For a fluid that does not follow Newtonian behavior, such as the emulsions investigated in this study (see Figure 5.3b), no assumption can be made about the relationship between its viscosity under shear stress and its viscosity under extensional stress. The viscosity of the milk model emulsion was too low for standard capillary-breakup extensional rheometry, however. Therefore, acoustically-driven microfluidic extensional rheometry was employed, which is designed to capture the extensional viscosity of low-viscosity samples (McDonnell et al., 2015a, McDonnell et al., 2015b). These measurements were conducted at room temperature (25 °C) at the School of Engineering, RMIT University in Melbourne, Australia. The rheometer and the mathemat-

ical analysis procedure have been described elsewhere (Bhattacharjee et al., 2011). In brief, a sessile droplet of 1 µl in volume (i.e. approximately 1.2 mm in diameter) was placed onto the piezoelectric substrate surface of a surface acoustic wave (SAW) device. A pulse of SAW energy was then applied to the droplet, causing it to elongate and to form a stable liquid bridge between the substrate and a parallel opposing surface at a gap length of 1.5 mm. At this point the SAW pulse was terminated, allowing the liquid bridge to thin under capillary forces and thus creating a uniaxial extensional flow. The diameter d [m] at the neck of the thinning emulsion filament was recorded with a high-speed camera until it had decreased to half of its initial value (d_0) (see Figure 5.1a as well as Video 2[3]). The evolution of the filament diameter with respect to time was determined with standard image analysis techniques. From this, the Ohnesorge number Oh [-] could be determined by comparison with a series of Newtonian reference samples of a wide range of viscosities, allowing calculation of the extensional viscosity μ_{ext} [Pa·s] by the following expression:

$$\mu_{ext} = 3 \cdot Oh \cdot \sqrt{\rho \cdot \gamma \cdot d_0/2} \tag{5.2}$$

where ρ was the emulsion density [kg/m^3] and γ the initial surface tension of the emulsion [N/m] at 25 °C as taken from Bertsch (1983). Every sample was analyzed by measurement of three individual droplets with ten runs per droplet, and from these the average value was taken and the standard deviation was calculated. As the intention of this analysis was to study the impact of the fat globules on the film disintegration, the emulsion preparation was slightly modified for the purpose of the extensional viscosity measurements. A mixture of lactose, calcium caseinate and whey protein powder was used instead of skim milk powder. Otherwise it would not have been possible to prepare emulsions with very low fat content, as skim milk powder itself still contains a significant amount of fat. Thus, a low-fat emulsion that contained hardly any fat (0.3 % w/w in d.m.) could be compared with regular-fat emulsions featuring 31.1 % w/w fat in d.m. (and 0 or 0.3 % w/w carrageenan). All of these emulsions had a solid content of 20 % w/w, and their ratio of lactose to protein as well as their proportion between caseinate and whey protein were equivalent to the earlier described standard emulsions.

5.4.3 Powder Analysis

5.4.3.1 Powder Production with Microfluidic Multi-Jet Spray Dryer

A microfluidic jet spray dryer, comprehensively described in Section 4.4.2, was used to dry the emulsions under production of monodisperse particles with uniform drying history. In short, the utilized atomization nozzle consisted of a glass tube with an orifice of 100 µm in diameter. A piezoelectric ceramic jacket surrounded the nozzle tip to impose a sinusoidal pulse of 12 kHz, causing disintegration of the feed emulsion jet into individual droplets with uniform size (see Figure 5.1b). The feed was pushed through the nozzle by pneumatic pressure of 34-53 kPa for respective carrageenan contents of 0-0.5 % w/w, accounting for the increasing viscosity. The nozzle was either operated detached from the

[3] Video 2: Thinning emulsion bridge during microfluidic extensional viscometry of a milk model emulsion with 31.1 % w/w fat in d.m. and no carrageenan. Available online as supplementary data: dx.doi.org/10.1016/j.foodhyd.2017.04.005

spray drying apparatus for cryogenic flash freezing of the atomized droplets (described in Section 5.4.3.2) or was positioned onto the drying tower for spray drying. The tower was 3.2 m in height and contained a concurrent drying air flow. The temperatures of the drying air at the top and bottom of the drying chamber were 200 °C and 88 °C, respectively.

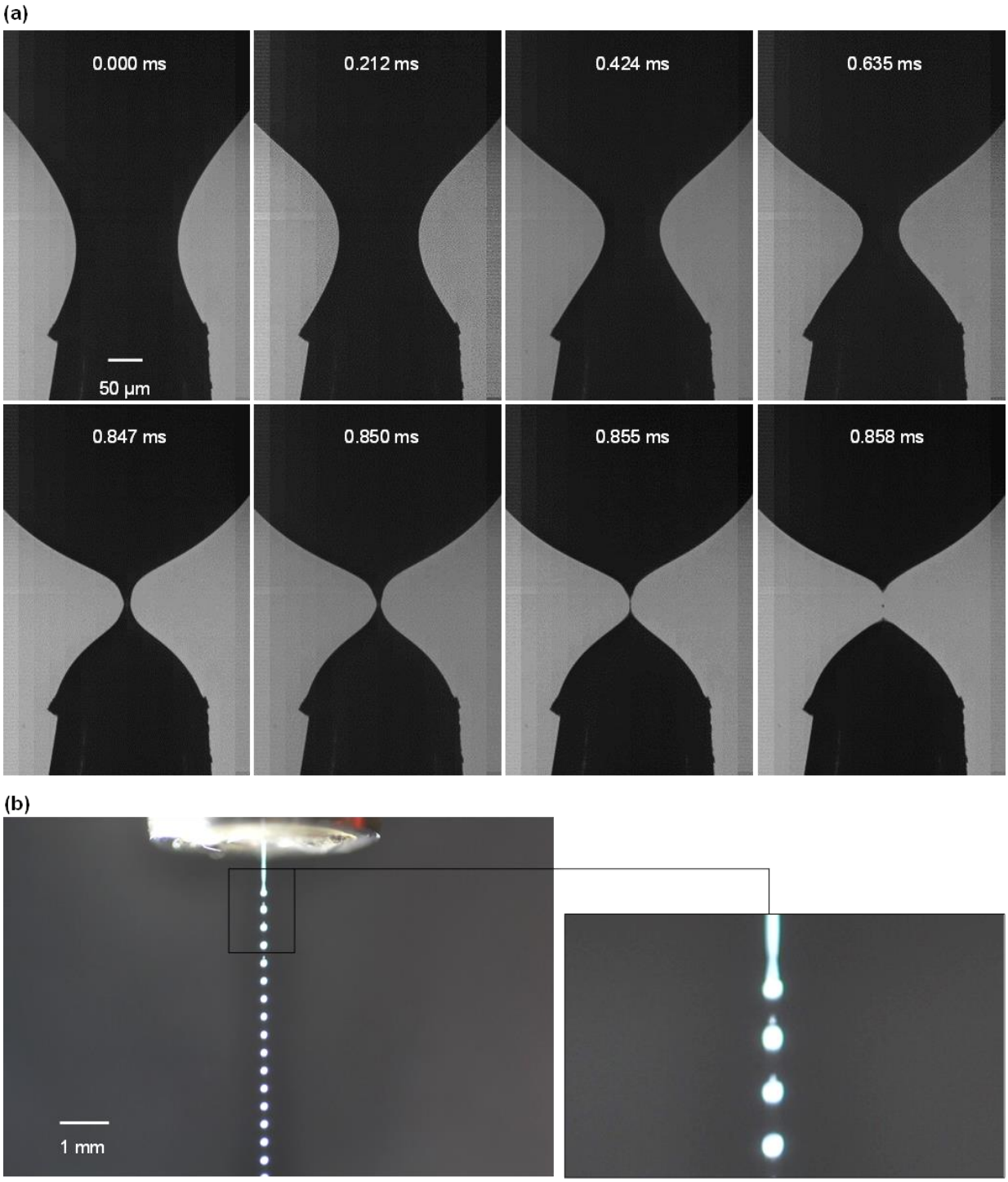

Figure 5.1: Visual comparison of elongational disintegration processes: (a) time sequence of an emulsion bridge during extensional viscometry from commencement of thinning until break-up, and (b) break-up of emulsion jet from microfluidic jet nozzle.

5.4.3.2 Cryogenic Flash Freezing of Atomized Droplets

To facilitate the study of the chemical surface composition and internal component distribution of emulsion droplets as present immediately after atomization, a modified methodology of Rogers et al. (2008) was applied. Milk model emulsion droplets with 0.3 % w/w carrageenan content were flash-frozen in liquid nitrogen at a distance of 10 cm from the microfluidic jet nozzle, which was operated outside of the spray dryer. Afterwards, the droplets were kept in frozen state by cooling with dry ice until freeze drying was carried out for 48 h at 0.1 mbar and with a collector temperature of -80 °C in a FreeZone 2.5 l benchtop freeze-dryer (Labconco Corp, USA). As the microfluidic atomization technique generated monodisperse particles, the mean size of the atomized droplets as well as of the corresponding spray dried particles could be determined by simple image analysis of a small powder sample (100 particles) with a light microscope (B1-211A, Motic, P.R. China) under 4× magnification.

5.4.3.3 Surface Fat Extraction

A modified method of the gentle surface fat extraction method proposed by Wang et al. (2016) was applied. This approach avoided fat removal from the inner part of the particles by limiting the time exposed to the solvent medium. While the free fat on the surface of a powder particle is quickly dissolved by organic solvents, the free fat in the inner part of the particles is extracted considerably slower (Kim et al., 2005b). 1 g of powder was weighed out on a filter paper with a pore size of 2.5 µm (Grade 1803, Filtech Pty Ltd, Australia), which was subsequently transferred into a Büchner funnel. The funnel was filled with 30 ml of petroleum ether (boiling point of 40-60 °C, Sigma-Aldrich Pty Ltd, Australia), wherein the powder rested for 2 min. Afterwards, vacuum filtration was commenced and the powder was washed three times with 20 ml of petroleum ether per pass. The powder filled filter paper was then kept in a drying oven at 33 °C for 24 h for evaporation of any remaining ether residue, prior to a second weighing to determine the extracted amount of surface fat. The study was conducted immediately after spray drying and the original powder samples were also stored at 33 °C ahead of the weighing and fat extraction process to eliminate any impact of adsorbed air humidity on the mass measurements. The surface fat content was determined for three powder samples that were collected for about 20 min each during the same spray drying run at 40, 60 and 80 min after a steady column temperature profile had been reached, and the standard deviation was determined. The amount of extracted free fat was presented as percentage relative to the particles' original total fat content.

5.4.3.4 Spectroscopic Surface Composition Measurements

The chemical surface composition of selected powders was estimated by XPS investigation with an AXIS Nova spectrometer (Kratos Analytical Inc., UK). The spray-dried particles of all carrageenan contents were analyzed, as well as the atomized droplets with 0.3 % w/w carrageenan after cryogenic flash freezing/freeze drying and the spray-dried powders from emulsions with 0.1 and 0.3 % w/w carrageenan after surface fat extraction. The instrument was equipped with a monochromated Al K_α X-ray

source and a hemispherical analyzer that was operated in the fixed analyzer transmission mode with the standard aperture (0.3 mm × 0.7 mm analysis area). The pressure inside the main vacuum chamber was of the order of 10^{-8} mbar. Shallow wells of a custom-built sample holder contained the powders, and two different locations were analyzed for each sample at a nominal photoelectron emission angle of 0º with respect to the surface normal. The actual emission angle is ill-defined in the case of particles (ranging from 0º to 90º), and hence the sampling depth ranged from 0 nm to approximately 10 nm. All detected elements were identified from survey spectra. The respective relative atomic concentrations were determined from the integral peak intensities and sensitivity factors provided by the manufacturer. The concentrations in lactose, protein and fat can be interpreted as linear combination of the atomic surface composition (Fäldt et al., 1993). Each component's fraction at the surface, expressed in atomic concentration, was thus estimated by linearization based on the representative structural formulas of lactose, milk protein and milk fat, as elaborated by Chew et al. (2014).

5.4.3.5 Confocal Laser Scanning Microscopy

The protein and fat distributions inside particles obtained from spray drying of milk model emulsions with 0, 0.3 and 0.5 % w/w carrageenan content were investigated by CLSM. The microscopy technique and the preceding labelling process with hydrophilic Fast Green FCF (bonded to protein) and hydrophobic Nile Red (bonded to the fat phase) have been described in Section 4.4.5.

5.4.3.6 Scanning Electron Microscopy

The morphology of the spray-dried particles was imaged with a field-emission scanning electron microscope (FEI Nova NanoSEM 450 FE-SEM, FEI Corp, USA) using a 5 kV electron beam. The internal features and porosity of particles that had been intentionally cleaved asunder with a thin razor blade were studied as well as the exterior morphology before and after surface fat extraction. The samples were coated with a 2 nm thick Iridium layer to prevent them from electrical charging.

5.4.3.7 Powder Dissolution and Wetting Behavior

Two studies to evaluate the reconstitution behavior of the spray-dried powders were undertaken. First, focused beam reflectance measurement (FBRM) was carried out to monitor *in situ* the dissolution as a function of time. FBRM uses the measured particle chord lengths and their corresponding count rates to quantify the decreasing particle size in the course of dissolution. The working principle of the FBRM device (Lasentec D 600 L-C22-K, Mettler Toledo Ltd, Australia) and the detailed experimental procedure have been described by Fang et al. (2010). In brief, 0.500 g of sample were added on the surface of 25 °C warm water that was contained in a flat 250 ml beaker. The FBRM laser probe was immersed into the water at a well-defined location and an angle of 45 °, and a magnetic stirrer operated at 900 rpm. The measurements had been executed for 20 min with data collection intervals of 2 s. The FBRM measurements were conducted in triplicate with three powder samples that were collected for about 10 min

each during the same spray drying run at 10, 20 and 30 min after a steady column temperature profile had been obtained.

Second, a modified approach of the Niro Analytical Method No. A5a (GEA, 2005) was used to determine the powders' wettability. The wettability, expressed in time in seconds, defines a dried powder's ability to penetrate a still water surface. For this, 0.500 g sample were passed through a funnel onto the quiet surface of Milli-Q purified water (25 °C), which had been filled into a 100 ml measuring cylinder up to the 90 ml mark. A camera (DCR-HC36, Sony Corp, Japan) recorded the wetting process from the time of powder addition until the last particle had overcome the water surface tension and consequently sunk down. The wettability study was run in duplicate with two powder samples that were collected for about 10 min each during the same spray drying run at 100 and 110 min after a steady column temperature profile had been established.

5.4.3.8 Peroxide Value Analysis for Oxidative Stability Study

The oxidative stability of the fat contained in the spray-dried particles of different carrageenan concentrations was compared by means of their peroxide values at intervals of seven days. The powders were stored for 35 days at accelerated storage conditions of 33 °C and ambient air in a drying oven. The peroxide value measurements were carried out following the guidelines given in the Official Methods of Analysis by the Association of Official Analytical Chemists (AOAC, 1990). In short, 2 g of sample were swirled for 30 s in 30 ml of a freshly prepared acetic acid (Univar Inc, USA)/chloroform (Merck KGaA, Germany) mixture (3:2 by volume) that contained 1 ml of a saturated potassium iodate (Sigma-Aldrich Pty Ltd, Australia) solution. The mixture was then kept in dark environment for 5 min prior to addition of 30 ml of water. Subsequently, titration with a 0.002 molar sodium thiosulfate (Sigma-Aldrich Pty Ltd, Australia) solution was conducted under stirring until the yellow color had disappeared. Lastly, 1 ml of an aqueous one per cent starch indicator solution was added and it was further titrated under stirring until the blue color had vanished. For each set of measurements, a blank control without powder was also carried out. The peroxide value PV in [milliequiv. peroxide/kg fat] was calculated by the following expression:

$$PV = S \cdot N \cdot 1000/m_{fat} \tag{5.3}$$

where S was the blank corrected titration volume in [ml], N the normality of the sodium thiosulfate solution in [mol/l] and m_{fat} the mass of fat comprised by 2 g of sample in [g]. The analysis was run in duplicate with samples that were collected for about 40 min each during the same spray drying run at 120 and 160 min after a steady column temperature profile had been reached.

5.5 Results and Discussion

5.5.1 Impact of λ-Carrageenan Content on Emulsion Properties

5.5.1.1 Stability of the Model Emulsions

The preparation of the model emulsions, as described in Section 5.4.1, resulted in complete dissolution of all components. The good water solubility of λ-carrageenan in comparison to the less charged κ and ι forms (Langendorff et al., 2000) permitted its dissolution at a relatively low temperature, which can mean better cost efficiency in industrial applications and the avoidance of protein denaturation leading to reduced emulsion stability (Millqvist-Fureby et al., 2001).

Turbiscan emulsion stability measurements (Figure 5.2) were performed to evaluate the capability of λ-carrageenan to alter the stability of the milk model emulsions at different concentrations as an indicator for the network strength between the oil and water phase. The homogeneity and stability or instability of the emulsions was evaluated by analyzing the Turbiscan backscattering data over sample height as a function of time. The more precisely the scans at different times overlapped, the more stable were the emulsions. The low backscattering values at a sample height of less than 0.6 cm and above 6 cm for even the most stable samples were ascribed to light scattering at the glass bottom of the measurement cell and more light transmission at the very sample top due to the meniscus curvature.

The emulsions without carrageenan and 0.1 % w/w carrageenan were least stable. They featured an increasing backscattering percentage over time throughout the sample height due to larger fat globules as a result of flocculation, and displayed a concomitant appearance of cream at the surface, as was observed from the more pronounced backscattering at the sample top (height > 6 cm) in comparison to the other samples.

The flocculation could be inhibited by the addition of more polysaccharide. According to the width of the backscattering bands, the stability of the emulsion with 0.2 % w/w carrageenan was improved in comparison to lower concentrations and greatest stability was reached for 0.3-0.4 % w/w carrageenan. This indicated that the λ-carrageenan bonded onto the protein of the fat globule membranes and thus stabilized the oil/water interface by preventing coalescence of the fat globules due to their increased electrostatic repulsion. There might have been an electrostatic attraction between carrageenan and whey protein, as suggested by Stone and Nickerson (2012). More often, though, the stabilization of milk emulsions has been attributed to interaction between carrageenan and casein (Dickinson, 1998, Gu et al., 2005, Langendorff et al., 2000), with the latter representing 80 % of the protein contained in bovine milk. The pH values of the milk model emulsions were measured to be in the range of 6.44 ± 0.03, exceeding the casein's isoelectric point of 4.6. While the casein thus carried a negative net charge, the κ-casein molecules still featured positive amino acid residue regions, as generally believed

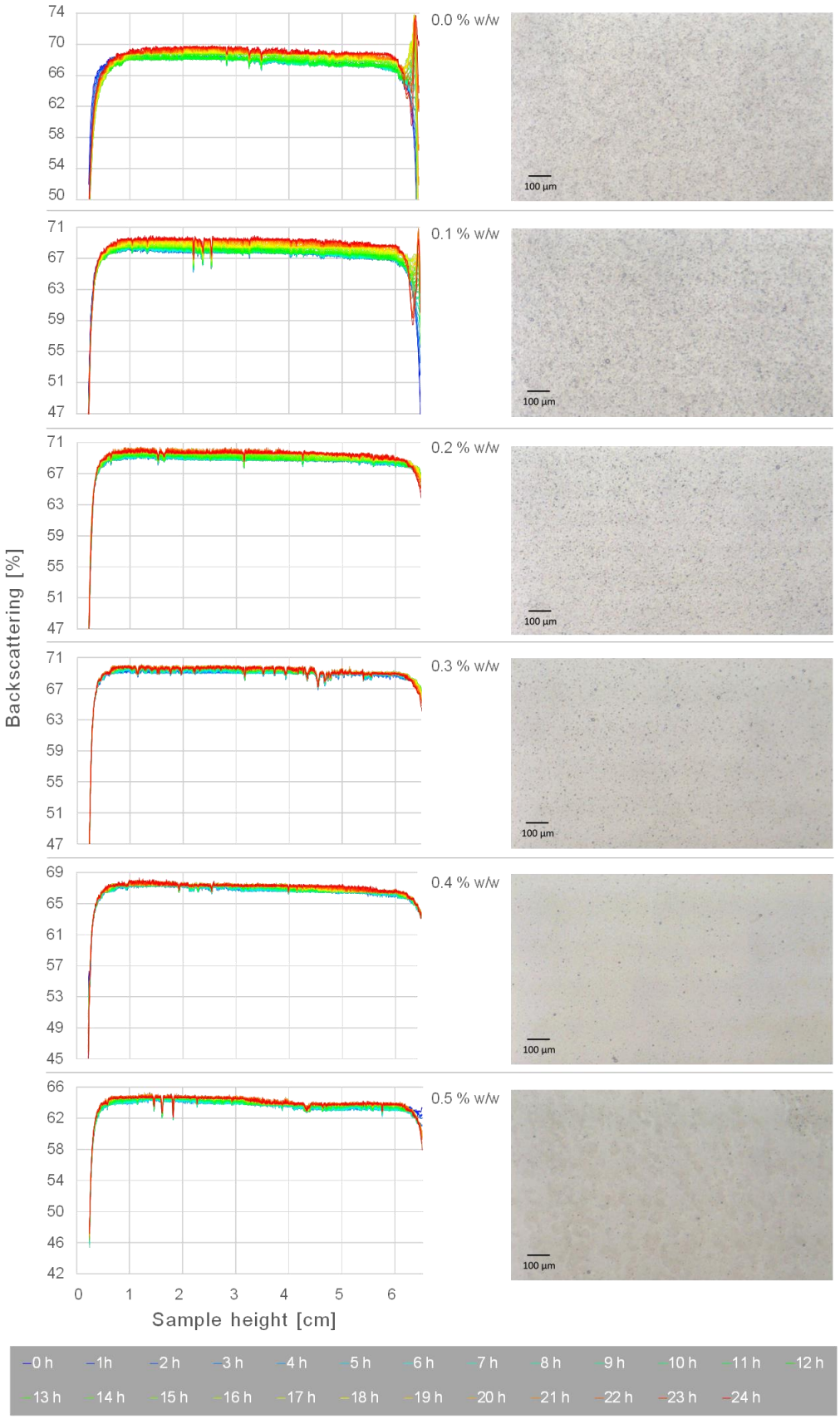

Figure 5.2: Model milk emulsion stabilities depending on λ-carrageenan content: Turbiscan backscattering measurements over time, and corresponding representative microscope images of the microstructures in the freshly prepared emulsions.

(Snoeren et al., 1975). This allowed absorbance of the negatively charged sulphate groups of the carrageenan at the positively charged patches of the membranes that surrounded the fat globules. The complexation increased the overall charge of the fat globule membranes towards more negative values. Dalgleish and Morris (1988) found from ζ-potential measurements using micro-electrophoresis that the negative charge density on casein/λ-carrageenan complexes in strongly diluted skim milk approximately doubled with very low carrageenan contents from about 0.001 to 0.01 % w/w. Higher concentrations lead to a further, though less sharp increase in charge density within the range investigated (maximum of approximately 0.02 % w/w). The flattening of the charge curve at greater carrageenan concentrations was ascribed to the cationic protein surfaces reaching saturation coverage, and it was presumed that this would have led to cross-linkage and depletion flocculation if the total solid content had been higher.

In agreement with the work by Dalgleish and Morris (1988), in the present study further carrageenan addition (from 0.4 to 0.5 % w/w) resulted in physical emulsion destabilization. The backscattering profile of the emulsion with 0.5 % w/w carrageenan resembled the one of 0.2 % w/w, being more constant over time than for 0 and 0.1 % w/w. However, the emulsion was less stable than for 0.3 and 0.4 % w/w, which presumably was as a result of depletion flocculation upon saturation surface coverage of the positively charged protein areas (see Appendix 4.B for a supporting theoretical calculation of the saturation concentration). Depletion flocculation is often observed in colloidal systems when the droplets of the dispersed phase are surrounded by an adsorbed layer of polymer, which simultaneously exists in excess inside the continuous phase. As discussed by Langendorff et al. (2000), if the carrageenan concentration exceeds the saturation level to a certain degree, the free carrageenan will repulse the carrageenan-covered surfaces of the fat globules and protein aggregates and will consequently induce coalescence of the lipid phase.

The Turbiscan stability results were compared with the corresponding microstructures of the freshly prepared emulsions as visualized by the microscopic images in Figure 5.2. The emulsion with 0.5 % w/w carrageenan had relatively large patches of darker shade, suggesting phase separation throughout the emulsion with the dark patches being interconnected areas of flocculated fat globules. These patches were not observed at concentrations of 0.3-0.4 % w/w carrageenan, where the microstructure appeared most homogeneous amongst all samples. Here only a few dark spots were observed, because the majority of the flat globules did not coalesce and thus were so finely dispersed inside the continuous phase (the brighter, grey regions in the images) that they were not visible under the microscope at the given magnification. In comparison, at lower polysaccharide contents the appearance of the emulsion microstructure was more heterogeneous with substantially more and larger dark spots, probably due to the formation of more and larger clusters by coalescence of fat globules. These most likely further coalesced over time, leading to the observed creaming. It was confirmed that the visual homogeneity of the microstructure correlated with the emulsion stability by tracking the changes over several days in an emulsion (0.3 % w/w carrageenan content), which was stored at 6 °C (Figure 5.8 in Appendix

4.A). While being relatively homogeneous initially, after the first 24 h larger coalesced lipid globules became visible and after ten days some grey patches had eventually emerged, similar in their appearance to what was observed for the fresh model emulsion of 0.5 % w/w carrageenan content. It can thus be concluded that the microstructure images supported the Turbiscan stability results.

5.5.1.2 Fat Globule Size Distribution and Shear Viscosity of the Model Emulsions

First and foremost, Figure 5.3a compares the impact of the λ-carrageenan concentration on the size distribution of the fat globules together with the free casein micelles inside the original, untreated model emulsions. At the lowest polysaccharide concentration of 0.1 % w/w, the fat globules featured maximal size with a mean emulsion diameter of 1.09±0.01 µm, which was slightly larger than in case of the carrageenan-free model emulsion. This observation was explained by bridging flocculation, where the polysaccharide chains are only loosely adsorbed on the protein of the fat globule membranes and hence may develop bridges between the fat globules, leading to physical instability. Such a bridging flocculation has also been reported for other emulsions at low polysaccharide concentration, such as by Serfert et al. (2013) for a fish oil/β-lactoglubin emulsion at 0.05-0.15 % w/w pectin concentration and by Dickinson and Pawlowsky (1997) for a n-tetradecane/bovine serum albumin emulsion at 0.001-0.04 % w/w ι-carrageenan concentration. In the present study, doubling the λ-carrageenan concentration to 0.2 % w/w prevented bridging flocculation and thus resulted in a sharp decline in fat globule size. The emulsion size was further reduced by adding more carrageenan of up to 0.4 % w/w, although the mean volumetric diameters for 0.3 and 0.4 % w/w only differed slightly. A minimal emulsion size of 0.66±0.0019 µm in diameter was thus achieved.

This minimum coincided with the previously described saturation surface coverage concentration and an establishment of optimum emulsion stability at 0.3-0.4 % w/w carrageenan (Appendix 4.B and Section 5.5.1.1). The physical stabilization with carrageenan prevented coalescence of the fat globules. As can be seen in Appendix 4.A (Figure 5.9), the volumetric size distribution of the emulsions was bimodal, consisting of two main peaks at approximately 0.2 and 1.5 µm. The first peak of the fat globule size distribution overlapped with the peak of the free casein micelles with their aforementioned volumetric mean diameter of 0.14 µm. The first peak was not representing the casein micelles alone, because its volume was closely related to the volume of the second peak as influenced by the carrageenan content. From 0.1 to 0.3 % w/w, the volume of the second peak decreased more and more (decrease in height from approximately 6.5 % to 4.5 % and 3.5 %). The mass of the fat phase was conserved with a corresponding increase in volume of the first peak (increase in height from approximately 5.5 % to 8.7 % and 9.6 %). This occurred because coalescence of the smaller fat globules was inhibited by greater electrostatic repulsion due to λ-carrageenan adsorption. Comparing the emulsion of 0.1 % w/w with the carrageenan-free emulsion, the size distribution shifted towards the larger fat globules of the second peak due to bridging flocculation.

Additionally, Figure 5.3a also illustrates the changes in fat globule size during film disintegration in the two investigated atomization nozzles. In both cases and independent from the carrageenan concentration, the fat globules did not coalesce during atomization, but underwent a decrease in mean diameter by 6 % in average. The mechanical stress inside the nozzles caused a break-up of some of the larger fat globules, as can be deduced from a slight reduction of the second peak in all atomized emulsions in comparison to the size distribution of the original emulsions (see Figure 5.9 in Appendix 4.A).

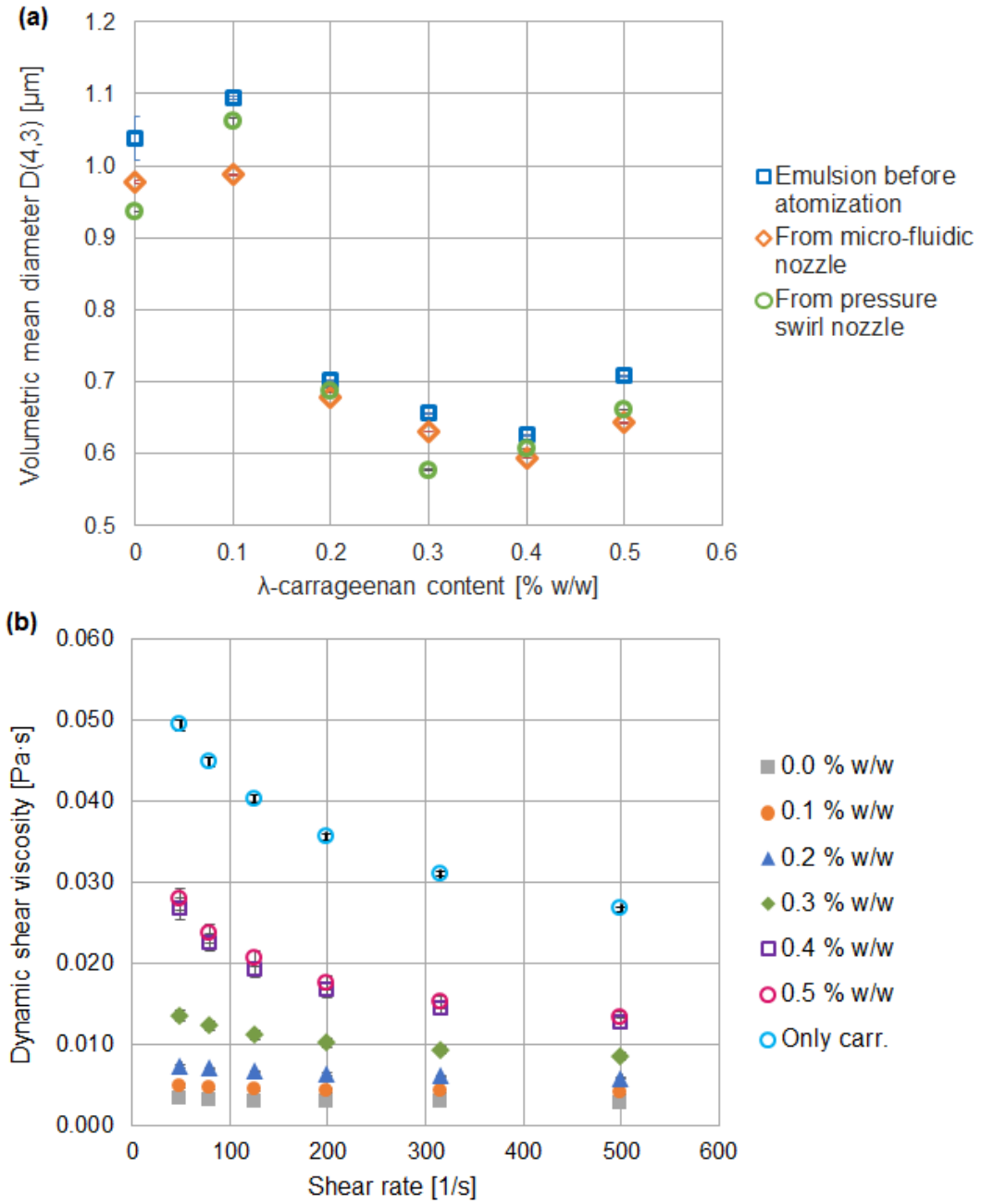

Figure 5.3: Properties of the model milk emulsions at different λ-carrageenan contents: (a) mean volumetric particle sizes in original emulsion and in collected emulsion after disintegration by one of the two atomization nozzles as measured with laser light scattering, and (b) dynamic shear viscosities obtained from cone and plate rheometer measurements (25 °C), including pure carrageenan solution with carrageenan/water ratio being similar to the emulsion with 0.5 % w/w carrageenan.

Aside from the observed reduction in droplet size of the dispersed phase, hydrocolloids can primarily enhance emulsion stabilities by means of their thickening effect. Despite λ-carrageenan being non-gelling, the dynamic shear viscosity of the model emulsions increased considerably with carrageenan content, particularly in the range of 0.2 to 0.4 % w/w (Figure 5.3b). An increase in carrageenan concentration to 0.5 % w/w lacked a further appreciable rise in shear viscosity. The increasing shear viscosity with higher carrageenan content presumably was a consequence of the increasing presence of adsorbed carrageenan on the milk fat globule membranes. Bridging flocculation at low carrageenan concentration (0.1 % w/w) is believed to be the reason why there was only a minor rise in dynamic shear viscosity in comparison to the carrageenan-free emulsion. At higher carrageenan concentrations, the shear viscosity increased simultaneous with improving emulsion stability until the saturation level of the protein surface areas of the fat globule membranes and casein micelles had been reached at about 0.4 % w/w carrageenan content. From 0.4 to 0.5 % w/w, the shear viscosity did not increase further to any significant extent, which can be explained by depletion flocculation. This is supported by comparison with the dynamic shear viscosity of the pure carrageenan solution, which had a water/carrageenan ratio similar to the emulsion with 0.5 % w/w. The shear viscosity of that solution was appreciably greater than the one of the 0.5 % w/w emulsion (for instance, 0.049 mPa·s in comparison to 0.028 mPa·s at a shear rate of 50 1/s), because there was no flocculation in the carrageenan-water solution and all of the carrageenan was unabsorbed, forming a network free of a dispersed phase. Variation of the shear rate revealed non-Newtonian, shear thinning behavior, being more distinct at greater carrageenan concentrations. As such, the viscosity under extensional stress was not computable from the shear viscosity, but had to be determined experimentally.

5.5.1.3 Impact of Fat and Carrageenan Content on Shear and Extensional Viscosities

It was hypothesized that the extensional viscosity can be a crucial factor of influence on the atomization behavior of emulsions during spray drying. The atomization technique of the microfluidic nozzle employed in this study was not based on shear stress, but it imposed a normal stress on the emulsion jet *via* a sinusoidal contraction of the orifice. Figure 5.1 visualizes the similarities between the microfluidic jet atomization and the acoustically-driven microfluidic extensional viscometry. In either case, the emulsion film was forming a fine thread that thinned more and more with distance from the nozzle orifice or with measurement time, respectively. At some point, depending on the viscous forces, excess surface energy was then reached, causing the thread to break up into an individual droplet to regain minimal surface energy. To better understand the impact of a dispersed fat phase and the emulsion stabilization with carrageenan, the extensional and shear viscosities of selected emulsions were compared (Table 5.1). The extensional viscosities were determined according to Eq. (5.2) from the data illustrated in Appendix 4.C (Figure 5.10).

The low-fat emulsion with a lipid content of only 0.3 % w/w in d.m. and the regular-fat emulsion with a fat content similar to the standard model emulsions (31.1 % w/w in d.m.) were compared to evaluate the

impact of the fat globules. Their presence caused a strong decrease in extensional viscosity to less than half the value of the low-fat emulsion (from 25.9 to 11.5 mPa·s). There was also a drop in dynamic shear viscosity, which, however, was marginal by comparison with 15 % from 3.75 to 3.17 mPa·s. The sharp decrease in extensional viscosity provides an explanation for the reduction in milk droplet size with higher fat content upon atomization with a microfluidic jet nozzle as observed in a previous study (Chapter 4), where similar emulsions were investigated. While the regular-fat emulsion had a solid content of 20 % w/w in the aforementioned study, the low-fat emulsion contained only 14 % w/w solids and thus featured a lower shear viscosity (2.4 mPa·s) than the regular-fat emulsion. Therefore, consideration of the shear viscosities could not explain the measurement of smaller droplet sizes in the presence of fat, as a greater viscosity typically favors the formation of bigger droplets (Lefebvre, 1989). In light of Table 5.1, not only the shear viscosity but in particular the extensional viscosity needs to be taken into account to describe the droplet disintegration mechanism during atomization in spray drying..

Table 5.1: Rheological impact of fat phase and λ-carrageenan: composition, dynamic shear viscosity (at shear rate of 199.1 s^{-1}) and uniaxial extensional viscosity of a low-fat emulsion without λ-carrageenan, a regular-fat emulsion without λ-carrageenan and similar fat content to the standard model emulsions, and a standard model emulsion with 0.3 % w/w λ-carrageenan.

Carrageenan content [% w/w]	Fat content [% w/w in d.m.]	Solid content [% w/w]	Shear viscosity [mPa·s]	Extensional viscosity [mPa·s]
0	0.3	20	3.75 ± 0.07	25.9 ± 1.5
0	31.1	20	3.17 ± 0.02	11.5 ± 0.8
0.3	31.1	20	10.20 ± 0.05	30.7 ± 2.8

A perforation mechanism induced by the fat globules is proposed to explain the observed sharp drop in extensional viscosity with the existence of a significant lipid content. The intrinsic milk emulsion stability might be locally reduced along the oil-water interfaces formed by the fat globules. With more fat globules being dispersed throughout the regular-fat emulsion, the emulsion became perforated by these areas of lower stability. During atomization under elongational stress, the film hence disintegrated preferably along the fat globules, following the lowest viscous resistance, figuratively speaking, like the ‘zipper of a jacket’. Such a perforation mechanism had already been briefly discussed several decades ago, when Dombrowski and Fraser (1954) and Zakarlan and King (1982) undertook photographic studies of the disintegration of fan-shaped, flat liquid sheets that were generated with a single-hole fan-spray nozzle. The films broke earlier, that is at greater film thickness, in the presence of a dispersed oil phase. Furthermore, recent investigations reported that during the spray drying of milk emulsions surface layers of fat existed on the droplets immediately after atomization for various kinds of atomization techniques: microfluidic jet nozzles of different orifice size, pressure swirl nozzles of different orifice size

and operated at different feed pressures, and droplet generation with a micro-volumetric syringe (compare to Chapter 4, Chapter 6 and Wu et al. (2014)).

A film disintegration localized along the dispersed fat phase would explain why the droplet surfaces were covered by fat as soon as individual droplets had been formed. If the emulsion preferably breaks up along the interface of the fat globules, the fat globules were immediately present on the surface of the formed droplets, presumably in form of a more or less consistent monolayer of fat globules that might either rupture or stay intact until completion of the spray drying process. In view of that, it was anticipated that the amount of surface fat on spray-dried milk particles should be reducible by decreasing the size of the fat globules inside the emulsions with the addition of λ-carrageenan. Also, the emulsion stabilization with carrageenan was hoped to shift the disintegration mechanism away from the fat globules.

Investigation of the impact of λ-carrageenan (0.3 % w/w) on the viscosity of the standard regular-fat emulsion showed that the carrageenan increased the extensional viscosity significantly (Table 5.1). The milk model emulsion with 0.3 % w/w λ-carrageenan featured an extensional viscosity of 30.7 mPa·s, which was by a factor of 2.7 greater than the one of the polysaccharide-free emulsion of identical fat content. The loss in extensional viscosity due to addition of the lipid phase was consequently overcome and the extensional viscosity was even greater than the one of the low-fat emulsion. Accordingly, the diameter of the monodisperse droplets immediately after atomization was slightly larger for 0.3 % w/w (122 ± 2 µm) in comparison to the carrageenan-free emulsion droplets (115 ± 2 µm). This indicated that the stabilized emulsions might have less preferably disintegrated along the dispersed fat phase.

5.5.2 Impact of λ-Carrageenan Content on the Spray-Dried Particles' Properties

5.5.2.1 Chemical Surface Composition

The amount of surface fat on the spray-dried particles was significantly reduced at certain carrageenan concentrations, as determined by surface fat extraction (Figure 5.4a). The surface fat amounted to 4.7 % for 0.3 % w/w carrageenan, in contrast to 13.8 % for the carrageenan-free powder. The extent of surface fat formation during spray drying was approximately inversely proportional to the emulsion stability, as the lowest amount was observed at intermediate carrageenan concentrations. Being at 0.2-0.3 % w/w, this was slightly offset from the optimum emulsion stability and fat globule size values at 0.3-0.4 % (Figure 5.2 and Figure 5.3a). In agreement with this finding, a more efficient fat encapsulation with decreasing fat globule size inside the emulsions to be spray-dried, indicating greater emulsion stability, was also reported in other studies (Jafari et al., 2008, Sarkar et al., 2016). A strengthened network between the lipid and aqueous phases through stabilization of the milk fat globules by adsorption of λ-carrageenan, as also reflected by the substantial increase in extensional viscosity, possibly led to a reduction of the in Section 5.5.1.3 discussed perforation mechanism. As the network along the fat globules was reinforced, it is believed that the emulsion film disintegrated less preferably along the phase

interfaces and thus a less fat emerged on the surfaces upon droplet formation. The emulsion stability seemed to entail a decisive influence, since the fat proportion at the surface went up again to 10.0 % for the emulsion with the highest carrageenan concentration of 0.5 % w/w, which presumably was subject to depletion flocculation. Other than that, the reduction in fat globule size in the stabilized emulsions (discussed in Section 5.5.1.2) possibly contributed directly to the observation of less surface fat.

From the fat extraction data, the thickness of the surface fat was roughly estimated under the assumption of a continuous fat layer that had the same composition as measured for the first few nanometers of the surface by XPS (albeit this is not the case in reality). Surface fat thicknesses of 1.0, 0.9, 0.4, 0.4, 0.6 and 0.6 µm were calculated for the respective powders from emulsions with 0-0.5 % w/w carrageenan. Interestingly, these estimations approximately corresponded to the respective sizes of the fat globules as measured inside the emulsions (Figure 5.3a). This suggested that about a monolayer of fat globules, albeit presumably to some extent in ruptured form, might have been present on the spray-dried particle surfaces. This is in conformity with the proposed surface fat formation mechanism in consequence of preferred disintegration along the dispersed fat phase during atomization. In view of this, a smaller fat globule size led to less thick surface fat on the generated droplets and thus on the spray-dried particles.

The analysis of the surface concentration (Figure 5.4b) only showed minor differences between the powder samples. As the XPS surface concentration in lactose, protein and fat on the various spray-dried powders was a linear estimation derived from the atomic concentrations, the small differences between the samples were not statistically significant. More generally, the XPS results showed that the powders consisted almost completely of fat (approximately 88-94 % v/v) at the outmost surface layer and addition of carrageenan could not inhibit the creation of a dominant fat coverage along the outmost particle surface. As such, XPS analysis did not reflect the strong influence of the carrageenan content on the extent of surface fat that was revealed by surface fat extraction. Protein took up the remaining volume of the analyzed surface layer, which was depleted in lactose.

For 0.3 % w/w carrageenan inside the model emulsion, Figure 5.4b also compares the surface concentration of spray-dried powder particles with the one of the corresponding droplets immediately after atomization for 0.3 % w/w carrageenan. Apparently, a surface fat layer had already been formed during atomization (77 % v/v fat) and the XPS surface concentration did not change significantly throughout the succeeding drying stage. It was concluded that at least some of the fat globule membranes got ruptured at the droplet surfaces by mechanical or thermal stress during atomization or drying, and the free fat could spread over wide areas of the droplet surface. If the majority of the membranes was still intact, the XPS measurement would most likely have indicated greater protein surface concentrations, because the thickness of the adsorbed casein layers in homogenized milk model emulsions are typically in the range of approximately 5-11 nm (Dalgleish et al., 1995, Fang and Dalgleish, 1993), which coincides with the XPS measurement depth of less than about 10 nm. Instead, as a result of the presumed membrane rupture of at least some of the fat globules at the surface, primarily the lipid phase was detected by

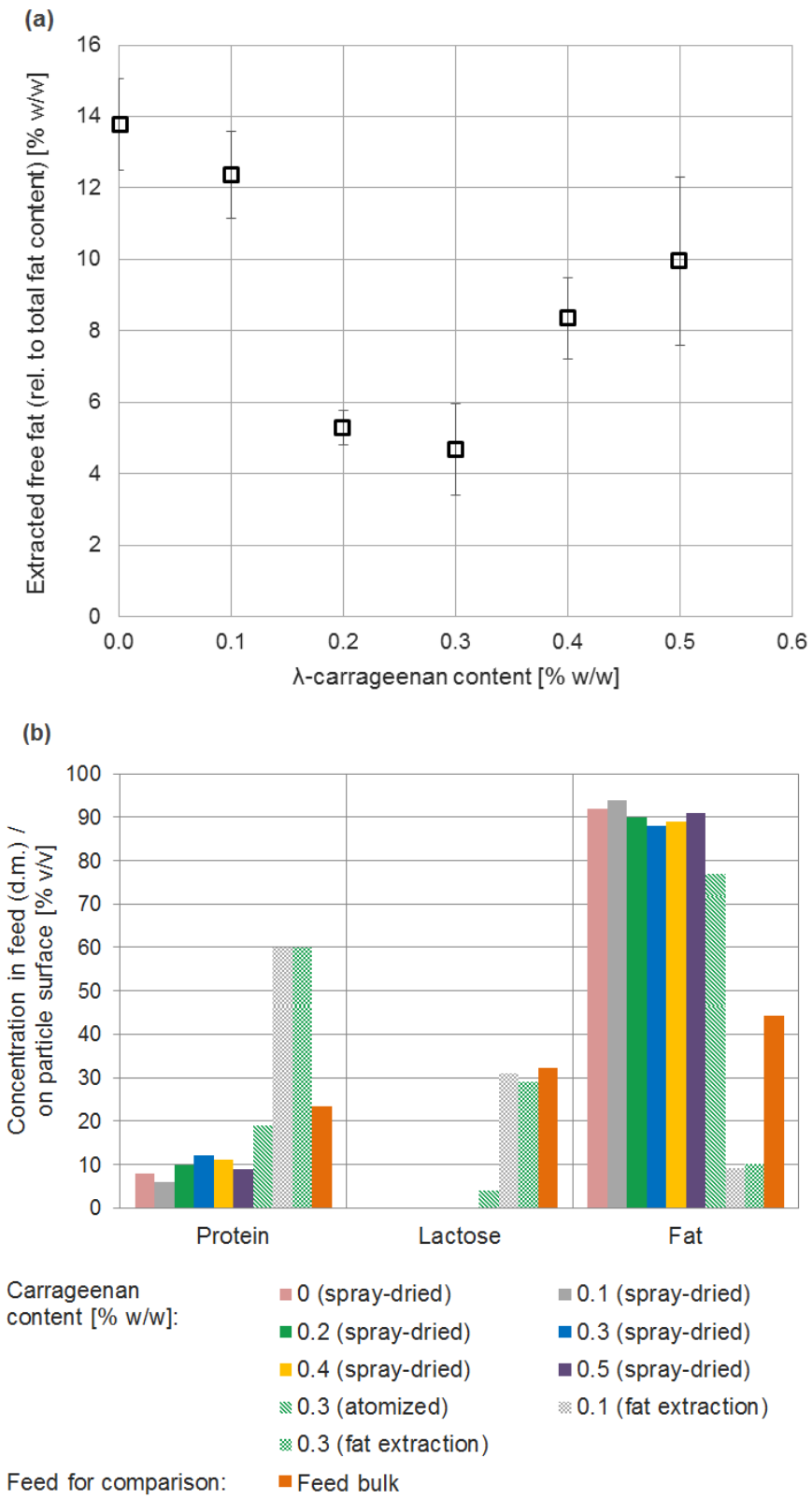

Figure 5.4: Impact of λ-carrageenan content of the model milk emulsions on the corresponding spray-dried particles' surface composition: (a) free surface fat from extraction study, and (b) estimated XPS surface composition of the spray-dried particles for all carrageenan concentrations, of the droplets with 0.3 % w/w directly after atomization and of the spray-dried particles from emulsions with 0.1 and 0.3 % w/w after surface fat extraction.

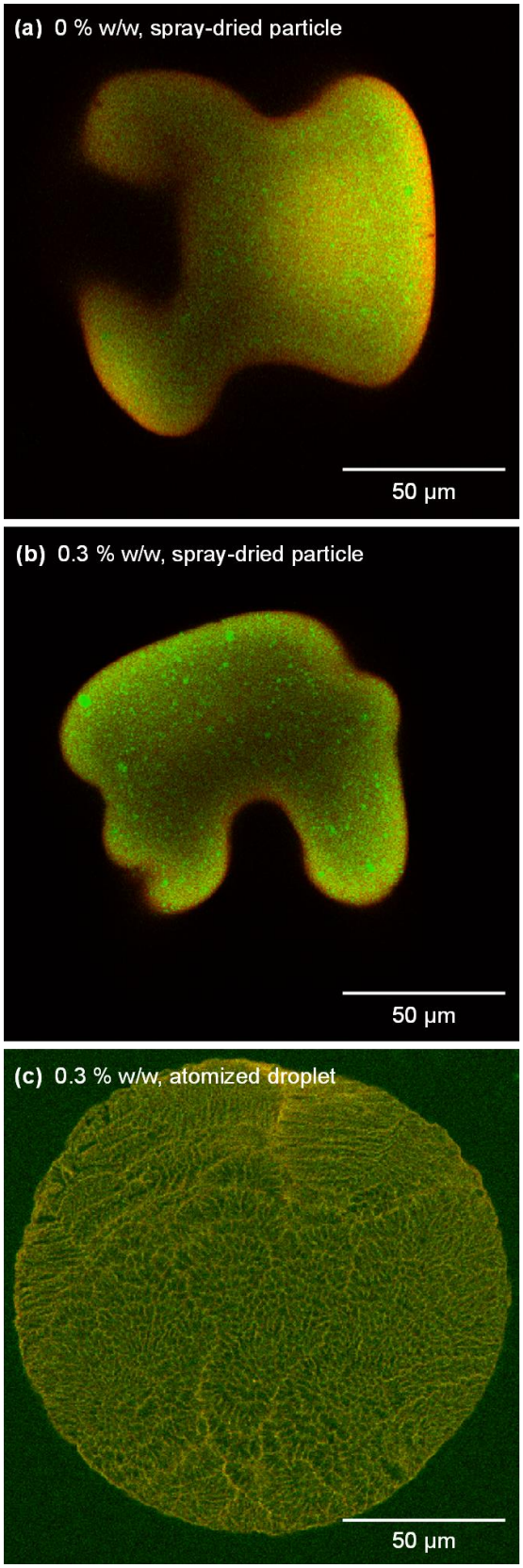

Figure 5.5: CLSM images of distribution of protein (signal from Fast Green FCF visualized in green) and fat (signal from Nile Red in red): (a,b) cross-section of spray-dried particles with λ-carrageenan contents of 0 and 0.3 % w/w, and (c) cross-section of atomized droplet (after flash freezing and freeze drying) with 0.3 % w/w λ-carrageenan.

XPS. The fat surface concentration did not reach 100 % v/v, nevertheless, because not all globules got ruptured at the surface (see Section 5.5.2.2) and some protein of the original membranes might have remained near the surface or other protein diffused to the surface during the drying stage due to its surface activity. Regarding the extent of globule rupture, the adsorbed carrageenan layers presumably had an indirect influence on the membrane stability: the membranes of the smaller fat globules, as for instance obtained by emulsion stabilization with carrageenan at intermediate concentrations, were less susceptible to rupture than the ones of the largest globules (Xu et al., 2013).

The protein and fat distributions obtained from confocal laser scanning microscopy showed that the surfaces of all spray-dried particles were covered by a fat layer (Figure 5.5a,b). Moreover, the thickness of the fat surface layers strongly varied with carrageenan content. For 0 % w/w, the signal of the surface fat was stronger and reached further into the inner of the particle in comparison to 0.3 % w/w (also compare to Video 3[4] and Video 4[5]). The component distribution in the atomized droplets of 0.3 % w/w carrageenan content appeared to already feature a hardly visible fat surface layer (Figure 5.5c). The low visibility of this thin surface layer was ascribed to the limited resolution of the CLSM image and the porous surface structure of the atomized droplets after freeze drying. The variation of the thickness of the surface fat observed from CLSM thus explained why the surface fat extraction demonstrated a strong dependence of the amount of surface fat on the carrageenan content. Additionally, as even for low surface fat contents the outmost surface was comprised predominantly by fat, the CLSM images also explained why the XPS measurements, which accounted only for the composition at the very particle surface due to the short sampling depth, detected a fat dominance at the surfaces throughout all spray-dried powders and on the atomized droplets.

5.5.2.2 Particle Morphology and Porosity

In addition to the chemical surface composition, also the particle morphology and porosity can affect the functional properties of milk powder. SEM investigation showed that the particle surfaces obtained from emulsions without carrageenan or with low concentration thereof featured convex bumps of 2-4 µm in diameter (Figure 5.6a,b). With more polysaccharide, the particle surfaces became smoother (Figure 5.6d,e). Comparing the particle surfaces at 0.1 % w/w before and after surface fat extraction (Figure 5.6b,c), the convex bumps had disappeared after the extraction process and instead concave dimples of approximately similar size and distribution density remained. It was hence concluded that the bumps consisted of fat and were formed during spray drying under coalescence of fat globules on the drying particles' surfaces. Accordingly, it appears that not all of the fat globule membranes that were located at the droplet surfaces underwent rupture (compare to Section 5.5.2.1). With the addition of λ-carrageenan, the negative charge of the fat globules' membranes rose and thus coalescence of fat globules on the surfaces was inhibited and less to no bumps were observed.

[4,5] Video 3 and Video 4: CLSM stack animations of protein (green) and fat (red) distribution inside spray-dried particles from emulsions without carrageenan and 0.3 % w/w carrageenan, respectively, from the top to about the middle in 1 µm steps. Available online as supplementary data: dx.doi.org/10.1016/j.foodhyd.2017.04.005

Comparing the CLSM images before and after the drying stage (Figure 5b,c), it appears that protein clusters had been formed during drying or storage, at least in the protein-rich inner of the particles. It is well known that in spray-dried high-casein powders the casein has a tendency to form networks of interconnected micelles with low solubility in aqueous media (Crowley et al., 2016, Schuck et al., 2007). Also, it has been suggested in literature that, at elevated temperature of sufficient height and duration, whey protein exposes hydrophobic amino acid residues that then undergo linkage with casein micelles, leading to hydrophobic aggregate formation (Corredig and Dalgleish, 1999). The reported protein aggregate formation occurred for particles that were very high in protein, whereas in the present study the particle surfaces were dominated by fat. It is hence doubtful whether here such hydrophobic protein aggregates could have developed at the particle surfaces.

Although the external surfaces of all powder samples were non-porous, the internal cross-sections contained macro-porous structures, which were more pronounced at lower carrageenan content (Figure 5.6f-i). It is hence believed that the strengthening of the emulsion network by addition of carrageenan translated into denser particles upon spray drying. This also explains why the spray-dried particles from emulsions with 0 and 0.3 % w/w carrageenan were of similar size (91 ± 4 and 90 ± 3 µm in diameter, respectively), despite the atomized droplets being about 7 µm larger for 0.3 % w/w (see Section 5.5.1.3). Thus, both the amount of surface fat as well as the particle porosity is to be taken into account when discussing the impact of carrageenan on the functional powder properties.

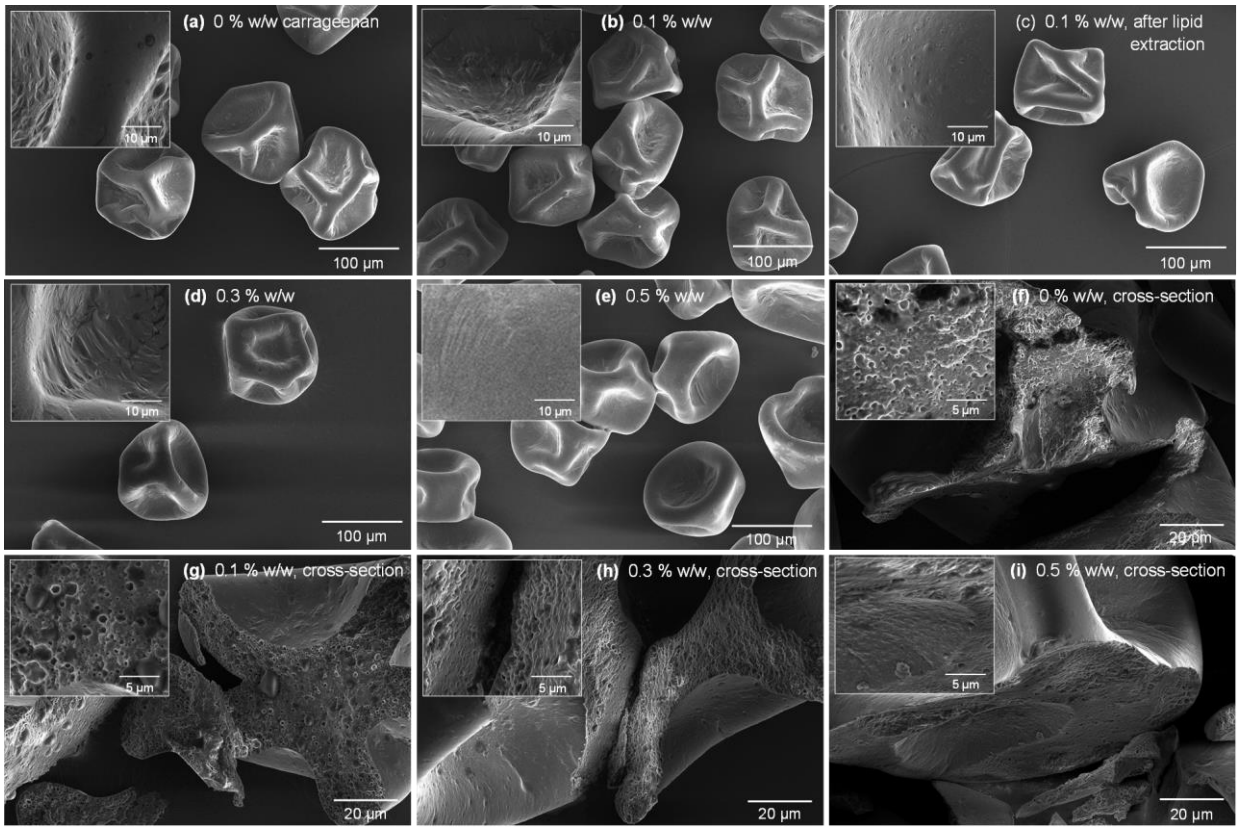

Figure 5.6: Morphology and porosity of spray-dried particles as influenced by λ-carrageenan content: (a-e) particle surfaces with (c) being after surface fat extraction, and (f-i) cross-sections.

5.5.2.3 Functional Powder Properties

Figure 5.7a illustrates the results of the dissolution and wettability studies. At the end of the FBRM dissolution test, the particle size, as represented by the median chord length, was generally larger for any λ-carrageenan concentration in comparison to the carrageenan-free powder.

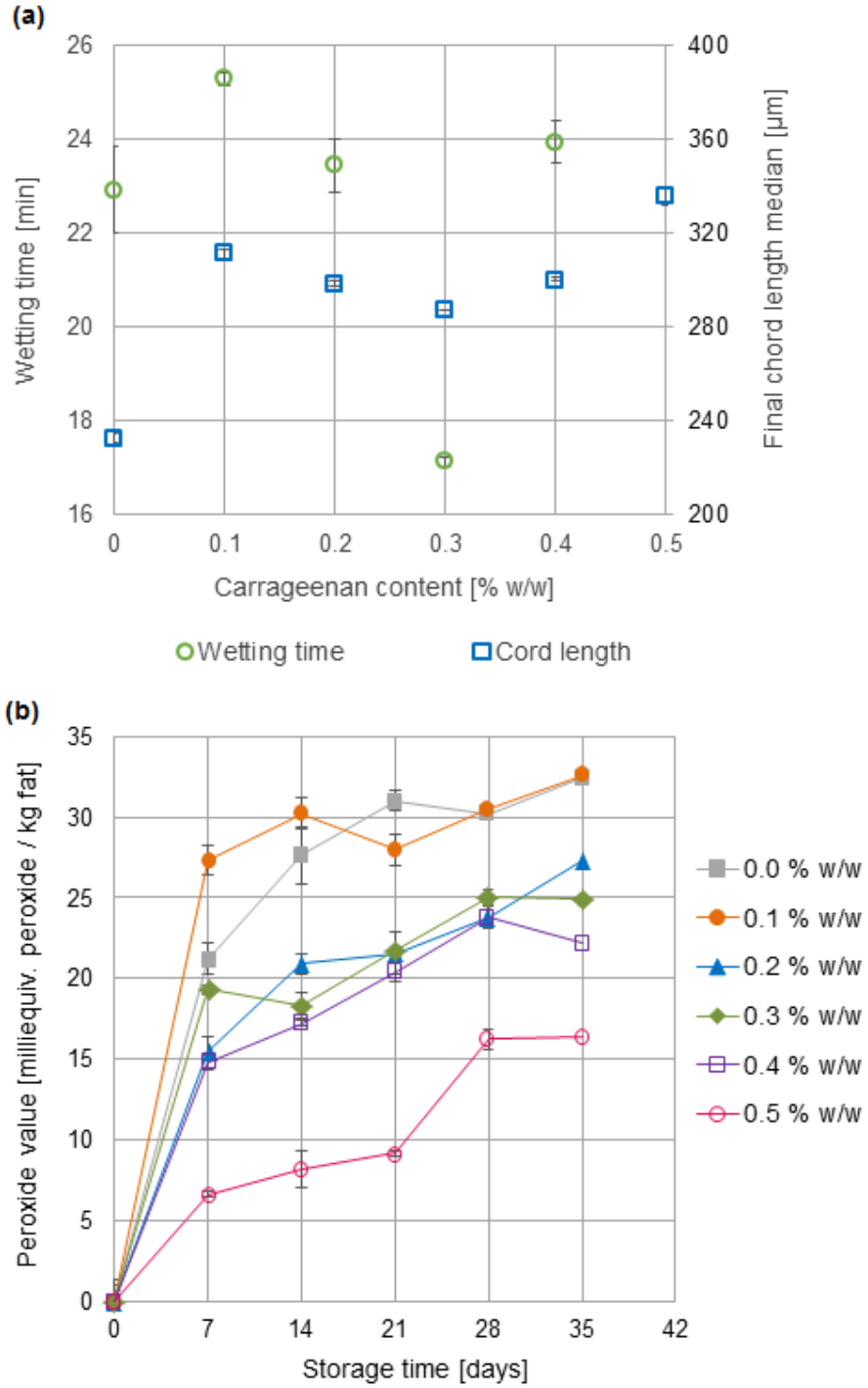

Figure 5.7: Functional properties of spray-dried powders in dependence of λ-carrageenan content: (a) wetting time on a quiescent water surface as well as median of the final particle chord length at the end of the FBRM dissolution analysis, and (b) peroxide value for quantification of the oxidative stability over storage time.

In the range of 0.1-0.5 % w/w, there was a local minimum in particle size at an intermediate carrageenan content of 0.3 % w/w. The curves of chord length over full dissolution time were in agreement with this and are provided in Appendix 4.D (Figure 5.11). The wettability study revealed that the samples containing 0.3 % w/w polysaccharide completed the penetration of the water surface the fastest in a time of about 17 min. The wetting times of the other samples (0, 0.1, 0.2 and 0.4 % w/w), defined as total time required for the last particle of each sample to penetrate the water surface, did not vary significantly from each other, lying between 23 to 25 min. No wetting time for powder samples obtained from spray drying of an emulsion with 0.5 % w/w carrageenan are displayed in the chart, because the majority of those particles had still not penetrated the water surface after one hour. The results of the wetting time were in line with photographic monitoring at 20, 60, 120 and 300 s, which also showed a superior wettability for 0.3 % w/w and a particularly limited wettability for 0.5 % w/w (Figure 5.12 in Appendix 4.D). For interpretation of these results, the dissolution and wettability studies need to be discussed in relation to each other.

The powder wettability seemed to influence the powder solubility, as the wettability curve over carrageenan content was similar in shape to the dissolution curve with a minimum at 0.3 % w/w carrageenan. The minimal value in chord length and wetting time at 0.3 % w/w is believed to be a consequence of the powders' different surface fat contents. As the amount of hydrophobic surface fat decreased from 0 to 0.3 % w/w of added carrageenan, the thereby improved wettability in aqueous medium counteracted, to some extent, the detrimental impact of the declining porosity that was observed from SEM imaging. Presumably as a result of lower particle porosities with greater carrageenan content, the powder dissolution rate was lowered by any carrageenan content in comparison to the polysaccharide-free powder. Therefore, an unwanted deterioration of the powder rehydration behavior was caused by emulsion stabilization with carrageenan.

Furthermore, the internal porosity of the powders also affected their peroxide values (Figure 5.7b). These were used as a measure of the extent to which the lipid's unsaturated fatty acid chains had undergone primary oxidation. Directly after spray drying (0 days), no difference in the degree of oxidation was observed between any sample (color of the initial analyte solutions was already similar to the blank tests prior to titration). Apparently, the fatty acids had not been appreciably oxidized during emulsion preparation or spray drying for any powder sample, and the peroxide values hence were approximated as being 0 milliequiv/kg. The most significant changes in peroxide value and the most distinct differences between the individual powder samples were found to occur during the first seven days. The greater the carrageenan content of each sample was, the less strongly increased the corresponding peroxide value, indicating an improved oxidative stability by the addition of carrageenan. This was explained by the decreasing internal powder porosity at higher carrageenan concentration, which impeded oxygen diffusion inside the particles. Therefore, the peroxide values of the 0.5 % w/w powder samples were by far the lowest (6-17 milliequiv/kg) over the whole storage study.

It should be noted that the difference in powder dissolution rate and wettability might have also affected the peroxide value measurement itself by influencing the accessibility of the titrant and the sample solution into the particles. In addition, a smaller amount of surface fat most likely supported lower peroxide values, too. For instance, there was a considerable difference in the peroxide values at the end of the storage study (35 days) between powders with a carrageenan content of 0 or 0.1 % w/w (approximately 33 milliequiv/kg) and 0.2-0.4 % w/w (27-22 milliequiv/kg). This corresponded well with the sharp drop in extracted surface fat from 0.1 to 0.2 % w/w (Figure 5.4a). That the lipid contained in particles can be protected from a high rate of oxidation by reducing the amount of surface fat was previously demonstrated by Granelli et al. (1996).

5.6 Conclusions

This study gave an understanding about the effect of λ-carrageenan, a linear sulphated polysaccharide, on milk model emulsions in terms of stability and disintegration behavior during spray drying for the purpose of improved milk powder properties by a reduction of surface fat.

From investigation of emulsions at different carrageenan concentrations, it was learnt that coalescence of the dispersed lipid phase can be inhibited by adsorption of λ-carrageenan's sulphate groups on the milk fat globule membranes and a consequent increase in negative charge of these oil-water interfaces. Optimum electrostatic emulsion stabilization and minimum fat globule size were obtained within a certain range of carrageenan concentrations (0.3-0.4 % w/w) for the given model emulsions, which agreed with a theoretical estimation of the saturation coverage of the cationic casein surface area.

The emulsion stabilization translated into a considerably thinner surface fat layer on the spray-dried particles. The fat in powders obtained from a carrageenan-free emulsion consisted of 13.8 % free surface fat, in contrast to only a third of this (4.7 %) for a carrageenan content of 0.3 % w/w. These fat extraction results were confirmed by confocal laser scanning microscopic images. It was concluded that the emulsion stabilization with carrageenan possibly reduced the proposed perforation mechanism along the dispersed fat phase and decreased the volume of the fat globules that appeared at the droplet surface through this disintegration process, contributing to the observation of less surface fat at intermediate carrageenan concentrations.

Rheological data suggested that during atomization the milk emulsions preferably disintegrated along the dispersed fat globules. The extensional viscosity was very sensitive to the addition of oil and λ-carrageenan. While the addition of a significant fat phase at constant total solid content resulted in a decrease from 25.9 to 11.5 mPa·s, the presence of carrageenan (0.3 % w/w) averted this trend by raising the extensional viscosity up to 30.7 mPa·s. The new insights into the connection between emulsion properties, atomization behavior and resulting surface composition of the corresponding particles is of

importance for industrial spray drying applications, since surface fat coverage affects the functional powder properties detrimentally. In light of these results, and as carrageenan is already being used in commercially available dairy drinks, the addition of carrageenan into milk emulsions for reduction of the powder surface fat coverage upon spray drying seems to be feasible from an economical and consumer point of view.

Besides a reduction in surface fat, the emulsion stabilization with λ-carrageenan also induced a decrease in internal particle porosity. With regard to the rehydration behavior in water, a trade-off was noted between the positive impact of reduced surface fat and the negative influence of a greater particle density with carrageenan. Since the effect of increased density was more dominant on the water solubility, methods to avoid a loss in powder porosity should be explored in future studies for the purpose of ideal functional milk powder properties in industrial applications. Yet, the higher powder density appeared to also have a favorable effect, as the powder's oxidative rancidity after storage was reduced with greater carrageenan content.

In a future study, it could be investigated how the improved emulsion stability and increased extensional viscosity by addition of carrageenan impacts the disintegration behavior and fat encapsulation efficiency in spray drying techniques that are commonly applied in industrial milk powder production. The charge density in emulsions containing skim milk powder and different λ-carrageenan concentrations could be investigated by ζ-potential measurements to also study how the electrostatic carrageenan/casein interaction is influenced by a variation in sodium or calcium cation concentrations.

5.7 Appendix

5.7.1 Appendix 4.A: Fat Globule Size Distributions and Changes in Emulsion Microstructure over Time

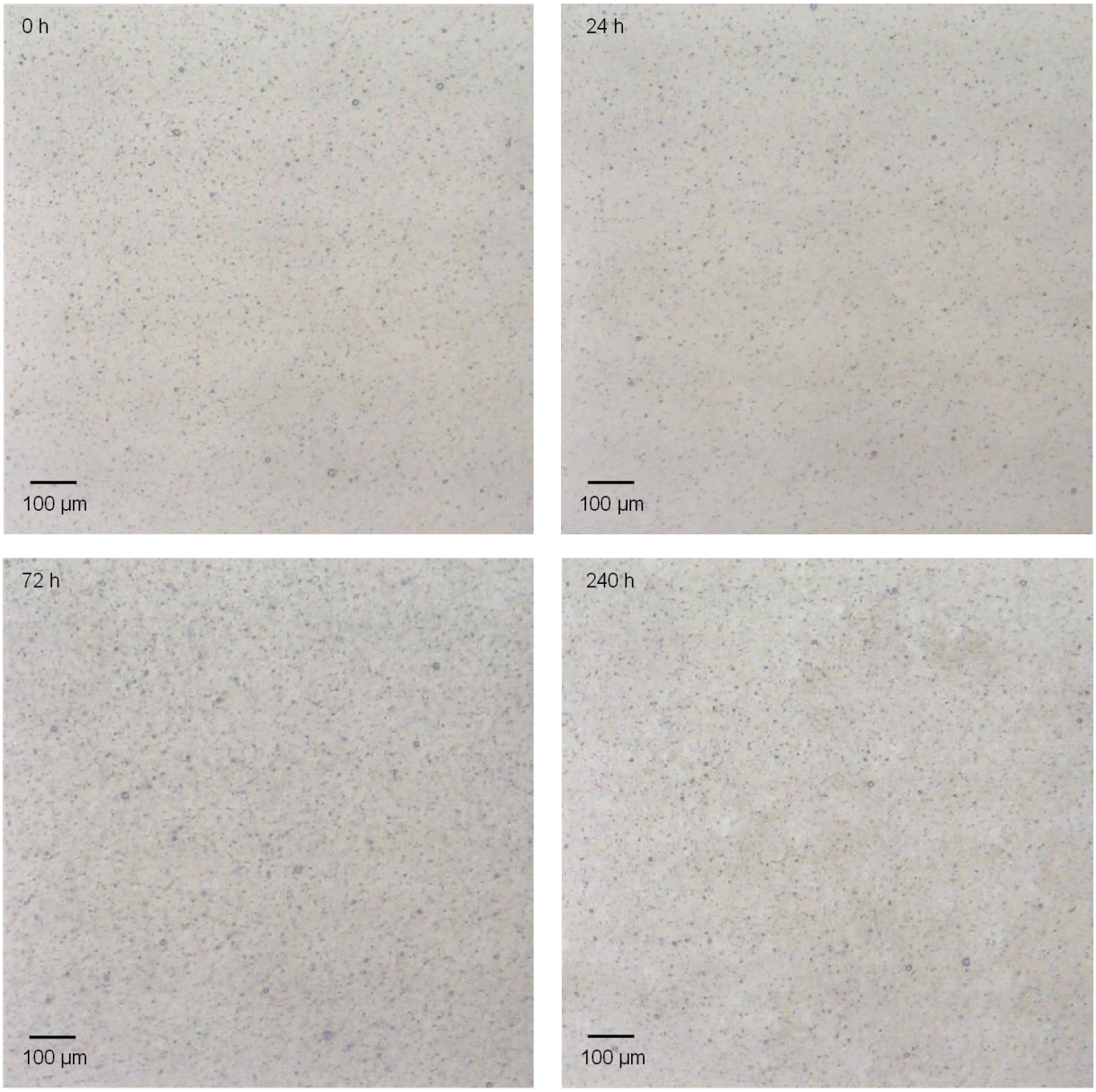

Figure 5.8: Emulsion homogeneity as a function of time: microscope images of the microstructure of a model emulsion (0.3 % w/w carrageenan) that was stored at 6 °C.

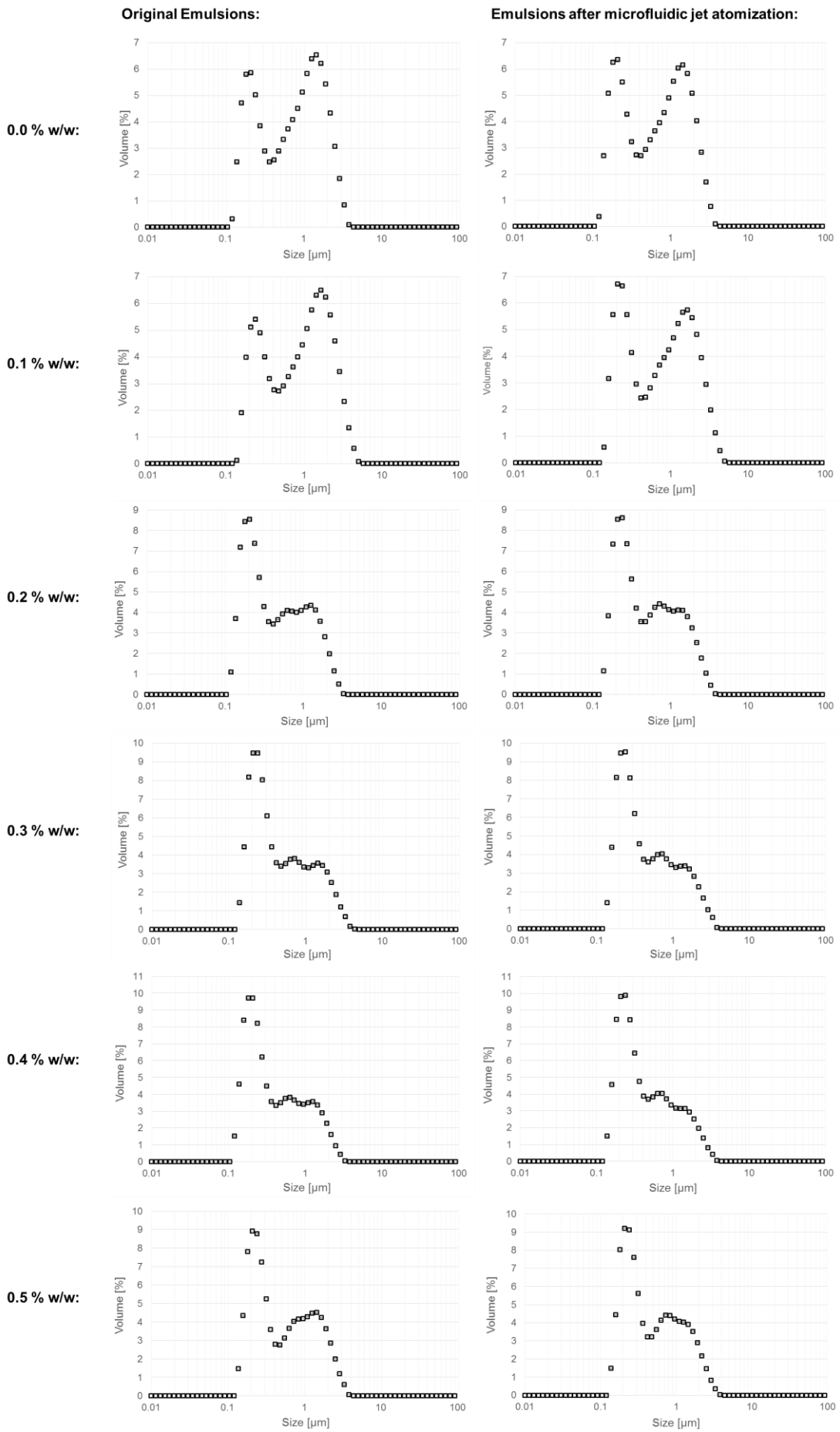
Original Emulsions:
Emulsions after microfluidic jet atomization:
0.0 % w/w:
0.1 % w/w:
0.2 % w/w:
0.3 % w/w:
0.4 % w/w:
0.5 % w/w:
Volume [%]
Size [µm]
0.01
0.1
1
10
100

Figure 5.9: Volumetric size distribution in model milk emulsions of different carrageenan contents obtained from laser light scattering measurements: in the original emulsions (first column) and after atomization in a microfluidic jet nozzle (second column).

5.7.2 Appendix 4.B: Estimation of the Saturation Coverage of the Protein Surfaces by Carrageenan

The emulsion stability investigation (Section 5.5.1.1) indicated that saturation coverage of the cationic surface areas of the protein of the casein micelles and around the fat globules, and as such optimum stability that deteriorates again for higher concentrations presumably due to depletion flocculation, occurred at approximately 0.4 % w/w carrageenan. This value was about 30 times greater than the values reported by Dalgleish and Morris (1988). This seemed reasonable, because the emulsions investigated in the present study contained a much higher fat content, leading to a greater protein surface area around the lipid globules, and a significantly higher concentration in protein (5.4 % w/w, in comparison to about 0.025 % w/w). Theoretical calculation, comparable to Dalgleish and Morris (1988), was undertaken to provide further supporting evidence that flocculation occurred due to excess carrageenan at a carrageenan concentration above 0.4 % w/w.

For this consideration, it was supposed that at saturation level the positively charged regions of the protein at the surface of the fat globules and the casein micelles were completely covered by a monolayer of carrageen. The fat globules featured a volumetric mean diameter of around 650 nm (Figure 5.3a), and their surface area was thus about 0.64 m^2/g emulsion for the given lipid concentration inside the model emulsions. Estimating a surface casein concentration on the fat globules of $1.50 \cdot 10^{-3}$ g/m^2 according to analyses by Srinivasan et al. (1996) of a soya oil/caseinate emulsion homogenized at high pressure, the non-adsorbed amount of casein was $5.30 \cdot 10^{-2}$ g/g emulsion. Together with the volumetric mean diameter of the casein micelles being previously measured as approximately 140 nm, this amounted to a surface area of casein micelles of about 1.82 m^2/g emulsion. Hence, the combined surface area available for carrageenan adsorption was 2.46 m^2/g emulsion. The carrageenan molecules were assumed to span an area of $6.0 \cdot 10^2$ m^2/g as adapted from Dalgleish and Morris (1988). This meant an absolute surface area of 0.60, 1.20, 1.80, 2.40 or 3.00 m^2/g emulsion held by the polysaccharide molecules for respective concentrations of 0.1, 0.2, 0.3, 0.4 or 0.5 % w/w. Consequently, the surface area of casein micelles and fat globules was approximately commensurate with the present carrageenan surface area for a carrageenan content of 0.4 % w/w, and at 0.5 % w/w there was more carrageenan inside the emulsion than could undergo electrostatic interaction with the positively charged protein regions.

The theoretical calculation thus agreed well with the observed emulsion stabilities (Section 5.5.1.1) and the results about the fat globule sizes as a function of carrageenan concentration (Section 5.5.1.2). The calculated saturation surface coverage corresponded to an adsorbed carrageenan amount of $1.62 \cdot 10^{-3}$ g/m^2.

5.7.3 Appendix 4.C: Time Curves of Neck Diameter during Extensional Viscosity Analysis

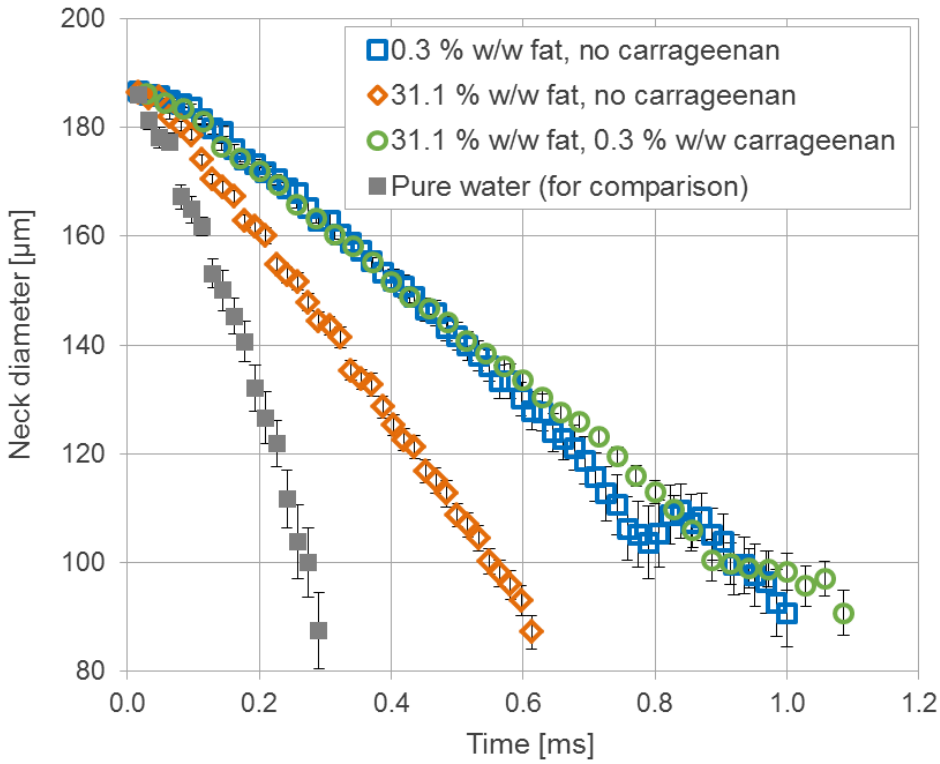

Figure 5.10: Extensional viscosity measurements: bridge neck diameter over time for low-fat emulsion, regular-fat emulsion, regular-fat emulsion with carrageenan (0.3 % w/w) and pure water for comparison.

5.7.4 Appendix 4.D: Full Results of FBRM Dissolution Study and Images Taken during Wettability Study

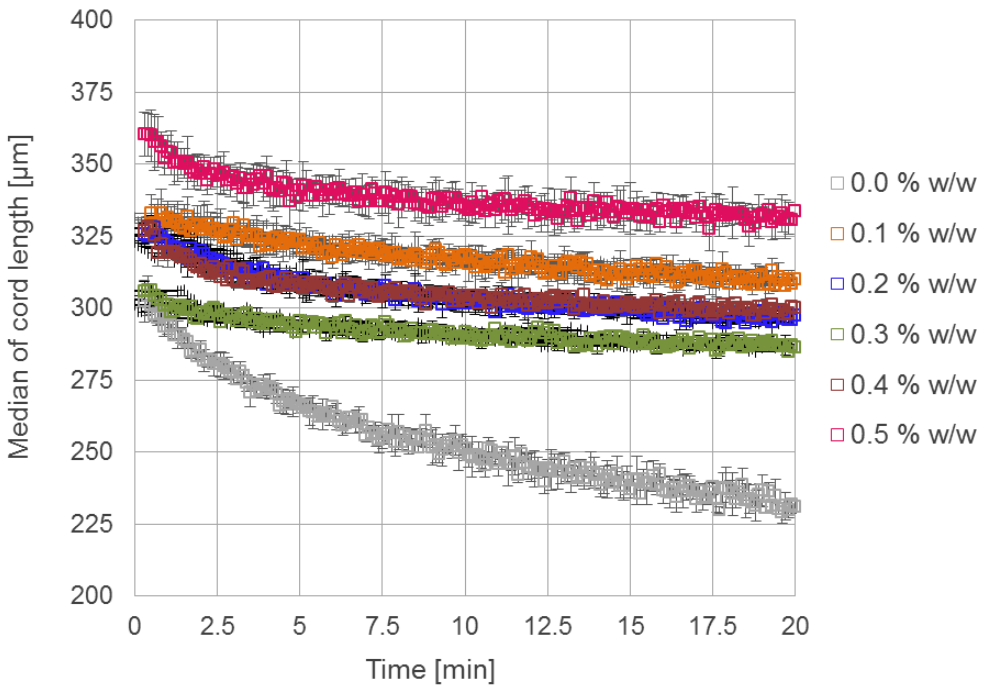

Figure 5.11: Impact of λ-carrageenan concentration on powder dissolution rate: median diameter of the particles' chord lengths as a function of dissolution time.

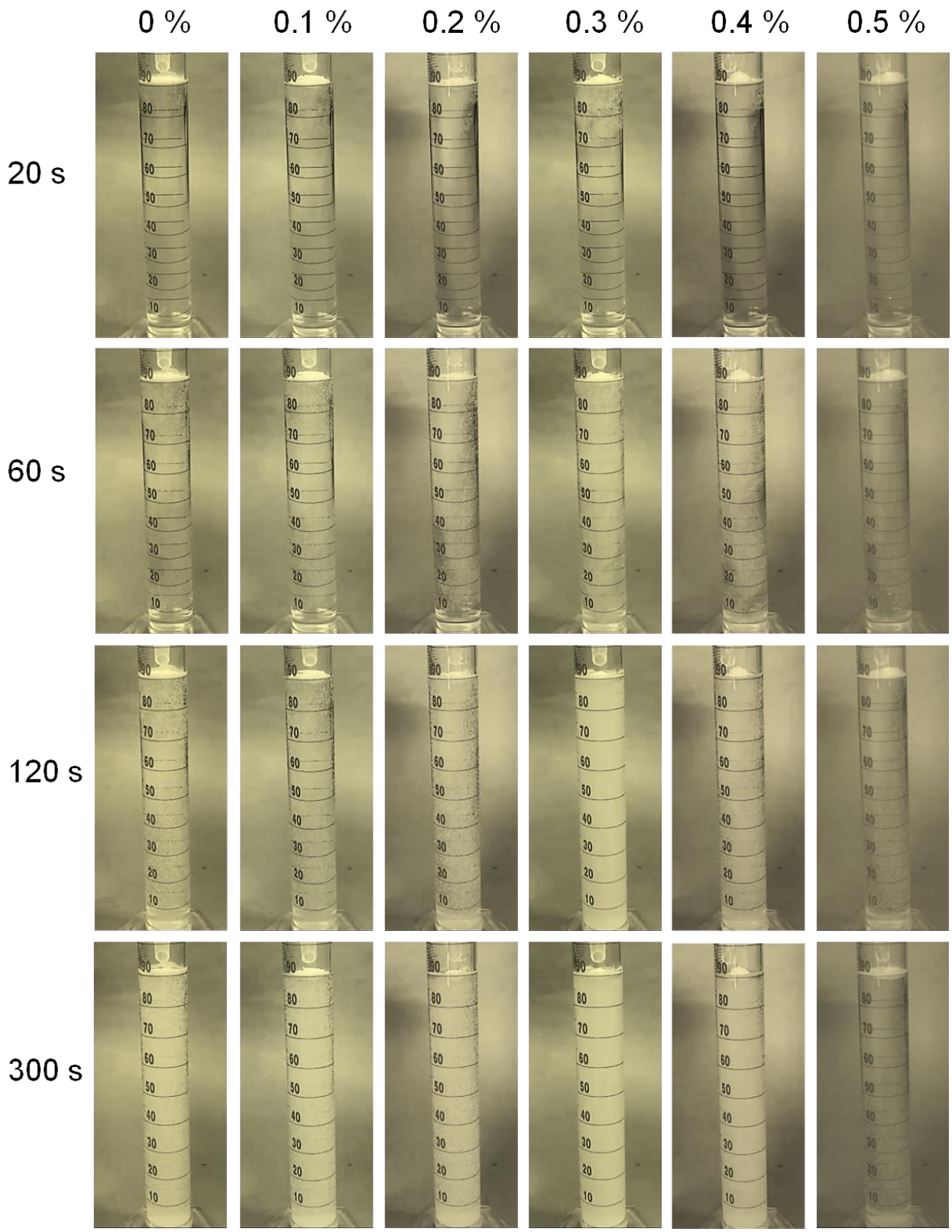

Figure 5.12: Impact of λ-carrageenan concentration on powder wettability: photographs taken at 20, 60, 120 and 300 s after addition of powder onto the water surface.

6 The Influence of the Chemical Surface Composition on the Drying Process of Milk Droplets

6.1 Preface

In the spray drying study of Chapter 4, a fat surface layer was observed on the regular-fat model emulsion droplets from immediately after atomization throughout the whole drying process until completed drying. With regards to an accurate CFD simulation of drying milk droplets for optimization of spray dryer designs and prediction of product characteristics, it was of interest how this droplet surface coverage by fat affects the droplets' drying and shrinkage rates. The suspended single droplet drying technique facilitates an accurate determination of the drying kinetics from measurement of the changes in diameter, temperature and mass of the drying milk droplets (see Section 2.3). To ensure that the single droplet drying process was comparable with spray drying, however, it needed to be validated that the chemical surface composition as a function of drying progress was similar to each other for both convective drying methods. For this reason, the conventional suspended single droplet drying method was extended by a new approach, where the changes in surface composition could be tracked over drying time. Thus, the impact of the chemical surface formation of low-fat and regular-fat emulsion droplets on the drying and shrinkage kinetics could be compared with each other.

The following study (Section 6.2-6.5) has been published by Elsevier B.V.:

Foerster, M., Gengenbach, T., Woo, M. W., Selomulya, C. The influence of the chemical surface composition on the drying process of milk droplets, Advanced Powder Technology, 2016, Vol. 27, p. 2324–2334, DOI: dx.doi.org/10.1016/j.apt.2016.07.004

This study was amended by numerical simulation work. The experimental results were compared with a mathematical model that was used for simulation of the radial concentration profiles of lactose, protein and fat in a low-fat model milk emulsion droplet during single droplet drying. It was endeavored to apply a suitable modelling approach by eliminating some weaknesses of previously published models of this kind (see Section 2.2.5). By means of this, it was expected to obtain an improved understanding of the component migration during drying to verify some hypotheses that have been made in the first part of Chapter 6. The experimentally measured drying and shrinkage kinetics were implemented into the numerical model for the purpose of a more realistic description of the impact of the forming crust on the water concentration profile and droplet diameter. Moreover, an improved validation method was

demonstrated by utilizing the knowledge about the changes in surface composition over time, which had been acquired from the experimental study.

Presented in Section 6.6 is a condensed and reworded form of the simulation work that has been published by John Wiley & Sons, Inc.:

Putranto, A., Foerster, M., Woo, M.W., Chen, X.D., Selomulya, C., A continuum-approach modelling of surface composition and ternary component distribution inside low fat milk emulsions during single droplet drying, AIChE Journal, in press, DOI: dx.doi.org/10.1002/aic.15657

At the end of this chapter, the conclusions of both studies are presented in combined form.

6.2 Abstract

The functional properties of multi-component particles are strongly affected by their chemical surface composition, for instance in pharmaceutical and food applications. The powders are often produced from emulsions and solutions by convective drying, such as spray drying. A detailed understanding of the drying and shrinkage kinetics of the material is hereby crucial to optimize process design and product characteristics. In this study, a modified analysis technique was implemented into filament single droplet drying to observe the changes in component distribution of two milk model emulsions with drying time as well as the impact thereof on the water evaporation resistance and shrinkage behavior. The drying droplets were cryogenically flash-frozen at discrete drying times and, subsequent to freeze drying, investigated in terms of their chemical surface composition and internal fat and protein distribution. The droplets of a regular-fat milk model emulsion were covered by a continuous fat film throughout the whole drying process, whereas the droplets of a low-fat model emulsion featured a surface overrepresentation of protein in comparison to the bulk concentration. The protein further enriched near the surface with increasing drying time. In the regular-fat system, the lipid surface film reduced the extent of particle shrinkage and impeded the drying process.

6.3 Introduction

A high content of fat on the surface of spray-dried milk particles, which greatly exceeds the bulk fat content, is typically encountered independent of the atomization process. This surface dominance of fat causes detrimental effects on the powder particles' oxidative stability (Granelli et al., 1996, Hardas et al., 2000, Keogh et al., 2001a), affinity to caking (Kim et al., 2005a, Nijdam and Langrish, 2006) and dispersibility as well as wettability during reconstitution in water (Fäldt and Bergenståhl, 1996b, Millqvist-Fureby et al., 2001). As a result, post-processing steps, such as coating with lecithin, are often

used in industry for further processing and to prolong storage. Various potential mechanisms have been proposed to describe the component segregation mechanism between lipid, protein and lactose that leads to this fat accumulation at the surface during convective drying of milk droplets. Previously, it has often been attributed to the components' different physical properties that come into effect during the actual drying process subsequent to film disintegration. These include surface activity (Adhikari et al., 2009, Fäldt and Bergenståhl, 1996a, Gaiani et al., 2006), diffusivity (Fu et al., 2011a, Kim et al., 2003, Meerdink, 1994, Nikolova et al., 2015a) and solubility (Charlesworth and Marshall, 1960, Kim et al., 2009b, Wang and Langrish, 2009). Yet, it has previously been shown that it was, in fact, the atomization process that induces the fat surface coverage (Chapter 3). Immediately after atomization, the surfaces of milk model droplets were found to have fat contents of 9-13 and 83-92 % v/v, respectively, for 0.5 and 44.2 % v/v of fat on dry matter basis in the feed emulsions. In the subsequent drying stage, the layer of fat remained on the surface, while protein accumulated underneath the fat layer as drying proceeded. The comparison between atomized droplets and fully spray-dried particles was made possible by flash freezing the atomized droplets. However, no information could be obtained on the droplet surface composition at intermediate drying times inside the drying tower. Moreover, the impact of the forming crust and of the corresponding surface composition on the drying and shrinkage kinetics of the droplets would be of great interest for optimization of industrial dryer design and operation.

In contrast to spray drying experiments, single droplet drying facilitates a direct monitoring of the convective drying of a solution or emulsion droplet at any point of the drying process (Sadek et al., 2014b, Walton, 2004). The filament single droplet drying technique, where an individual droplet is suspended at a thin filament and dried in a conditioned air stream, has often been applied for this purpose, for instance the drying of aqueous droplets containing fruit pulp, milk and lactose (Chen et al., 2001, Chen and Lin, 2005, Lin and Chen, 2006). Parameters such as relative air velocity, drying air humidity and temperature can be adjusted to observe the resulting changes in droplet mass, diameter and temperature *in situ*. Chen and Xie (1997) introduced a semi-empirical model, the Reaction Engineering Approach, to process this experimental data for description of the 'apparent activation energy of evaporation' as a measurement of the evaporation resistance of the emerging crust as a function of the droplet moisture content. Evaporation is hereby treated as an activation process that has to overcome a certain energy barrier. The single droplet drying technique does not allow for the complex droplet-droplet and droplet-air interactions encountered within spray dryers and the droplet size is significantly larger than in spray drying. It offers, however, a practical way of replicating the actual drying process of an individual droplet to determine the characteristic convective drying behavior of a certain material system. This information can then be fed into CFD simulations to predict the changes in moisture content and droplet size for the given material system in a spray dryer environment. In this way, the evaporation and shrinkage kinetics, even for complex solidification processes, are described with high accuracy (Putranto et al., 2011, Woo et al., 2008, Zhu et al., 2011).

Mezhericher et al. (2007) proposed an incorporation of REA into a numerical model of the mass and temperature change in drying skim milk droplets for a more realistic account of the water diffusion resistance caused by crust formation. Chew et al. (2014) undertook an investigation of the surface composition of fully dried milk protein concentrate particles subsequent to completion of the single droplet drying. The dried particles were analyzed regarding to their chemical surface concentration *via* X-ray photoelectron spectroscopy, and it was found that smaller droplet sizes as well as higher temperatures resulted in a decreasing fat content on the particle surface, although there was always a significant overrepresentation of fat on the surface. Fu et al. (2011a) conducted a wetting and dissolution study of fresh whole and skim milk particles obtained from single droplet drying to qualitatively classify the surface as hydrophobic or hydrophilic. After certain drying times, the air flow was stopped and a solvent droplet (ethanol or water) was attached to the (semi-)dried droplet. Based on the wetting behavior observed with a camera, conclusions about the nature of the developed surfaces were drawn. Interpretation, however, was limited to a relative comparison between whole and skim milk, and the wettability until about 35 s from drying commencement could not be studied because of too high moisture contents.

In order to gain a better understanding of the component segregation process that occurs in convective drying of milk droplets, the final surface concentration alone or ambiguous dissolution test videos are insufficient. To date, single droplet drying has not yet been applied for quantitative analysis of the surface composition at intermediate drying stages and directly after droplet generation. The aim of the present study was to widen the hitherto employed extent of single droplet drying analyses to also monitor, for the first time, the changes in surface composition and internal component distribution over drying time and over the corresponding droplet moisture content. Single droplet drying of low and regular-fat milk model emulsions was interrupted at discrete drying times by cryogenic flash freezing, and, following freeze drying, the particles were analyzed in terms of surface composition by XPS and internal component distribution by CLSM. The data were compared with drying and shrinkage kinetics obtained from conventional single droplet drying experiments for a better understanding of surface formation and its impact on the convective drying behavior of milk droplets. A requirement for these results to be representative for the surface composition and drying characteristics in a spray dryer were comparable initial droplet states. It was hence to be validated that the component distribution in the droplets generated for single droplet drying matched the one of droplets atomized during conventional spray drying.

6.4 Material and Methods

6.4.1 Emulsion Preparation

Two model milk emulsions of different fat contents were investigated, as summarized in Table 6.1. A regular-fat model milk emulsion featured a composition typical for both bovine whole milk and com-

mercially sold fat filled milk powder. It contained 40.8 % w/w lactose, 31.1 % w/w fat and 27.0 % w/w protein in d.m. A low-fat model milk emulsion resembled the composition of the RFMM in terms of protein-lactose ratio and solid content, whereas the fat content was significantly reduced to 0.3 % w/w. The emulsions were prepared by dissolving α-lactose monohydrate (Sigma-Aldrich Co., USA), calcium caseinate isolate (Nutrients Direct Pty Ltd, Australia) and whey protein isolate (Nexius Pty Ltd, Australia) with a caseinate/whey ratio of 4:1 in water. For the RFMM emulsion, sustainably sourced refined *Elaeis guineensis* palm oil fat (Auroma Pty Ltd, Australia) was added. Both emulsions were mixed with deionized water at 45 °C for 1 h, prior to pre-homogenization in a high-speed colloidal mill (WiseMix Homogenizer HG-15D, Daihan Scientific, South Korea) at 1000 rpm. This was followed by three passes at 1,000 bar and two subsequent passes at 500 bar through a high pressure homogenizer (EmulsiFlex-C5, Avestin, Canada). The fat globule size distributions of each emulsion were measured by dynamic light scattering (Zetasizer Nano ZS, Malvern Instruments Ltd, UK) to ensure consistency (volume weighted mean diameter had to be $D(4,3) = 1.0\ \mu m \pm 0.05\ \mu m$).

Table 6.1: Volumetric composition of the solid contents in the LFMM and RFMM emulsions.

	Abbreviation	Solid concentration [% w/w]	Fat content (d.m.) [% v/v]	Protein content (d.m.) [% v/v]	Lactose content (d.m.) [% v/v]
Low-fat	LFMM	20.0	0.5	41.8	57.7
Regular-fat	RFMM	20.0	44.2	23.5	32.4

6.4.2 Changes in Component Distribution over Drying Time *via* Cryogenic Flash Freezing

Information about changes in the internal and surface distribution of lactose, protein and fat with proceeding drying time was acquired from single droplet drying experiments conducted inside a suspension rig with well-defined drying environment. Compressed air flowed through a dehumidifying column (KF-DDF-125, Knight Pneumatics, Australia) and was electrically heated before entering the drying chamber from the bottom and leaving it through its top. The conditioned air stream had a temperature of 70 °C, a velocity of 0.75 m/s and a humidity of 0.0001 kg/kg. Individual RFMM and LFMM droplets of 3 µl (± 0.05 µl standard deviation) were generated by means of a 5 µl micro-volume syringe (5FX, SGE Analytical Science, Australia) and were then suspended at the tip of a thin, vertically mounted glass filament. The tip of the filament consisted of a knob which had a hydrophilic coating at its lower half and a hydrophobic one at its upper half. The beginning of the drying process was controlled with a bypass slider separating the chamber from the air stream. The drying process was stopped abruptly after certain drying times to virtually freeze the component distribution. At 0, 20, 50, 100 and 200 s, the drying droplets were flash-frozen directly inside the drying chamber by immersing them in cryogenic vials that were filled with liquid nitrogen and that were raised from the chamber bottom up towards the drop-

let (Figure 6.1a). The frozen droplets were then immediately taken out of the drying chamber together with their glass filament by pulling the filaments down from the filament holder, to which they had been connected loosely with adhesive tape. For a drying time of 0 s, the generated droplets were directly immersed from the syringe into liquid nitrogen. The flash-frozen droplets were stored in the liquid nitrogen filled vials, which were kept sufficiently cool by dry ice, until freeze drying. Freeze drying was performed with a FreeZone 2.5 l benchtop freeze dry system (Labconco Corp., USA) at -80 °C and 0.1 mbar for 24 h. The component distribution in particles dried for 420 s was also analyzed, but did not require flash freezing, because the drying process of those particle was already completed. All of these singe droplet drying runs were performed in duplicate.

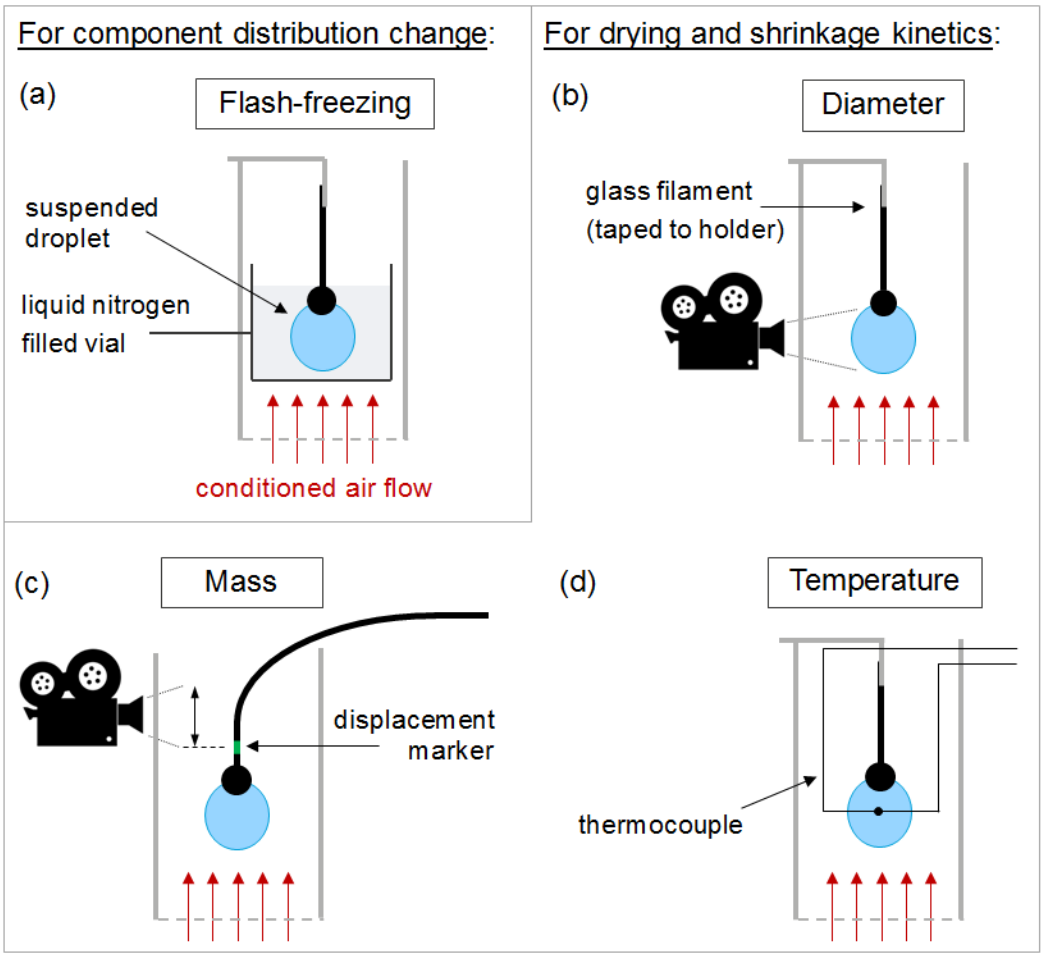

Figure 6.1: Schematic illustration of the experimental single droplet drying set-ups: (a) component distribution analysis; (b) diameter change analysis; (c) mass change analysis; (d) temperature change analysis.

6.4.3 Spectroscopic Surface Composition Analysis

XPS was employed to analyze the chemical surface compositions of the flash-frozen and fully dried particles of both model emulsions. Analyses were performed either on an AXIS Ultra DLD or an AXIS

Nova (Kratos Analytical Inc., UK), both spectrometers equipped with a monochromatic Al K_α source, a hemispherical analyzer operating in the fixed analyzer transmission mode and using the standard aperture (analysis area of 0.3 mm × 0.7 mm). The particles were mounted on custom-built sample holders by taping their glass filaments to the holder so that the particles themselves remained suspended in space, without coming into contact with the holder. Each particle was analyzed at a nominal photoelectron emission angle of 0º with respect to the surface normal. As the actual emission angle is ambiguous in the case of particles, varying between 0º and 90º, the sampling depth varied between 0 nm and approximately 10 nm. The pressure in the main vacuum chamber during analysis was of the order of 10^{-8} mbar. All detected elements were identified from survey spectra. Their relative atomic concentrations were computed from the integral peak intensities and the sensitivity factors provided by the manufacturer. The concentrations in lactose, fat and protein can be assumed to be linear combinations of the atomic surface composition (Fäldt et al., 1993). The fraction of each component at the surface, expressed in atomic concentrations, was hence estimated by linearization based on the representative structural formulas of lactose, milk fat and milk protein, as elaborated elsewhere (Chew et al., 2014). For duplicate measurements, two particles for each drying time were analyzed and the respective standard deviations were calculated.

6.4.4 Confocal Laser Scanning Microscopy

The protein and fat distribution in flash-frozen as well as fully dried RFMM particles were analyzed *via* CLSM. Based on the procedure described by Taneja et al. (2013), dual labelling with fluorescent dyes was performed during emulsion preparation. The molten fat and the reconstituted protein powder were stained with 0.02 % w/w hydrophobic Nile Red and 0.01 % w/w hydrophilic Fast Green FCF, respectively (Sigma Aldrich Co., USA). Similar to the above described procedure, the constituents were then mixed and the emulsion was homogenized. The labelled droplets were subsequently dried in the single droplet drying rig for discrete drying times, followed by freeze drying to remove the remaining moisture, if applicable. The resulting particles were mounted on a microscope slide with DPX (Sigma Aldrich Co., USA) and investigated by CLSM with a Nikon A1+ confocal microscope (Nikon Corp., Japan). Nile Red, attached to the fat, and Fast Green FCF, attached to the protein, were sequentially excited by respective laser lights from a helium-neon (637 nm) and an argon (487 nm) source. The images were taken through a 4× magnification lens with a resolution of 2048×2048 pixels in the x-y plane at different z-depths inside the particles.

6.4.5 Change in Droplet Diameter, Mass and Temperature over Drying Time

In addition to the component distribution study, single droplet drying was also conducted in the conventional way to obtain information about the temperature, mass and diameter profiles of the model milk droplets. The experimental procedure followed the methodology described by Fu et al. (2011b), and a

schematic illustration is given in Figure 6.1b-d. In brief, droplets with an initial volume of 1, 2 or 3 µl were generated and attached to vertical glass filaments inside the drying chamber, similar to the above described procedure. In this case, however, the drying process was not interrupted by flash freezing. Instead, *in situ* analyses were conducted simultaneously to the drying process. The profiles of droplet diameter, mass and temperature changes were obtained from separate single droplet drying runs. Firstly, as illustrated in Figure 6.1b, the projected droplet areas were recorded with a camcorder (DCR-HC36, Sony Corp., Japan) equipped with five 4× close-up lenses (Marumi Optical Co. Ltd., Japan) to estimate the droplet volume and thus the equivalent droplet diameter over time. Secondly, the changes in droplet mass during drying were monitored by attaching the droplets at the tip of an elastic glass filament (Figure 6.1c). The displacement of a marker at the filament was recorded with the camera and the correlating mass change was derived from a previously performed calibration with standard weights consisting of agglomerated glass beads. Thirdly, changes in temperature over drying time were measured by inserting a type K thermocouple (Omega Engineering Inc., USA), which was attached to a Picolog TC-08 data logger (Pico Technology, United Kingdom), into the droplets (Figure 6.1d). The videos of the droplet diameter and mass change analyses were rendered into a sequence of individual images with Blender 2.69 (Stichting Blender Foundation, The Netherlands) and processed using ImageJ 1.48 (National Institutes of Health, USA). Each of these single droplet drying runs was run in triplicate. The obtained data was processed according to the hereafter described REA methodology.

6.4.6 Drying and Shrinkage Kinetics from Single Droplet Drying Data

Data about the changes in droplet diameter, mass and temperature, which had been obtained from single droplet drying experiments as described above, was processed according to the Reaction Engineering Approach. The REA describes convection drying as a result of differences in the vapor density between drying air and droplet surface, as will be briefly described in the following and outlined in detail elsewhere (Chen and Xie, 1997). The drying rate $\mathrm{dm_w/dt}$ as loss in water content $\mathrm{m_w}$ [kg] over time t [s] was calculated by:

$$dm_w/dt = -h_m \cdot A \cdot (\rho_{v,s} - \rho_{v,b}) \tag{6.1}$$

where h_m was the convective mass transfer coefficient [m/s], A the surface area of the droplet [m^2], and $\rho_{v,s}$ and $\rho_{v,b}$ the vapor density at the droplet surface and of the bulk air, respectively [kg/m^3]. The convective mass transfer coefficient was computed with a modified Ranz-Marshall correlation (Lin and Chen, 2002, Ranz and Marshall, 1952a, Ranz and Marshall, 1952b), which is well suited for high vapor fluxes as they occur in single droplet drying. The surface vapor density changed with drying time, and was correlated with the saturated surface vapor density $\rho_{v,sat}$ by means of the fractionality coefficient ψ [-]:

$$\rho_{v,s} = \psi \cdot \rho_{v,sat}(T_s) \tag{6.2}$$

where T_s was the temperature at the interface [K]. The fractionality coefficient depended on the apparent activation energy of water evaporation ΔE_{vap} [J/mol], as described by the following formulation of an Arrhenius equation:

$$\psi = exp\{-\Delta E_{vap}/(\mathcal{R} \cdot T_d)\} \tag{6.3}$$

where $\mathcal{R}$ was the universal gas constant [8.314 J/(mol·K)]. Since the Biot number lies well below unity in single droplet drying applications (Patel et al., 2005), the temperature gradient inside the droplet could be neglected and the surface temperature could be approximated with the internal droplet temperature T_d [K]. The activation energy reflected the vapor concentration depression at the interface of the droplet as a result of a reduction in free surface water due to influences such as component precipitation and crust formation. Eq. (6.2) and Eq. (6.3) substituted into Eq. (6.1) lead to the following expression of the drying rate:

$$dm_w/dt = -h_m \cdot A \cdot \left[\rho_{v,sat} \cdot exp\{-\Delta E_{vap}/(\mathcal{R} \cdot T_d)\} - \rho_{v,b}\right] \tag{6.4}$$

For a given convective drying condition, the drying rate can hence be predicted if the activation energy is known as a function of droplet moisture content. This correlation was determined *via* single droplet drying experiments by recording the changes in droplet mass, droplet temperature and droplet surface area, as rearrangement of Eq. (6.4) shows:

$$\Delta E_{vap} = -\mathcal{R} \cdot T_d \cdot ln\left[(-(dm_w/dt) \cdot (1/(h_m \cdot A)) + \rho_{v,b})/\rho_{v,sat}\right] \tag{6.5}$$

The experimentally established activation energy over droplet moisture content was described in normalized form by its maximum value $\Delta E_{vap,max}$, which eventuated when the vapor densities at the surface and in the bulk air of temperature T_b reached equilibrium:

$$\Delta E_{vap,max} = -\mathcal{R} \cdot T_b \cdot ln\left(\rho_{v,b}/\rho_{v,sat}(T_b)\right) \tag{6.6}$$

The normalized activation energy over the free moisture content $(\bar{X} - X_e)$ of the overall droplet volume was to be described with the fitting parameters *a,b,c* [-] in the following form:

$$\Delta E_{vap}/\Delta E_{vap,max} = a \cdot exp\{b \cdot (\bar{X} - X_e)^c - 1\} + 1 \tag{6.7}$$

where $\bar{X}$ was the global droplet moisture content and X_e the equilibrium moisture content [kg/kg]. The latter one was found *via* the Guggenheim–Anderson–de Boer desorption isotherm following Chen and Lin (2005). In addition, an empirical relationship for the normalized droplet diameter was determined from the same single droplet drying experiments with fitting parameter *B* [-]:

$$\mathrm{r_s}/\mathrm{r_0} = B + (1 - B) \cdot (\bar{X} - X_e)/X_0 \tag{6.8}$$

where X_0 was the initial global droplet moisture content and r_s/r_0 the ratio between the droplet radius during drying and the initial radius. In the first approximation, linear correlations usually describe the droplet shrinkage with sufficient accuracy for food drying applications (Rahman, 2009).

6.5 Results and Discussion

6.5.1 Qualitative Distribution of Fat and Protein in the Particles

Figure 6.2 illustrates the qualitative fat and protein distribution in drying RFMM droplets of 3 µl initial volume by taking the example of a fully dried RFMM particle. The component distributions after an earlier interruption of the drying process were found to be similar to the one presented here in case of the RFMM emulsion. The fat and the protein of the RFMM emulsion could be stained individually prior to mixing of both phases, and thus the two components were clearly distinguishable in the CLSM analysis. Yet, the image quality of the LFMM particles was not satisfying, since the fat phase could not be visualized. The fat content of the LFMM emulsion originated directly from the protein isolates and thus the fat globules were not available in isolated form without a surrounding protein membrane, which inhibited penetration by the Nile Red stain. In Figure 6.2, the response channels obtained from sequential excitation of the RFMM particle were superimposed. The signal emitted from Nile Red, being attached to the lipid phase, is depicted as brownish red and the signal from Fast Green FCF, which attached to the protein, is represented in green color. Areas of relatively high concentrations in both protein and fat appear yellow. 60 high resolution images were taken at a step size of 35 µm from the very particle surface towards the inner of the particle at a location far away from the contact point of the glass filament. From both the x-y and the z-y plane, it can be seen that the outermost particle surface was dominated by fat, as a consistent fat film encased the whole particle. The pixel size of the CLSM images was 1.6 µm, and hence in the same order of magnitude than the individual fat globules present in the emulsions. The existence of a fat film rather than individual lipid islands suggested that, in case of the RFMM, the globules were ruptured by mechanical stress during the droplet generation process and thus spread over the whole droplet surface. Directly underneath the fat surface film, there was generally a high accumulation of protein. With an average of about 30-60 µm, the radial thickness of the transition region from the surface fat film to protein domination was very thin in relation to the total droplet and particle radii (approximately 600-800 µm).

Below the outer fat film and the subjacent protein, no fluorescent signal was received from the inside of the particles (large black internal space in Figure 6.2). Theoretically, this could mean that that region was completely free of fat and protein, being filled with lactose and/or voids only. However, it was cal-

culated by simple mass balance that the volume of the ‘surface shell’ that was visible in the CLSM images accounted for only about 30-35 % of the total fat and protein volume contained in a 3 µl RFMM droplet. Also, scanning electron microscopic analysis of sliced particles (not shown here) showed that the particle centers did not consist of any significant voids or hollows, but the whole particle matrix was interspersed with a network of small pores due to the freeze drying step. Therefore, it was concluded that at a certain radial depth the exciting laser light and the emitted fluorescent signal had become too weak to produce a detectable response. Limited penetration depths due to low signal strength is a typical problem in conventional confocal microscopy, since scattered light is not detected by the spatial pinhole (Helmchen and Denk, 2005). Accordingly, as can be seen in the z-y plane of Figure 6.2 by the thinning ‘surface shell’ with increasing depth, the fluorescent response signal became weaker in z-direction with increasing distance from the instrument’s laser source and detector until vanishing completely. In the x-y plane, this effect was enhanced by the relatively low protein and fat concentrations in the inside of the particles. Since there was an overrepresentation of these components neat the surface, it is realistic to consequently assume a stoichiometric overrepresentation of lactose in the particle middle.

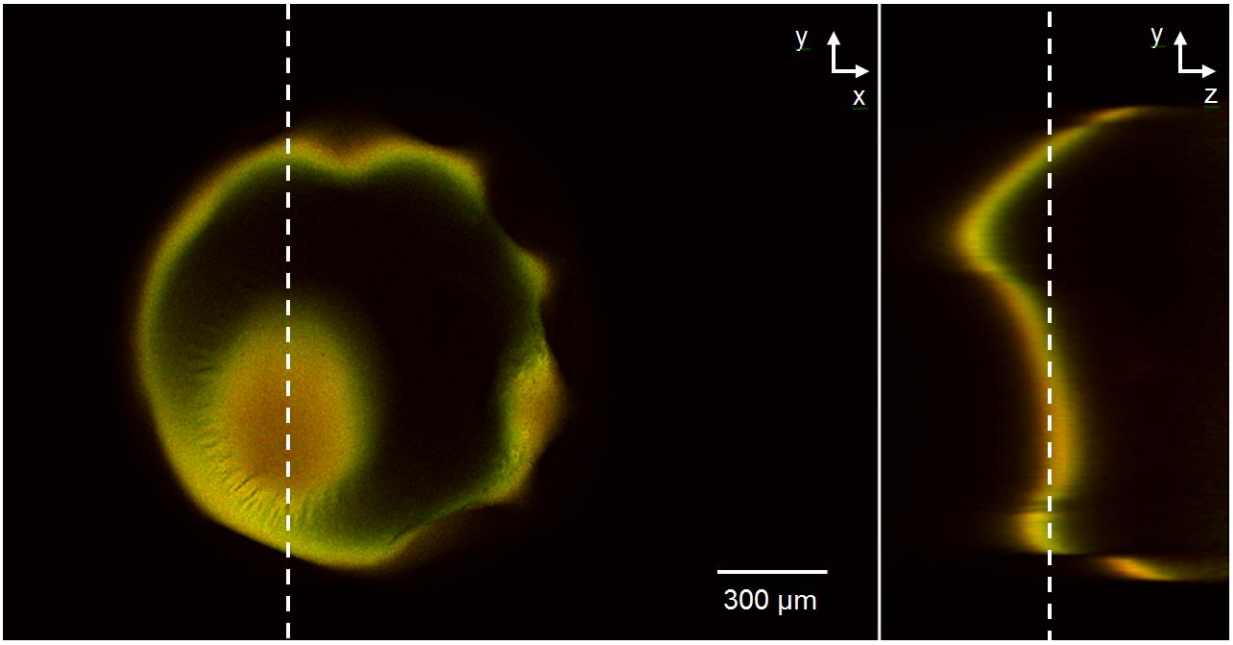

Figure 6.2: Fat and protein distribution in a RFMM particle after completed single droplet drying (420 s) as obtained by CLSM: two cross-sections through the three-dimensional image stack as indicated by the dotted lines, Nile Red (fat dye) and Fast Green FCF (protein dye) are depicted in red and in green, respectively.

Despite the different size scale and generation technique of the droplets, the existence of a surface fat layer with adjacent protein accumulation agrees well with the analysis of the CLSM images of spray-dried milk particles and their corresponding freshly atomized droplets from a microfluidic multi-jet spray dryer (Chapter 3). For detailed discussion of the potential reasons for the observed component

segregation mechanism that occurred during the single droplet drying process, the quantitative surface composition analysis *via* XPS needs to be taken into account.

6.5.2 Chemical Surface Composition of the Regular-Fat Emulsion Droplets at Discrete Drying Times

Figure 6.3 illustrates the surface composition of the drying RFMM and LFMM droplets, obtained from XPS analysis, as a function of the free moisture content ($\bar{X} - X_e$). Defined as total water content over total solid content [kg/kg], the moisture content $\bar{X}$ was calculated from the experimentally obtained mass change data. It decreased from 4 kg/kg until approximating the calculated equilibrium moisture content, and the equilibrium moisture content was taken as the final moisture content. In addition, also the corresponding drying time is given for each analysis point. After 7 min the droplets were fully dried and could be directly analyzed, whereas for any shorter drying time (0, 20, 50, 100 and 200 s) the droplets were flash-frozen and subsequently freeze-dried prior to XPS. The standard deviations in the relative atomic concentrations were relatively small and are depicted in Figure 6.3. The absolute values in lactose, protein and fat surface concentration should nonetheless be treated as estimates only, because some uncertainty might have been introduced by the linearization step.

Most notably was for the RFMM droplets that their surface consisted almost exclusively of fat (Figure 6.3a). The fat accounted for a concentration of 90 to nearly 100 % v/v throughout the whole drying process, which was more than double as high as the overall fat concentration in the emulsion. This corresponds well with the CLSM observation of a consistent fat film, which appeared thicker than the maximum XPS sampling depth of approximately 10 nm. The fat concentration did not reach a total 100 % v/v, however, owing to small amounts of protein. These presumably had been part of the protein membrane around the fat globules in the emulsion and hence became entrapped inside the fat surface film. The fat is believed to have already emerged at the droplet surface at the time of droplet generation, as the initial fat concentration of 92.6 % v/v indicates. Due to its hydrophobicity, the lipid phase might have accumulated at the droplet surface while the droplet was formed with the micro-volume syringe. Transport to the surface might have occurred by means of convection currents and circulation inside the droplet upon its generation. It is interesting that a similar atomization induced fat surface accumulation has also been reported in Chapter 3, although the droplets were generated with a microfluidic jet nozzle, a pressure swirl nozzle and a rotary disc nozzle and their size was substantially smaller. Further study of the droplet formation process will be required in order to better understand the underlying mechanisms that led to the observed initial surface composition independent from the type of film disintegration. In the case of 0 s drying time, approximately two to three seconds elapsed until the droplet was immersed in liquid nitrogen following the droplet generation. Droplet generation typically took about one to two seconds. This duration was most likely not sufficient to allow a considerable amount of fat globules to travel towards the droplet surface by diffusion, given their relatively slow diffusivity at room tempera-

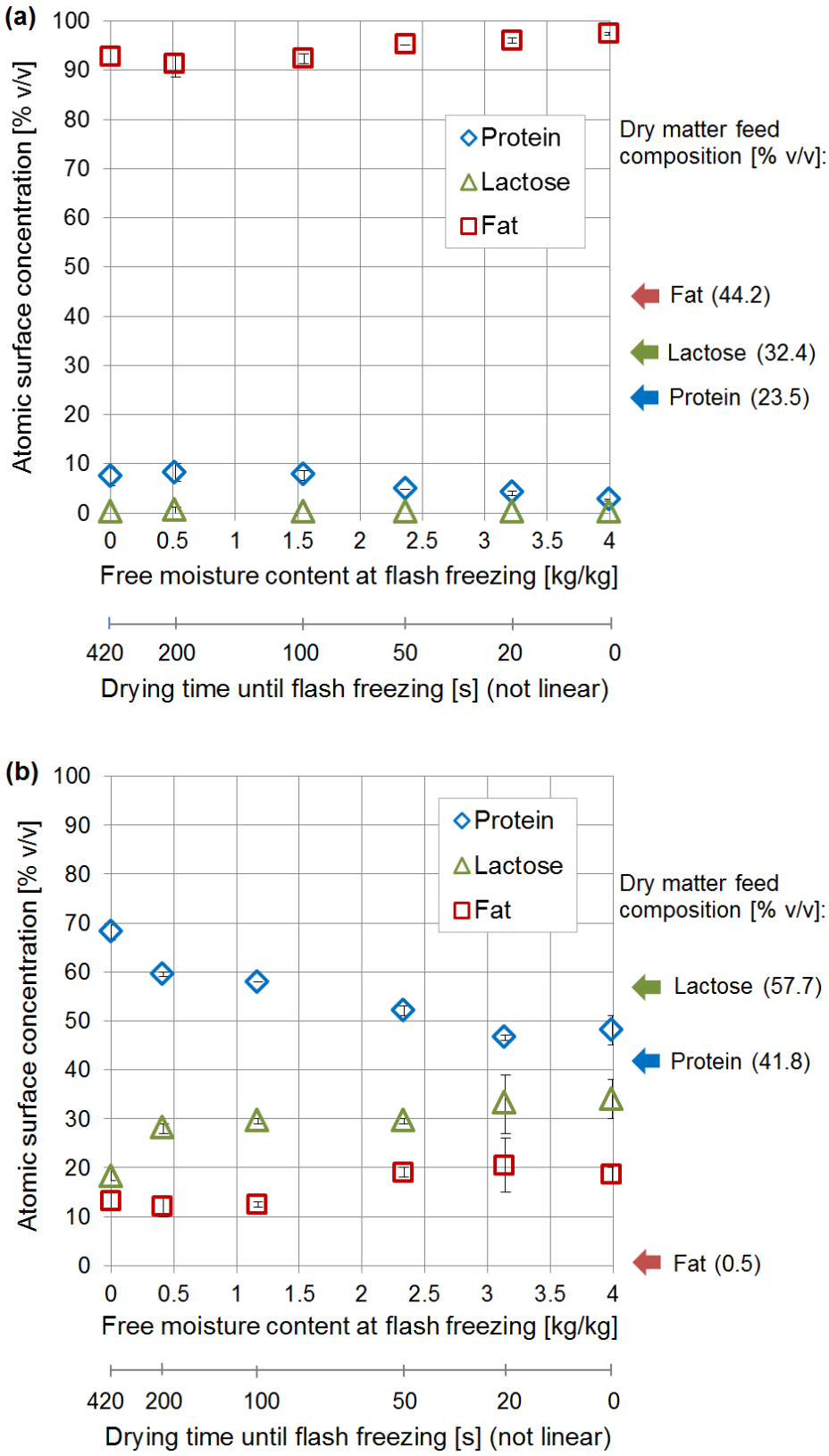

Figure 6.3: Estimated XPS particle surface composition in protein, lactose and fat for certain drying times and the corresponding free moisture contents, in comparison with the overall dry matter compositions of the feed emulsions: (a) RFMM droplets; (b) LFMM droplets. Droplets were flash-frozen and freeze-dried prior to analysis for drying times of 0-200 s.

ture as shown in Table 6.2. The presented diffusion time scales τ_i over a diffusion length x of 50 µm were approximated with the aid of binary diffusion coefficients, which were calculated with the Stokes-Einstein's equation (Einstein, 1905):

$$\tau_i = x^2/D_i \tag{6.9}$$

$$D_i = k_B \cdot T/(6 \cdot \pi \cdot \mu_w \cdot R_i) \tag{6.10}$$

The resulting values only represent qualitative comparison of the relative diffusivities between fat globules, protein and lactose. The absolute values must be treated with caution, considering the uncertainty about the exact diameter of the species during drying and the very limited validity of the Stoke-Einstein's equation, particularly due to an infinite dilution assumption.

Table 6.2: Binary diffusion coefficients of fat globules, caseinate and lactose: in water at infinite dilution from Eq. (6.10) together with the corresponding diffusion time scales for a length of 50 µm from Eq. (6.9). The radii were determined by dynamic light scattering for fat and protein and taken from Bylund (2003) for lactose.

	Mean radius [nm]	Diffusivity [m^2/s]		Diffusion time scale [s]	
		at 25 °C	at 50 °C	at 25 °C	at 50 °C
Fat globules	1000	$2.2 \cdot 10^{-13}$	$1.2 \cdot 10^{-12}$	5724	1056
Protein (caseinate)	75	$2.9 \cdot 10^{-12}$	$1.6 \cdot 10^{-11}$	429	79
Lactose	0.5	$4.4 \cdot 10^{-10}$	$2.4 \cdot 10^{-09}$	2.9	0.53

In the drying process subsequent to droplet generation, the droplet surface remained covered by the fat film due to its hydrophobicity. There was, however, a trend of increasing protein content at the surface from 4.4 to 7.5 % v/v.

6.5.3 Chemical Surface Composition of the Low-Fat Emulsion Droplets at Discrete Drying Times

The investigation of the LFMM emulsion behavior during single droplet drying (Figure 6.3b) gave a better insight into the protein migration process. Also in this case the fat was highly overrepresented at the surface in comparison to the bulk composition. With a fat concentration of 0.5 % v/v in d.m. in the feed emulsion, a multiple thereof was present at the droplet surface, starting with 18.5 % v/v and then declining marginally to approximately 13.5 % v/v. However, this time the fat did not dominate at the surface. Again, the surface compositions of the droplets generated with the micro-volume syringe were

similar to droplets of the same milk model emulsion after atomization in different spray dryers as reported in Chapter 3. Consequently, the observed surface formation and drying kinetics could be considered as representative for droplets in a spray dryer. On a general note, however, such an agreement in initial droplet surface state between single droplet drying and spray drying is not guaranteed, because the droplet generation process in single droplet drying is different to the disintegration mechanism in an atomization nozzle. This hence needs to be validated case-by-case.

Due to the lower fat content at the surface in comparison to the RFMM droplets, a significant rise in protein surface concentration with proceeding drying time could be observed. This protein migration to the surface was presumably governed by diffusion, since the diffusion time of the caseinate molecules possibly lay within the range of the singe droplet drying time scale (Table 6.2). The cause of this diffusion could have been twofold. First, the drying process induced a radial gradient in water concentration from the inner of the droplet towards the surface, where water was continuously removed as a result of evaporation. Consequently, concentration gradients in fat, lactose and protein developed in reverse direction from the surface towards the droplet center and induced inward diffusion. As there was a considerable difference in the diffusivities of the components (Table 6.2), they diffused at dissimilar speeds. The diffusivity of lactose exceeded the one of caseinate by about two orders of magnitude. This might have led to enrichment of protein, in comparison to the lactose concentration, at the outer droplet regions. Second, caseinate molecules are surface active and therefore a part of them could adsorb at the air/water interface of the droplets (Graham and Phillips, 1979). As such, the adsorption at the surface reduced the concentration gradient in free diffusing protein molecules and thus counteracted the above described protein movement towards the droplet center.

While an efficient encapsulation of the fat phase in the particle middle is desired in industrial applications for optimum functional properties, high amounts of protein at the particle surface can also imply detrimental effects. For instance, it has been shown that native casein micelles are prone to form an interlinked network between the surfaces of aggregated powders, hence reducing the dispersibility and water penetration ability (Crowley et al., 2016, Schuck et al., 2007). Figure 6.3b further shows that, concomitant with the increase in protein concentration, the lactose surface concentration declined from 34.0 to 18.3 % v/v. The comparatively low lactose surface content potentially influenced the particles' solubility in aqueous medium adversely (Anema et al., 2006, Baldwin and Truong, 2007).

Although the diffusivity of the fat globules was even about one order of magnitude smaller than the one of caseinate, the surface of the LFMM droplets did not further enrich in fat over drying time. The reason for this might be that the high protein-to-fat ratio in the low-fat emulsion, in combination with the low fat globule size of 1 µm in diameter, lead to an extensive encapsulation of the fat globules by thick protein membranes that were bound to them. Thus, despite a potential concentration of the slow diffusing fat globules at the droplet surface, the surface fat content did not exceed a certain threshold. The comprehensive protein membranes were also believed to prevent rupture of the fat globules and consequent

spreading of a consistent fat film over the droplet surface, unlike the observations made for the RFMM droplets.

The results of this modified single droplet drying technique were compared with the study conducted by Fu et al. (2011a), where the same single droplet drying rig at identical drying air temperature and flow rate was used for 2 µl skim and whole milk droplets. In agreement with the results discussed in respect to Figure 6.2 and Figure 6.3, after a drying time of 50-80 s both investigated emulsions featured semi-dried droplets with hydrophobic shells, which were less water-wettable for whole milk in comparison to skim milk. Yet, they concluded an increasing surface fat content with drying time from a rise in repulsion of attached water droplets, which does not correspond with the outcomes of this study. The wettability might have been impaired by a proceeding crust formation rather than by a supposed increase in fat content on the surface of that crust. The interpretation of the dissolution study was ambiguous due to overlapping influences between different rates of crust formation for whole and skim milk and the actual difference in composition between those crusts. In conclusion, the advantage of the proposed single droplet drying technique over such a dissolution study seems to be that it allows to, firstly, investigate droplets immediately subsequent to their generation at any moisture content and, secondly, to observe the change in the components' surface concentration itself.

6.5.4 Changes in Droplet Mass, Temperature and Size

How the observed changes in component distribution near the surface of drying RFMM and LFMM droplets influenced their drying and shrinkage characteristics was evaluated on the basis of the other single droplet drying measurements. Excerpts of the corresponding data about the droplet mass, temperature and diameter behavior over drying time are shown in Figure 6.4. The evaporation rate was identified to be considerably faster in the early drying stage (Figure 6.4a,b). The curve shapes agreed well with mass change data from literature for 20 % w/w skim milk droplets of 1.6 µl initial volume at 91.4 °C drying air temperature (Chen and Lin, 2005). The final particle masses were proportional to the initial droplet volumes. The mass changes at early drying were most rapid, as with proceeding drying the crust formation built up an increasing mass transfer resistance for moisture movement towards the surface. This was also reflected in the horizontal axes of Figure 6.3: for instance, the free moisture content of the 3 µl RFMM droplets had been reduced from 4.0 to 1.55 kg/kg after the initial 100 s of drying, whereas it only altered by about 1.0 kg/kg to 0.52 kg/kg in the following 100 s. In comparison, during the first 100 s of drying of the 3 µl LFMM droplets, the free moisture content sank more significantly to 1.17 kg/kg. This indicated that a lower fat content (at equal total solid content) favored water transport to the surface and hence evaporation from the surface.

It can be seen from Figure 6.4c,d that the temperature profiles approached asymptotically the bulk temperature of the drying air (70 °C). Slight dips in the temperature rise took place at the wet bulb temperature of around 25-30 °C after 15-40 s drying time. There were no distinct temperature plateaus as for

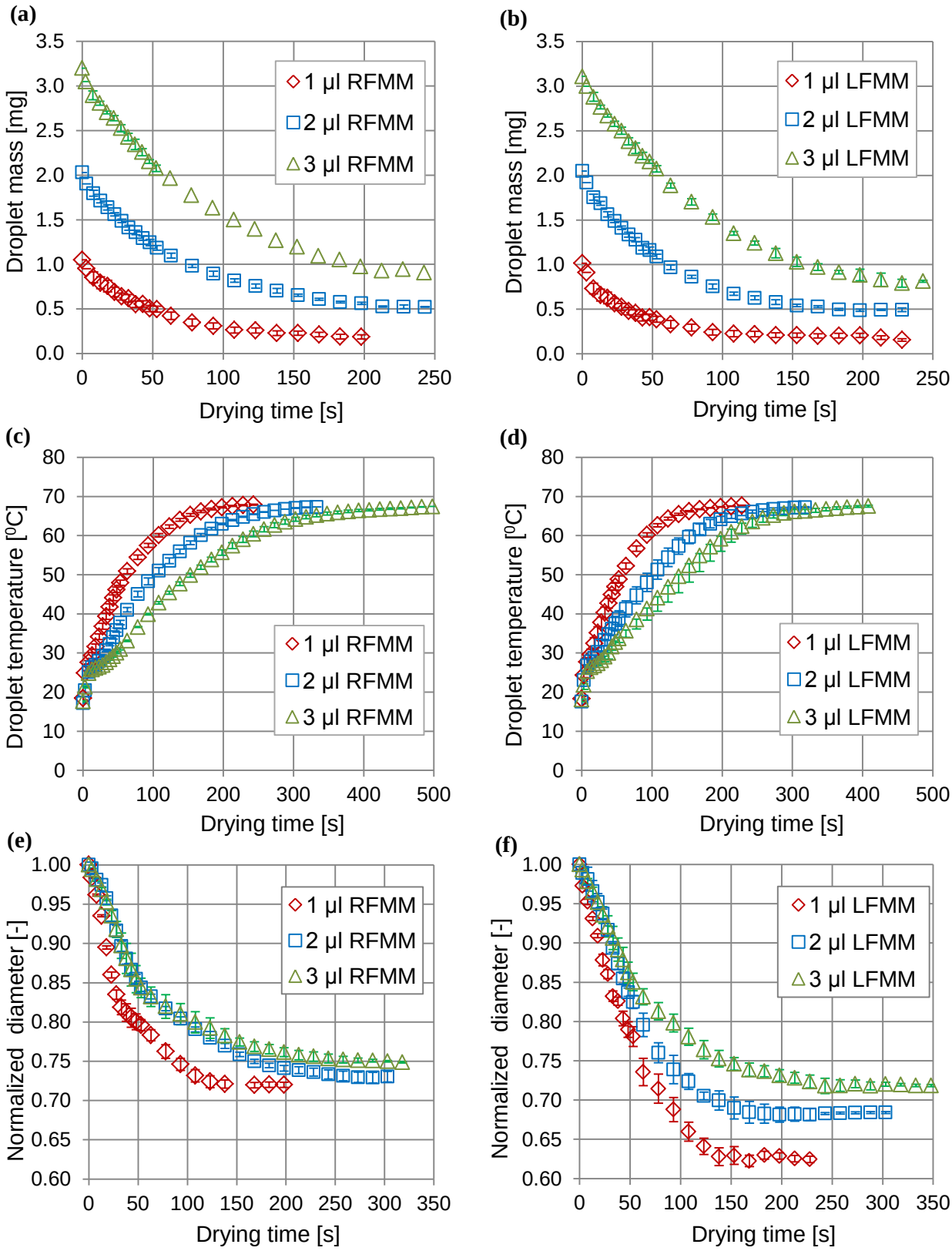

Figure 6.4: Experimental results from single droplet drying for RFMM and LFMM droplets with different initial volumes over drying time: (a), (b) droplet mass; (c), (d) droplet temperature; (e), (f) normalized equivalent spherical droplet diameter.

example found during single droplet drying of lactose solutions by Fu (2012), since lactose is not shell forming and thus allowed free surface water during most of the drying. The immediate formation of a hydrophobic fat film on the surfaces of both model emulsions presumably further contributed to the very low free surface water and the consequent lack of a temperature plateau at wet bulb temperature.

The shape of the droplets remained almost spherical (circular projected cross-section) throughout the drying process for all initial droplet volumes and both samples until some buckling occurred in the final drying stages. As such, the reported equivalent spherical diameter can practically be considered as approximate true diameter of spherical droplets. The observed profiles of the normalized droplet diameters over drying time (Figure 6.4e,f) corresponded well with the results obtained by Chew et al. (2013), where skim milk droplets of 40 % w/w initial solid content were investigated in the same single droplet drying rig at various drying air conditions. Yet, the shrinkage was less pronounced in the experiments conducted by Chew et al. (2013) due to a higher solid content. The bigger the initial droplet volume was, the longer was the existence of an appreciable change in diameter and the larger was the final normalized diameter of the dried particle. For larger initial droplets, it is believed that full crusts at the surface had been developed earlier relative to the remaining total amount of moisture inside the droplets. These solidified shells decelerated the moisture transport to the droplet surfaces and inhibited the degree of shrinkage relative to the initial diameter. Furthermore, comparison between Figure 6.4e and Figure 6.4f revealed that more considerable shrinkage occurred for a lower fat content. In consideration of that, the fat content seemed to also have a significant influence on the shrinkage kinetics and the final particle size, as will be discussed in the following in respect to the REA outcomes.

6.5.5 Shrinkage Kinetics

The temperature, mass and diameter data were processed by means of REA to produce correlations between the normalized diameter and the free moisture content as well as between the normalized activation energy of evaporation and the free moisture content. As can be seen in Figure 6.5a, the normalized diameter curves for the different initial droplet sizes of RFMM emulsions lied close together and featured a proportional relationship between normalized diameter and free moisture content. The r^2 value and the fitting parameter B of the corresponding linear trend line, which was expressed in accordance to Eq. (6.8), are given in Table 6.3. In contrast, the normalized diameter curves of the LFMM droplets varied appreciably with their initial volumes of 1, 2 and 3 µl, as reflected by the considerably lower r^2 value of the linear fitting curve of all LFMM points. In particular once the moisture contents came below 0.5 kg/kg, the curves of the different initial LFMM droplet sizes deviated significantly. For the smallest initial size, the droplets experienced a significant further shrinkage at low moisture content, whilst the diameter hardly changed anymore for droplets with an initial volume of 2 and 3 µl. This was in agreement with a study conducted by Chew et al. (2015), where out of three milk model emulsions the one with the highest fat content featured the least shrinkage, particularly at low moisture content. In

addition, also at intermediate moisture contents (3.5-1 kg/kg) the normalized diameter curves described different trends, in particular comparing the drying droplets of 1 and 3 µl initial volume.

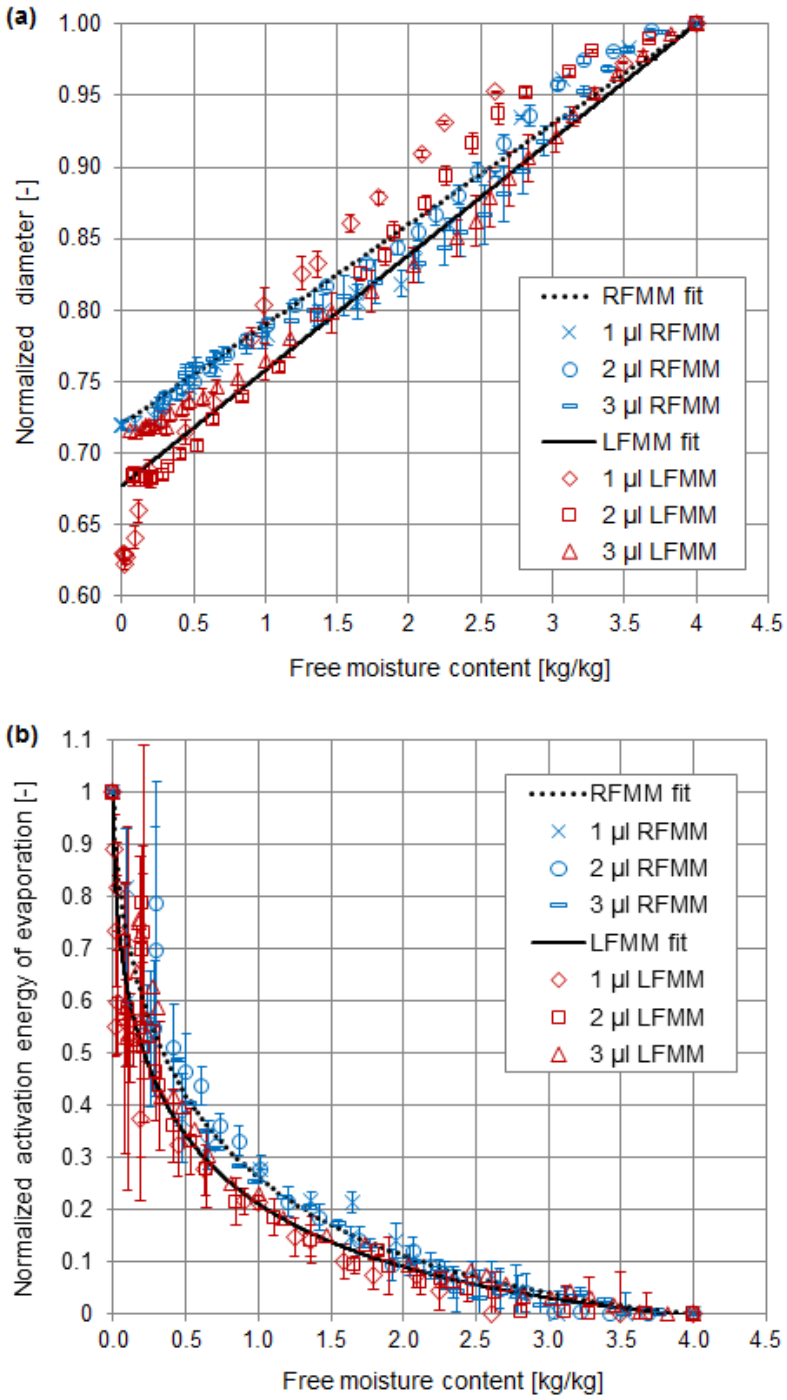

Figure 6.5: From single droplet drying experiments derived drying and shrinkage kinetics: RFMM and LFMM droplets with different initial volumes over free moisture content, including one trend line fitting for all volumes of each sample and propagated error bar,: (a) normalized droplet diameter and (b) normalized activation energy of evaporation.

Comparing the normalized diameter profiles of the two model emulsions, the low-fat droplets experienced more shrinkage relative to the initial diameter owing to a more significant decrease in diameter in

the second drying half (2.0-0 kg/kg free moisture content). All these described differences in the normalized diameter curves for different initial droplet sizes (in case of the LFMM emulsion) and for different fat contents were clearly greater than the depicted standard deviations. It was therefore concluded that the different fat contents and the surface composition of the drying droplets exerted crucial impact on the shrinkage characteristics. As a result of water evaporation from the surface, the droplets became enriched in their non-aqueous components near the surface with an increase in water concentration towards the center. The RFMM droplets were covered by a fat film throughout the whole drying process. Consequently, the crust that was forming in the surface region featured hydrophobic properties and, as such, inhibited shrinkage of the drying droplet due to repulsion towards the moisture in the droplet center. In comparison, the shells of the LFMM droplets underwent more contraction, because they did not contain a dominating amount of fat in their peripheral areas. Instead, 48-68 % v/v of the surface was occupied by protein (Figure 6.3b). Because of attractive forces between the hydrophilic groups of the protein and the water contained inside the droplets, the surface shell presumably was less resistive to changes in diameter in comparison to the RFMM droplets.

The complex impact of various kinds of protein on the shell behavior in drying droplets is an area of high interest for various applications. The physical properties, such as sol-gel transition, molecular weight and conformation behavior, can vary widely, even for the different protein types encountered in milk. For instance, native casein micelles tend to arrange in soft, flexible shells. In contrast, whey protein has been shown to form hard, brittle shells with higher restraint to deformation at high concentration regimes (Sadek et al., 2014a, Sadek et al., 2015). In the present study, the protein component consisted to 80 % w/w of calcium caseinate and to only 20 % w/w of whey protein. As such, the protein shell of the LFMM droplets was relatively flexible. Though caseinate molecules do not assemble in micelle structures like native casein, they feature strong hydration ability and a dynamic molecule structure, in particular in comparison to the denser, hydrophobic fat phase. In view of that, it is proposed that with advancing solidification at the droplet surface, the caseinate molecules were able to pack into a denser configuration under dehydration and reconfiguration. As a result, the shells of the LFMM droplets, which were high in caseinate, remained more deformable than the high-fat shells and exhibited a plastic behavior at low moisture contents. Accordingly, despite ongoing solidification with longer drying time, the shell of the LFMM droplets still possessed relatively high water permeability and flexibility in terms of shrinkage at low moisture contents, as the protein surface content was rising simultaneously (for instance from 59.5 % v/v at a moisture content of 0.42 kg/kg to 68 % v/v at completed drying). This could have allowed the above described considerable extent of shrinkage at a late drying stage. Possibly, a less rigid shell was also responsible for the LFMM droplets being more prone to shell expansion and collapse as subject to vapor pressure in the droplet center (if internal evaporation occurred) and capillary force. This is believed to have led to the above described, distinct deviations in the normalized diameter curves for 1, 2 and 3 µl initial droplet volume. For example, the rise in protein surface concentration might have been more pronounced for a shorter diffusion length and hence the

normalized diameter curve of the 1 µl LFMM droplets showed stronger deviation from linear behavior in comparison to 2 µl and 3 µl LFMM droplets.

Table 6.3: Correlations of the normalized activation energy of evaporation and the normalized droplet diameter over free moisture content: fitting constants a, b, c, B and coefficients of determination r^2 with regard to Eq. (6.7) and Eq. (6.8), respectively.

	Norm. activation energy				Norm. diameter	
	a	b	c	r^2	B	r^2
RFMM	1.092	-1.130	0.575	0.952	0.720	0.962
LFMM	1.104	-1.256	0.471	0.951	0.677	0.700

6.5.6 Drying Kinetics *via* Reaction Engineering Approach

The activation energy of evaporation was calculated as a function of moisture content according Eq. (6.5) and its maximum value $\Delta E_{v,max}$ was determined by Eq. (6.6) in order to plot Figure 6.5b. The standard deviations of the normalized activation energy points were reasonably low, except from the low moisture content region below 0.5 kg/kg. At slow evaporation rates the mass changes tended to go towards zero and so, along with a significant standard deviation in mass change relative to the absolute mass change, the propagated error in activation energy became large in this region. The normalized activation energy of evaporation increased exponentially with smaller free moisture content for both model emulsions. The reason for this was a rise in the apparent resistance to evaporation, as the vapor pressure at the droplet surface and the effective water diffusivity declined the further the crust formation had been advanced. Therefore, the water movement to the surface and the evaporation rate decelerated with preceding drying. Furthermore, the activation energy of the RFMM droplets was slightly higher than the one of the LFMM droplets at moisture contents of around 2.0 kg/kg and below.

Because of the previously discussed hydrophobic character of the fatty surface shell that occurred in the RFMM droplets, the water movement to the droplet surface was additionally repelled in the drying RFMM droplets. Whereas the shell of the RFMM droplets was dominated by lipids throughout the whole single droplet drying process, the shell of the LFMM droplets contained less than a quarter of this fat amount and protein enriched more and more with declining moisture content. In view of that, it was concluded that the higher fat content slowed down the drying process and concurrently limited the particle shrinkage. The obtained activation energy data did not scatter significantly between the different initial droplet volumes, and thus one trend curve for all RFMM and another trend curve for all LFMM points could be applied (r^2 value of 0.952 and 0.951, respectively). The mathematical expression of the trend curves followed Eq. (6.7), and the fitting parameters are presented in Table 6.3. This agreed with the results from previous studies of a range of solutions and emulsions with initial solid contents below

40 % w/w, where the normalized activation energy curves were also approximately independent from the initial droplet volume (Chen, 2008, Fu et al., 2011b). In industry, such correlations for the activation energy of evaporation and droplet diameter can be implemented into CFD simulations to optimize process conditions, and to predict the moisture content and particle size of resulting powders, in response to fluctuations in the feed properties. In combination with component distribution data obtained from the modified single droplet drying analysis, the approach should allow a better understanding of a range of process conditions to control functional powder properties, such as stickiness.

6.6 Modeling Approach for Validation of Concepts

6.6.1 Spatiotemporal Simulation of the Component Distribution

A numerical model was developed to validate the concepts that were employed in Chapter 6.5 to explain the experimentally measured formation of the chemical surface composition of drying milk droplets. The purpose of the model was a prediction of the concentration profiles of the three main milk components (lactose, protein and fat) as a function of drying time. As opposed to the capability of the previous modeling approaches that are available in literature (see Section 2.2), this model allowed for protein surface activity and the influence of the solidification process on the component and water diffusivities as well as on the evaporation rate. Equations describing the conservation of heat, momentum and mass transfer were coupled with the semi-empirical drying and shrinkage kinetics that had been described by REA correlations as obtained from the above single droplet drying experiments. The simulation was performed for a LFMM droplet with an initial volume of 3 µl under drying conditions similar to the experimental investigation (drying air temperature of 70 °C, velocity of 0.75 m/s and humidity of 0.0001 kg/kg). Radial symmetry and no interaction between the species were assumed. Spatially resolved profiles of moisture content, temperature and concentration of lactose, protein and fat were computed over time by solving a set of partial differential equations, which will be summarized in the following, with the Method of Lines in MATLAB R2013a (MathWorks, United States).

6.6.1.1 Heat and Momentum Balances

The heat balance was expressed as:

$$\rho \cdot c_p \cdot \left(\frac{\partial T_d}{\partial t} + v_r \cdot \frac{\partial T_d}{\partial r}\right) = \frac{1}{r^2}\left(\frac{\partial}{\partial r}\left(k \cdot r^2 \cdot \frac{\partial T_d}{\partial r}\right)\right) \tag{6.11}$$

where ρ was the droplet density [kg/m^3], c_p the specific heat capacity of the droplet [J/(kg·K)], t the drying time [s], v_r the shrinkage velocity of the droplet [m/s], k the thermal conductivity [W/(m·K)] and r the radial coordinate [m]. The thermal conductivity was derived from a modified Ranz-Marshall correlation (Ranz and Marshall, 1952a, Ranz and Marshall, 1952b) according to Lin and Chen (2002).

The momentum balance was written as:

$$\rho \cdot \left(\frac{\partial v_r}{\partial t} + v_r \cdot \frac{\partial v_r}{\partial r}\right) = \mu \cdot \left(\frac{\partial}{\partial r}\frac{1}{r^2}\frac{\partial (r^2 \cdot v_r)}{\partial r}\right) \tag{6.12}$$

where μ was the droplet's dynamic shear viscosity [Pa·s].

The initial and boundary conditions for Eq. (6.11) and Eq. (6.12) were:

$$t = 0: \quad T = T_0, \;\; v_r = v_0 \tag{6.13}$$

$$r = 0: \;\; \frac{dT}{dr} = 0, \;\; v_r = 0 \tag{6.14}$$

$$r = r_0: \; k \cdot \frac{\partial T}{\partial r} = h_h \cdot (T_b - T_s) - h_m \cdot \left(\rho_{v,s} - \rho_{v,b}\right) \cdot \Delta H_v \tag{6.15}$$

where h_h was the convective heat transfer coefficient [W/(m^2·K)], T_s the droplet surface temperature [K] and ΔH_{vap} the enthalpy of evaporation [J/kg].

6.6.1.2 Incorporation of REA for Drying and Shrinkage Kinetics

In order to account for the resistance to evaporation and diffusion of water imposed by the crust formation, the reduction in surface vapor density (from saturated density $\rho_{v,sat}$ to a lower density $\rho_{v,s}$) was incorporated by the fractionality coefficient ψ as per Eq. (6.2). The fractionality coefficient was computed as a function of the global droplet moisture content, as described in Eq. (6.3), by means of the empirically determined REA activation energy of evaporation ΔE_{vap}. The activation energy of evaporation was defined by Eq. (6.7) with the kinetic parameters (*a*, *b*, *c*) for LFMM droplets presented in Table 6.3. Likewise, the droplet shrinkage was expressed by the REA shrinkage correlation of Eq. (6.8) with the corresponding kinetic parameter (*B*) taken from Table 6.3. Thereby, the assumption of perfect shrinkage, which is typically made in comparable models, could be omitted and a reliable expression for the retardation of water diffusion to the surface and vapor transfer from the surface to the drying air was implemented.

6.6.1.3 Water and Component Mass Balances and Diffusion Coefficients

The water mass balance was formulated in the following way:

$$\frac{\partial (C_s \cdot X)}{\partial t} = \frac{1}{r^2}\left(\frac{\partial}{\partial r}\left(D_w \cdot r^2 \cdot \frac{\partial (C_s \cdot X)}{\partial r}\right)\right) \tag{6.16}$$

where X was the radius dependent moisture content [kg/kg], C_s the solids concentration [kg/m^3] and D_w the water diffusivity [m^2/s].

The initial and boundary conditions of the water mass balance were:

$$t = 0: \quad X = X_0 \tag{6.17}$$

$$r = 0: \quad \frac{dX}{dr} = 0 \tag{6.18}$$

$$r = r_0: \quad -C_s \cdot D_w \cdot \frac{dX}{dr} = h_m \cdot (\rho_{v,s} - \rho_{v,b}) \tag{6.19}$$

The change in concentration of a component i (lactose, protein or fat) over time at a certain radial position was expressed by a combination of the convective mass flux and the diffusive mass flux according Fick's second law of diffusion, following Gardner (1965):

$$\frac{\partial C_i}{\partial t} + v_r \cdot \frac{\partial C_i}{\partial r} = \frac{1}{r^2}\left(\frac{\partial}{\partial r}\left(D_i \cdot r^2 \frac{\partial C_i}{\partial r}\right)\right) \tag{6.20}$$

where C_i was the concentration of component i [kg/m^3] and D_i its diffusivity [m^2/s].

The component diffusivities were calculated depending on the moisture content by means of a modified Stokes-Einstein equation. When simulating a full drying process where the component concentrations vary from diluted until almost dry, it needs to be accounted for the influence of the solids concentration on the medium viscosity and hence on the diffusivities. As suggested by Chen et al. (2013), this crowding effect can be described by Quemada's model (Quemada, 1982) with a correction factor f:

$$D_i = \frac{k_B \cdot T}{6 \cdot \pi \cdot \mu_w \cdot R_i} \cdot f \tag{6.21}$$

$$f = \left(1 - \frac{\Phi}{\Phi_{max}}\right)^2 \tag{6.22}$$

where μ_w was the dynamic water viscosity [Pa·s], R_i the component radius according Table 6.2 [m], Φ the global volume fraction of all three components combined [m^3/m^3], and Φ_{max} the theoretical maximum packing volume fraction [m^3/m^3]. Using the Quemada's value for the maximum packing volume fraction under the assumption of perfect uniformly sized spheres, values of approximately 0.7 were obtained. Though a value of 0.95 would be more realistic, the ratio Φ/Φ_{max} will still be accurate.

6.6.1.4 Boundary and Initial Conditions of the Component Mass Balances (Case 1 and Case 2)

In its standard form, the model's initial surface ratio between lactose, protein and fat was set to be equivalent to the experimentally measured initial surface composition directly after droplet generation, which was implemented by means of a step change near the surface (case 1). Also a second scenario was studied where the bulk composition was set as initial surface composition (case 2).

Initial conditions of Eq. (6.20) - case 1:

$$t = 0, (r_0 - 25\ \mu m) < r < r_0: \quad C_i = C_{i,exp} \tag{6.23}$$

$$t = 0, r < (r_0 - 25\ \mu m): \quad C_i = C_{i,bulk,corr} \tag{6.24}$$

where $c_{i,exp}$ was the experimentally determined initial surface concentration and $c_{i,bulk,corr}$ the corresponding bulk concentration after correction by the relative excess or shortfall of component i due to accumulation or depletion in the surface layer [kg/m^3].

Initial conditions of Eq. (6.20) - case 2:

$$t = 0: \quad C_i = C_{i,bulk} \tag{6.25}$$

where $C_{i,bulk}$ was the bulk concentration [kg/m^3].

In either case, the protein mass balance was complemented by a description of adsorption at the air/water interface. The boundary conditions of Eq. (6.20) thus were:

$$r = r_s: \ D_{lac} \cdot \frac{dC_{lac}}{dr} = C_{lac} \cdot v_s \ , \qquad D_{fat} \cdot \frac{dC_{fat}}{dr} = C_{fat} \cdot v_s \ ,$$
$$D_{prot} \cdot \frac{dC_{prot}}{dr} = C_{prot} \cdot v_s + k_a \cdot C_{prot} - k_d \cdot Q_{prot} \tag{6.26}$$

$$r = 0: \ \frac{dC_i}{dr} = 0 \tag{6.27}$$

where the subscript $i = lac, fat, prot$ denoted lactose, fat and protein, respectively. As further elaborated in Appendix 5.A, k_a was the kinetic adsorption parameter [m/s], k_d the kinetic desorption parameter [1/s] and Q_{prot} the concentration of adsorbed protein at the surface [kg/m^2].

6.6.2 Comparison of Simulation Results with Experimental Data (Case 1 and Case 2)

Model validation was performed in two ways. Firstly, validation by means of the change in droplet temperature or drying rate has been the method of choice employed in many studies on comparable droplet drying models (see Table 2.4 in Section 2.2). Therefore, in this work, the simulated changes in global droplet temperature and global droplet moisture content over drying time (using case 1 for the initial conditions of the component mass balances) were compared with the results observed during experimental single droplet drying (see Figure 6.9 in Appendix 5.B). Good agreement between the simulated and experimental profiles was found, indicated by r^2 values of 0.998 for each profile. It was hence concluded that the model computed accurately both droplet moisture content and temperature with proceeding drying. The temperature profiles were found to be uniform over the droplet radius at any given drying time (data not presented here, see publication for further information) as a result of a relatively slow temperature change at the surface in comparison to the heat conduction inside the droplet.

Secondly, a small number of numerical models on the chemical surface formation of drying droplets were validated by comparison with the XPS surface composition of spray-dried particles (Chen et al., 2011, Wang et al., 2013). Although this approach is of particular value for modeling applications that investigate the component segregation during drying, the comparability between simulation and experiments was limited, because the drying environment of the model did not precisely replicate the spray drying environment, and only evaluation of the surface compositions after completed spray drying was possible. In the present study, the development of the above described single droplet drying technique coupled with cryogenic flash freezing allowed for experimental surface composition data at various drying times under single droplet drying conditions that were similar to the model. These experimental results (presented in Figure 6.3) were compared with the simulation outcomes utilizing the initial conditions according to either case 1 or case 2 for the component mass balances (see Section 6.6.1.4).

In literature, it is typically reported that the bulk composition was used for the initial surface concentrations. This simplifies the methodology, as no experimental analysis of the droplet surface composition after droplet generation is required. It was therefore tested if the bulk composition of lactose, protein and fat can be employed as initial surface condition of the component mass balances according to Table 6.1 (case 2, Eq. (6.25)). As presented in Figure 6.6a, the protein surface composition corresponded reasonably well with the experimental data (difference of -2.4, -5.6, -8.0, -1.6 and 5.2 % v/v after respective drying times of 20, 50, 100, 200, 420 s). However, the model significantly over-predicted the lactose surface concentration (Figure 6.6b) throughout the whole drying process (difference of 22.4, 23.8, 20.2, 13.9, 8.4 % v/v after 20, 50, 100, 200, 420 s, respectively). Particularly deficient was the simulation of the fat surface content, where the predicted values were a manifold of magnitudes smaller than the experimental results (Figure 6.6c). Whereas the lowest experimentally determined fat surface concentration was 12 % v/v (at a corresponding drying time of 200 s), the simulation predicted values of 0.5 % w/w or lower at any drying time. This consequently demonstrated that the simulation under application of case 2 did not capture the overrepresentation of fat on the surface of drying milk droplets.

Figure 6.6 further illustrates the results obtained when case 1 was employed for the initial conditions of the component mass balances (Eq. (6.23) and Eq. (6.24)). The simulated surface concentrations in protein after various drying times were in good agreement with the experimental study, as well as with the simulation when applying case 2 (Figure 6.6a). The reason for this was that the experimentally determined initial surface concentration did not differ significantly from the bulk composition (6 % v/v overrepresentation, see Figure 6.3) and both modeling scenarios accounted for the protein surface activity. Regarding the lactose surface concentration (Figure 6.6b), simulation utilizing case 1 led to a strongly improved accuracy (difference of 11.8, 14.5, 11.4, 5.0, 0.5 % v/v after 20, 50, 100, 200, 420 s, respectively), as compared to case 2. The reason for this was that the experimental study showed a significant underrepresentation of lactose at the surface after droplet generation in relation to the bulk composition (by about 24 % v/v), which was only accounted for by the initial surface conditions of case

1. While an appreciable deviation from the experimental data was formed during the first 20 s of drying, the lactose surface concentrations agreed progressively better with proceeding drying. Figure 6.6c highlights that simulation under utilization of the experimentally determined initial surface composition still underestimated the amount of surface fat (difference of -7.8, -8.7, -3.7, -4.6, -7.7 % v/v after 20, 50, 100, 200, 420 s, respectively), but featured a considerably better accuracy than when neglecting the atomization induced enrichment of fat at the droplet surface.

While the absolute values agreed reasonably well with each other, in relative terms the simulated values were already 40 % below the experimental results after the first 20 s of drying. The discrepancy in fat surface composition remained throughout the remaining drying time due to a monotonic decrease in simulated fat surface concentration with longer drying time. This can be explained by the hydrophobic nature of the fat phase, which had not been accounted for in the model. Due to the distinct overrepresentation of fat at the surface of the freshly generated droplet and the much lower fat concentration in the bulk, the model predicted a strong diffusive flux of fat towards the inner of the droplet along this gradient. In reality, however, the repulsion between the water inside the droplet and the hydrophobic fat layer inhibited this diffusion process and caused the surface fat to remain at the air/water interface to greater extent than computed by the model. Qualitatively, nevertheless, the model described the surface fat content reasonably well and with considerably greater precision than when the bulk composition was used as initial condition. This highlights that coupling single droplet drying experiments with cryogenic flash freezing to track the change in the chemical surface composition of drying droplets can be very useful for application in a corresponding mathematical model in two respects; for finding suitable initial conditions and for validation of the model.

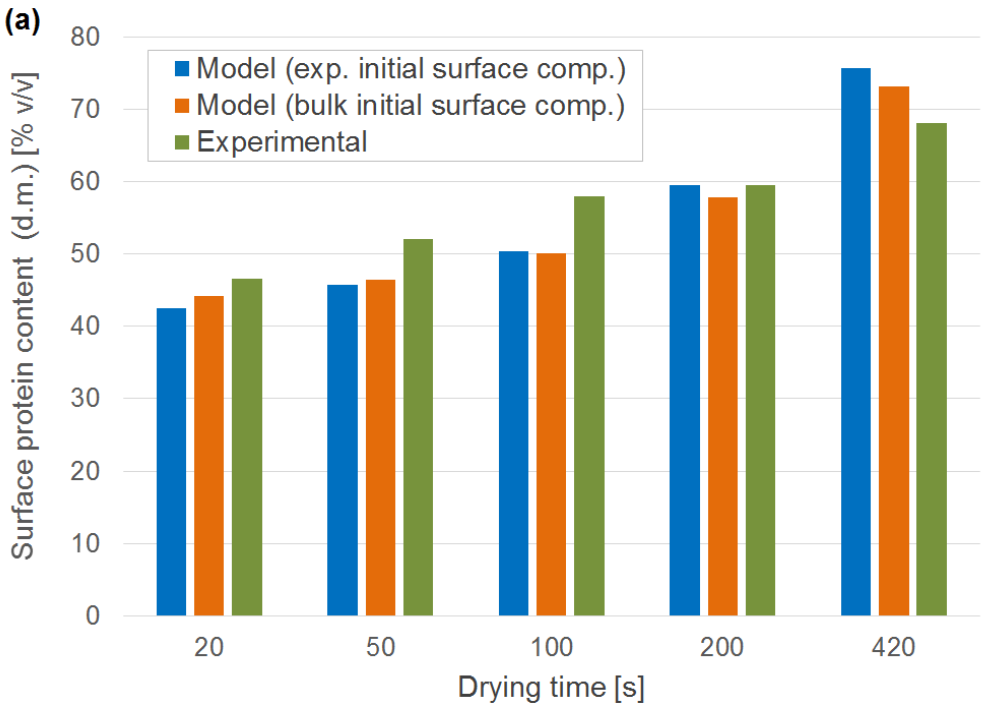

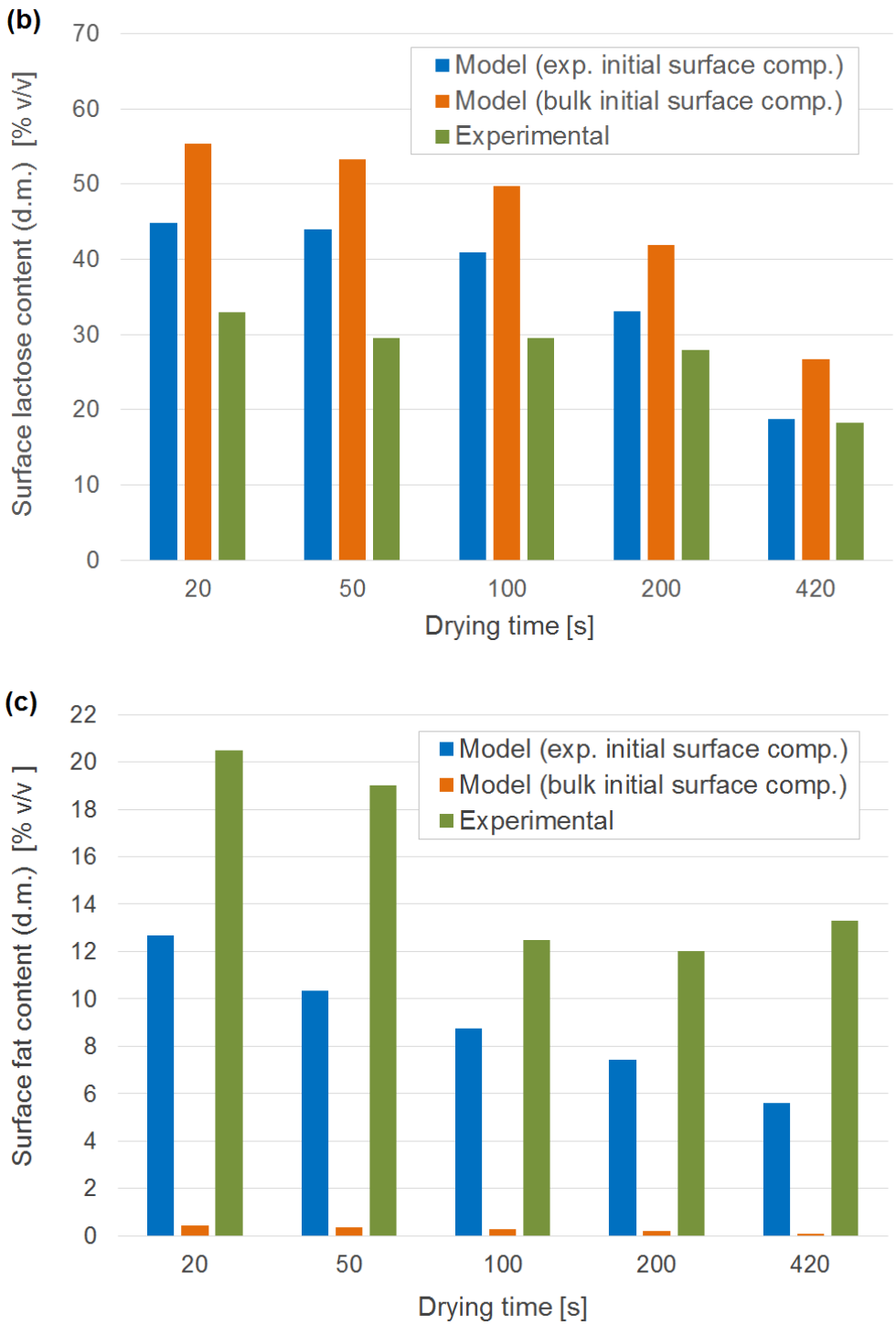

Figure 6.6: Simulated surface concentrations after certain times during single droplet drying of a LFMM droplet with an initial volume of 3 µl: comparison with experimentally obtained values (green) for (a) protein, (b) lactose, and (c) fat. Either the experimentally measured initial surface composition (case 1, blue) or the bulk composition (case 2, orange) was used as initial surface condition.

6.6.3 Simulated Component Segregation at the Droplet Surface (Based on Case 1)

Using case 1, the numerical model was demonstrated to be applicable for the estimation of the surface composition during single droplet drying of milk. Under consideration of its limitations regarding the simulation of the fat concentration as discussed in Section 6.6.2, it thus can be utilized to verify the assumptions about the component segregation process made from the experimental observations in Section 6.5. In Figure 6.7, the spatial profiles of the moisture content at different drying times are presented for increasing radius from the droplet center (0 mm) to the surface (approximately 0.9 mm initially). The simulation data confirmed the existence of a declining concentration in water from the surface towards the center because of evaporation from the surface. During the early drying stages the gradients were particularly distinct, whereas they decreased with proceeding drying until the end of drying. The slopes of the moisture profiles were more pronounced in proximity to the droplet surface than near the droplet center. As such, component segregation as a result of the strong variance in diffusivity of lactose, protein and fat (compare to Table 6.2) can be expected to be particularly significant close to the surface. In addition, the concentration gradients of protein and especially of fat near the surface were enhanced by the difference between initial surface composition and bulk composition.

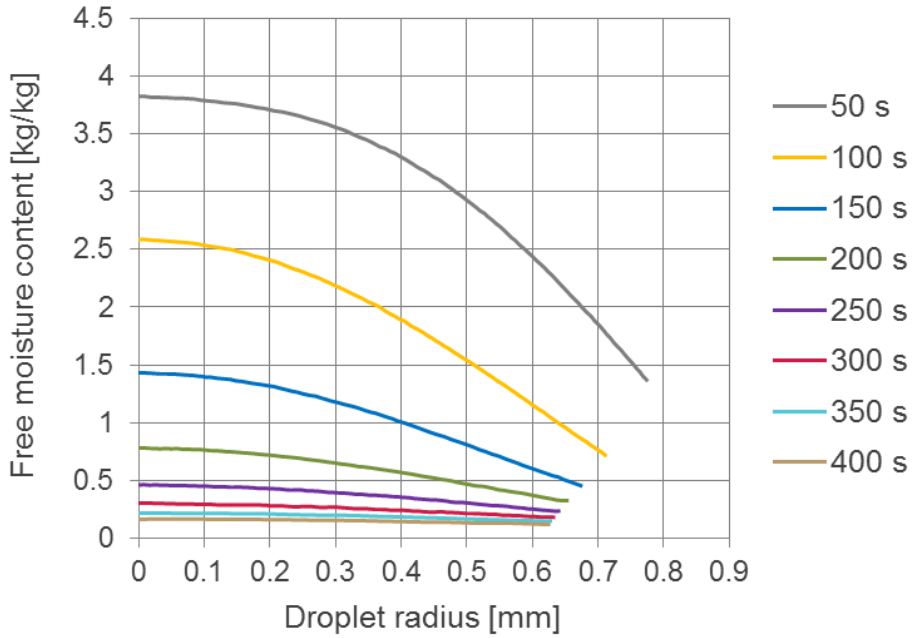

Figure 6.7: Simulated moisture content profiles at certain times during single droplet drying. The experimentally measured initial surface composition was used as initial surface condition (case 1).

Figure 6.6 shows that the surface concentration of every component experienced significant changes over drying time. As lactose featured the smallest hydrodynamic radius amongst the three components, it underwent strong depletion at the surface (Figure 6.6b), which was in line with the experimentally obtained surface composition. In addition, the decrease in lactose surface composition with proceeding drying time was amplified by the protein's surface activity. Protein enriched at the surface (Figure 6.6a),

attracted by its adsorption at the air/water interface. The model also predicted a significant decline in fat overrepresentation at the surface (Figure 6.6c). Already ahead of the actual drying process, a fat overrepresentation existed at the droplet surface, whose origin will be discussed in Section 6.6.4. Consequently, the concentration gradient in fat was more pronounced than for the other two components, causing a relatively fast inward diffusion process, despite the lower diffusivity of fat in comparison to lactose and protein. Furthermore, the transport of protein to the surface due to its surface activity enhanced the decrease in fat surface content. As such, the model confirms that during the drying process the component distribution is influenced by the protein surface activity and, to lesser extent, by the differences in the component diffusivities. However, a decisive impact on the final particle surface was also exerted by atomization induced component segregation, particularly in respect to the surface fat formation. As discussed before, the model did not accurately describe the retention of the surface fat, whilst this had been observed in the experimental analysis (presumably due to the fat's hydrophobicity).

6.6.4 Diffusion Controlled Segregation between Droplet Generation and Flash Freezing

As Figure 6.3 highlights, the experimentally measured surface composition of the LFMM droplets already differed significantly from the bulk composition ahead of the drying process (0 s). As such, it was concluded that component segregation must have occurred prior to drying. This segregation could either have been taking place during droplet formation or during the time that elapsed between droplet generation and commencement of drying (or flash freezing of the sample, respectively). To examine the latter possibility, the change in component distribution in a LFMM droplet without drying was simulated. In the experiments, the droplets were not exposed to a drying air flow during their transfer from the syringe to the suspension filament or into the liquid nitrogen bath, but only to quiescent air at room temperature. The equations that described the evaporation of water and the heating of the droplet (Eq. (6.11) - Eq. (6.19)) were therefore omitted for this simulation. The initial surface composition was set to equal the bulk composition (case 2 in the component mass balances). If the experimentally obtained surface concentrations were primarily caused by diffusion during the time between droplet generation and commencement of drying or flash freezing, the model should predict a similar surface composition within the first few simulated seconds when implementing the bulk composition as initial condition.

As can be seen from Figure 6.8, the simulation predicted that the protein and lactose components would need an approximate time of 50 s and 200 s, respectively, to reach the experimentally measured initial surface contents. Throughout the full simulated time of 7 min, the computed fat concentration at the droplet surface stayed well below the initial surface fat content that had been determined in the single droplet drying experiments. Moreover, the model predicted a decline in surface concentration of the fat due to replacement by surface active protein. As a result, a diffusion controlled segregation process cannot be considered to be responsible for the experimentally observed surface fat. In addition, con-

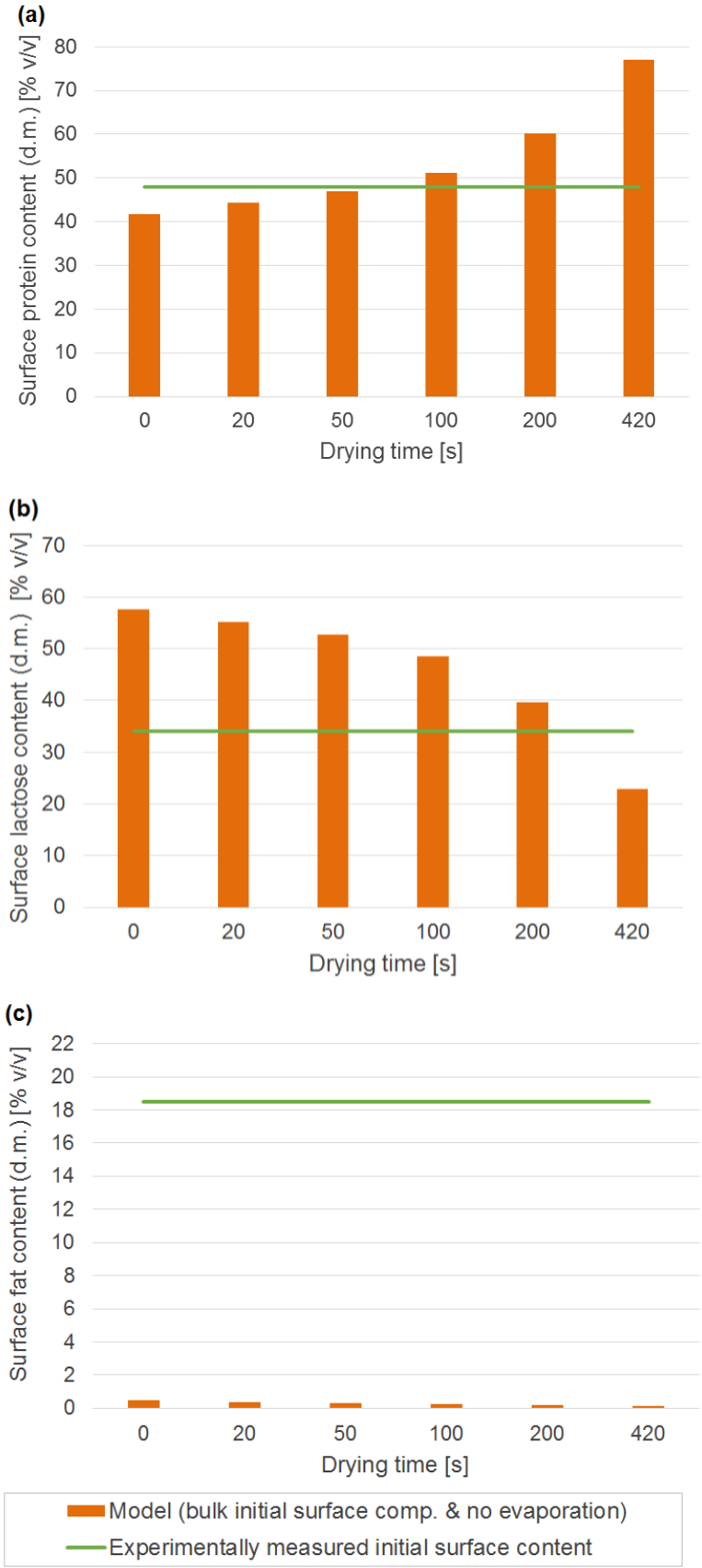

Figure 6.8: Simulated surface concentrations at certain times after droplet generation without evaporation: (a) protein, (b) lactose, and (c) fat. The bulk composition was used as initial surface condition (case 2).

sidering the relatively short duration between commencement of droplet generation and cryogenic flash freezing in comparison to the time necessary for lactose and protein to attain the experimentally measured surface concentrations, also the surface composition in lactose and protein cannot be ascribed to a diffusion controlled process. The droplet generation process took only 1-2 s and the subsequent transfer of the droplet into liquid nitrogen for flash freezing required 2-3 s. Convection, which could have been formed during droplet generation, might have accelerated the transport of the hydrophobic fat or surface active protein to the surface during this time. In light of the previous results about the segregation process in spray-dried milk droplets (compare to Chapter 3 and Chapter 5), however, it seems most likely that a similar, atomization induced mechanism also took place during droplet generation in the single droplet drying experiments and that this mechanism was primarily responsible for the observed surface fat. The simulation results strengthen the hypothesis made in Section 6.5.2 that the difference between the bulk and measured initial surface composition was a result of the previously proposed disintegration mechanism. As a consequence thereof, the fat phase covered the droplet surface immediately after droplet formation, independent from diffusion or convection controlled transport phenomena.

6.7 Conclusions

The drying behavior of droplets from two milk model emulsions with different fat contents was studied in a filament single droplet drying rig. The study demonstrated the modification of suspended single droplet drying by a flash freezing approach to interrupt the drying process at certain times in order to record the changes in component distribution and chemical surface composition. This new analysis method facilitated two complementary studies: an experimental observation of the connection between droplet surface composition and drying kinetics, and a mathematical simulation of the drying process with accurate initial surface conditions and a robust validation technique.

Firstly, the influence of the composition of the developing surface shell on the drying characteristics was experimentally investigated. The initial surface composition during single droplet drying of the investigated milk model emulsions was found to be consistent with the one of spray-dried milk droplets directly after atomization, which was reported in Chapter 3. Therefore, the observed surface formation and its impact on the drying and shrinkage kinetics with proceeding single droplet drying could be considered as representative for a spray drying process under comparable conditions. For the higher fat content emulsion, the droplet shrinkage was less distinct and the evaporation process was slower. This was explained by the existence of a hydrophobic fat film, which had occurred at the surface immediately after droplet generation and remained until completion of the drying process. The surface of the low-fat model emulsion droplets also featured an overrepresentation of fat in respect to the bulk composition, but the absolute surface concentration was lower than the one of protein. The protein further enriched near the surface with increasing drying time, presumably by diffusion due to its surface activity

and its lower diffusivity in comparison to lactose. It thus imposed a more hydrophilic, flexible character of the surface shell. This caused the shell of the low-fat model emulsion droplets to be more susceptible to shrinkage and more permeable for evaporating moisture.

Secondly, the measured change in surface concentration during single droplet drying of low-fat milk model droplets was applied on a numerical simulation model for computation of the spatiotemporal distribution of lactose, protein and fat. It was demonstrated that the choice of the initial surface composition was critical for accurate simulation of the component segregation in drying milk droplets. Furthermore, the experimentally obtained surface composition data was valuable for validation of the simulation results. Also the experimentally derived drying and shrinkage kinetics, which had been shown to be characteristic for each milk model emulsion, were incorporated into the model for a reliable description of the forming crust's influence on the evaporation rate and droplet shrinkage. Diffusion processes as well as protein surface activity were included into the model, and both exercised an important influence over the component distribution. The results confirmed the hypothesis that the protein's surface activity was responsible for its enrichment at the air/water interface. The strong diffusivity of lactose in comparison to the other components additionally contributed to a depletion of lactose near the surface. Component segregation during droplet generation was identified as the reason for the observation of highly overrepresented surface fat from the beginning of drying onwards until completed drying. A modified simulation model without evaporation and with the bulk composition as initial surface condition in the component mass balances was applied, which suggested that the initial difference between bulk and surface composition cannot be ascribed to diffusion induced component segregation. This finding supported the previously suggested concept of a disintegration mechanism along the dispersed fat globules inside the milk emulsions that causes the fat phase to be accumulated at the surface as soon as a droplet has been formed.

As a future study, it is recommended to apply and test the here proposed simulation model at smaller droplet sizes under spray drying conditions in order to predict the surface composition of industrially produced milk powder. In conjunction with this, phenomena associated with surface properties such as stickiness, crystallinity, flow and rehydration behavior are expected to be predictable by utilization of this model. It should also be attempted to further develop the model's mathematical description to account for precipitation and the influence of the fat phase's hydrophobicity. Furthermore, the here described experimental methodology of coupling single droplet drying with cryogenic flash freezing can be adopted for other milk emulsions and other food or pharmaceutical particle systems to better understand their respective behavior during convective drying. Applicability of the obtained results on an industrial spray drying process will yet depend on whether the surface composition of the generated droplets agrees with the initial state of droplets produced with the corresponding atomization nozzle that is utilized on industrial scale.

6.8 Appendix

6.8.1 Appendix 5.A: Parameters for Protein Adsorption and Temperature Dependent Physical Properties

A formulation for the kinetic adsorption and desorption parameters of albumin at an air/water interface (Hansen and Myrvold, 1995) was utilized for estimation of the protein surface activity (Eq. (6.26)). Considering that several types of protein are present in milk and that these have a complex dependency on pH, protein bulk concentration and temperature (Hansen and Myrvold, 1995), the kinetic parameters had to be fine-tuned to achieve good agreement with the experimental data. It was found that the data was best represented by increasing the reported value of the kinetic adsorption parameter by 30 % and retaining the reported value of the desorption parameter. This seemed reasonable since surface tension measurements have indicated that casein is more surface active than bovine albumin (Fäldt and Bergenståhl, 1994).

Equations for the temperature dependency of the density and thermal conductivity of water, lactose, protein and fat were derived from data by Choi (1986). Temperature correlations for the dynamic viscosity of water and the saturation vapor pressure were obtained from Haynes (2012). A regression curve fit for the diffusion coefficient of water vapor in air was provided by Bolz and Tuve (1976). The change in enthalpy of water evaporation with temperature was correlated from data published by Sabbah et al. (1999).

6.8.2 Appendix 5.B: Simulation of Global Droplet Temperature and Moisture Profiles

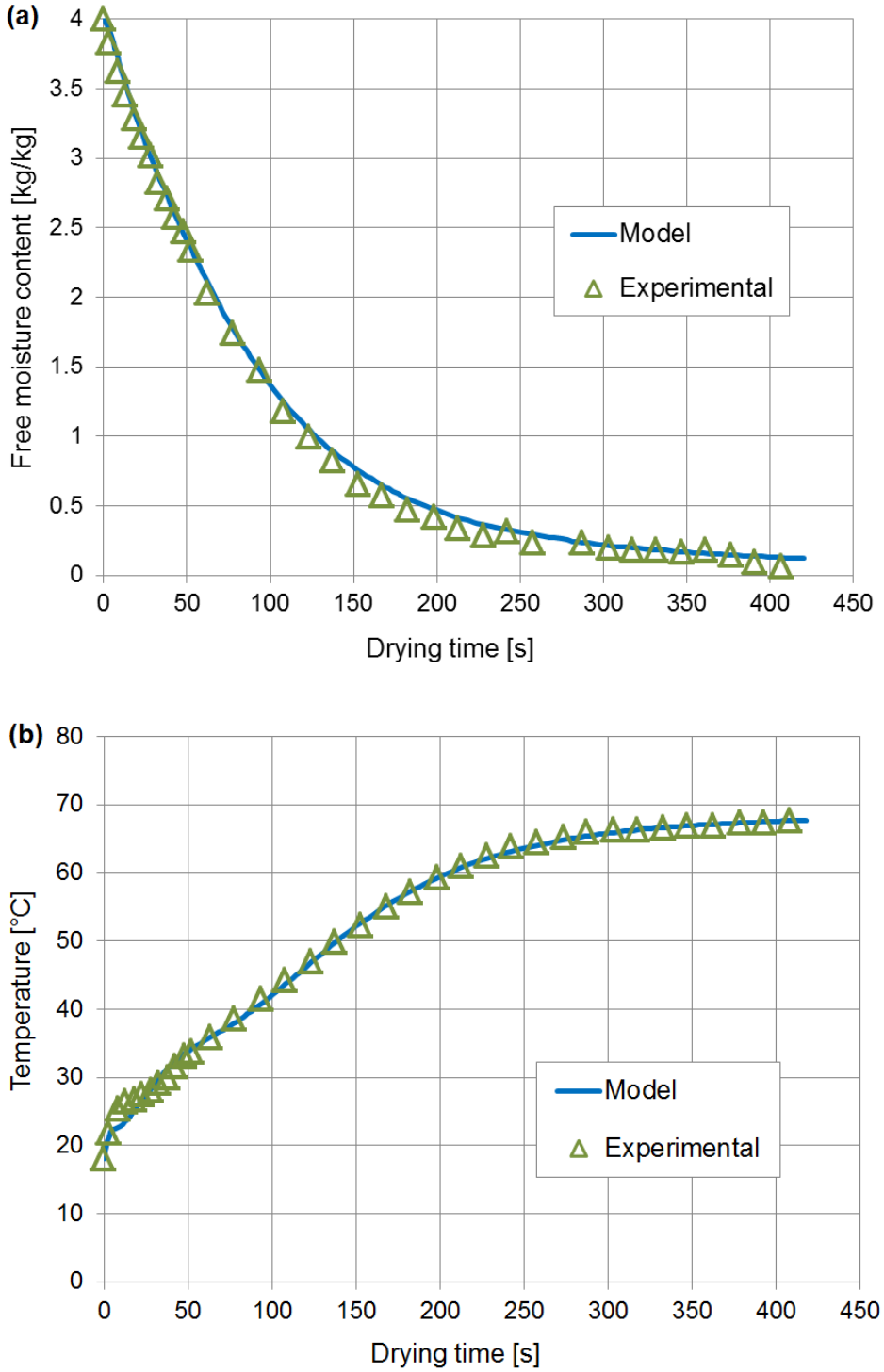

Figure 6.9: Simulated global properties during single droplet drying: volumetric averages over droplet radius of (a) free droplet moisture content, and (b) droplet temperature. The experimentally measured initial surface composition was used as initial surface condition (case 1).

7 Conclusions and Recommendations

7.1 Conclusions

Detailed insights into the component segregation that takes place in drying milk droplets were obtained by a systematic investigation using two convective drying methods and modifying these with cryogenic flash freezing techniques. This gave a new understanding of the mechanism that is responsible for the formation of surface fat on spray-dried milk powder, how this influences the drying kinetics and how the chemical surface composition can be improved for more desirable functional powder properties. In both drying methods, a regular-fat milk model emulsion (20 % w/w solid content, dry matter composition: 40.8 % w/w lactose, 31.1 % w/w fat, 27.0 % w/w protein with 80% whey protein and 20% casein) and a low-fat milk model emulsion (0.3 % w/w fat in d.m.) were studied.

Firstly, microfluidic multi-jet spray drying facilitated the production of monodisperse particles with uniform drying history for direct correlation between different emulsion compositions or nozzle orifice sizes and their influence on the powder surface composition. Cryogenic flash freezing of the generated droplets immediately after atomization allowed distinguishing the influence of the atomization stage from the one of the drying stage. The droplets after atomization featured diameters of 50-150 µm. Comparison with a pressure-swirl single-fluid spray nozzle and a pilot-scale rotary disk spray dryer indicated that the results obtained from microfluidic atomization were representative for atomization techniques that are commonly used on an industrial scale. The spray drying studies were extended by modifying the regular-fat emulsion prior to spray drying with the addition of λ-carrageenan, a linear sulphated polysaccharide, at different concentrations from 0-0.5 % w/w.

Secondly, single droplet drying allowed the *in situ* observation of droplet changes in mass, diameter and temperature, as well as tracking of the chemical surface composition over time by stopping the drying process by immersion in liquid nitrogen after discrete drying times in a new single droplet drying technique. The droplets were substantially larger than in spray drying with an initial size of approximately 1.2-1.8 mm in diameter. The single droplet drying experiments were compared with a numerical model that was applied for simulation of the radial component distribution of lactose, protein and fat during single droplet drying of a low-fat milk model droplet.

In spray drying, the surfaces of both the atomized droplets and the spray-dried particles were found to feature an overrepresentation of fat in comparison to the bulk composition, as observed *via* X-ray photoelectron spectroscopy and confocal laser scanning microscopy. Surface fat contents of 9-13 and 83-92 % v/v in d.m. were detected on the atomized droplets of the low-fat and regular-fat emulsions, respectively. As the surface compositions remained relatively unchanged throughout the following drying

stage, the findings indicated that the final surface composition of spray-dried milk powder should not be attributed to the drying process, but is already formed during the atomization stage. In light of that, it was concluded that the capacity for a reduction in surface fat on spray-dried milk particles by adjusting the conditions of the drying stage is very limited. As an alternative, it was demonstrated that strengthening the milk emulsions prior to spray drying can translate into improved fat encapsulation in the spray-dried particles. Successful emulsion stabilization was achieved by reducing the coalescence of the dispersed lipid phase as a result of electrostatic repulsion amongst the milk fat globule membranes, whose negative charge was increased by adsorption of λ-carrageenan. Smaller fat globule size and improved emulsion stability occurred at carrageenan contents of 0.3-0.4 % w/w, when the protein membranes presumably reached saturation with carrageenan. The emulsions experienced creaming as a result of depletion flocculation at higher carrageenan concentration (0.5 % w/w) and bridging flocculation at lower carrageenan concentration (0.1 % w/w).

The stabilized emulsions translated into spray-dried particles with a significantly reduced surface fat thickness. Whereas the carrageenan-free emulsion consisted of 13.8 % surface fat as determined *via* surface fat extraction, only a third of this amount (4.7 %) was measured on particles obtained from an emulsion with 0.3 % w/w carrageenan. The extensional viscosity of the model emulsions was found to be very sensitive to the presence of λ-carrageenan or a dispersed fat phase. While the shear viscosity only dropped slightly under an increase in fat content of the carrageenan-free emulsions, the extensional viscosity experienced a sharp decrease from 25.9 to 11.5 mPa·s. This explained why the size of the atomized droplets decreased with increasing fat content during spray drying. The addition of carrageenan (0.3 % w/w) raised the extensional viscosity up to 30.7 mPa·s again. Based on these results, it was proposed that the surface fat formation during atomization occurred because of a perforation mechanism that was induced by the fat globules. As the interface between the aqueous continuous phase and the dispersed lipid phase has appeared to be less stable against film disintegration under extensional shear than the other parts of the emulsions, it was concluded that the emulsions preferably broke up along the fat globules during atomization. The fat globules were consequently at the surface as soon as individual droplets had been formed. Emulsion stabilization with λ-carrageenan reduced the amount of surface fat, presumably by reducing the fat globule size and inhibiting this perforation mechanism. This demonstrated that emulsion stabilization ahead of the spray drying of milk powder might become a cost and resource efficient alternative to the conventional milk powder production process in the dairy industry.

In single droplet drying, it was demonstrated experimentally how the existence of a fat dominated surface shell influenced the drying and shrinkage kinetics. The new cryogenic flash freezing technique revealed that the regular-fat droplets featured a comprehensive fat film directly after droplet generation and throughout the whole drying process (between 91-97 % v/v fat in d.m.). This was similar to the observations on spray drying, although the droplet generation in single droplet drying was performed by a different technique, utilizing a micro-volumetric syringe. It was thus shown that the component segre-

gation during single droplet drying resembled the spray drying process reasonably well. Also consistent with the spray drying experiments was that protein enriched in the surface-near regions with proceeding drying time of the low-fat milk model emulsion droplets (increase from 48 to 68 % v/v in d.m.), while fat was also present in over-stoichiometric amounts (between 13-19 % v/v fat in d.m.). The temperature, mass and diameter data was processed with the Reaction Engineering Approach to describe the shrinkage kinetics and the declining vapor pressure at the droplet surface due to decreasing effective water diffusivities with advancing crust formation. The hydrophobic fat shell of the regular-fat emulsion imposed a greater resistance to evaporation and was subject to less shrinkage, particularly at low moisture contents, in comparison to the high-in-protein shell of the low-fat emulsion.

The drying and shrinkage kinetics were implemented into a numerical model to simulate the component distribution during single droplet drying of a low-fat milk droplet. A few novelties of this model eliminated some weaknesses that previously published models for the prediction of the chemical surface composition of dried particles with multiple components have had in common. Firstly, the semi-empirical correlations from the single droplet drying experiments were adopted in order to realistically describe the impact of the emerging crust on the shrinkage and evaporation rates. Secondly, a modified Stokes-Einstein equation accounted for the decreasing diffusion rates with lower water content, and the protein surface activity was introduced as a boundary condition. Thirdly, the experimentally determined initial surface composition after droplet generation was required as initial condition for accurate simulation. For model validation, knowledge of the change in surface concentration over drying time proved to be useful, whereas previous models of similar kind were only validated in terms of moisture content and temperature profiles or the surface composition after completed drying. The model was demonstrated to be suitable for the description of the spatiotemporal component distribution in drying milk droplets. Modeling of the component migration without evaporation and the bulk composition as the initial surface composition did not result, within any time, in surface concentrations that matched the measured values of the atomized droplets. This confirmed that the difference between the initial surface composition and the bulk composition prior to drying must be a direct result of the proposed film disintegration mechanism during atomization, and could not have happened due to diffusion. Furthermore, the simulation work supported the hypothesis that during the following drying stage the further depletion of lactose at the surface was determined by its relatively fast diffusivity and that the protein enrichment at the surface was intensified by its surface activity.

In summary, by means of modified spray drying and single droplet drying analysis techniques as well as numerical simulation, this study has provided a better understanding of the chemical surface formation of spray-dried milk powder and of a possible way to reduce the amount of surface fat. The demonstrated investigation approach and the obtained insights are expected to provide value to the research of spray drying processes of emulsions in general, beyond milk powder. For the dairy industry, this research

contributes towards an optimization of milk powder production in terms of efficiency and product quality.

7.2 Recommendations for Future Work

It is envisaged that the findings of this research will contribute towards a more efficient and sustainable milk powder production in the dairy industry. A few further studies are proposed to continue this ambition.

Firstly, in respect to industrial applications, the effort to improve the functional properties of spray-dried milk powder by prior emulsion stabilization should be continued. Since the internal porosity of emulsions that were stabilized with carrageenan was reduced to the detriment of the solubility, further research on how to prevent the densification of the milk particles during spray drying should be conducted. Regarding an industrial utilization of carrageenan for reduction of the surface fat formation during spray drying, it would also be interesting to explore the interaction between carrageenan and fresh whole milk emulsions. It is proposed that such a study would also take into account the influence of varied homogenization pressures. A future study could also explore how an increased extensional viscosity and improved stability of milk emulsions through the addition of carrageenan influences the disintegration behavior and thus the fat encapsulation efficiency in spray drying techniques that employ high shear forces, as typically found in industrial powder production. A deeper understanding of the adsorption process of λ-carrageenan and the electrostatic interaction in the milk emulsions could be obtained by ζ-potential measurements. Moreover, other stabilizers or surfactants instead of carrageenan could be tested in respect to their impact on spray-dried milk powder, and in particular regarding their influence on the droplet surface formation during atomization. Other food-safe, natural and economical excipients such as rice dreg protein hydrolysate or modified starch would be possible options for this purpose.

From an economical perspective, a comprehensive cost analysis of the addition of carrageen regarding its viability for emulsion modification prior to industrial spray drying of milk powder would be valuable. It could be compared with other treatments that might have similar effects, as future studies might find out. Also a market analysis of the consumer acceptance of added carrageenan in milk powder will be an important part of implementing carrageenan addition into commercial milk powder manufacturing.

Secondly, on a more fundamental level, it seems to be worth exploring new ways to further understand and visualize the disintegration mechanism of milk emulsions into individual droplets during atomization. So far, the proposed perforation and disintegration mechanism has been supported indirectly by the observed droplet sizes after atomization, the reduction in surface fat through emulsion stabilization,

extensional viscosity measurements and a small number of previously published studies. However, the disintegration mechanism itself has not been observed directly yet. As a first step towards this objective, fluorescence microscopy could be coupled with the acoustically-driven microfluidic extensional rheometer or the microfluidic jet atomizer to observe the position of the fat globules in relation to the break-up location of the emulsion. If the time resolution of the fluorescent microscopy did not prove to be sufficient for these fast disintegration processes, fluorescent tracking of the fat globules during an elongational stretching of a small emulsion volume in a stagnation point of a microfluidic channel would possibly be a practical alternative. In addition to that, experimental or simulation work could also be conducted to gain insights into the convective flow pattern in milk droplets upon atomization to investigate if fast convection processes exist which could have an impact on the component segregation during droplet generation.

Thirdly, the developed numerical model for simulation of the concentration gradients in drying milk droplets can provide a powerful tool for optimizing the spray drying conditions in milk powder production. After being validated for single droplet drying, the model can now be applied on spray drying processes. Further, the computed surface compositions may be used to predict the functional powder properties, such as reconstitution behavior and stickiness. For this purpose, it will be worthwhile to test an extension of the numerical model by implementing a description of solute precipitation upon saturation and by accounting for the hydrophobicity of the (surface) fat.

Last but not least, on a more general note, the new experimental and numerical investigation techniques that have been demonstrated in the present work will be available for application on other microencapsulation systems. The undertaken approach can be expanded onto various emulsions and solutions to explore whether atomization also creates wanted or unwanted component segregation in other food or pharmaceutical spray drying processes. For instance, the surface composition of droplets consisting of food oils or oleoresins together with acacia gum, modified starch or maltodextrin as wall materials could be investigated.

8 List of Awards and Scholarships

The following awards and scholarships have been received in the course of this research work:

Awards

1st Prize, Manfred Kroger Graduate Student Research Paper Oral Competition, IFT 16, Chicago, USA, July 2016

2nd Prize, 3 Minute Thesis, Department of Chemical Engineering, Monash University, Australia, July 2016

Best Poster Award, Concentrated and Dried Milk Products, IDF Parallel Symposia 2016, Dublin, Ireland, April 2016

Scholarships

Postgraduate Publication Award scholarship, Round 1/2017, April – May 2017, sponsored by Monash University

Travel scholarship for the Crawford Fund Parliamentary Conference, Canberra, Australia, sponsored by the Gardiner Foundation, August 2015

Monash Graduate Scholarship & Monash International Postgraduate Research Scholarship, March 2014 - March 2017, sponsored by Monash University

9 Consolidated Bibliography

Adhikari, B., Howes, T. & Bhandari, B. R. 2007. Use of solute fixed coordinate system and method of lines for prediction of drying kinetics and surface stickiness of single droplet during convective drying. *Chemical Engineering and Processing: Process Intensification,* 46**,** 405-419.

Adhikari, B., Howes, T., Bhandari, B. R. & Langrish, T. a. G. 2009. Effect of addition of proteins on the production of amorphous sucrose powder through spray drying. *Journal of Food Engineering,* 94**,** 144-153.

Adhikari, B., Howes, T., Bhandari, B. R. & Troung, V. 2003. Surface stickiness of drops of carbohydrate and organic acid solutions during convective drying: experiments and modeling. *Drying Technology,* 21**,** 839-873.

Adhikari, B., Howes, T., Bhandari, B. R. & Troung, V. 2004. Effect of addition of maltodextrin on drying kinetics and stickiness of sugar and acid-rich foods during convective drying: experiments and modelling. *Journal of Food Engineering,* 62**,** 53-68.

Agboola, S. O. & Dalgleish, D. G. 1996a. Enzymatic hydrolysis of milk proteins used for emulsion formation. 2. Effects of calcium, pH, and ethanol on the stability of the emulsions. *Journal of Agricultural and Food Chemistry,* 44**,** 3637-3642.

Agboola, S. O. & Dalgleish, D. G. 1996b. Kinetics of the calcium-induced instability of oil-in-water emulsions: studies under quiescent and shearing conditions. *LWT-Food Science and Technology,* 29**,** 425-432.

Alexander, K. & Judson King, C. 1985. Factors governing surface morphology of spray-dried amorphous substances. *Drying Technology,* 3**,** 321-348.

Anema, S. G., Pinder, D. N., Hunter, R. J. & Hemar, Y. 2006. Effects of storage temperature on the solubility of milk protein concentrate (MPC85). *Food Hydrocolloids,* 20**,** 386-393.

Aoac 1990. *Official Methods of Analysis of the Association of Official Analytical Chemists,* Arlington, USA, Association of Official Analytical Chemists.

Baldwin, A. J. & Truong, G. N. T. 2007. Development of insolubility in dehydration of dairy milk powders. *Food and Bioproducts Processing,* 85**,** 202-208.

Bertsch, A. J. 1983. Surface tension of whole and skim-milk between 18 and 135 C. *Journal of Dairy Research,* 50**,** 259-267.

Bhattacharjee, P. K., Mcdonnell, A. G., Prabhakar, R., Yeo, L. Y. & Friend, J. 2011. Extensional flow of low-viscosity fluids in capillary bridges formed by pulsed surface acoustic wave jetting. *New Journal of Physics,* 13**,** 023005.

Bixler, H. J., Johndro, K. & Falshaw, R. 2001. Kappa-2 carrageenan: Structure and performance of commercial extracts: II. Performance in two simulated dairy applications. *Food Hydrocolloids,* 15**,** 619-630.

Bolz, R. E. & Tuve, G. L. 1976. CRC handbook of tables for applied engineering. New York, USA: CRC Press.

Brenn, G., Rensink, D., Tropea, C. & Yarin, A. L. 1997. Investigation of droplet drying characteristics using an acoustic-aerodynamic levitator. *International Journal of Fluid Mechanics Research,* 24.

Buchheim, W. 1982. Electron microscopic localization of solvent-extractable fat in agglomerated spray-dried whole milk powder particles. *Food Structure,* 1**,** 12.

Buma, T. J. 1971. Free fat in spray-dried whole milk. 2. Evaluation of methods for determination of free-fat content. *Netherlands Milk and Dairy Journal-Nederlands-Nederlands Melk En Zuiveltijdschrift,* 25**,** 42-50.

Bylund, G. S. 2003. *Dairy processing handbook,* Lund, Tetra Pak Processing Systems AB.

Charlesworth, D. H. & Marshall, W. R. 1960. Evaporation from drops containing dissolved solids. *AIChE Journal,* 6**,** 9-23.

Chen, X., Boyko, V., Rieger, J., Reinhold, F., Reck, B., Perlich, J., Gehrke, R. & Men, Y. 2012. Buckling-induced structural transition during the drying of a polymeric latex droplet on a solid surface. *Soft Matter,* 8**,** 12093-12098.

Chen, X. D. 2008. The basics of a reaction engineering approach to modeling air-drying of small droplets or thin-layer materials. *Drying Technology,* 26**,** 627-639.

Chen, X. D. & Lin, S. X. Q. 2005. Air drying of milk droplet under constant and time ‐ dependent conditions. *AIChE Journal,* 51**,** 1790-1799.

Chen, X. D. & Peng, X. 2005. Modified Biot number in the context of air drying of small moist porous objects. *Drying Technology,* 23**,** 83-103.

Chen, X. D., Pirini, W. & Ozilgen, M. 2001. The reaction engineering approach to modelling drying of thin layer of pulped Kiwifruit flesh under conditions of small Biot numbers. *Chemical Engineering and Processing: Process Intensification,* 40**,** 311-320.

Chen, X. D. & Putranto, A. 2013. *Modelling drying processes: A Reaction Engineering Approach,* Cambridge, UK, Cambridge University Press.

Chen, X. D., Sidhu, H. & Nelson, M. 2011. Theoretical probing of the phenomenon of the formation of the outermost surface layer of a multi-component particle, and the surface chemical composition after the rapid removal of water in spray drying. *Chemical Engineering Science,* 66**,** 6375-6384.

Chen, X. D., Sidhu, H. & Nelson, M. 2013. On the addition of protein (casein) to aqueous lactose as a drying aid in spray drying - theoretical surface composition. *Drying Technology,* 31**,** 1504-1512.

Chen, X. D. & Xie, G. Z. 1997. Fingerprints of the drying behaviour of particulate or thin layer food materials established using a reaction engineering model. *Food and Bioproducts Processing,* 75**,** 213-222.

Cheong, H. W., Jeffreys, G. V. & Mumford, C. J. 1986. A receding interface model for the drying of slurry droplets. *AIChE Journal,* 32**,** 1334-1346.

Chew, J. H., Fu, N., Gengenbach, T., Chen, X. D. & Selomulya, C. 2015. The compositional effects of high solids model emulsions on drying behaviour and particle formation processes. *Journal of Food Engineering,* 157**,** 33-40.

Chew, J. H., Fu, N., Woo, M. W., Patel, K., Selomulya, C. & Chen, X. D. 2013. Capturing the effect of initial concentrations on the drying kinetics of high solids milk using reaction engineering approach. *Dairy Science & Technology,* 93**,** 415-430.

Chew, J. H., Liu, W., Fu, N., Gengenbach, T., Chen, X. D. & Selomulya, C. 2014. Exploring the drying behaviour and particle formation of high solids milk protein concentrate. *Journal of Food Engineering,* 143**,** 186-194.

Choi, C.-H. & Kim, C. J. 2009. Droplet evaporation of pure water and protein solution on nanostructured superhydrophobic surfaces of varying heights. *Langmuir,* 25**,** 7561-7567.

Choi, Y. 1986. Effects of temperature and composition on the thermal properties of foods. *Food Engineering and Process Applications,* 1**,** 93-101.

Corredig, M. & Dalgleish, D. G. 1999. The mechanisms of the heat-induced interaction of whey proteins with casein micelles in milk. *International Dairy Journal,* 9**,** 233-236.

Crowley, S. V., Kelly, A. L., Schuck, P., Jeantet, R. & O'mahony, J. A. 2016. Rehydration and solubility characteristics of high-protein dairy powders. *In:* MCSWEENEY, P. L. H., O'MAHONY, J.A. (ed.) *Advanced Dairy Chemistry. Volume 1B: Proteins: Applied Aspects. Fourth Edition.* Heidelberg, Germany: Springer.

Cussler, E. L. 2009. *Diffusion: mass transfer in fluid systems,* Cambridge, UK, Cambridge University Press.

Dalgleish, D. G. 1997. Adsorption of protein and the stability of emulsions. *Trends in Food Science & Technology,* 8**,** 1-6.

Dalgleish, D. G. & Morris, E. R. 1988. Interactions between carrageenans and casein micelles: electrophoretic and hydrodynamic properties of the particles. *Food Hydrocolloids,* 2**,** 311-320.

Dalgleish, D. G., Srinivasan, M. & Singh, H. 1995. Surface properties of oil-in-water emulsion droplets containing casein and Tween 60. *Journal of Agricultural and Food Chemistry,* 43**,** 2351-2355.

Dewan, R. K., Chudgar, A., Mead, R., Bloomfield, V. A. & Morr, C. V. 1974. Molecular weight and size distribution of bovine milk casein micelles. *Biochimica et Biophysica Acta (BBA)-Protein Structure,* 342**,** 313-321.

Dickinson, E. 1998. Stability and rheological implications of electrostatic milk protein–polysaccharide interactions. *Trends in Food Science & Technology,* 9**,** 347-354.

Dickinson, E. & Pawlowsky, K. 1997. Effect of ι-carrageenan on flocculation, creaming, and rheology of a protein-stabilized emulsion. *Journal of Agricultural and Food Chemistry,* 45**,** 3799-3806.

Dombrowski, N. & Fraser, R. P. 1954. A photographic investigation into the disintegration of liquid sheets. *Philosophical Transactions of the Royal Society of London. Series A, Mathematical and Physical Sciences***,** 101-130.

Drusch, S., Serfert, Y., Scampicchio, M., Schmidt-Hansberg, B. & Schwarz, K. 2007. Impact of physicochemical characteristics on the oxidative stability of fish oil microencapsulated by spray-drying. *Journal of Agricultural and Food Chemistry,* 55**,** 11044-11051.

Einhorn-Stoll, U., Ulbrich, M., Sever, S. & Kunzek, H. 2005. Formation of milk protein–pectin conjugates with improved emulsifying properties by controlled dry heating. *Food Hydrocolloids,* 19**,** 329-340.

Einstein, A. 1905. Über die von der molekularkinetischen Theorie der Wärme geforderte Bewegung von in ruhenden Flüssigkeiten suspendierten Teilchen. *Annalen der Physik,* 4.

El-Sayed, T. M., Wallack, D. A. & King, C. J. 1990. Changes in particle morphology during drying of drops of carbohydrate solutions and food liquids. 1. Effect of composition and drying conditions. *Industrial & Engineering Chemistry Research,* 29**,** 2346-2354.

Erbil, H. Y. 2012. Evaporation of pure liquid sessile and spherical suspended drops: A review. *Advances in Colloid and Interface Science,* 170**,** 67-86.

Eslamian, M. & Ashgriz, N. 2007. Evaporation and evolution of suspended solution droplets at atmospheric and reduced pressures. *Drying Technology,* 25**,** 999-1010.

Fäldt, P. & Bergenståhl, B. 1994. The surface composition of spray-dried protein-lactose powders. *Colloids and Surfaces A: Physicochemical and Engineering Aspects,* 90**,** 183-190.

Fäldt, P. & Bergenståhl, B. 1995. Fat encapsulation in spray-dried food powders. *Journal of the American Oil Chemists' Society,* 72**,** 171-176.

Fäldt, P. & Bergenståhl, B. 1996a. Spray-dried whey protein/lactose/soybean oil emulsions. 1. Surface composition and particle structure. *Food Hydrocolloids,* 10**,** 421-429.

Fäldt, P. & Bergenståhl, B. 1996b. Spray-dried whey protein/lactose/soybean oil emulsions. 2. Redispersability, wettability and particle structure. *Food Hydrocolloids,* 10**,** 431-439.

Fäldt, P., Bergenstahl, B. & Carlsson, G. 1993. The surface coverage of fat on food powders analyzed by ESCA (electron spectroscopy for chemical analysis). *Food Structure,* 12**,** 225-234.

Fang, Y. & Dalgleish, D. G. 1993. Dimensions of the adsorbed layers in oil-in-water emulsions stabilized by caseins. *Journal of Colloid and Interface Science,* 156**,** 329-334.

Fang, Y., Selomulya, C. & Chen, X. D. 2010. Characterization of milk protein concentrate solubility using focused beam reflectance measurement. *Dairy Science & Technology,* 90**,** 253-270.

Fao 1987. Production and Utilization of Products from Commercial Seaweeds. *In:* MCHUGH, D. J. (ed.) *Food and Agriculture Organization of the United Nations, Chapter 3: Production and utilization of products from commercial seaweeds*

Fda 2016. 21CFR172.620. *Title 21, Volume 3, Part 172.* US Food & Drug Administration, Code of Federal Regulations.

Ferrari, G., Meerdink, G. & Walstra, P. 1989. Drying kinetics for a single droplet of skim-milk. *Journal of Food Engineering,* 10**,** 215-230.

Fonseca, C. R., Bento, M. S. G., Quintero, E. S. M., Gabas, A. L. & Oliveira, C. a. F. 2011. Physical properties of goat milk powder with soy lecithin added before spray drying. *International Journal of Food Science & Technology,* 46**,** 608-611.

Fu, N. 2012. *Single droplet drying of food and bacterium containing liquids and particle engineering.* Thesis (Ph.D.), Monash University. Faculty of Engineering. Department of Chemical Engineering.

Fu, N., Woo, M. W. & Chen, X. D. 2011a. Colloidal transport phenomena of milk components during convective droplet drying. *Colloids and Surfaces B: Biointerfaces,* 87**,** 255-266.

Fu, N., Woo, M. W., Moo, F. T. & Chen, X. D. 2012a. Microcrystallization of lactose during droplet drying and its effect on the property of the dried particle. *Chemical Engineering Research and Design,* 90**,** 138-149.

Fu, N., Woo, M. W., Qi Lin, S. X., Zhou, Z. & Chen, X. D. 2011b. Reaction Engineering Approach (REA) to model the drying kinetics of droplets with different initial sizes - experiments and analyses. *Chemical Engineering Science,* 66**,** 1738-1747.

Fu, N., Woo, M. W., Selomulya, C., Chen, X. D., Patel, K., Schuck, P. & Jeantet, R. 2012b. Drying kinetics of skim milk with 50wt.% initial solids. *Journal of Food Engineering,* 109**,** 701-711.

Fu, N., Zhou, Z., Jones, T. B., Tan, T. T., Wu, W. D., Lin, S. X., Chen, X. D. & Chan, P. P. 2011c. Production of monodisperse epigallocatechin gallate (EGCG) microparticles by spray drying for high antioxidant activity retention. *International Journal of Pharmaceutics,* 413**,** 155-166.

Furuta, T., Tsujimoto, S., O Azaki, M. & Toei, R. 1983. Effect of drying on retention of ethanol in maltodextrin solution during drying of a single droplet. *Drying Technology,* 2**,** 311-327.

Fyfe, K., Kravchuk, O., Nguyen, A. V., Deeth, H. & Bhandari, B. 2011. Influence of dryer type on surface characteristics of milk powders. *Drying Technology,* 29**,** 758-769.

Gaiani, C., Ehrhardt, J., Scher, J., Hardy, J., Desobry, S. & Banon, S. 2006. Surface composition of dairy powders observed by X-ray photoelectron spectroscopy and effects on their rehydration properties. *Colloids and Surfaces B: Biointerfaces,* 49**,** 71-78.

Gaiani, C., Morand, M., Sanchez, C., Tehrany, E., Jacquot, M., Schuck, P., Jeantet, R. & Scher, J. 2010. How surface composition of high milk proteins powders is influenced by spray-drying temperature. *Colloids and Surfaces B: Biointerfaces,* 75**,** 377-384.

Gaiani, C., Schuck, P., Scher, J., Desobry, S. & Banon, S. 2007. Dairy powder rehydration: influence of protein state, incorporation mode, and agglomeration. *Journal of Dairy Science,* 90**,** 570-581.

Gardner, C. 1965. Asymptotic concentration distribution of an involatile solute in an evaporating drop. *International Journal of Heat and Mass Transfer,* 8**,** 667-668.

Gea. 2005. *GEA Niro Analytical Methods. No. A 5 a - Wettability* [Online]. Germany: GEA Group AG. Available: http://www.gea.com/global/en/binaries/A%205%20a%20-%20Wettability_tcm11-30909.pdf [Accessed 31 June 2016.

Gharsallaoui, A., Saurel, R., Chambin, O., Cases, E., Voilley, A. & Cayot, P. 2010. Utilisation of pectin coating to enhance spray-dry stability of pea protein-stabilised oil-in-water emulsions. *Food Chemistry,* 122**,** 447-454.

Gopireddy, S. R. & Gutheil, E. 2013. Numerical simulation of evaporation and drying of a bi-component droplet. *International Journal of Heat and Mass Transfer,* 66**,** 404-411.

Graham, D. E. & Phillips, M. C. 1979. Proteins at liquid interfaces: I. Kinetics of adsorption and surface denaturation. *Journal of Colloid and Interface Science,* 70**,** 403-414.

Granelli, K., Fäldt, P., Appelqvist, L. Å. & Bergenståhl, B. 1996. Influence of surface structure on cholesterol oxidation in model food powders. *Journal of the Science of Food and Agriculture,* 71**,** 75-82.

Groenewold, C., Möser, C., Groenewold, H. & Tsotsas, E. 2002. Determination of single-particle drying kinetics in an acoustic levitator. *Chemical Engineering Journal,* 86**,** 217-222.

Gu, Y. S., Regnier, L. & Mcclements, D. J. 2005. Influence of environmental stresses on stability of oil-in-water emulsions containing droplets stabilized by β-lactoglobulin–ι-carrageenan membranes. *Journal of Colloid and Interface Science,* 286**,** 551-558.

Guzey, D., Kim, H. & Mcclements, D. J. 2004. Factors influencing the production of o/w emulsions stabilized by β-lactoglobulin–pectin membranes. *Food Hydrocolloids,* 18**,** 967-975.

Hampton, M. A., Nguyen, T. a. H., Nguyen, A. V., Xu, Z. P., Huang, L. & Rudolph, V. 2012. Influence of surface orientation on the organization of nanoparticles in drying nanofluid droplets. *Journal of Colloid and Interface Science,* 377**,** 456-462.

Handscomb, C. S., Kraft, M. & Bayly, A. E. 2009. A new model for the drying of droplets containing suspended solids after shell formation. *Chemical Engineering Science,* 64**,** 228-246.

Hansen, F. K. & Myrvold, R. 1995. The kinetics of albumin adsorption to the air/water interface measured by automatic axisymmetric drop shape analysis. *Journal of Colloid and Interface Science,* 176**,** 408-417.

Hardas, N., Danviriyakul, S., Foley, J., Nawar, W. W. & Chinachoti, P. 2000. Accelerated stability studies of microencapsulated anhydrous milk fat. *LWT-Food Science and Technology,* 33**,** 506-513.

Harvie, D. J. E., Langrish, T. a. G. & Fletcher, D. F. 2002. A computational fluid dynamics study of a tall-form spray dryer. *Food and Bioproducts Processing,* 80**,** 163-175.

Havea, P. 2006. Protein interactions in milk protein concentrate powders. *International Dairy Journal,* 16**,** 415-422.

Haynes, W. M. 2012. *CRC Handbook of Chemistry and Physics,* Boca Raton, USA, CRC Press.

Helmchen, F. & Denk, W. 2005. Deep tissue two-photon microscopy. *Nature Methods,* 2**,** 932-940.

Iserles, A. 2009. *A first course in the numerical analysis of differential equations,* Cambridge, UK, Cambridge University Press.

Ishwarya, S. P., Anandharamakrishnan, C. & Stapley, A. 2014. Spray Freeze Drying: A novel process for the drying of foods and bioproducts. *Trends in Food Science & Technology,* 41**,** 161–181.

Jafari, S. M., Assadpoor, E., Bhandari, B. & He, Y. 2008. Nano-particle encapsulation of fish oil by spray drying. *Food Research International,* 41**,** 172-183.

Jin, Y. & Chen, X. D. 2009. Numerical study of the drying process of different sized particles in an industrial-scale spray dryer. *Drying Technology,* 27**,** 371-381.

Kastner, O., Brenn, G., Rensink, D. & Tropea, C. 2001. The acoustic tube levitator–a novel device for determining the drying kinetics of single droplets. *Chemical Engineering & Technology,* 24**,** 335-339.

Keey, R. B. 1991. *Drying of loose and particulate materials,* New York, USA, Hemisphere Publishing Corperation.

Kelly, G. M., O'mahony, J. A., Kelly, A. L., Huppertz, T., Kennedy, D. & O'callaghan, D. J. 2015. Influence of protein concentration on surface composition and physico-chemical properties of spray-dried milk protein concentrate powders. *International Dairy Journal,* 51**,** 34-40.

Kelly, J., Kelly, P. M. & Harrington, D. 2002. Influence of processing variables on the physicochemical properties of spray dried fat-based milk powders. *Le Lait,* 82**,** 401-412.

Kentish, S., Davidson, M., Hassan, H. & Bloore, C. 2005. Milk skin formation during drying. *Chemical Engineering Science,* 60**,** 635-646.

Keogh, M. K. & O'kennedy, B. T. 1999. Milk fat microencapsulation using whey proteins. *International Dairy Journal,* 9**,** 657-663.

Keogh, M. K., O'kennedy, B. T., Kelly, J., Auty, M. A., Kelly, P. M., Fureby, A. & Haahr, A. M. 2001a. Stability to oxidation of spray-dried fish oil powder microencapsulated using milk ingredients. *Journal of Food Science,* 66**,** 217-224.

Keogh, M. K., O'kennedy, B. T., Kelly, J., Auty, M. A., Kelly, P. M., Fureby, A. & Haahr, A. M. 2001b. Stability to oxidation of spray‐dried fish oil powder microencapsulated using milk ingredients. *Journal of Food Science,* 66**,** 217-224.

Kim, E. H.-J., Chen, X. D. & Pearce, D. 2005a. Effect of surface composition on the flowability of industrial spray-dried dairy powders. *Colloids and Surfaces B: Biointerfaces,* 46**,** 182-187.

Kim, E. H.-J., Chen, X. D. & Pearce, D. 2005b. Melting characteristics of fat present on the surface of industrial spray-dried dairy powders. *Colloids and Surfaces B: Biointerfaces,* 42**,** 1-8.

Kim, E. H.-J., Chen, X. D. & Pearce, D. 2009a. Surface composition of industrial spray-dried milk powders. 1. Development of surface composition during manufacture. *Journal of Food Engineering,* 94**,** 163-168.

Kim, E. H.-J., Chen, X. D. & Pearce, D. 2009b. Surface composition of industrial spray-dried milk powders. 2. Effects of spray drying conditions on the surface composition. *Journal of Food Engineering,* 94**,** 169-181.

Kim, E. H.-J., Dong Chen, X. & Pearce, D. 2003. On the mechanisms of surface formation and the surface compositions of industrial milk powders. *Drying Technology,* 21**,** 265-278.

Kinzer, G. D. & Gunn, R. 1951. The evaporation, temperature and thermal relaxation-time of freely falling waterdrops. *Journal of Meteorology,* 8**,** 71-83.

Kravtchenko, T. P., Parker, A. & Trespoey, A. 1995. Colloidal stability and sedimentation of pectin-stabilized acid milk drinks. *In:* ERIC DICKINSON, D. L. (ed.) *Food Macromolecules and Colloids.* France: Royal Society of Chemistry.

Lallbeeharry, P., Tian, Y., Fu, N., Wu, W. D., Woo, M. W., Selomulya, C. & Chen, X. D. 2014. Effects of ionic and nonionic surfactants on milk shell wettability during co-spray-drying of whole milk particles. *Journal of Dairy Science,* 97**,** 5303–5314.

Landström, K., Bergenståhl, B., Alsins, J. & Almgren, M. 1999. A fluorescence method for quantitative measurements of specific protein at powder surfaces. *Colloids and Surfaces B: Biointerfaces,* 12**,** 429-440.

Langendorff, V., Cuvelier, G., Michon, C., Launay, B. & Parker, A. 2000. Effects of carrageenan type on the behaviour of carrageenan/milk mixtures. *Food Hydrocolloids,* 14**,** 273-280.

Langrish, T. a. G. & Kockel, T. K. 2001. The assessment of a characteristic drying curve for milk powder for use in computational fluid dynamics modelling. *Chemical Engineering Journal,* 84**,** 69-74.

Le, H. P. 1998. Progress and trends in ink-jet printing technology. *Journal of Imaging Science and Technology,* 42**,** 49-62.

Lefebvre, A. H. 1989. *Atomization and Sprays,* New York, USA, CRC Press.

Leman, J., Kinsella, J. E. & Kilara, A. 1989. Surface activity, film formation, and emulsifying properties of milk proteins. *Critical Reviews in Food Science & Nutrition,* 28**,** 115-138.

Lin, J.-C. & Gentry, J. W. 2003. Spray drying drop morphology: experimental study. *Aerosol Science & Technology,* 37**,** 15-32.

Lin, S. X. Q. & Chen, X. D. 2002. Improving the glass-filament method for accurate measurement of drying kinetics of liquid droplets. *Chemical Engineering Research and Design,* 80**,** 401-410.

Lin, S. X. Q. & Chen, X. D. 2004. Changes in milk droplet diameter during drying under constant drying conditions investigated using the glass-filament method. *Food and Bioproducts Processing,* 82**,** 213-218.

Lin, S. X. Q. & Chen, X. D. 2005. Prediction of air-drying of milk droplet under relatively high humidity using the reaction engineering approach. *Drying Technology,* 23**,** 1395-1406.

Lin, S. X. Q. & Chen, X. D. 2006. A model for drying of an aqueous lactose droplet using the reaction engineering approach. *Drying Technology,* 24**,** 1329-1334.

Liu, W., Chen, X. D. & Selomulya, C. 2015. On the spray drying of uniform functional microparticles. *Particuology,* 22**,** 1-12.

Manukyan, S., Sauer, H. M., Roisman, I. V., Baldwin, K. A., Fairhurst, D. J., Liang, H., Venzmer, J. & Tropea, C. 2013. Imaging internal flows in a drying sessile polymer dispersion drop using Spectral Radar Optical Coherence Tomography (SR-OCT). *Journal of Colloid and Interface Science,* 395**,** 287-293.

Masters, K. 1991. *Spray Drying Handbook,* Harlow, UK, Longman Scientific and Technical.

Mcdonnell, A. G., Gopesh, T. C., Lo, J., O'bryan, M., Yeo, L. Y., Friend, J. R. & Prabhakar, R. 2015a. Motility induced changes in viscosity of suspensions of swimming microbes in extensional flows. *Soft Matter,* 11**,** 4658-4668.

Mcdonnell, A. G., Jason, N. N., Yeo, L. Y., Friend, J. R., Cheng, W. & Prabhakar, R. 2015b. Extensional viscosity of copper nanowire suspensions in an aqueous polymer solution. *Soft Matter,* 11**,** 8076-8082.

Mchale, G., Aqil, S., Shirtcliffe, N. J., Newton, M. I. & Erbil, H. Y. 2005. Analysis of droplet evaporation on a superhydrophobic surface. *Langmuir,* 21**,** 11053-11060.

Mckenna, A. B., Lloyd, R. J., Munro, P. A. & Singh, H. 1999. Microstructure of whole milk powder and of insolubles detected by powder functional testing. *Scanning,* 21**,** 305-315.

Meerdink, G. 1994. Drying of liquid food droplets enzyme inactivation and multicomponent diffusion. *Drying Technology,* 12**,** 981-982.

Meerdink, G. & Van't Riet, K. 1995. Modeling segregation of solute material during drying of liquid foods. *AIChE Journal,* 41**,** 732-736.

Mezhericher, M., Levy, A. & Borde, I. 2007. Theoretical drying model of single droplets containing insoluble or dissolved solids. *Drying Technology,* 25**,** 1025-1032.

Michalski, M.-C., Michel, F., Sainmont, D. & Briard, V. 2002. Apparent ζ-potential as a tool to assess mechanical damages to the milk fat globule membrane. *Colloids and Surfaces B: Biointerfaces,* 23**,** 23-30.

Millqvist-Fureby, A. 2003. Characterisation of spray-dried emulsions with mixed fat phases. *Colloids and Surfaces B: Biointerfaces,* 31**,** 65-79.

Millqvist-Fureby, A., Elofsson, U. & Bergenståhl, B. 2001. Surface composition of spray-dried milk protein-stabilised emulsions in relation to pre-heat treatment of proteins. *Colloids and Surfaces B: Biointerfaces,* 21**,** 47-58.

Millqvist-Fureby, A. & Smith, P. 2007. In-situ lecithination of dairy powders in spray-drying for confectionery applications. *Food Hydrocolloids,* 21**,** 920-927.

Mimouni, A., Deeth, H. C., Whittaker, A. K., Gidley, M. J. & Bhandari, B. R. 2010. Rehydration of high-protein-containing dairy powder: Slow-and fast-dissolving components and storage effects. *Dairy Science & Technology,* 90**,** 335-344.

Mondragon, R., Hernandez, L., Enrique Julia, J., Carlos Jarque, J., Chiva, S., Zaitone, B. & Tropea, C. 2011. Study of the drying behavior of high load multiphase droplets in an acoustic levitator at high temperature conditions. *Chemical Engineering Science,* 66**,** 2734-2744.

Mondragón, R., Juliá, J. E., Hernández, L. & Jarque, J. C. 2013. Modeling of drying curves of silica nanofluid droplets dried in an acoustic levitator using the Reaction Engineering Approach (REA) model. *Drying Technology,* 31**,** 439-451.

Müller-Buschbaum, P., Gebhardt, R., Roth, S. V., Metwalli, E. & Doster, W. 2007. Effect of calcium concentration on the structure of casein micelles in thin films. *Biophysical Journal,* 93**,** 960-968.

Munoz-Ibanez, M., Nuzzo, M., Turchiuli, C., Bergenståhl, B., Dumoulin, E. & Millqvist-Fureby, A. 2016. The microstructure and component distribution in spray-dried emulsion particles. *Food Structure,* 8**,** 16-24.

Murrieta-Pazos, I., Gaiani, C., Galet, L. & Scher, J. 2012. Composition gradient from surface to core in dairy powders: agglomeration effect. *Food Hydrocolloids,* 26**,** 149-158.

Nešić, S. & Vodnik, J. 1991. Kinetics of droplet evaporation. *Chemical Engineering Science,* 46**,** 527-537.

Nijdam, J. J. & Langrish, T. a. G. 2005. An investigation of milk powders produced by a laboratory-scale spray dryer. *Drying technology,* 23**,** 1043-1056.

Nijdam, J. J. & Langrish, T. a. G. 2006. The effect of surface composition on the functional properties of milk powders. *Journal of Food Engineering,* 77**,** 919-925.

Nikolova, Y., Petit, J., Gianfrancesco, A., Sanders, C. F. W., Scher, J. & Gaiani, C. 2015a. Impact of spray-drying process parameters on dairy powder surface composition and properties. *Drying Technology,* 33.13**,** 1654-1661.

Nikolova, Y., Petit, J., Sanders, C., Gianfrancesco, A., Desbenoit, N., Frache, G., Scher, J. & Gaiani, C. 2014. Is it possible to modulate the structure of skim milk particle through drying process and parameters? *Journal of Food Engineering,* 142**,** 179-189.

Nikolova, Y., Petit, J., Sanders, C., Gianfrancesco, A., Scher, J. & Gaiani, C. 2015b. Toward a better determination of dairy powders surface composition through XPS matrices development. *Colloids and Surfaces B: Biointerfaces,* 125**,** 12-20.

Patel, K. C., Chen, X. D. & Kar, S. 2005. The temperature uniformity during air drying of a colloidal liquid droplet. *Drying Technology,* 23**,** 2337-2367.

Perdana, J., Fox, M. B., Schutyser, M. a. I. & Boom, R. M. 2011. Single‐Droplet Experimentation on Spray Drying: Evaporation of a Sessile Droplet. *Chemical Engineering & Technology,* 34**,** 1151-1158.

Perdana, J., Fox, M. B., Schutyser, M. a. I. & Boom, R. M. 2013. Mimicking spray drying by drying of single droplets deposited on a flat surface. *Food and Bioprocess Technology,* 6**,** 964-977.

Perré, P. 2015. The proper use of mass diffusion equations in drying modeling: introducing the drying intensity number. *Drying Technology,* 33**,** 1949-1962.

Picknett, R. G. & Bexon, R. 1977. The evaporation of sessile or pendant drops in still air. *Journal of Colloid and Interface Science,* 61**,** 336-350.

Pısecký, J. 1997. Handbook of milk powder manufacture. *Niro A/S, Copenhagen,* 3.

Porowska, A., Dosta, M., Heinrich, S., Fries, L., Gianfrancesco, A. & Palzer, S. 2015. Influence of feed composition and drying parameters on the surface composition of a spray-dried multicomponent particle. *Drying Technology,* 33**,** 1911-1919.

Putranto, A., Chen, X. D., Xiao, Z. & Webley, P. A. 2011. Simple, accurate and robust modeling of various systems of drying of foods and biomaterials: A demonstration of the feasibility of the reaction engineering approach (REA). *Drying Technology,* 29**,** 1519-1528.

Quemada, D. 1982. Lecture notes in physics: stability of thermodynamic systems. *In:* J. CASAS-VASQUES, L., G. (ed.). Berlin, Germany: Springer.

Rahman, M. S. 2009. *Food properties handbook,* Boca Raton, USA, CRC Press.

Ranz, W. E. & Marshall, W. R. 1952a. Evaporation from drops Part I. *Chemical Engineering Progress,* 48**,** 141-146.

Ranz, W. E. & Marshall, W. R. 1952b. Evaporation from drops Part II. *Chemical Engineering Progress,* 48**,** 173-180.

Rayleigh, F. R. S. On the instability of jets. Proceedings of the London Mathematical Society, 1879. 4-13.

Rogers, S., Wu, W. D., Lin, S. X. Q. & Chen, X. D. 2012. Particle shrinkage and morphology of milk powder made with a monodisperse spray dryer. *Biochemical Engineering Journal,* 62**,** 92-100.

Rogers, S., Wu, W. D., Saunders, J. & Chen, X. D. 2008. Characteristics of milk powders produced by spray freeze drying. *Drying Technology,* 26**,** 404-412.

Rosenberg, M., Kopelman, I. J. & Talmon, Y. 1985. A scanning electron microscopy study of microencapsulation. *Journal of Food Science,* 50**,** 139-144.

Sabbah, R., Xu-Wu, A., Chickos, J. S., Leitão, M. L. P., Roux, M. V. & Torres, L. A. 1999. Reference materials for calorimetry and differential thermal analysis. *Thermochimica Acta,* 331**,** 93-204.

Sadek, C., Li, H., Schuck, P., Fallourd, Y., Pradeau, N., Le Floch-Fouéré, C. & Jeantet, R. 2014a. To what extent do whey and casein micelle proteins influence the morphology and properties of the resulting powder? *Drying Technology,* 32**,** 1540-1551.

Sadek, C., Pauchard, L., Schuck, P., Fallourd, Y., Pradeau, N., Le Floch-Fouéré, C. & Jeantet, R. 2015. Mechanical properties of milk protein skin layers after drying: Understanding the mechanisms of particle formation from whey protein isolate and native phosphocaseinate. *Food Hydrocolloids,* 48**,** 8-16.

Sadek, C., Schuck, P., Fallourd, Y., Pradeau, N., Jeantet, R. & Le Floch-Fouéré, C. 2016. Buckling and collapse during drying of a single aqueous dispersion of casein micelle droplet. *Food Hydrocolloids,* 52**,** 161-166.

Sadek, C., Schuck, P., Fallourd, Y., Pradeau, N., Le Floch-Fouéré, C. & Jeantet, R. 2014b. Drying of a single droplet to investigate process-structure-function relationships: a review. *Dairy Science & Technology***,** 1-24.

Sadek, C. L., Tabuteau, H., Schuck, P., Fallourd, Y., Pradeau, N., Le Floch-FouéRé, C. C. & Jeantet, R. 2013. Shape, shell, and vacuole formation during the drying of a single concentrated whey protein droplet. *Langmuir,* 29**,** 15606-15613.

Sano, Y. & Keey, R. B. 1982. The drying of a spherical particle containing colloidal material into a hollow sphere. *Chemical Engineering Science,* 37**,** 881-889.

Sarkar, A., Arfsten, J., Golay, P.-A., Acquistapace, S. & Heinrich, E. 2016. Microstructure and long-term stability of spray dried emulsions with ultra-high oil content. *Food Hydrocolloids,* 52**,** 857-867.

Scf 2003. Opinion of the Scientific Committee on Food on Carrageenan. *SCF/CS/ADD/EMU/199.* European Commission - Health & Consumer Protection Directorate - Scientific Committee on Food.

Schiffter, H. & Lee, G. 2007a. Single‐droplet evaporation kinetics and particle formation in an acoustic levitator. Part 1: Evaporation of water microdroplets assessed using boundary‐layer and acoustic levitation theories. *Journal of Pharmaceutical Sciences,* 96**,** 2274-2283.

Schiffter, H. & Lee, G. 2007b. Single‐droplet evaporation kinetics and particle formation in an acoustic levitator. Part 2: Drying kinetics and particle formation from microdroplets of aqueous mannitol, trehalose, or catalase. *Journal of Pharmaceutical Sciences,* 96**,** 2284-2295.

Schuck, P. 2002. Spray drying of dairy products: state of the art. *Le Lait,* 82**,** 375-382.

Schuck, P., Mejean, S., Dolivet, A., Gaiani, C., Banon, S., Scher, J. & Jeantet, R. 2007. Water transfer during rehydration of micellar casein powders. *Le Lait,* 87**,** 425-432.

Serfert, Y., Schröder, J., Mescher, A., Laackmann, J., Rätzke, K., Shaikh, M., Gaukel, V., Moritz, H.-U., Schuchmann, H. P. & Walzel, P. 2013. Spray drying behaviour and functionality of emulsions with β-lactoglobulin/pectin interfacial complexes. *Food Hydrocolloids,* 31**,** 438-445.

Seydel, P., Sengespeick, A., Blömer, J. & Bertling, J. 2004. Experiment and mathematical modeling of solid formation at spray drying. *Chemical Engineering & Technology,* 27**,** 505-510.

Shamaei, S., Seiiedlou, S. S., Aghbashlo, M., Tsotsas, E. & Kharaghani, A. 2016. Microencapsulation of walnut oil by spray drying: Effects of wall material and drying conditions on physicochemical properties of microcapsules. *Innovative Food Science & Emerging Technologies*.

Singh, H. & Gallier, S. 2016. Nature's complex emulsion: The fat globules of milk. *Food Hydrocolloids,* 68**,** 81–89.

Singh, H., Tamehana, M., Hemar, Y. & Munro, P. A. 2003. Interfacial compositions, microstuctures and properties of oil-in-water emulsions formed with mixtures of milk proteins and κ-carrageenan: 1. Sodium caseinate. *Food Hydrocolloids,* 17**,** 539-548.

Sloth, J., Kiil, S., Jensen, A. D., Andersen, S. K., Jørgensen, K., Schiffter, H. & Lee, G. 2006. Model based analysis of the drying of a single solution droplet in an ultrasonic levitator. *Chemical Engineering Science,* 61**,** 2701-2709.

Snoeren, T. H. M., Payens, T. a. J., Jeunink, J. & Both, P. 1975. Electrostatic interaction between kappa-carrageenan and kappa-casein. *Milchwissenschaft,* 30**,** 393-396.

Soottitantawat, A., Yoshii, H., Furuta, T., Ohkawara, M. & Linko, P. 2003. Microencapsulation by spray drying: influence of emulsion size on the retention of volatile compounds. *Journal of Food Science,* 68**,** 2256-2262.

Srinivasan, M., Singh, H. & Munro, P. A. 1996. Sodium caseinate-stabilized emulsions: factors affecting coverage and composition of surface proteins. *Journal of Agricultural and Food Chemistry,* 44**,** 3807-3811.

Stone, A. K. & Nickerson, M. T. 2012. Formation and functionality of whey protein isolate–(kappa-, iota-, and lambda-type) carrageenan electrostatic complexes. *Food Hydrocolloids,* 27**,** 271-277.

Sugiyama, Y., Larsen, R. J., Kim, J.-W. & Weitz, D. A. 2006. Buckling and crumpling of drying droplets of colloid-polymer suspensions. *Langmuir,* 22**,** 6024-6030.

Sunkel, J. M. & King, C. J. 1993. Influence of the development of particle morphology upon rates of loss of volatile solutes during drying of drops. *Industrial & Engineering Chemistry Research,* 32**,** 2357-2364.

Surh, J., Decker, E. A. & Mcclements, D. J. 2006. Influence of pH and pectin type on properties and stability of sodium-caseinate stabilized oil-in-water emulsions. *Food Hydrocolloids,* 20**,** 607-618.

Taneja, A., Ye, A., Jones, J. R., Archer, R. & Singh, H. 2013. Behaviour of oil droplets during spray drying of milk-protein-stabilised oil-in-water emulsions. *International Dairy Journal,* 28**,** 15-23.

Tian, Y., Fu, N., Wu, W. D., Zhu, D., Huang, J., Yun, S. & Chen, X. D. 2014. Effects of co-spray drying of surfactants with high solids milk on milk powder wettability. *Food and Bioprocess Technology,* 7**,** 3121-3135.

Tran, T. T. H., Jaskulski, M., Avila-Acevedo, J. G. & Tsotsas, E. 2016. Model parameters for single droplet drying of skim milk and its constituents at moderate and elevated temperatures. *Drying Technology,* 35**,** 444-464.

Tsapis, N., Dufresne, E. R., Sinha, S. S., Riera, C. S., Hutchinson, J. W., Mahadevan, L. & Weitz, D. A. 2005. Onset of buckling in drying droplets of colloidal suspensions. *Physical Review Letters,* 94**,** 018302.

Twomey, M., Keogh, M. K., O'kennedy, B. T., Auty, M. & Mulvihill, D. M. 2000. Effect of milk composition on selected properties of spray-dried high-fat and skim-milk powders. *Irish journal of Agricultural and Food Research*, 79-94.

Van Krevelen, D. W. & Hoftijzer, P. J. 1949. Drying of granulated materials. Part I. Drying of a single granule. *Journal of the Society of Chemical Industry,* 68**,** 59-66.

Van Mil, P. J. J. M., Hols, G. & Klok, H. J. Spray drying of concentrated milk: relation between initial droplet size and final particle size. *In:* BRUIN, S., ed. Preconcentration and drying of food materials: Thijssen Memorial Symposium: proc of the International Symposium on Preconcentration and Drying of Foods, 1987 Eindhoven, The Netherlands. Elsevier.

Vega, C. & Roos, Y. H. 2006. Invited review: spray-dried Dairy and dairy-like emulsions - compositional considerations. *Journal of Dairy Science,* 89**,** 383-401.

Vehring, R. 2008. Pharmaceutical particle engineering via spray drying. *Pharmaceutical Research,* 25**,** 999-1022.

Vehring, R., Foss, W. R. & Lechuga-Ballesteros, D. 2007. Particle formation in spray drying. *Journal of Aerosol Science,* 38**,** 728-746.

Vignolles, M.-L., Jeantet, R., Lopez, C. & Schuck, P. 2007. Free fat, surface fat and dairy powders: interactions between process and product. A review. *Le Lait,* 87**,** 187-236.

Vignolles, M. L., Lopez, C., Madec, M. N., Ehrhardt, J. J., Méjean, S., Schuck, P. & Jeantet, R. 2009a. Fat properties during homogenization, spray-drying, and storage affect the physical properties of dairy powders. *Journal of Dairy Science,* 92**,** 58-70.

Vignolles, M. L., Lopez, C., Madec, M. N., Ehrhardt, J. J., Méjean, S., Schuck, P. & Jeantet, R. 2009b. Protein-lactose matrix effects on fat encapsulation during the overall spray-drying process of dairy powders. *Australian Journal of Dairy Technology,* 64**,** 75.

Walton, D. E. 2000. The morphology of spray-dryied particles: A qualitative view. *Drying Technology,* 18**,** 1943-1986.

Walton, D. E. 2004. The evaporation of water droplets. A single droplet drying experiment. *Drying Technology,* 22**,** 431-456.

Wang, S., Langrish, T. & Adhikari, B. 2013. A multicomponent distributed parameter model for spray drying: model development and validation with experiments. *Drying Technology,* 31**,** 1513-1524.

Wang, S. & Langrish, T. a. G. 2009. A distributed parameter model for particles in the spray drying process. *Advanced Powder Technology,* 20**,** 220-226.

Wang, Y., Liu, W., Chen, X. D. & Selomulya, C. 2016. Micro-encapsulation and stabilization of DHA containing fish oil in protein-based emulsion through mono-disperse droplet spray dryer. *Journal of Food Engineering,* 175**,** 74-84.

Wijlhuizen, A. E., Kerkhof, P. J. a. M. & Bruin, S. 1979. Theoretical study of the inactivation of phosphatase during spray drying of skim-milk. *Chemical Engineering Science,* 34**,** 651-660.

Woo, M. W. 2016. *Computational fluid dynamics simulation of spray dryers: an engineer's guide,* Boca Raton, USA, CRC Press.

Woo, M. W., Daud, W. R. W., Mujumdar, A. S., Talib, M. Z. M., Hua, W. Z. & Tasirin, S. M. 2008. Comparative study of droplet drying models for CFD modelling. *Chemical Engineering Research and Design,* 86**,** 1038-1048.

Wu, D. 2010. *A Novel micro-fluidic-jet-spray-dryer equipped with a micro-fluidic-aerosol-nozzle: Equipment development and applications in making functional particles.* Thesis (Ph.D.), Monash University. Faculty of Engineering. Department of Chemical Engineering.

Wu, W. D., Lin, S. X. & Chen, X. D. 2011. Monodisperse droplet formation through a continuous jet break‐up using glass nozzles operated with piezoelectric pulsation. *AIChE Journal,* 57**,** 1386-1392.

Wu, W. D., Liu, W., Gengenbach, T., Woo, M. W., Selomulya, C., Chen, X. D. & Weeks, M. 2014. Towards spray drying of high solids dairy liquid: effects of feed solid content on particle structure and functionality. *Journal of Food Engineering,* 123**,** 130-135.

Wulsten, E. & Lee, G. 2008. Surface temperature of acoustically levitated water microdroplets measured using infra-red thermography. *Chemical Engineering Science,* 63**,** 5420-5424.

Xiao, J. & Chen, X. D. 2014. Multiscale modeling for surface composition of spray‐dried two‐component powders. *AIChE Journal,* 60**,** 2416-2427.

Xu, W. & Choi, C.-H. 2012. Effects of surface topography and colloid particles on the evaporation kinetics of sessile droplets on superhydrophobic surfaces. *Journal of Heat Transfer,* 134.

Xu, Y. Y., Howes, T., Adhikari, B. & Bhandari, B. 2013. Effects of emulsification of fat on the surface tension of protein solutions and surface properties of the resultant spray-dried particles. *Drying Technology,* 31**,** 1939-1950.

Yanes, M., Durán, L. & Costell, E. 2002. Effect of hydrocolloid type and concentration on flow behaviour and sensory properties of milk beverages model systems. *Food Hydrocolloids,* 16**,** 605-611.

Yarin, A. L., Brenn, G., Kastner, O., Rensink, D. & Tropea, C. 1999. Evaporation of acoustically levitated droplets. *Journal of Fluid Mechanics,* 399**,** 151-204.

Yarin, A. L., Brenn, G., Keller, J., Pfaffenlehner, M., Ryssel, E. & Tropea, C. 1997. Flowfield characteristics of an aerodynamic acoustic levitator. *Physics of Fluids (1994-present),* 9**,** 3300-3314.

Yarin, A. L., Pfaffenlehner, M. & Tropea, C. 1998. On the acoustic levitation of droplets. *Journal of Fluid Mechanics,* 356**,** 65-91.

Yu, Y.-S., Wang, Z. & Zhao, Y.-P. 2012. Experimental and theoretical investigations of evaporation of sessile water droplet on hydrophobic surfaces. *Journal of Colloid and Interface Science,* 365**,** 254-259.

Zakarlan, J. A. & King, C. J. 1982. Volatiles loss in the nozzle zone during spray drying of emulsions. *Industrial & Engineering Chemistry Process Design and Development,* 21**,** 107-113.

Zhu, P., Patel, K., Lin, S., Méjean, S., Blanchard, E., Chen, X. D., Schuck, P. & Jeantet, R. 2011. Simulating industrial spray-drying operations using a reaction engineering approach and a modified desorption method. *Drying Technology,* 29**,** 419-428.